Diagenèse expérimentale du quartz en présence d'hydrocarbures

Stéphane Teinturier

Faculté des Sciences — UMR 7566

U.F.R. S.T.M.P.
Ecole Doctorale :
RP²E (Ressources, Produits, Procédés et Environnement)

Thèse
présentée pour l'obtention du titre de

Docteur de l'Université Henri Poincaré, Nancy I
en Sciences de l'Univers

par
Stéphane TEINTURIER

Diagenèse expérimentale du quartz en présence d'hydrocarbures

Soutenue publiquement le 15 novembre 2002

Membres du jury :

Président	M. J. Leroy	Professeur, Université Henri Poincaré, Nancy 1
Rapporteurs	M. M. Pagel	Professeur, Université Paris XI, Orsay
	M. O. Vidal	Directeur de Recherche CNRS, Université J.F., Grenoble
Directeur de thèse	M. J. Pironon	Chargé de Recherche CNRS, G2R–CREGU, Nancy
Examinateurs	M. E. Deloule	Directeur de Recherche CNRS, CRPG, Nancy
	M. F. Walgenwitz	Ingénieur TotalFinaElf, Pau
Invités	M. J.P. Girard	Ingénieur BRGM, Orléans
	M. A. Aplin	Professeur, Université de Newcastle, Grande Bretagne

AVANT PROPOS & REMERCIEMENTS

Ce mémoire a été réalisé à l'UMR G2R 7566-CREGU de Nancy avec le soutien financier du CREGU, de l'Université Henri Poincaré (UMR G2R) et de TotalFinaElf.

Qu'est ce qu'une thèse ? Dure question...et je n'ai pas la prétention d'y répondre ici...En revanche, il est clair que la thèse permet d'acquérir plus qu'un simple savoir, elle permet d'approfondir sa connaissance des autres et de soi-même. A cette occasion, je voudrais donc remercier ici, les personnes qui ont eu un rapport de près ou de loin avec "ma thèse".

- **mon directeur de thèse**

Jacques PIRONON, alias le maître de cérémonie qui m'a transmis son goût et sa passion pour la recherche et a su me guider dans les méandres de la thèse. Ce fut un réel plaisir de travailler avec toi.

- **les membres du Jury** qui ont participé et accepté de juger ce travail.

Andrew APLIN, Etienne DELOULE, Jean-Pierre GIRARD, Jacques LEROY, Maurice PAGEL, Olivier VIDAL et Frédéric WALGENWITZ.

- **les personnes** qui ont apporté leur aide, leur soutien technique et scientifique à ce travail.

A l'UMR G2R-CREGU à Nancy : Marcel ELIE pour l'analyse des huiles; Régine MOSSER-RUCK et Hélène LEGROS pour leurs aides concernant les expériences réalisées en autoclave; Jean DUBESSY et Thérèse LHOMME pour leurs aides scientifiques et techniques, en expérimentation et au Raman; Cédric DEMEURIE pour la confection des lames.

Au LCM de l'Université de Nancy : Frédéric DIOT et Alain KOHLER pour les observations en cathodoluminescence.

Au CRPG de Nancy : Michel CHAMPENOY, Denis MANGIN et Claire ROLLION-BARD pour les analyses sur la sonde ionique; Christian FRANCE-LANORD et Caroline GUILMETTE pour les analyses isotopiques des solutions. Bruno PORCU pour le polissage des échantillons de sonde.

A l'IBMP de Strasbourg : Jérôme MUTTERER pour nos excellentes séances de microscopie confocale "à l'Alsacienne".

Diverses personnes rencontrées lors de tests chez des constructeurs : Alexander PIRY (®Bruker) pour l'imagerie IR; Jean Louis COUPIER (®Olympus) et Dan (®Bio-Rad) pour la microscopie confocale.

Je remercie également Benoît MARTINET et Régis THIERY pour les améliorations apportées au logiciel PIT.

- **mes compagnons de travail**

Le bureau A508
Tout d'abord, je tiens à remercier ma collègue de bureau Delphine, qui m'a supporté pendant plus de 2 ans. Je n'oublierai jamais nos longues conversations sur la vie !

La famille "Hulk"
Dona, ma "frangine de thèse", la chanteuse au grand cœur qui n'est à l'aise que sur une "bleu"... et au volant d'un camion !
Jörgy, alias le mythe, la MaxiWurst,... qui ne sait toujours pas ce qui est le plus important dans sa vie: la bière ou sa coccinelle...?

La famille "AB Production"
Cécile (*AblatGirl)* et son capitaine Anthony *Stubing*, pour nos nombreux fous rires et délires en tout genre...ainsi que Norman alias Return to the base.

La famille "Modèle"
Stéphane *(Bushman, Mini-moi*) et sa femme Karine pour la maîtrise et la sagesse de leurs actes et aussi pour nos délires...raisonnables !

Jean V (*alias Père Jean*) pour sa bénédiction et ses "conseils visuels". Les voix impénétrables du Seigneur lui ont donné comme mission d'évangéliser les Equatoriens... et les Suisses.

Guillaume Lorilleux (*BP*) pour nos longues conversations métaphysiques. Sa R5 hantera encore longtemps la place de stationnement devant l'entrée 3B.

Damien (*EvilRisson*) pour son aide et son incroyable faculté de travail. Mais quel est ton secret ?

Emilie (*EmiliX*) pour sa "capacité d'excitation" au pot de thèse, vous verrez.

Philippe (*K-67*) pour son humour, son enthousiasme et ses incroyables histoires...

Régine* (*Maîtresse des Confs.*) pour sa bonne humeur et sa philosophie...

Bocar pour sa phrase désormais culte lors de mon entrée à l'UMR: *"Moi de toute façon l'eutectique, je l'ai jamais vu !"*

Même si je m'arrête au 5ème étage, je n'oublie pas le 6ème (Lubna, Pierre, Marcel, Vincent, Laurence, Laure...), les amis de passage Halim (SONATRACH) et Mustapha ainsi que toute l'équipe du G2R-CREGU des deux étages et du rez de chaussée !

- **Mes amis réels, virtuels et électroniques** qui m'ont accompagné ces 3 années

Seb, Pimprenelle, Simon, Alhambra Project, les Zergs, les membres d'Audiofanzine, ma GIBSON et mon VIRUS !

Enfin je ne pourrais conclure sans une immense pensée pour Carole

RESUME

La cimentation du quartz est un processus diagénétique important puisqu'elle influence directement la qualité d'un réservoir pétrolier, notamment en régulant la porosité et donc son potentiel en huile ou en gaz. Cependant, la possibilité de cimenter ou non du quartz en présence d'hydrocarbures reste un sujet de controverse. Bien souvent, la reconstitution et la compréhension des processus diagénétiques se basent sur l'étude des inclusions fluides. Or de nombreuses questions concernant la représentativité et la lecture des inclusions des auréoles des environnements pétroliers demeurent toujours sans réponse.

Les expériences réalisées en système silice±eau±sels±huile±gaz ont permis de simuler et d'approcher les conditions de la diagenèse siliceuse d'un réservoir pétrolier naturel et d'améliorer la compréhension des mécanismes de formation des inclusions fluides et de croissance de quartz en milieu aqueux et/ou hydrocarboné. Des courbes de calibrage permettant de calculer la teneur en méthane des inclusions dans le système H_2O-CH_4-NaCl ont été obtenues à partir de l'analyse en spectroscopie Raman et grâce à la synthèse d'inclusions utilisées comme standards. L'utilisation d'inclusions synthétiques et naturelles de référence a permis un calibrage de l'analyse quantitative de CH_4, CO_2 et des alcanes des inclusions hydrocarbonées par spectroscopie IR.

Des inclusions aqueuses ont été synthétisées dans des microfractures de grains de quartz, en présence de méthane dès 150°C-200 bar, en présence d'hydrocarbures à partir de 184°C-163 bar et dans des surcroissances en présence d'hydrocarbures à partir de 277°C-330 bar. Des inclusions hydrocarbonées ont été synthétisées avec différents rapports eau/huile (E/H), dans des microfractures de quartz (0<E/H<50%, 209-350°C; 175-400 bar), ainsi que dans des auréoles de croissance (10<E/H<50%, 289-350°C; 350-400 bar). La composition des inclusions hydrocarbonées est représentative de la composition du fluide parent jusqu'à des températures et pressions de 250°C et 212 bars respectivement. A 350°C-400 bar, des processus de cracking ont été mis en évidence aussi bien dans les inclusions fluides que dans l'huile parent et les propriétés PVTX des inclusions fluides hydrocarbonées sont modifiées par la présence d'eau dissoute dans l'huile en grande quantité. Aucun processus de rééquilibrage et d'infiltration post-auréole n'a été observé dans les auréoles des quartz lors d'une baisse de température. En revanche, quelques inclusions fluides ont pu être rééquilibrées et marquées au lithium ou au méthane en appliquant des températures expérimentales supérieures aux T_h des inclusions préexistantes.

La croissance de quartz et la formation d'inclusions fluides sont donc possibles même à forte saturation en hydrocarbures seulement si les quartz sont mouillés à l'eau. Dans des conditions expérimentales extrêmes (350°C-400 bar; E/H =10%), le fait que la quasi-totalité de l'eau soit dissoute dans la phase hydrocarbonée implique que la présence d'un film d'eau suffit à faire pousser du quartz en milieu à forte saturation en huile, dans l'hypothèse ou l'eau reste le seul vecteur et transporteur de silice. Les données expérimentales obtenues en SIMS ont montré que les auréoles générées en présence d'huile avaient des $\delta^{18}O$ supérieures, d'environ 10‰ par

rapport à celles crées en milieu strictement aqueux dans les conditions expérimentales à 350°C et 400 bar. Si l'on fait le parallèle entre l'étude des auréoles naturelles des réservoirs pétroliers et les auréoles expérimentales, il est fort probable que les valeurs maximales en $\delta^{18}O$ des auréoles naturelles soient les témoins d'une saturation en huile du réservoir au moment de leur formation.

Mot-clés: quartz, hydrocarbures, experimentation, diagenèse

ABSTRACT

Quartz cementation has a great impact on petroleum reservoir quality by controlling the porosity and thus the gas or oil storage. However, the possible cementation of quartz during petroleum emplacement is still debated. In most cases, the reconstitution and the understanding of diagenetic processes is based on fluid inclusions studies. However, many questions concerning the representativeness and the reading of the fluid inclusions still remains misunderstood.

The experiments were carried out in a silica±water±salts±oil±gas system with the objective to simulate the siliceous diagenesis of natural petroleum reservoirs and to better understand the mechanisms of fluid inclusions formation and quartz cementation in a water and/or petroleum system. Calibration curves have been established using Raman microspectroscopy and synthetic reference inclusions to calculate the methane content of aqueous inclusions in the H_2O-CH_4-NaCl system. A quantitative procedure for FT-IR microspectrometry has been developed to obtain, from individual petroleum fluid inclusions, mole % concentrations of methane, alkanes and carbon dioxide as constraints to thermodynamic modelling.

Synthetic aqueous inclusions were created within quartz microfractures, with methane (from 150°C-200 bar), with petroleum (from 184°C-163 bar) and inside quartz overgrowths with the presence of hydrocarbons (from 277°C-300 bar). Synthetic petroleum inclusions were created with different water/oil ratios (W/O) within quartz microfractures (0<E/H<50%, 209-350°C; 175-400 bar), and in quartz overgrowths (10<E/H<50%, 289-350°C; 350-400 bar). The composition of the petroleum inclusions is representative to their parent oil composition up to 250°C and 212 bars. At 350°C-400 bar, cracking processes have been observed as well inside petroleum inclusions as for its residual parent oil in the autoclave. Moreover, the presence of water has modified the PVTX properties of fluid inclusions. On the other hand, no reequilibration processes have been observed with a continuous decrease of temperature. In contrast, few natural inclusions marked with lithium and methane have been reequilibrated by applying higher experimental temperatures than the trapping temperature of pre-existing fluid inclusions.

The quartz cementation as well as the fluid inclusion formation is thus possible even at high oil saturation. These processes require that the quartz is water-wet. In extreme experimental conditions (350°C-400 bar; E/H =10%), the almost entire dissolution of water into the petroleum phase involve that a simple water film is sufficient to generate quartz overgrowth into a high oil saturation. This hypothesis implies that water still remains the silica vector. SIMS profiles shows that $\delta^{18}O$ values of quartz overgrowths created with the presence of petroleum are higher (+10‰) than those created in a strict water system, at 350°C and 400 bar. If we project these observations in natural petroleum reservoirs, it could be possible that the maximum $\delta^{18}O$ values of diagenetic quartz overgrowths correspond to a possible episode of petroleum migration.

Keywords: quartz, petroleum, experimentation, diagenesis

TABLES DES MATIERES

TABLE DES ILLUSTRATIONS

FIGURES

TABLEAUX

A. INTRODUCTION GENERALE

INTRODUCTION GENERALE

Objectif de l'étude

La cimentation du quartz est un processus diagénétique important puisqu'elle influence directement la qualité d'un réservoir pétrolier, notamment en régulant la porosité et donc son potentiel en huile ou en gaz. Cette cimentation de quartz correspond à la cicatrisation des fractures des grains et plus généralement à la croissance d'auréoles et dépend en grande partie de la disponibilité de silice et du contrôle de son transport en solution aqueuse de sa source jusqu'à son site de précipitation (Figure A-1).

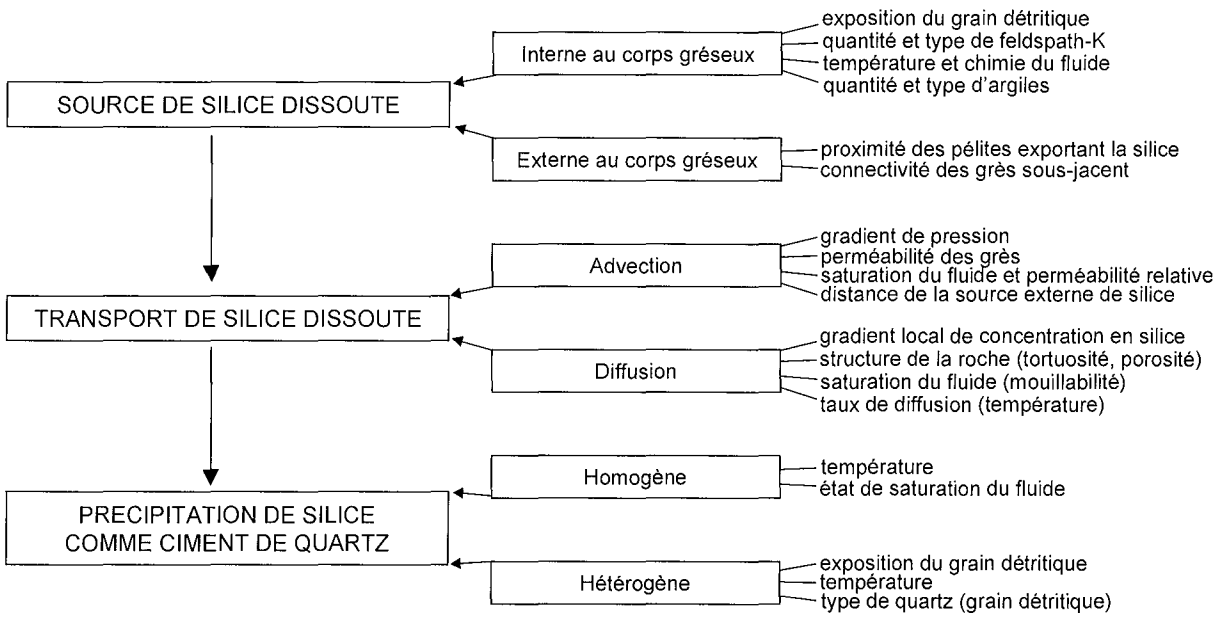

Figure A-1: Contrôles géochimiques de la cimentation du quartz (Worden et Morad, 2000). Les trois contrôles fondamentaux permettant la cimentation du quartz sont (1) le ou les apports de silice, (2) le transport de silice en solution aqueuse et (3) la précipitation de silice (ciment) à partir de cette solution aqueuse. Ces trois processus sont contrôlés par des paramètres secondaires, eux-mêmes influencés par des facteurs listés à droite du diagramme.

Les relations entre la cimentation du quartz et la mise en place des hydrocarbures dans un bassin pétrolier restent un sujet de controverse. Diverses études ont montré que cette cimentation de quartz était possible même dans un milieu à forte saturation en huile ou en gaz (Ramm, 1992; Saigal et al., 1992; Walderhaug, 1990). Cependant, de nombreux auteurs soutiennent le fait que la migration d'hydrocarbures puisse stopper ou du moins ralentir la cimentation de quartz, en se

basant notamment sur des différences importantes de porosité entre les zones à eau et à huile de divers réservoirs pétroliers (Dixon et al., 1989; Gluyas et al., 1993; Marchand et al., 2001). Le degré d'inhibition devrait alors dépendre principalement de la saturation en eau restante, de la mouillabilité des quartz et de la pression fluide exercée sur les quartz (Figure A-2).

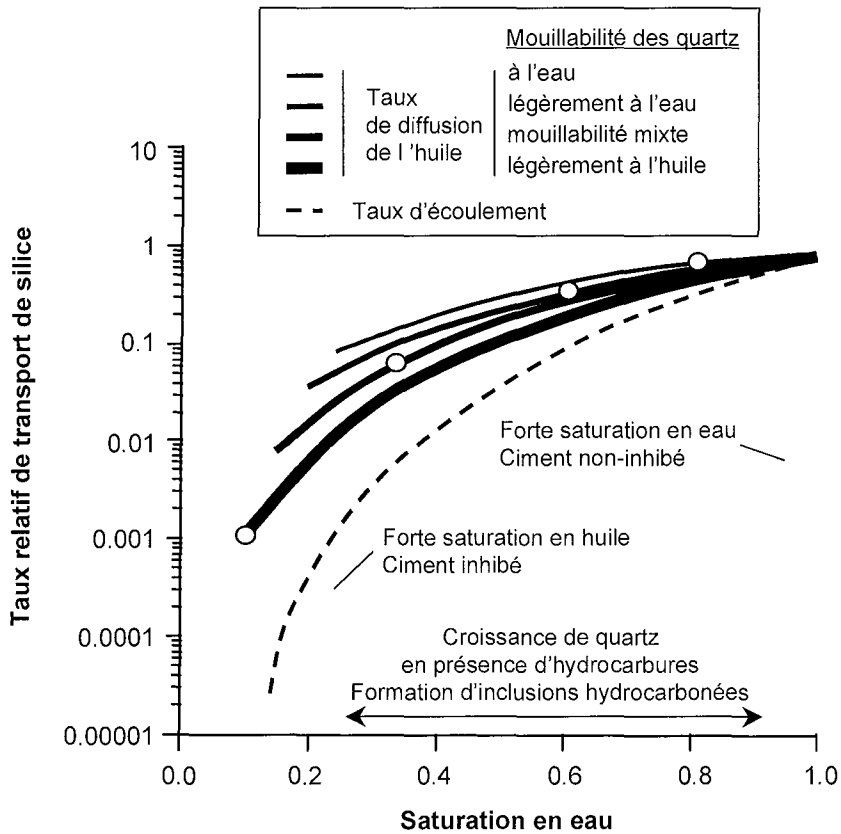

Figure A-2: Effets relatifs de la présence d'huile sur le taux de diffusion et d'advection des fluides aqueux riches en silice. Les taux de diffusion de la silice dans l'eau ont été calculés pour différents rapports E/H et différents états de mouillabilité en eau et/ou huile. Les cercles blancs représentent l'évolution d'un système roche-eau-huile au cours du remplissage en huile du réservoir. Le taux d'advection (écoulement) est fortement affectée par la baisse des rapports eau/huile. Une fenêtre de piégeage des inclusions hydrocarbonées pour des rapports E/H compris entre 25 et 95% est proposé. (Worden et Morad, 2000).

En général, la reconstitution et la compréhension des processus diagénétiques se basent sur l'étude de la matière organique, des traces de fissions, des isotopes, de la pétrographie et/ou des inclusions fluides. Concernant les inclusions fluides, de nombreuses questions concernant la représentativité et la lecture des inclusions des auréoles demeurent toujours sans réponse. Les problèmes de rééquilibrage et de la simultanéité du piégeage des inclusions des auréoles avec les différentes époques de cimentation peut complètement fausser l'interprétation des données d'inclusions fluides. C'est dans cette optique que le groupe TotalFinaElf (TFE) s'est joint à l'UMR-

G2R 7566-CREGU de Nancy pour développer une approche expérimentale consacrée à l'étude des caractéristiques physiques et chimiques de la limite grain-auréole et de leur accès par les fluides dans le système eau-huile-silice. Cette étude s'inscrit dans un projet TFE qui a permis la réalisation d'une thèse à l'Université Paris XI Orsay sous la direction de Maurice Pagel, intitulé "Origine, conditions et processus de la silicification diagénétique de réservoirs gréseux en Mer du Nord" (Blanchet, 2002).

Le travail développé ici permet également de s'interroger sur les mécanismes liés à la cimentation de quartz et aux conditions de formation des inclusions fluides aqueuses et/ou hydrocarbonées. Quelles sont les effets de la température, de la pression sur la croissance de quartz ? Est-ce que la croissance de quartz est possible en milieu hydrocarboné? Quelle saturation en eau/huile/gaz est nécessaire pendant la croissance pour donner naissance à des inclusions hydrocarbonées ? Est-ce que le rapport huile/eau (E/H) des inclusions reflète la saturation en huile du réservoir ? Est-ce que la formation d'inclusions est un processus rapide ou lent ? Quelle est la représentativité des inclusions fluides vis à vis du quartz et du fluide de départ? Est-ce que le quartz contient une empreinte isotopique de la présence d'eau et/ou d'huile lors de sa croissance?

Avant d'entreprendre l'étude expérimentale de la croissance de quartz et la formation d'inclusions fluides en milieu aqueux et/ou hydrocarboné, il est bon de rappeler ce qu'est une inclusion fluide piégée dans un quartz.

Une inclusion est une microcavité intracristalline qui correspond à un défaut lors de la croissance d'un minéral ou lors de sa recristallisation totale ou partielle. Les quartz des bassins pétroliers peuvent contenir plusieurs générations d'inclusions correspondant à différents épisodes de cristallisation. Ces inclusions sont localisées dans des microfractures dans les grains de quartz détritiques et/ou dans les auréoles de croissance des quartz diagénétiques (Figure A-3). L'apport interne et/ou externe de silice est variable selon l'objet à cimenter. Il sera négligeable dans le cas de fractures nanométriques où la redistribution locale de silice peut suffire à former des ponts liant les parois de la structure et ainsi cicatriser la nanofracture. Il sera un peu plus important pour cimenter des microfractures (<5µm) et créer des inclusions classiquement observables au microscope. En revanche, un fort apport en silice sera nécessaire pour pouvoir former des auréoles de quartz de plusieurs dizaines, voir plusieurs centaines de microns.

Les inclusions hydrocarbonées se différencient des inclusions aqueuses par leur contenu riche en carbone et en hydrogène. Cependant, ces inclusions peuvent piéger des composés non-hydrocarbonés tels que CO_2, H_2O, N_2, H_2S... Lors du piégeage de composés immiscibles tels que l'huile et l'eau, le rapport volumique E/H des inclusions peut varier en fonction du pourcentage initial de chacun des composés dans l'émulsion, de leurs propriétés respectives de mouillabilité, de la vitesse de cristallisation, de la nature de la microporosité...

Les quartz des bassins naturels ont des propriétés géochimiques et cristallographiques variables suivant leurs origines et leurs histoires. Le taux d'hydratation, les défauts, les impuretés, les éléments traces caractéristiques d'un quartz vont notamment influencer la croissance d'auréole, d'un point de vue morphologique et chimique. Deux types de quartz ont été utilisés dans nos expériences, comme analogues des quartz des réservoirs naturels : un germe de quartz de synthèse et un germe de quartz naturel brésilien. La concentration en groupements silanol semble plus importante pour le quartz de synthèse que pour les quartz naturels d'origine métamorphique ou ignée (Giletti and Yund, 1984). La combinaison de ces deux types de quartz devrait être représentative de la plupart des quartz naturels des réservoirs. En effet, les réservoirs silicoclastiques contiennent des grains de quartz détritiques d'origine diverses: métamorphique, ignée et/ou sédimentaire. Les sources de silice des quartz néoformés sont également variées: biogénique, volcanique, quartz détritique, argiles, feldspaths...

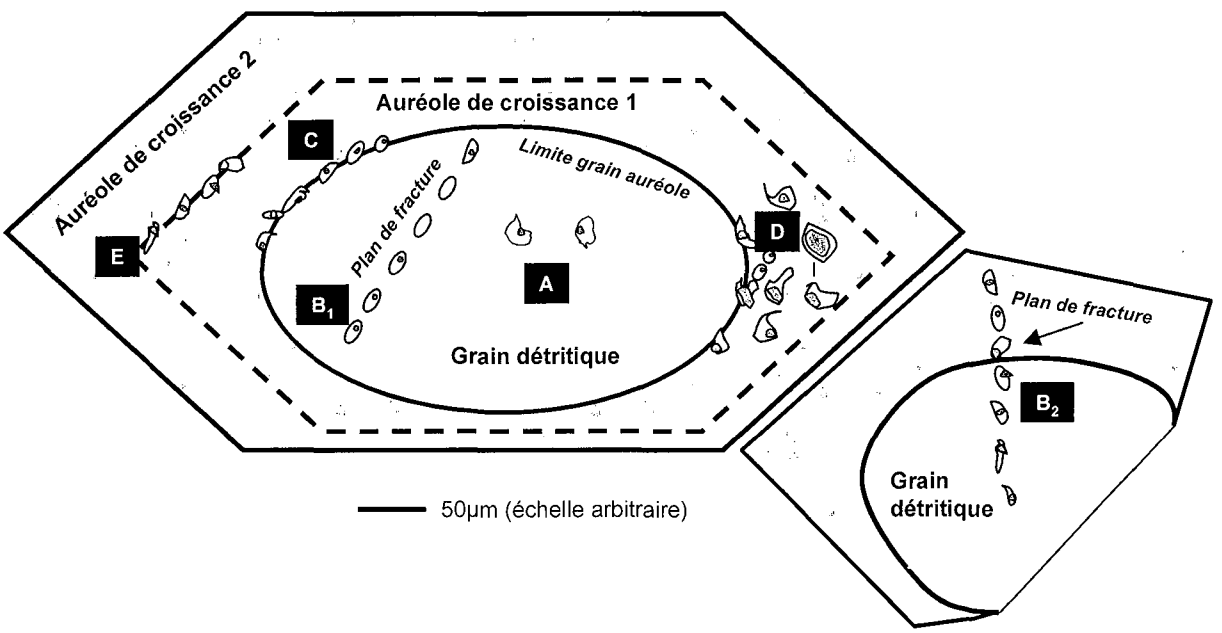

Figure A-3: Schéma représentant deux grains détritiques et leurs surcroissances. Les inclusions fluides sont présentes dans les microfractures des grains détritiques et/ou dans les auréoles de croissance des quartz. A. inclusions héritées du grain détritique. B_1.inclusions situées dans une microfracture du grain détritique. B_2: inclusions situées dans une microfracture recoupant le grain détritique et l'auréole. C. inclusions en limite grain-auréole. D. inclusions dans l'auréole. E. inclusions en limite de zone de surcroissance

Organisation de l'étude

Ce mémoire s'organise en 3 parties principales et est composé de 9 articles publiés, sous presse, soumis ou en préparation pour des revues internationales. En raison de la forte dépendance et la forte interaction entre ces articles, il a été décidé de les grouper en fin de chapitres et de présenter les problématiques et les principaux résultats en début de chapitre. Une première partie sera consacrée aux méthodes analytiques et expérimentales développées ou utilisées lors de cette thèse. La deuxième partie traitera des résultats expérimentaux des synthèses d'inclusions et des croissances de quartz et posera le problème de la représentativité des inclusions dans les quartz diagénétiques. Les mécanismes de croissances de quartz en milieu aqueux et hydrocarboné seront également discutés. Enfin, une étude d'un cas naturel situé dans la région d'Haltenbanken en zone offshore conclura ce mémoire. Ce cas local mais complexe permettra de visualiser l'ensemble des problèmes relatifs à la cimentation de quartz et à l'interprétation des données d'inclusions fluides (necking-down, rééquilibrage...) dans un réservoir pétrolier de la Mer de Norvège.

B. METHODES EXPERIMENTALES, TECHNIQUES ANALYTIQUES ET MODELISATION

METHODES EXPERIMENTALES, TECHNIQUES ANALYTIQUES ET MODELISATION

1 SYNTHESE DE QUARTZ ET DES INCLUSIONS FLUIDES

1.1 Préparation des échantillons

Les expériences en autoclave ont été réalisées sur des cristaux de quartz brésiliens (< 1cm) et sur des quartz de synthèse (1-3cm) découpés perpendiculairement à leur axe de croissance *c*. Des morceaux de lames épaisses polies provenant de la zone d'Alwyn (3/14b9-3630.5m) ont également été utilisés dans certaines expériences.

Avant expérience, les quartz sont préalablement chauffés à 700°C afin de décrépiter d'éventuelles inclusions préexistantes. Selon l'expérience, les quartz sont fracturés lors d'une trempe thermique (environ 400°C) dans l'eau pure et séchés pendant une demi-journée à 80°C.

Technique analytique	Préparation des échantillons	Nettoyage ou rinçage	Observation
Microthermométrie	Aucune	Ethanol ou méthanol	Transmission
Microspectroscopie Raman, infrarouge (et imagerie infrarouge)	Aucune	Ethanol ou méthanol Dichlorométhane ou chloroforme	Transmission
Microscopie confocale	Collage sur lame de verre (baume du Canada)	Ethanol	Transmission réflexion
Cathodoluminescence	Collage sur lame de verre ou enrobage des grains dans une résine d'Araldite métallisation au carbone	-	réflexion
Sonde ionique	Enrobage des grains dans une résine d'Araldite métallisation à l'or	-	réflexion

Tableau B-1 : Préparation des échantillons en fonction du type d'analyse (polissage inclus).

Après expérience, les quartz sont récupérés et nettoyés (tableau B-1). Les quartz des expériences réalisées en milieu aqueux sont nettoyés à l'éthanol ou au méthanol. Les quartz des expériences réalisées en présence d'huile sont rincés au dichlorométhane ou au chloroforme puis à l'éthanol. Ces quartz vont être étudiés, observés sous divers microscopes et appareils analytiques différents, ce qui implique souvent un collage et un décollage sur lame de verre

(microscopie confocale notamment). Il est donc important de proscrire certaines colles (super-glue...) ou solvants (acétone...) lors du nettoyage des échantillons qui peuvent grandement perturber les analyses en microspectroscopie infrarouge ou Raman. Les quartz sont polis manuellement avec beaucoup de précaution. Cette démarche permet d'éviter les destructions d'auréole ou la perte d'inclusions de surface.

1.2 Protocoles expérimentaux

La croissance de quartz secondaire et la synthèse d'inclusions aqueuses et/ou hydrocarbonées sont deux processus difficilement réalisables en laboratoire à basse pression et à basse température. La cimentation des fractures des grains de quartz et/ou la formation d'auréoles de croissance vont conditionner les protocoles expérimentaux. Il est donc nécessaire de développer un protocole qui permette à la fois d'augmenter la cinétique de réaction tout en gardant des conditions P-T réalistes et proches de celles des bassins pétroliers.

Deux approches expérimentales ont été envisagées. La première, dans des gammes de pression-température comprises entre 130-212 bars et 100-270°C respectivement. Ces expériences sont réalisées dans un autoclave à pression de gaz permettant d'utiliser le méthane comme gaz vecteur de pression. La seconde, dans des gammes de pression-température plus élevées, de la pression de vapeur saturante (P_{sat}) à 1200 bars et de 300 à 400°C, en adoptant ainsi une cinétique de réaction plus importante. Ces expériences ont été menées dans des capsules d'or scellées, placées dans des autoclaves à pression fluide de marque ®Autoclave Engeneer.

1.2.1 Autoclave à pression gaz ou à prélèvement (GPA)

L'autoclave à prélèvement est utilisé ici non pas pour prélever mais pour injecter une pression connue de méthane à l'intérieur d'une enceinte fermée, composée d'un alliage titane/nickel. Le volume interne maximal de cette enceinte est de 250 cm^3 mais se réduit à environ 150 cm^3 si l'enceinte est téflonée. L'avantage est alors de réduire d'éventuels risques de contaminations liées aux interactions entre la solution et les parois internes de l'autoclave. L'autoclave à prélèvement dispose d'une vanne d'entrée (V1) dans la phase liquide et d'une vanne de sortie (V2) dans la phase vapeur. Une bouteille de méthane connectée à l'autoclave via la vanne V1 permet d'introduire dans l'enceinte une pression connue de méthane en le faisant buller dans la solution (Figure B-1). Une fois chargé, l'ensemble du dispositif fonctionne en système fermé et peut être amené à une température maximale de 300°C et une pression de 233 bars (3380 PSI).

Contrairement aux expériences réalisées en capsule en domaine monophasique liquide (§ B-1.2.2), celles en autoclave à prélèvement sont réalisées en domaine biphasique. L'équilibre des phases liquides et gazeuses en présence permet de considérer les températures d'homogénéisation (T_h) des inclusions égales aux températures de piégeage (T_p) du fluide de ces mêmes inclusions.

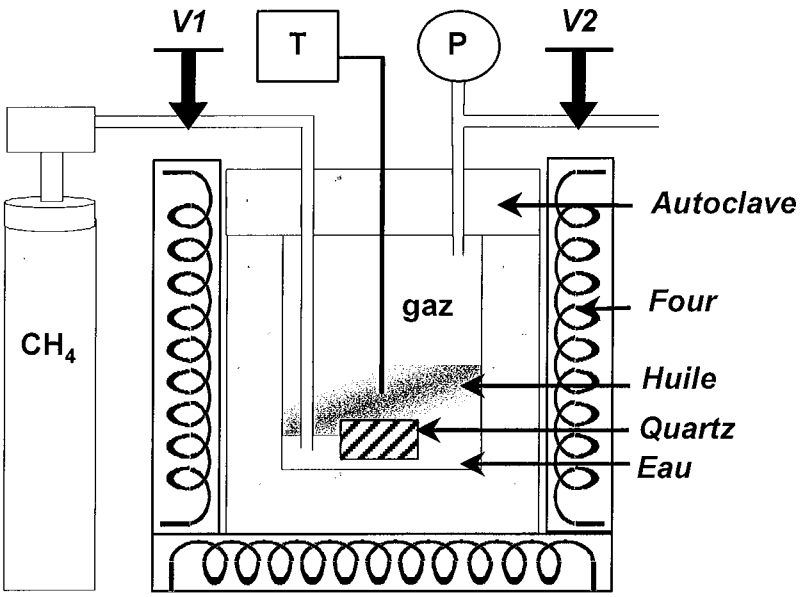

Figure B-1: Autoclave à pression gaz (GPA). V1 : vanne d'entrée, V2 : vanne de sortie, T : Thermocouple relié à un multimètre, P : Manomètre

Les échantillons de quartz sont placés au fond de l'autoclave avec du gel de silice. En présence d'huile, l'ordre de remplissage de l'autoclave peut-être modifié (tableau B-2), les échantillons sont donc préférentiellement mouillés à l'eau ou à l'huile. En fonction du degré de remplissage, du rapport eau/huile (W/O) et de l'épaisseur des quartz, ces derniers peuvent parfois baigner à la fois dans l'eau et dans l'huile. Cette configuration permet d'augmenter la formation d'inclusions aqueuses et hydrocarbonées dans un même échantillon. Dans ce cas, l'eau ou l'huile s'infiltre via le réseau de fracture des quartz. Le méthane est introduit une première fois par la vanne d'entrée (V1) pour évacuer l'air de la phase gazeuse et l'air dissous dans la solution. Après fermeture de la vanne de sortie (V2) et avant la montée en température, la pression de méthane est ajustée ; la pression est alors supérieure à la pression de vapeur saturante dans l'eau pure ou dans une solution saline.

La température et la pression d'expérimentation sont atteintes en quelques heures, puis ajustées si nécessaire. Un manomètre et un thermocouple reliés à l'autoclave permettent à tout instant une vérification des conditions thermobariques. Une fois le temps d'expérimentation écoulé, le circuit de chauffage est coupé et l'autoclave se refroidit jusqu'à température ambiante. L'autoclave est ouvert.

1.2.2 Autoclave à pression fluide (FPA)

Cette technique permet d'appliquer une pression externe à une capsule en or, dans une gamme de pressions (0.3 à 1.2 Kbars) analogue ou supérieure à celle que l'on peut mesurer dans les bassins sédimentaires. Cette pression (dans notre cas, inférieure ou égale à 400 bar) est générée par une pompe à air et transmise dans l'autoclave par un mélange eau-huile (Hydraulub 16mg/l) qui circule dans une ligne hydrostatique connectée à chaque autoclave par une série de vannes. La température (inférieure ou égale à 400°C) est contrôlée par des régulateurs reliés aux thermocouples de chaque four (Figure B-2). Les autoclaves sont placés dans des fours annulaires. Un thermocouple est placé dans l'autoclave à proximité des capsules, un deuxième est situé dans le four. L'autoclave peut contenir jusqu'à 8 capsules. A l'issue de l'expérience, l'autoclave est refroidi dans un système à circulation d'eau.

Selon l'expérience, les quantités connues de quartz, de gel de silice, de solution et/ou d'huile sont placées dans des capsules en or (diamètre de 5 mm, longueur de 6 cm, épaisseur de 0.5 mm) dont une extrémité a été préalablement soudée. L'or est choisi pour son inertie chimique et ses propriétés de malléabilité et de conductivité thermique assurant une bonne transmission de la pression et de la température. Les capsules des expériences réalisées en milieu aqueux sont scellées à l'air ambiant. Celles réalisées en présence d'huile ont été scellées sous atmosphère inerte, sous argon pour empêcher tout risque d'oxydation de l'huile. Les capsules d'or sont ensuite soudées sous un flux d'azote liquide de façon à contrebalancer l'échauffement thermique et ainsi éviter l'évaporation de la solution. Avant de placer les capsules dans l'autoclave pour toute la durée de l'expérience, celles-ci sont pesées avant et après une chauffe à 150°C pendant 2 heures. Celles qui présentent une différence de masse supérieure à 0.2% sont immédiatement retirées pour (1) éviter de modifier la concentration des espèces en solution et (2) garder le maximum de solution pour la croissance et la synthèse d'inclusions. Les capsules en or sont ensuite placées dans l'autoclave. Les températures et pressions maximales d'expérimentation sont atteintes en quelques heures. Une fois le temps d'expérimentation écoulé, l'autoclave est ramené à température et pression ambiante. Les capsules récupérées sont lavées avec du chloroforme afin d'éliminer d'éventuels dépôts d'huile. Les capsules sont pesées puis ouvertes.

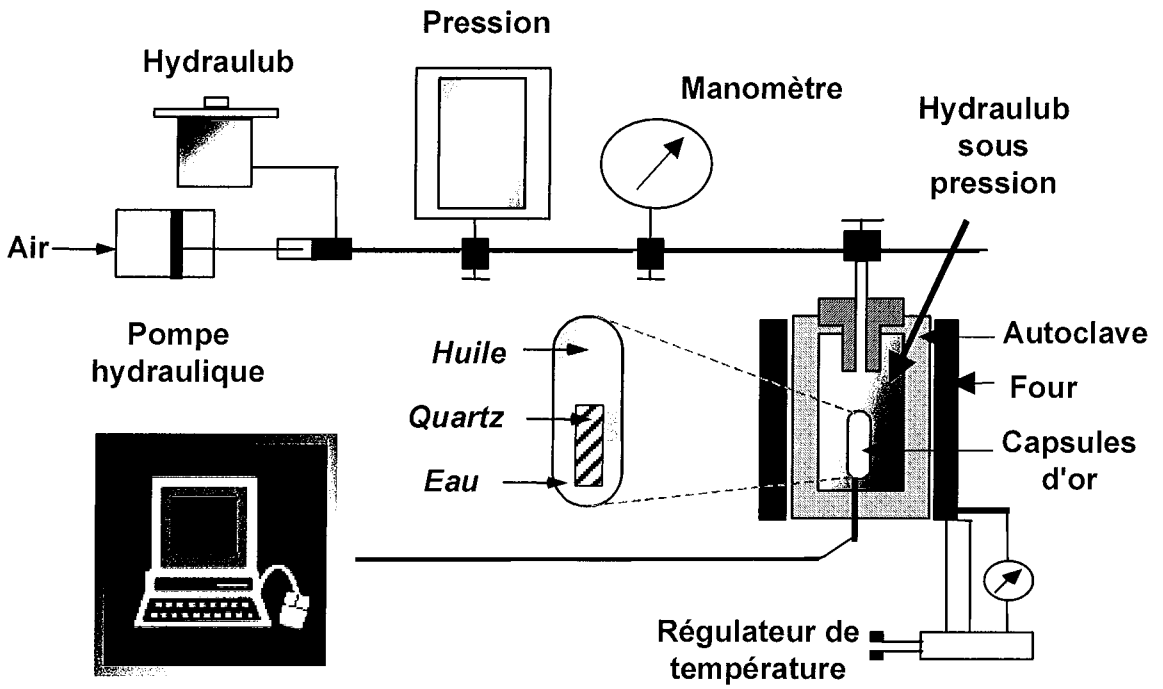

Figure B-2 : Dispositif expérimental des expériences en capsules en or utilisant un autoclave à pression fluide (FPA)

1.3 Conditions expérimentales

Les conditions générales expérimentales des différentes expériences menées dans les deux types d'autoclaves sont présentées tableau B-2. Ces expériences ont été réalisées dans des milieux aqueux et/ou hydrocarbonés, en présence ou non de méthane et d'ions dissous dans la phase aqueuse tels que NH_4^+, Cl^- ou Na^+. Différents rapports eau/huile ont été utilisés et différents ordres de remplissage de l'autoclave ont été testés. Dans toutes ces expériences, du gel de silice a été ajouté pour faciliter la saturation en silice de la solution.

Les premières expériences G1 à G4 et F1 à F4 ont servi de banc d'essai aux expériences suivantes que ce soit pour la formation de quartz secondaire et/ou la synthèse d'inclusions. La cinétique de réaction a notamment été accentuée en faisant varier soit la température, soit la pression, soit les deux. Les variations thermobarométriques ont toujours été effectuées après que la solution ait atteint son niveau de saturation en silice maximum. La température et/ou la pression maximale d'expérimentation est maintenue constante pendant une durée définie. Puis, la température (et/ou la pression) est abaissée jusqu'à une autre température. L'effet souhaité est de sursaturer la solution en silice, d'augmenter la précipitation de quartz et ainsi favoriser la formation d'inclusions fluides et de surcroissance.

Les risques d'oxydation de l'huile durant l'expérience sont réduits au maximum. Dans les expériences réalisées en autoclave à pression gaz, l'essentiel de l'oxygène de l'air est soustrait du

système avant la chauffe par le transit d'une faible pression de méthane dans l'autoclave pendant 30 minutes. Dans les expériences réalisées dans les autoclaves à pression fluide, le chargement et la fermeture des capsules sont effectuées sous atmosphère inerte, sous argon. Selon les expériences, une solution à NH_4Cl a été utilisée. Celle-ci maintient un potentiel redox constant par le tampon NH_4/N_2 similaire au tampon hématite/magnétite. De plus, une faible quantité de fer métal (Fe^0) a constamment été adjointe à la solution pour maintenir un Eh faible (autour de 250°C).

	Exp.	Système[1]	Autoc./capsule ordre de remplissage[2]	variation p-T?		conditions p-T		Durée	rapport eau/huile	Croissance quartz		Inclusions fluides			CH_4
				T	P	max	min	(jour)	%	CF[3]	AC[4]	Aqueuses	Hydroc.	3-phase	incl. Aq.[5]
Autoclave à pression gaz (gas pressure autoclave)	G1	CH_4+H_2O+NaCl	S-W	non	non	250°C-200bar		30	-	non	non		-	-	-
	G2	CH_4+H_2O+LiCl	S-W	oui	oui	200°C-200bar	150°C-170bar	30	-	oui	sa.	oui	-	-	saturation
	G3	CH_4+H_2O+NaCl +(Na_2CO_3-NaOH)	S-W	oui	oui	200°C-200bar	102°C-130bar	30	-	oui	sa.	non	-	-	-
	G4	CH_4+H_2O+NaCl	S-W	non	non	100°C-200bar		10	-	non	non	non	-	-	-
	G5	CH_4+H_2O+NaCl	S-W	non	non	150°C-200bar		10	-	oui	non	oui	-	-	saturation
	G6	CH_4+H_2O+NaCl	S-W	non	non	200°C-200bar		10	-	oui	pyr.	oui	-	-	saturation
	G7	CH_4+H_2O	S-W	oui	oui	210°C-201bar	174°C-162bar	20	-	oui	pyr.	oui	-	-	saturation
	G8	HC+CH_4+H_2O+NH_4Cl	S-W-HC	oui	oui	250°C-212bar	150°C-141bar	30	10	oui	pyr.	oui	oui	-	sous-saturé
	G9	HC+CH_4+H_2O+NH_4Cl	S-HC-W	oui	oui	250°C-209bar	150°C-136bar	30	20	oui	pyr.	oui	oui	-	non détecté
	G10	HC+CH_4	HC	oui	oui	250°C-200bar	150°C-200bar	25	0	non	non	non	non	-	-
	G11	HC+CH_4+H_2O+NaCl	S-W-HC	non	non	270°C-200bar		30	5	oui	pyr.	oui	oui	-	non détecté
Autoclave à pression fluide (fluid pressure autoclave)	F1	H_2O+NaCl	S-W	non	non	400°C-700bar		30	-	oui	pyr.	oui	-	-	-
	F2	H_2O+LiCl	S-W	non	non	400°C-700bar		25	-	oui	pyr.	oui	-	-	-
	F3	H_2O+LiCl	S-W	non	non	400°C-1200 Kbar		25	-	oui	oui	oui	-	-	-
	F4	H_2O+(Na_2CO_3-NaOH)	S-W	oui	non	400°C-400bar	400°C-300bar	25	-	oui	oui	oui	-	-	-
	F5	H_2O+NaCl	S-W	non	oui	400°C-400bar	400°C-Psat	20	-	oui	oui	oui	-	-	-
	F6	H_2O+NaCl	S-W	oui	non	400°C-400bar	300°C-400bar	20	-	oui	oui	oui	-	-	-
	F7	HC+H_2O+NaCl	S-HC	non	non	350°C-400bar		25	0	oui	non	non	oui	-	-
			S-W-HC	non	non	350°C-400bar		25	5	oui	pyr.	oui	oui	-	non détecté
			S-W-HC	non	non	350°C-400bar		25	10	oui	oui	oui	oui	oui	non détecté
			S-W-HC	non	non	350°C-400bar		25	20	oui	oui	oui	oui	oui	non détecté
			S-W-HC	non	non	350°C-400bar		25	50	oui	oui	oui	oui	oui	non détecté
	F8	H_2O+NaCl	S-W	non	non	350°C-400bar		20	-	oui	oui	oui	-	-	-

[1]HC: huile morte; [2]S: échantillon, W: solution aqueuse, HC: huile morte; [3]CF: cimentation des fractures; [4]AC: auréole de croissance, pyr.: pyramide de quartz (faible croissance), sa.:plaquette de silice amorphe; [5]detection Raman

Tableau B-2: Conditions générales expérimentales des expériences réalisées en autoclave à pression gaz (GPA) et dans des capsules d'or en autoclave à pression gaz (FPA).

2 ETUDE DES INCLUSIONS FLUIDES

2.1 Microscopie optique et fluorescence

Les échantillons ont été observés en lumière transmise naturelle, polarisée et réfléchie. Les inclusions hydrocarbonées ont été identifiées grâce à leur fluorescence sous éclairage ultraviolet (UV).

2.2 Microthermométrie

L'étude microthermométrique consiste à observer les changements de phase que peut subir une inclusion fluide lors d'un chauffage ou d'un refroidissement. Cette technique permet d'obtenir des renseignements sur la nature et la composition du ou des fluides piégés dans l'inclusion. Grâce à l'acquisition des températures d'homogénéisation (T_h) et de fusion de la glace (T_f), la microthermométrie est la technique de base permettant de remonter aux conditions PVTX de piégeage des inclusions aqueuses et/ou hydrocarbonées.

Les mesures par microthermométrie ont été réalisées au laboratoire UMR G2R-CREGU. Au cours de mes travaux, diverses platines ont été utilisées: une platine ®Chaix-Meca (Poty et al., 1976) pour les T_f, une platine ®USGS (Goldstein and Reynolds, 1994) pour les T_h et une platine ®Linkam MDS 600 équipée d'un écran vidéo pour les T_h et T_f. Les platines ®Chaix-Meca et ®USGS disposent d'une chambre de mesure assez grande pour y insérer des échantillons épais, notamment les quartz de synthèse.

Ces platines microthermométriques ont été calibrées avec des inclusions standards à CO_2 pur (T_f = -56.6°C) et des inclusions synthétiques très peu salées (T_f = -0.4°C) pour les basses températures, et divers cristaux organiques et/ou d'inclusions de synthèse (H_2O-CO_2) à haute température. Les transitions de phases des inclusions ont été observées avec des objectifs x40, x50 et x80.

2.3 Microspectroscopie Raman

La spectrométrie Raman permet dans la plupart des cas, d'identifier et d'analyser quantitativement les gaz (CH_4, CO_2, N_2...) contenus dans la phase volatile ou dissous dans la phase aqueuse des inclusions fluides. Son principe repose sur le phénomène de vibration des espèces moléculaires, lorsqu'elles sont excitées par une source lumineuse monochromatique. Ce phénomène est alors observé pour toute espèce polyatomique. Les gaz sont reconnus et

quantifiés grâce aux longueurs d'onde et intensités des vibrations des liaisons moléculaires obtenues sur les spectres. L'analyse Raman est non destructive et ponctuelle.

Les analyses Raman ont été effectuées à l'UMR G2R-CREGU sur un spectromètre ®Labram Dilor couplé à un laser à argon ionisé à 514,5 nm dont la puissance généralement utilisée en sortie de tube est de 300 mW. Les temps d'acquisition peuvent varier de 1 à 100 secondes selon l'inclusion. Pour analyser le méthane dissous des inclusions aqueuses, un spectre est enregistré entre 2800 et 3500 cm^{-1} (Dubessy et al, 2000). Cette fenêtre spectrale permet l'acquisition simultanée du spectre de l'eau et du méthane à la T_h en couplant au spectromètre Raman une platine microthermométrique ®Linkam MDS 600. L'intensité intégrée de chaque pic est calculée. Ce rapport d'intensité est ensuite corrélé à une concentration de méthane grâce à des courbes de calibrage. Ces courbes ont été obtenues grâce à des inclusions de synthèse contenant du méthane et différentes concentrations en sels, de 0 à 3.5 molal NaCl (Guillaume et al, 2002). Cet article est présenté dans ce chapitre B-§5.

Il convient de rappeler que la fluorescence est l'ennemi du Raman. Selon les échantillons, cette fluorescence peut-être intense et a plusieurs origines possibles: 1) des inclusions hydrocarbonées proches des inclusions aqueuses analysées, 2) des imprégnations d'hydrocarbures naturels en bordure de grain, 3) des contaminations par des produits organiques lors de la confection des lames.

2.4 Microspectroscopie infrarouge

Les analyses par microspectromètrie infrarouge à transformé de Fourier (IR-TF) sont ponctuelles (10 µm) et non-destructives. Elles permettent de caractériser le contenu des inclusions hydrocarbonées : teneurs en gaz (CH_4, CO_2), et en alcanes (longueur moyenne de chaîne aliphatique). Les spectres obtenus couvrent le moyen infrarouge. Des analyses IR ont également été réalisées sur l'huile morte utilisée dans les expériences avant et après expérience.

L'utilisation d'inclusions synthétiques et naturelles de référence a permis un calibrage de CH_4, CO_2 et des alcanes des inclusions. Les données compositionnelles sont obtenues après traitement de spectre (ligne de base, soustraction) et prise en compte des coefficients d'absorption relatifs des espèces dosées (Pironon et al, 2001). Cet article est présenté dans ce chapitre B-§6.

Les spectres ont été acquis au Laboratoire d'environnement et de minéralogie (LEM) de l'ENSG de Nancy sur un microscope ®Bruker, couplé à un spectromètre Equinox 55. La résolution spectrale est de 4 cm^{-1}, le temps d'accumulation est voisin de 4 minutes et l'ouverture est choisie afin d'analyser la totalité de l'inclusion. Les analyses ont été effectuées à température ambiante en mode transmission.

Les inclusions inférieures à 10 µm n'ont pu être analysées. La présence de contaminations organiques naturelles ou dues à la préparation des lames a souvent perturbé l'analyse des inclusions.

2.5 Microscopie confocale à balayage laser

La microscopie confocale à balayage laser (CSLM) permet l'acquisition d'images 2D et 3D sur des objets millimétriques à micrométriques. Elle permet, par sa résolution (qui peut atteindre 0,1 µm en résolution latérale et 0,3 µm en résolution axiale), d'être complémentaire à l'échelle micrométrique des microscopies électroniques à balayage et d'améliorer considérablement les performances de la microscopie de fluorescence. L'objectif de l'utilisation de la microscopie confocale appliquée aux inclusions fluides est à terme de reconstituer le volume en huile et en gaz de ces inclusions (Aplin et al, 1999; Pironon et al, 1998).

Les systèmes confocaux sont composés d'une ou plusieurs sources laser, d'un système de balayage, d'un microscope optique, d'un ou plusieurs détecteurs (photomultiplicateur) et d'une unité informatique dédiée à l'acquisition et au traitement d'images. En dehors du mode en transmission, deux autres modes d'observations ont été utilisés. Le premier est le mode en fluorescence qui utilise un laser incident à λ=488nm et collecte l'intensité du signal à une longueur d'onde $\lambda>\lambda_0$. Ce mode est utilisé pour détecter l'huile des inclusions. Le second mode d'observation est le mode réflexion qui utilise un laser incident à 637nm et collecte l'intensité du signal à la même longueur d'onde. Ce mode est très sensible aux changements d'index de réfraction et principalement utilisé pour détecter l'eau des inclusions.

Au cours de ces travaux, plusieurs microscopes ont été utilisés, notamment lors de test chez divers constructeurs: ®Biorad (Radiance 2000), ®Olympus (FV 300) et ®Zeiss (LSM 510). Mais l'essentiel des acquisitions a été effectué sur un microscope ®Zeiss LSM 510 à l'Institut de Biologie Moléculaire des Plantes (IBMP) à Strasbourg.

Des inclusions HC fluorescentes des expériences ou de lames épaisses de Mer du Nord ont été observées; le but étant de reconstituer leur volume respectif. Les plans confocaux ont été dans la plupart des cas choisis tous les 0,5 et 1µm, en fonction de la taille de l'inclusion. Le calcul du volume a été effectué sous Igor (Pironon et Canals, 1997) après seuillage de l'image en 256 niveaux de gris. La morphologie de certaines inclusions HC et de leur bulle de gaz à 23°C rend parfois le calcul du volume plus difficile. Dans la plupart des cas, la bulle de gaz s'apparente à une sphère. Dans d'autres cas, celle-ci a été assimilée à un cylindre.

2.6 Modélisation PIT

Le programme PIT (Petroleum Inclusion Thermodynamics) (Thiéry et al, 2000) a pour but de modéliser les propriétés thermodynamiques et la composition des pétroles fossiles piégés dans les minéraux des roches des réservoirs naturels. Ces données permettent de reconstituer les conditions de migration des hydrocarbures (profondeur, temps, température, calage temporel) et de comparer les compositions des huiles fossiles et des huiles actuelles. Deux approches permettent de reconstituer ces conditions de piégeage :

- soit par traçage direct des isoplèthes caractéristiques de l'huile dans un diagramme P-T. Dans ce cas, la composition de l'huile doit être connue.
- soit par la modélisation des huiles, basée sur deux paramètres α et β (figure B-3) représentant respectivement la composition de la fraction d'alcanes lourds (≥ C_{10}) et d'alcanes légers (C_1 à C_{10}). Dans ce cas, les données de départ sont: (1) la T_h des inclusions fluides hydrocarbonées, acquise par microthermométrie, (2) le volume de la bulle de gaz (ici à 23°C), calculé à partir des données de microscopie confocale.

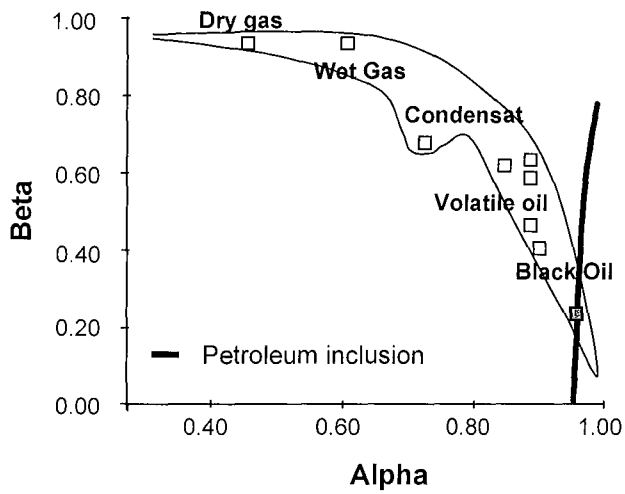

Figure B-3: Diagramme compositionnel alpha-beta caractérisant une huile naturelle piégée.

L'objectif de la modélisation PIT sur les inclusions hydrocarbonées de synthèse est triple. Il s'agit de (1) retrouver des conditions P-T de piégeage de l'huile cohérents avec la composition obtenue en laboratoire, (2) générer un modèle de composition compatible avec la composition de l'huile piégée dans l'inclusion et ainsi (3) valider le modèle.

3 ETUDE DES HUILES MORTES

3.1 Extraction et séparation

Les asphaltènes de l'huile brute ont été précipités dans un large excès d'hexane pendant 15 minutes à 60°C sur une plaque magnétique chauffante, sous une colonne réfrigérante. Les asphaltènes sont séparés des maltènes par filtration. Chacune des fractions est quantifiée par pesée. Les maltènes obtenus sont fractionnés sur une colonne d'alumine activée au moyen du dichloromethane. Cette étape permet de séparer les résines (récupérées avec un mélange méthanol/dichlorométhane 50/50) qui restent piégées sur la colonne des hydrocarbures saturés et aromatiques. Les hydrocarbures sont ensuite fractionnés sur une colonne de silice activée. Les hydrocarbures saturés sont élués avec du pentane et les aromatiques avec un mélange pentane dichlorométhane (65/35). Les résines et les fractions aromatiques et saturées ainsi récupérées sont quantifiées.

3.2 Chromatographie en phase gazeuse (GC-MS)

Les hydrocarbures saturés ont été analysés avec un chromatographe en phase gazeuse (HP 6890) couplé à un spectromètre de masse (HP 5971A). L'injecteur utilisé est un split/splitless en mode splitless dont le programme de température suit celui du four du chromatographe. La séparation chromatographique est réalisée avec une colonne capillaire en silice fondue DB-5 J&W Scientific (longueur=60m, diamètre=0.25mm, épaisseur du film=0.1µm) à phase non polaire (5% phénylméthylpolysiloxane) selon le programme de température : 40-130°C à 15°C/min, 130°C-300°C à 3°C/min, palier de 15 min à 300°C. Le débit d'hélium étant constant à 1 ml/min. Les molécules sont fragmentées dans le spectre de masse sous l'action d'un faisceau d'électrons de 70eV. La température de la source est de 180°C et la ligne de transfert est chauffée à 280°C.

Pour chacune des fractions, deux injections chromatographiques ont été réalisées. La première consistait à utiliser le spectromètre de masse en mode fullscan afin d'analyser tous les ions produits par l'ionisation des composés et dont les masses varient de m/z=50 jusqu'à m/z=550. Pour la seconde injection, le spectromètre de masse a été utilisé en mode MID (Multiple Ion Detection). Ce mode permet de sélectionner des masses m/z et donc d'augmenter la sensibilité de détection de composés peu abondants tels que les biomarqueurs.

4 ETUDE DES AUREOLES DE CROISSANCE

4.1 Cathodoluminescence

La cathodoluminescence (CL) permet de différencier le grain détritique des auréoles de croissance, d'observer les zonations à l'intérieur même d'une auréole ainsi que le ou les réseaux de fractures à l'intérieur d'un grain ou d'une auréole (Holness et Watt, 2001).

La CL correspond à l'émission de photons d'un échantillon soumis à un bombardement électronique. La CL intrinsèque est caractéristique du réseau cristallin et correspond à la recombinaison directe d'électrons et de trous entre bandes de valence et bande de conduction. Elle peut être rehaussée par plusieurs phénomènes tels que la non-stoechiométrie, les imperfections structurales ou des impuretés. La CL extrinsèque est liée à la présence d'ions activateurs. Dans ce cas, l'excitation et l'émission apparaissent comme le résultat de transition entre les niveaux de l'ion activateur sans participation des bandes de valence et de conduction. Les longueurs d'onde et les intensités d'émission caractérisent le minéral et/ou les impuretés qu'il contient.

L'observation en CL a été effectuée au Laboratoire commun d'analyses de Nancy sur un ®Oxford mono-CL couplé à un microscope à balayage laser (MEB). Les échantillons ont été métallisés au carbone et observés en utilisant un voltage de 20-25kV et un courant de 6nA.

4.2 Sonde ionique

La sonde ionique permet de mesurer à l'échelle microscopique, les concentrations et les compositions isotopiques de tous les éléments connus, même à des teneurs très faibles. Le bombardement ionique d'une zone d'un matériau provoque l'émission d'une partie des éléments qui la constituent sous forme d'ions secondaires. Ces ions secondaires sont ensuite accélérés et séparés par un champ électrostatique en fonction de leur énergie initiale, puis par un champ magnétique en fonction de leur masse. Enfin, le mode de détection en multicollection permet d'analyser simultanément les différents isotopes de certains éléments, notamment ceux de l'oxygène.

L'analyse des isotopes de l'oxygène a été réalisée au laboratoire du CRPG à Nancy sur la sonde ionique ®IMS 1270 suivant l'approche de (Hervig et al, 1995; Girard et al, 2001). Les mesures ont été effectuées sur des grains détritiques et des auréoles de croissance des quartz des expériences ainsi que sur des quartz naturels de lames épaisses de Mer du Nord et d'Argentine. Le diamètre des cratères d'impact produits lors du bombardement du faisceau d'ions primaires Cs+ sont de l'ordre de 10-20µm et sont sub-circulaires. Le fractionnement de masse de l'instrument est corrigé par l'analyse répétée de standards (BOG1, NL615, QZ-CWRU, QZ-BRA).

Sur l'ensemble des mesures, l'erreur totale sur la composition isotopique exprimée en $\delta^{18}O_{SMOW}$ varie de ±0.1 à ±0.6‰.

4.3 Imagerie infrarouge

L'imagerie IR est une technique encore peu utilisée dans l'étude des échantillons géologiques. L'approche conventionnelle utilisée en microspectroscopie IR-TF pour analyser un échantillon en 2D consiste à acquérir ponctuellement des spectres en des points précis de l'échantillon. Cependant, le mapping d'échantillons de grande taille et à haute résolution est relativement long et fastidieux. Pour palier à ce problème, une nouvelle instrumentation destinée à l'imagerie d'échantillons a été développée. Elle comporte un système de détection basée sur un alignement de plan focal. Cette technique d'imagerie IR est présentée plus en détails dans l'article situé à la fin de ce chapitre B-§7.

Des quartz des expériences, ainsi que des échantillons de réservoir pétroliers ont été analysés sur un appareil ®Bruker ®IRscope II équipé d'un détecteur HYPERION™. Une zone de 250 x 250 µm peut être ainsi analysée simultanément à une résolution spatiale de 4µm. L'intensité du signal à une fréquence IR est caractéristique de certaines liaisons ou molécules (O-H, H2O, C-O, C=O...).

5 Article 1: CALIBRATION OF METHANE ANALYSIS BY RAMAN SPECTROSCOPY IN H_2O-NaCl-CH_4 FLUID INCLUSIONS.

Des courbes de calibrage permettant de calculer la teneur en méthane des inclusions dans le système H_2O-CH_4-NaCl ont été obtenues. Les rapports CH_4/H_2O des données de spectroscopie Raman ont été effectués sur des inclusions de synthèse contenant différentes concentrations en sels (de 0 à 3.5 molal NaCl). Les spectres Raman de l'eau et du méthane présents dans la phase aqueuse des inclusions ont été collectés à différentes températures, ainsi qu'à des températures légèrement supérieures à la T_h des inclusions. La composition de la phase aqueuse ($T<T_h$) a été calculée avec un logiciel utilisant le modèle de Duan et al. (1992). Les résultats montrent la relation entre les concentrations en CH_4 et la salinité: à concentration constante, le rapport des aires CH_4/H_2O des bandes Raman baisse avec l'augmentation de la salinité de 0 à 1.6 molal et reste constante au-delà de 3.5 molal. La projection P-T de l'isoplèthe d'une inclusion fluide naturelle est ainsi déduite de sa T_h, de sa teneur en sels (mNaCl eq.) et de l'analyse Raman (mCH_4). Cette méthode a été appliquée sur un échantillon naturel de dépôt MVT située dans le sud de l'Illinois (fluorite-Pb-Zn district, Cave-in-Rock, USA), présentant des inclusions fluides hydrocarbonées associées à des inclusions aqueuses du système H_2O-CH_4-NaCl. L'isochore du système hydrocarboné recoupent l'isochore du système H_2O-NaCl-CH_4 à la Th, ce qui valide la procédure.

CALIBRATION OF METHANE ANALYSIS BY RAMAN SPECTROSCOPY IN H_2O-NaCl-CH_4 FLUID INCLUSIONS.

Damien GUILLAUME, Stéphane TEINTURIER, Jean DUBESSY and Jacques PIRONON

UMR G2R (7566) and CREGU, Université Henri Poincaré, BP 239, 54506 Vandœuvre-lès-Nancy, France

Soumis à Chemical Geology (accepté)

ABSTRACT

Calibration of the determination of CH_4/H_2O ratio using Raman spectroscopy is carried out using synthetic fluid inclusions at different NaCl concentration (0, 0.05, 0.66, 0.98, 1.00, 1.60, 2.25 and 3.5 molal NaCl). Spectra of the stretching bands of methane and water in the aqueous phase were collected at variable temperatures up to a few degrees above the homogenisation temperature. The composition of the aqueous phase for temperatures below the homogenisation temperature was calculated with a computer program, using the model of Duan et al. (1992). Results show the dependency of the estimate of the CH_4 concentration on salinity: at constant CH_4 concentration, the CH_4/H_2O area ratio of Raman bands decreases with increasing salinity from 0 to 1.6 molal and remains constant up to 3.5 molal NaCl. The P-T projection of the isopleth of a natural fluid inclusion is deduced from the homogenisation temperature, its composition obtained from cryometry (mNaCl eq.) and Raman analysis (mCH_4) ratio. This methodology was applied to a sample from the Cave-in-Rock MVT deposit (fluorite-Pb-Zn district, southern Illinois, USA) presenting petroleum fluid inclusions associated with fluid inclusions of the system H_2O-NaCl-CH_4. Hydrocarbon isochore intersects the isopleth of the H_2O-NaCl-CH_4 inclusions at the homogenization temperature, which validates this procedure.

Keywords: fluid inclusions, H_2O-CH_4-NaCl system, methane analysis, Raman spectroscopy, petroleum fluid inclusions, diagenetic fluids.

5.1 Introduction

P-T-t path reconstruction of a sedimentary basin is a key parameter for the evaluation of oil potential of sedimentary basins. Fluid inclusions which trap diagenetic fluids are a powerful tool for the reconstruction of P-T conditions provided the composition is correctly determined. Natural crude oils are made of a mixture of hydrocarbons. The solubility of individual hydrocarbon components in water decreases rapidly with increasing molecular weight. Methane is the main hydrocarbon whose solubility in water is significant in the P-T conditions of sedimentary basins (Price 1981).

The methane concentration in formation waters in sedimentary basins is often low, below 0.3 molal, and its quantification using microthermometric measurements is not possible (Dubessy et al., 2001). However, neglecting small concentrations of methane may result in incorrect interpretation of fluid inclusion observations because the pressure at the homogenisation temperature along the L-V isopleth curve is underestimated (Figure B-4). Bulk concentration of methane in aqueous fluid inclusions can be obtained a few degrees above the homogenisation in the H_2O-CH_4 system (Dubessy et al., 2001). However, NaCl is always present in diagenetic fluids. In a P-T diagram, the salting out effect shifts the L-V isopleth to higher pressure (Figure B-4). Cl^- ion is an hydrogen bond breaker that strongly modifies the profile of the Raman band of the stretching vibration of water (Dubessy et al., 2002), and prevents a priori any extrapolation of the calibration of the H_2O/CH_4 ratio obtained from H_2O-CH_4 fluids. Therefore, the analysis of methane dissolved in H_2O-NaCl fluid requires specific calibration as a function of the NaCl concentration. Such calibration is carried out using synthetic fluid inclusions prepared in fluorite and quartz crystals.

Petroleum fluids, which always contain significant amounts of methane, often more than 30 mole %, coexist with aqueous fluids during their migration in sedimentary basins. Methane being the most soluble hydrocarbon in aqueous phase, this gas component is expected to be present in the aqueous solutions at equilibrium with hydrocarbons. Therefore, P-T conditions of trapping can be deduced from fluid inclusions representative of hydrocarbons and methane bearing aqueous solutions. This approach is applied to a sample from the Cave-in-Rock MVT deposit (fluorite-Pb-Zn district, southern Illinois, USA) with the PIT modelling of the P-T projection of the bubble curve and isochore of the petroleum inclusions (Thiéry et al., 2000).

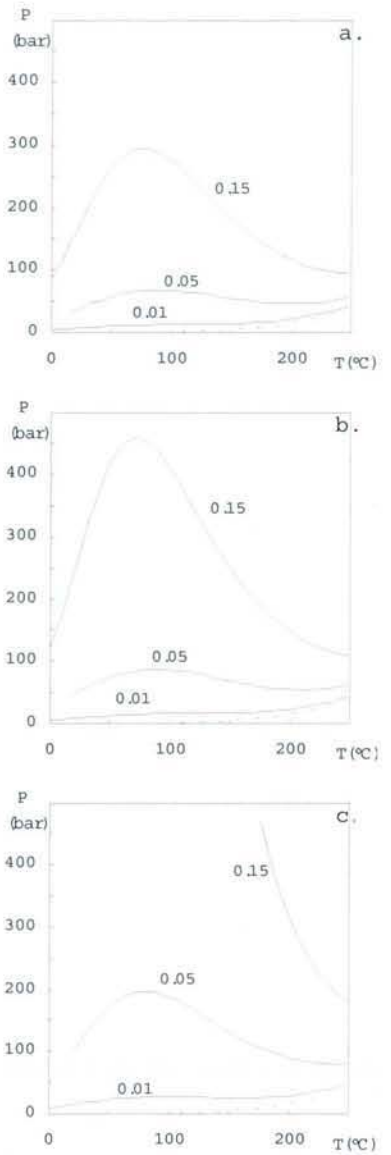

Figure B-4: Projection of the isopleth in the P-T plane of the H_2O-CH_4-NaCl system calculated using the model of Duan et al. (1992). a: 0 molal NaCl; b: 1 molal NaCl; c: 4 molal NaCl. Labels refer to CH_4 concentration (molality scale), dashed lines: 0 molal CH_4.

5.2 Experimental procedure

5.2.1 Starting materials

Synthetic fluid inclusions were produced in natural Brazilian quartz and synthetic fluorite (® SOREM). Water was taken from the laboratory distilled water supply (Millipore MILLI-Q ® Reagent water system). CH_4 was supplied by Air Liquide ® (99,9% minimum purity) and NaCl by Aldrich ® (98% minimum purity).

5.2.2 Formation of fluid inclusions

In quartz crystals, fluid inclusions were formed using pre-existing inclusion cavities (20-40µm) which were previously decrepitated. In fluorite crystals, cavities were made using the laser ablation method (Dubessy et al., 2000). All experiments were conducted in a gas-pressure autoclave. The major advantage of this autoclave is to maintain the equilibrium between liquid and vapour phase at run conditions. Crystal samples with pre-formed cavities were put inside the aqueous liquid phase of known salinity inside the autoclave. Oxygen and nitrogen gases of the air above the aqueous solution were flushed out by methane bubbling at room temperature before heating. Temperature and pressure were controlled during the experiments (Table B-3). For runs 6 and 7, a gentle cooling was applied to enhance quartz cementation (5°C per day during 10 days). In fluorite crystals, two types of fluid inclusions were produced: inclusions with cavities around 15 µm diameter (Figure B-5a) and smaller inclusions in the sealed cracks around the cavities. Figure B-5b shows the typical morphology of inclusions obtained in quartz crystals. The methane concentration in the aqueous phase is calculated using the thermodynamic model of Duan et al. (1992).

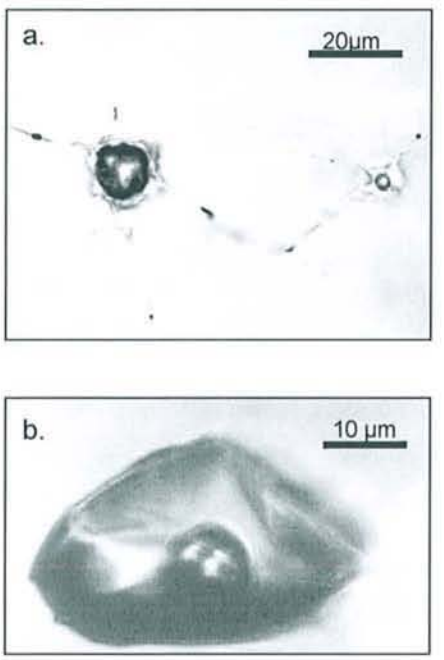

Figure B-5: 2a. Photomicrograph of inclusions obtained in sealed-cavities formed by laser ablation in fluorite crystal. 2b. Photomicrograph of a fluid inclusion obtained using pre-existing decrepitated-inclusion in natural quartz crystal.

Exp.	T_{exp} (°C)	*P (bar)*	mCH_4	Tm_{ice} (°C)	$Th_{L+V\rightarrow L}$ (°C)	*mNaCl*
1	200 ± 1	100 ± 5	0.102 ± 0.010	-3.9 ± 0.1	200 ± 1	1.00 ± 0.03
2	201 ± 1	200 ± 5	0.195 ± 0.019	-6.2 ± 0.1	201 ± 1	1.60 ± 0.03
3	200 ± 2	100 ± 5	0.083 ± 0.008	-7.9 ± 0.1	201 ± 1	2.25 ± 0.03
4	200 ± 2	120 ± 5	0.074 ± 0.007	-14.2 ± 0.1	201 ± 1	3.50 ± 0.03
5	150 ± 2	200 ± 5	0.130 ± 0.013	-3.3 ± 0.1	150 ± 1	0.98 ± 0.03
6	250 – 200	205 ± 5	0.298 ± 0.030	-2.2 ± 0.05	234 ± 1	0.66 ± 0.02
7	200 – 150	195 ± 5	0.210 ± 0.021	-0.2 ± 0.05	186 ± 1	0.05 ± 0.02
8	198 ± 2	205 ± 5	0.240 ± 0.024	0.0 ± 0.05	197 ± 1	0.00 ± 0.02

Table B-3. Experimental conditions of synthesis of fluid inclusions in the H2O-CH4-NaCl system and microthermometric data. Exp.: experiments. 1 to 4: Fluorite experiments, 5 to 8: Quartz experiments. P(bar): total pressure measured at experimental temperature T (°C); mCH4: CH4 molality calculated at Th (°C), for measured total pressure and NaCl concentration calculated using the model of Duan et al. (1992). Tmice (°C): ice melting temperature. ThL+V→L (°C): homogenisation temperature to the liquid phase.

5.2.3 Analytical techniques

Microthermometric measurements were obtained using a Chaix Meca heating and freezing stage (Poty et al., 1976). The Raman microprobe is a Labram type (®Dilor) with a ®Notch filter and with a CCD detector cooled at -30°C. The exciting radiation at 514.532 nm is provided by an Ar^+ laser (type 2020, ®Spectraphysics). A grating of 1800 grooves per mm is chosen to combine good spectral resolution (around 2 cm^{-1}) and convenient spectral window. The Raman spectra are collected between 2800 and 3900 cm^{-1} to get simultaneously the symmetric stretching vibration of methane at 2910 cm^{-1} and the broad band corresponding to the stretching vibrations of water. Raman data were obtained below and a few degrees above homogenisation temperature using a Chaix Meca or Linkam stage fixed on the microscope of the Raman microprobe.

5.3 Results

5.3.1 Calibration

Temperatures of ice melting and bulk homogenisation to the liquid phase were measured (Table B-3). NaCl concentration is determined from the ice melting temperature of the inclusion and is in good agreement with the salt concentration of the initial aqueous solution introduced into the autoclave. Samples obtained at constant temperature display fluid inclusion homogenisation temperatures equal to the measured experimental temperatures within the experimental errors (±1 or 2°C, runs 1 to 5 and 8, Table B-3). This feature is in agreement with the trapping of a liquid phase coexisting with a vapour phase (Ramboz et al., 1982). Thus, the aqueous inclusions can be considered to be representative of the liquid aqueous phase at equilibrium with the methane-bearing vapour phase. This finding is also confirmed by other experiments. First, healing of fractures around the laser ablation cavities occurs after one week (Dubessy et al., 2000). Secondly, experiments of solubility of ethylbenzene in aqueous solutions (Sawamura et al., 1989; Guillaume et al., 2001) have shown that the time to reach equilibrium was less than one day. Finally, if equilibrium was not achieved, the homogenisation temperature should be smaller than the experimental temperature. Therefore, the validation of the equilibrium between the aqueous and vapour phases justifies the calculation of the bulk methane concentration with the model of Duan et al. (1992). For samples prepared during cooling experiments, equilibrium between vapour and liquid aqueous phases is assumed to have occurred at a temperature equal to the homogenisation temperature. At temperatures lower than the homogenisation temperature, the inclusion is in the two-phase field and the methane concentration in the liquid aqueous phase is calculated with the algorithm of Dubessy et al. (2001).

Raman spectra obtained for different temperatures and for a given salt concentration are plotted in figure B-6. They show the increase of the band intensity assigned to the symmetric stretching vibration of methane (λ_1) around 2910 cm^{-1} indicating the progressive dissolution of methane in the aqueous solution. On the other hand, it has been observed that its wavenumber does not change with temperature and salt concentration, indicating that the perturbation endeavoured by the molecules of methane remains constant over this range of density, composition and temperature.

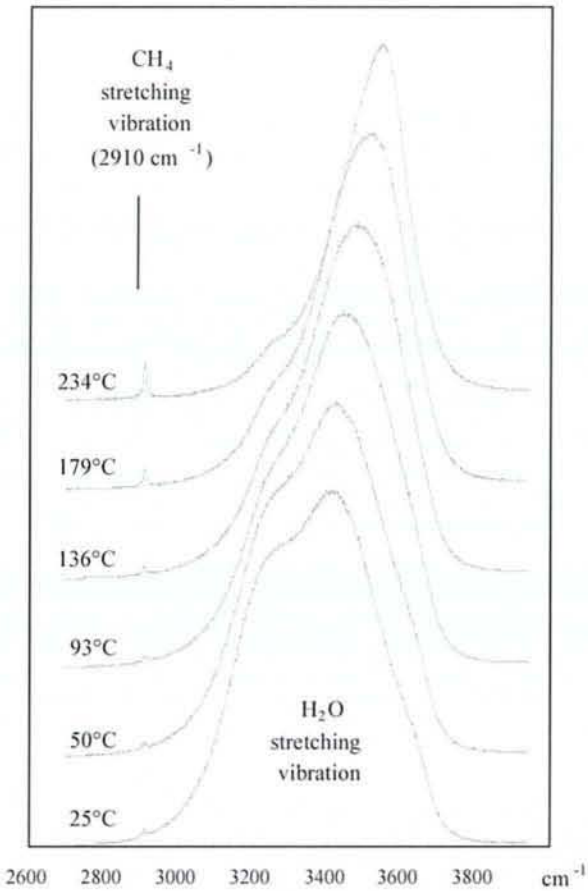

Figure B-6 : Raman spectra obtained at several temperatures for a fluid inclusion in quartz having the following composition: NaCl: 0.66 molal; CH_4: 0.298 molal.

Plot of mCH_4 versus the Raman band area ratio $[I(CH_4)/I(H_2O)]$ (Fig. B-7) shows the following features: first, for a given salt concentration, data plot along a straight line although the temperatures are different along each line. The effect of temperature over the range of measurements (100°C to 250°C) is weak and does not modify the CH_4 molar estimate. Second, the different iso-salinity lines have a slope that depends on the salt concentration. A plot of this slope as a function of salinity is given on figure B-8. For increasing salinity, the slope increases exponentially. The methane concentration (mCH_4) can be calculated with equation [1].

$$mCH_4 = [I(CH_4)/I(H_2O)] \times [72 - 35 \times \exp(-1.1 \times mNaCl)] \qquad R^2 = 0.99 \qquad [1]$$

where mNaCl is the salinity (molality scale) calculated from ice melting temperature of the inclusion and $[I(CH_4)/I(H_2O)]$ is the Raman band area ratio.

The accuracy varies with the signal/background ratio. This ratio is dependent to the inclusion geometry and location to the surface of the sample. However, for the synthetic inclusions used for the calibration (up to 40 µm in size and 10 to 60 µm in depth) the accuracy determined from the R^2 value is around 10 %. Equation [1] integrates the apparatus function.

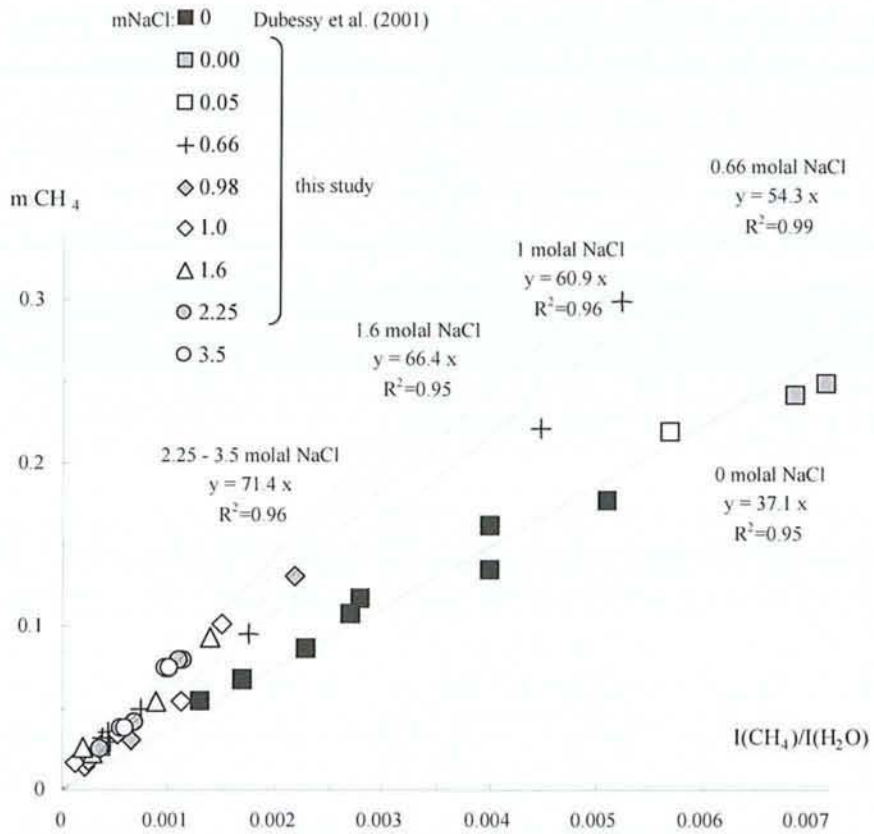

Figure B-7: Plot of the methane concentration (molality scale) versus the Raman band area ratio $I(CH_4)/I(H_2O)$. Labels indicate the salt concentration (molality scale), the regression line equation calculated from experimental data and the R^2 values of the fitted lines.

It is reasonable to expect that the Raman scattering cross-section of the symmetric stretching band of methane remains quasi constant at fixed temperature and for different salinities and thus can be considered as an internal standard. These new data suggest that the Raman scattering cross-sections of OH oscillators increases with increasing NaCl concentration. The slope (Fig. B-8) increases with increasing NaCl concentration, but this effect is weak above 1 molal NaCl and the absence of salinity effects above 1.6 molal indicate that the structure of water is strongly modified between 0 and 1.6 molal NaCl concentration.

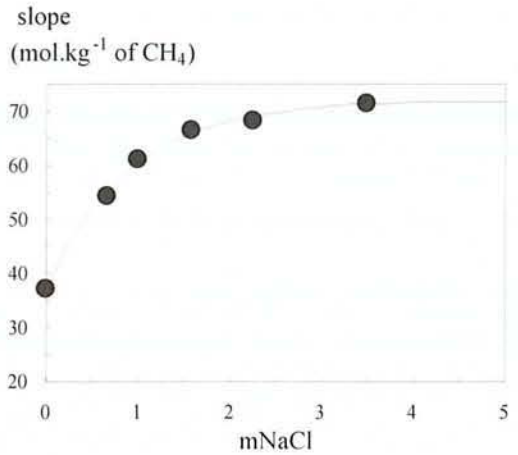

Figure B-8: Plot of the slope obtained by regression along data (Fig. B-7) versus the corresponding NaCl concentration (molality scale).

5.3.2 Effect of host mineral nature and orientation

Calibration curves that have been calculated from run 1 (200°C, 1 molal NaCl, in isotropic fluorite crystal) and run 5 (150°C, 0.98 molal NaCl, in birefringent quartz crystal) are consistent. This observation first confirms that there is no significant effect of host mineral nature. It also illustrates that temperature has no significant effect on mCH_4 estimate between 150 and 200°C.

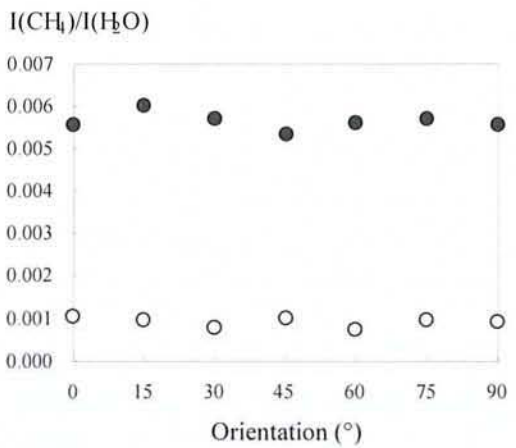

Figure B-9 : $I(CH_4)/I(H_2O)$ ratio of a single fluid inclusion (run 5) for various orientation of birefringent host mineral (quartz). 0° = extinction. Spectra were collected in the liquid phase at 25°C (open circles) and above homogenisation temperature (170°C, filled circles). Maximum deviation is below 5%.

Spectra have been collected in the liquid phase of a single fluid inclusion (run 5) at 25°C and 270°C (above the homogenisation temperature) for various orientations of the crystal. Results are presented on figure B-9. It appears that the orientation of birefringent mineral (quartz) has no significant effect on the calculated $I(CH_4)/I(H_2O)$ ratio and, as a consequence, no influence on the calculation of the methane concentration. Maximum deviation is below 5%.

5.3.3 Application to a case study

We studied inclusions trapped in fluorite from the Cave-in-Rock MVT deposit, fluorite-Pb-Zn district, southern Illinois, USA (Richardson & Pinckney, 1984; Roedder, 1984; Pironon et al., 1998). In a sample of fluorite, we studied a particular plane of fluid inclusions containing petroleum inclusions (5) together with aqueous fluid inclusions (>20) (Fig. B-10), this indicating that these palaeofluids were contemporaneous. Therefore, the petroleum fluid inclusions and aqueous fluid inclusions are interpreted as the two immiscible fluids at equilibrium. The bulk homogenisation of fluid inclusions representative of the two end-members should be the same and representative of the temperature of trapping. The aqueous fluid inclusions of this particular plane homogenise at 145 ± 2°C, whereas the petroleum inclusions homogenise at 112 ± 1°C. Vapour filling of hydrocarbon inclusion, measured with confocal scanning laser microscope (Pironon et al., 1998) is 9 ± 0.5% at room temperature. The phase transition measured for petroleum inclusions is the homogenisation temperature of the petroleum phase and its significance deserves to be discussed. The solubility of water in petroleum is around 1 weight % at 150°C (Tsonopoulos & Wilson, 1983; Heidman et al., 1985; Sawamura et al., 1989; Guillaume et al., 2001). Such water concentration corresponds approximately to a coating of water with a thickness smaller than 0.1 µm, a value much smaller than the resolving power of the optical microscope. Consequently, the true homogenisation temperature of hydrocarbon fluid inclusions is expected to be higher than the temperature of partial homogenisation of the hydrocarbon part that can never be interpreted as the trapping temperature (Pironon et al., 2000). Therefore a good approximation of the P-T conditions of trapping is the intersection of the petroleum inclusion isochore with the isopleth of the methane-bearing aqueous inclusion.

Figure B-10: Photomicrograph of petroleum and aqueous contemporaneous fluid inclusions in fluorite crystal from the Cave-in-Rock MVT deposit, fluorite-Pb-Zn district, southern Illinois, USA.

Eutectic temperatures of aqueous inclusions near -27°C confirm that sodium is the dominant cation. The salinity, determined by ice melting temperature, is 4 molal equivalent NaCl. The P-T projection of the possible bubble curves of the hydrocarbon part of the inclusion was calculated with the PIT software program (Thiéry et al. 2000) for an hydrocarbon homogenisation temperature of 112 ± 1°C and a vapour volume fraction of 0.09 ± 0.005 (Fig. B-11). The homogenisation pressure is 98 bar and the isochores correspond to the possible P-T couples of data for trapping conditions. For coexisting petroleum and aqueous inclusions the trapping conditions should be located at T = 145 ± 2°C (aqueous inclusions Th) and then at a pressure of P = 230 ± 15 bar. For such P-T conditions and NaCl concentration of 4 molal in aqueous inclusions, the methane concentration at saturation calculated from the model of Duan (1992) is 0.069 ± 0.007 m. This value is in good accordance with the concentration of methane in the aqueous fluid inclusion determined by Raman analysis which is mCH_4 = 0.071 ± 0.007 molal. The Raman analysis of CH_4 in water-salt inclusions is consistent with the coexistence of aqueous and hydrocarbon fluids during the trapping of inclusions in the Cave-in-Rock sample.

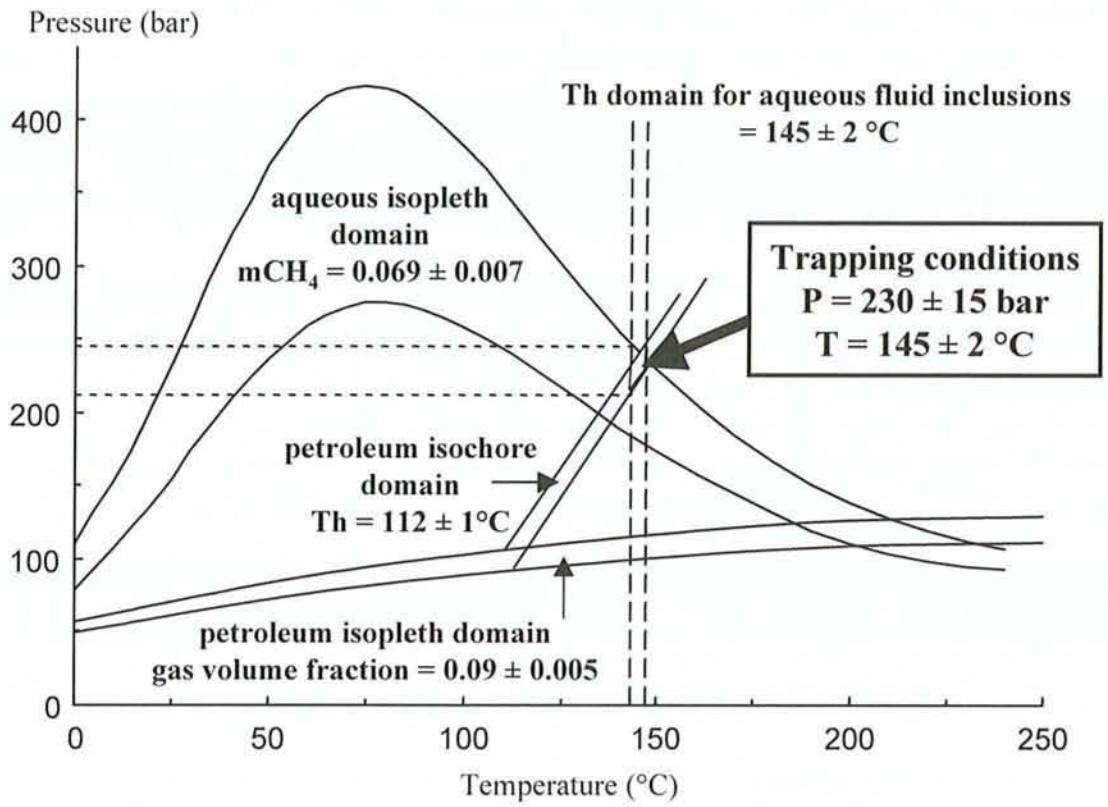

Figure B-11: P-T diagram showing isopleths and isochores plotted from data obtained on petroleum and aqueous inclusions from the Cave-in-Rock fluorite deposit (Illinois).

5.4 Conclusion

The analysis of methane in NaCl - bearing aqueous rich fluid inclusions by Raman spectroscopy was calibrated using synthetic fluid inclusions in fluorite and quartz crystals between 100 and 200 °C and for NaCl concentration from 0 to 3.5 molal. The inclusions were obtained between 150 and 250°C in the liquid aqueous solution coexisting with a methane bearing vapour phase in a gas-pressure autoclave. The concentration of methane in the aqueous solution was calculated using a computer programme (developed in Dubessy et al., 2001) incorporating the model of Duan et al. (1992). The Raman data obtained below and just above the homogenisation temperature were regressed as a function of temperature and NaCl concentration. This calibration allows the determination of the homogenisation pressure of methane-bearing aqueous fluid inclusions provided their salinity and homogenisation temperatures are known. If aqueous fluid inclusions are coexisting with petroleum fluid inclusions, the P-T conditions of hydrocarbon migration can be accurately determined.

Further work is necessary to evaluate the effect of temperature on the intensity of the water band for different salinities. The effect of different salts (NaCl, $CaCl_2$, ...), having different interactions with water molecules should be explored for the analysis of methane concentration in salt-bearing aqueous solutions. Finally, the effect of other gases, potentially present in petroleum environments (CO_2, H_2S, N_2) could be checked and their concentration measurement could be calibrated in the same way.

Acknowledgement

The authors greatly acknowledge A.M. van den Kerkhof and R.C. Burruss for their constructive reviews of this paper, and F. Noronha as associated editor.

References

Duan, Z., Moller, N., Greenberg, J., Weare, J.H., 1992. The prediction of methane solubility in natural waters to high ionic strength from 0 to 250°C and from 0 to 1600 bars. Geochim. Cosmochim. Acta 56, 1451-1460.

Dubessy, J., Guillaume, D., Buschaert, S., Fabre, C., Pironon, J., 2000. Production of synthetic fluid inclusions using laser ablation in fluorite and quartz. An application to the H_2O-CH_4-NaCl system. Eur. J. Mineral. 12, 1083-1091.

Dubessy, J., Buschaert, S., Lamb, W., Pironon, J., Thiéry, R., 2001. Methane-bearing aqueous fluid inclusions: Raman analysis, thermodynamic modelling and application to petroleum basins. Chem. Geol. 173, 193-205.

Dubessy, J., L'Homme, T., Boiron, M.C., Rull, F., 2002. Determination of chlorinity in aqueous fluids using Raman spectroscopy of the stretching band od water at room temperature: application to fluid inclusions. Applied Spectroscopy, in press.

Guillaume, D., Tkachenko, S., Dubessy, J., Pironon, J., 2001. High temperature and high pressure water solubility in ethylbenzene to 200°C and 1kbar and the acetic acid effect. Geochim. Cosmochim. Acta 65, 3319-3324.

Heidman, J.L., Tsonopoulos, C., Brady, C.J., and Wilson, G.M., 1985. High-temperature mutual solubilities of hydrocarbons and water. AIChE Journal 31, 376-384.

Pironon, J., Canals, M., Dubessy, J., Walgenwitz, F., Laplace-Builhe, C., 1998. Volumetric reconstruction of individual oil inclusion by confocal scanning laser microscopy. Eur. J. Mineral. 10, 1143-1150.

Pironon, J., Thiéry, R., Teinturier, S., Walgenwitz, F., 2000. Water in petroleum inclusions. Evidence from Raman and FT-IR measurements, PVT consequences. Journal of Geochemical Exploration 69-70, 663-668.

Poty, B., Leroy J., Jachimowicz, L., 1976. Un nouvel appareil pour la mesure des températures sous le microscope: l'installation de microthermométrie Chaix-Méca. Bull. Soc. fr. Minéral. Cristallogr. 99, 182-186.

Price, L.C., 1981. Aqueous solubility of crude oil to 400°C and 2,000 bar pressure in the presence of gas. J. Pet. Geol. 4, 195-223.

Ramboz, C., Pichavant, M., Weisbrod, A., 1982. Fluid immiscibility in natural processes: use and misuse of fluid inclusion data. II. Interpretation of fluid inclusion data in terms of immiscibility. Chem. Geol. 37, 39-48.

Richardson , C.K., Pinckney, D.M., 1984. The chemical and thermal evolution of the fluids in the Cave-in-Rock fluorspar district, Illinois; mineralogy, paragenesis, and fluid inclusions. Economic Geology and the Bulletin of the Society of Economic Geologists 79, 1833-1856.

Roedder, E., 1984. Fluid inclusions. Reviews in Mineralogy 12. Mineralogical Society of America. 644 p.

Sawamura, S., Kitamura, K., Taniguchi, Y., 1989. Effect of pressure on the solubilities of benzene and alkylbenzenes in water. J. Phys. Chem. 93, 4931-4935.

Thiéry, R., Pironon, J., Walgenwitz, F., Montel, F., 2000. PIT (Petroleum Inclusion Thermodynamic): a new modelling tool for the characterisation of hydrocarbon fluid inclusions from volumetric and microthermometric measurements. Journal of Geochemical Exploration 69-70, 701-704.

Tsonopoulos, C., Wilson, G.M., 1983. High-temperature mutual solubilities of hydrocarbons and water. Part I: benzene, cyclohexane and n-hexane. AIChE Journal 29, 990-999.

6 Article 2: FT-IR MEASUREMENTS OF PETROLEUM FLUID INCLUSIONS: METHANE, N-ALKANES AND CARBON DIOXIDE QUANTITATIVE ANALYSIS

Une des récentes avancée en géochimie pétrolière est de modéliser la composition des huiles fossiles en utilisant les données microthermométriques et volumétriques des inclusions fluides. La spectroscopie infrarouge (IR) peut enregistrer les informations compositionnelles d'une inclusion hydrocarboné: les gaz (CH_4 and CO_2) mais aussi la teneur en alcanes. Dans cette étude, une procédure quantitative couplée à la spectroscopie infrarouge a été développée pour obtenir les concentrations (en mole %) en méthane, alcanes et dioxyde de carbone des inclusions hydrocarboné. Une inclusion hydrocarbonée de la région du Québec (City Promontory nappe) a été utilisé comme standard pour l'enregistrement du spectre de référence du méthane. La procédure analytique est basé sur les mesures des rapports d'aires des rapports CH_4/alkane and CH_4/CO_2. Les rapports d'aires des bandes CH_4/alkane ont été obtenus par soustraction du spectre méthane de référence. Ce rapport d'aire, qui est affecté par des intensités absolues d'absorption du méthane, du méthyle et du méthylène, produit un rapport molaire CH_4/alkane. Les rapports méthyle/méthylène (CH_2/CH_3) est obtenu suivant la procédure établis dans des études antérieures. Le rapport de concentration CO_2/CH_4 est estimé à partir des intensité d'absorption absolues. L'application de cette méthode aux inclusions fluides naturelles de différents environnements montre une bonne corrélation entre la quantification IR et la modélisation PIT (Petroleum Inclusion Thermodynamics).

FT-IR MEASUREMENTS OF PETROLEUM FLUID INCLUSIONS: METHANE, N-ALKANES AND CARBON DIOXIDE QUANTITATIVE ANALYSIS

Jacques PIRONON[1], Régis THIERY[2], Mohamed AYT OUGOUGDAL[3], Stéphane TEINTURIER[1], Georges BEAUDOIN[3] & Frédéric WALGENWITZ[4]

[1]*UMR G2R-CNRS, Univ. H. Poincaré, BP 239, F-54506 Vandœuvre-lès-Nancy, France*
[2]*UMR 6524, Univ. B. Pascal, 5, rue Kessler, F-63038 Clermont-Ferrand, France*
[3]*MEDEF, Dép. de Géologie et de Génie Géologique, Univ. Laval, Québec, G1K 7P4, Canada*
[4]*CSTJF, ElfTotalFina, Avenue Larribau, F-64018 Pau, France*

Geofluids (2001), Vol 1, pp.2-10

ABSTRACT

A recent advancement in petroleum geochemistry is to model fossil oil composition using microthermometric and volumetric data acquired from individual fluid inclusion analysis. Fourier Transform Infrared (FT-IR) microspectroscopy can record compositional information related to gas (CH_4 and CO_2) and alkane contents of petroleum inclusions. In this study, a quantitative procedure for FT-IR microspectrometry has been developed to obtain, from individual fluid inclusions, mole % concentrations of methane, alkanes and carbon dioxide as constraints to thermodynamic modelling. A petroleum inclusion in a sample from the Quebec City Promontory nappe area, was used as standard to record a reference spectrum of methane. The analytical procedure is based on the measurement of CH_4/alkane and CH_4/CO_2 band area ratios. CH_4/alkane infrared band area ratio is obtained after spectral subtraction of the reference methane spectrum. This area ratio, affected by absolute absorption intensities of methane, methyl and methylene, provides a molar CH_4/alkane ratio. Methyl/methylene ratio (CH_2/CH_3) ratio is obtained following procedures established in previous work. CO_2/CH_4 concentration ratio is estimated from relative absolute absorption intensities. Application to natural inclusions from different environments shows good correlation between FT-IR quantification and PIT (Petroleum Inclusion Thermodynamic) modelling.

Key words: petroleum fluid inclusions, infrared intensity, microspectrometry, methane, carbon dioxide, n-alkane, PIT

6.1 Introduction

Petroleum inclusions are common in petroleum reservoirs and may be considered as fossil oils, which have preserved the original oil composition. Petroleum inclusion composition and phase equilibrium are related to the PVTX conditions at the time of trapping. Phase equilibrium data, such as homogenisation temperature, obtained by microthermometry, and volumetric estimate of the gas/oil ratio, obtained by Confocal Scanning Laser Microscopy (CSLM), are the only data currently required to constrain thermodynamic models (VTFlinc, PIT) applied to petroleum inclusions (Aplin et al., 1999, Thiéry et al., 2000). Bulk methods such as GC-MS (Bratus et al., 1975, Horsfield & Mc Limans, 1984, George et al., 1997), HPLC (Pang et al., 1998) or NMR (Dereppe et al., 1994) can provide bulk compositions of petroleum inclusions. However, these techniques may provide incorrect compositions if the sample contains multiple generations of oil inclusions, trapped in a single diagenetic mineral.

Analysis of individual inclusions is possible using molecular spectroscopies: visible Raman microspectroscopy can be applied in the case of non-fluorescent inclusions (Pironon, 1993). Near Infrared FT-Raman can be applied in the case of weakly-fluorescent inclusions but is still affected by fluorescence for most inclusions (Pironon et al., 1991). Fourier Transform Infrared (FT-IR) is the most powerful molecular microspectroscopic technique for analysing oil inclusions (Barrès et al., 1987, Guilhaumou et al., 1990, Wopenka et al., 1990, Pironon et al., 1991). Recent development of laser micropyrolysis coupled with GC-MS also offers the potential for chemical characterisation of individual inclusions (Greenwood et al., 1998). All of these techniques, whilst useful in a qualitative sense, have severe limitations that frequently prevent a quantitative approach. Limitations in FT-IR spectrometry can be minimised using synchrotron excitation (Guilhaumou et al., 1999), but this cannot be considered a routine technique applied to the characterisation of petroleum inclusions. Synchrotron sources are not always available, analyses are time and money consuming.

The objective of this work is to decipher quantitative chemical information from conventional infrared spectra to constrain petroleum modelling. An analytical procedure will be defined and applied to reference inclusions. Results from FT-IR quantification will be compared to the results obtained from compositional modelling of these same inclusions. Quantification has been focussed on methane, alkane and carbon dioxide concentrations by the analysis of the CH and CO stretching vibrations.

6.2 Equipment

The LEM laboratory (ENSG - Vandœuvre-lès-Nancy, France) uses a Bruker IFS 55 Fourier transform spectrometer, coupled with a Bruker microscope, which collects the infrared beam with cassegrain objectives (x15 or x36). Analysis of petroleum inclusions in thin (i.e. less than 300 µm) doubly-polished sections is done by transmission, using a circular or a knife-edge diaphragm with a variable diameter aperture (> 8 µm). Spectral resolution is 4 cm^{-1}, and integration time is longer than 2 min. and increases as the inclusion size decreases. Spectra are plotted in absorbance units in the mid-infrared range. The analytical limit is 2000 cm^{-1} for inclusions in quartz and 800 cm^{-1} for inclusions in fluorite owing to absorption by the host mineral. Spectra of atmospheric CO_2 and H_2O vapours, are subtracted. The atmospheric CO_2 spectrum shows a band doublet at 2360 and 2339 cm^{-1} clearly different from the single band infrared spectra of CO_2 under pressure or dissolved in oil. For each measurement, a reference spectrum is recorded in air or in an inclusion-free area of the host mineral. A Linkam microthermometric stage is coupled to the infrared microscope to record FT-IR spectra between –180°C and +600°C. We use BaF_2 windows, which are transparent in the mid-infrared range. Each spectrum is processed using the OPUS program (®Bruker). Band areas of CH and CO stretching bands are calculated. Bands with intensity higher than 1.3 are not taken into account because of MCT detector saturation.

Microthermometric measurements (homogenisation and melting temperatures) have been acquired with a Chaix-meca stage (Poty et al, 1976) on a conventional optical microscope.

Gas/oil volumetric ratios have been measured with Biorad 1024 and Olympus Fluoview confocal scanning laser microscopes following procedure determined by Pironon et al. (1998). Volume of fluorescent liquid oil is measured at room temperature by CSLM whereas the volume of the gas bubble is approximated to a sphere and calculated from its diameter, which is measured by conventional transmission optical microscopy.

6.3 Samples

Twelve different inclusions, taken from seven samples from different settings, have been selected for application of the FT-IR quantitative analysis.

Two samples of petroleum inclusion-rich fluorite have been analysed:

(1) An inclusion from the Cave-in-Rock fluorite-Pb-Zn district, southern Illinois, USA, described by Roedder (1984) and Pironon et al. (1998). It is a two-phase yellow oil inclusion with a homogenisation temperature to the liquid phase at 112.6 (±0.1) °C. The gas volume percentage at 25°C is 9 (±0.5) %. This primary oil inclusion is associated with aqueous inclusions rich in CO_2 and

CH_4, detected by Raman microspectrometry (Dubessy et al., 2000), homogenising to the liquid phase between 140 and 146°C.

(2) A spherical petroleum inclusion from Boujabeur (Jebel Guebli-South of Tunis), described by Bouhlel et al. (1988) and Guilhaumou et al. (1988). It is a multi-phase inclusion, with a gas volume of 9.5% at 25°C and a homogenisation temperature to the liquid phase of 110.1°C. The inclusions contain several solid phases (i.e. anhydrite and "organic" solids) attached to the inclusion wall in equal proportion for all inclusions. These organic solids could originate from post-trapping precipitation of aromatic fraction of the oil. Consequently, they should not interfere with FT-IR procedure and PIT modelling which only take into account the aliphatic fraction of the oil. Associated aqueous inclusions have Th ranging from 110 to 140°C and salinities between 15 and 17 wt.% NaCl equivalent.

Five samples of petroleum inclusion-rich quartz have been selected:

(3) Eight inclusions from four different boreholes of the North Sea basin have been analysed. Seven have been collected between 3400 to 3700 m in depth in the Brent formation for Alwyn area. They are located in healed microfractures inside the detrital quartz grains. Inclusion 3a has a guitar-like shape, is 45 µm long, and homogenises at 81.6°C to the liquid phase. The gas phase volume is 21.8% at room temperature. Inclusion 3b has an irregular shape with a length of 80 µm. The gas volume is 25% at 25°C and it homogenises at a temperature of 94.7°C. Inclusion 3c has a simple parallelepiped shape, a size of 25 µm along the main axis, a low gas volume of 6.3% at 25°C and a homogenisation temperature of 86.1°C. Inclusion 3d has a triangular shape, a 15 µm length size. It has a weak gas volume fraction at 25°C (3.1%) and a low homogenisation temperature (68.7°C). Inclusion 3e has an ellipsoid shape, a length of 8 µm, a gas volume of 9% at 25°C and a homogenisation temperature of 79.4°C. Inclusion 3f has an irregular shape and a length of 40 µm. The gas volume is 5.8% at room temperature and it homogenises at 74.6°C. Inclusion 3g has an irregular shape, a length of 25 µm, a gas volume of 5.8% at 25°C and a homogenisation temperature of 99.7°C. These petroleum inclusions are associated with aqueous inclusions homogenising between 105 and 115°C.

The inclusion from Haltenbanken area belongs to the sandstones of the Garn formation cored at 3700 m. This inclusion is located inside quartz overgrowth and has an irregular shape with terminal thin channels. The gas volume is 80% at 25°C and it homogenises at 121°C in gaseous phase. L+L+G —> L+G transition at low temperature occurs at – 53°C. This inclusion is not associated with aqueous inclusion but it contains a few amount of water wetting the inclusion wall.

(4) Two negative crystal-shaped inclusions (Q21 and 5) within euhedral quartz in quartz-calcite-bitumen fractures from the Quebec City Promontory nappe (Cambrian to Ordovician). The homogenisation of inclusion Q21 is to the liquid phase near 54°C, and inclusion 5 is by critical behaviour at 33°C. The gas volume of Q21 and 5 at room temperature is near 40%. Similar inclusions have been described by Levine et al. (1991). At low temperature, a L+L+G —> L+G

transition occurs at -68.6°C for inclusion 5 and at –65°C for inclusion Q21. Rare associated aqueous inclusions have salinities close to 10 wt % NaCl equivalent and Th near 85°C.

6.4 Analytical procedure

The FT-IR analytical procedure involves three steps: 1) recording of a methane reference spectrum, 2) methane, alkane and CO_2 spectral area measurement in the unknown inclusion, 3) calibration of the quantitative FT-IR approach.

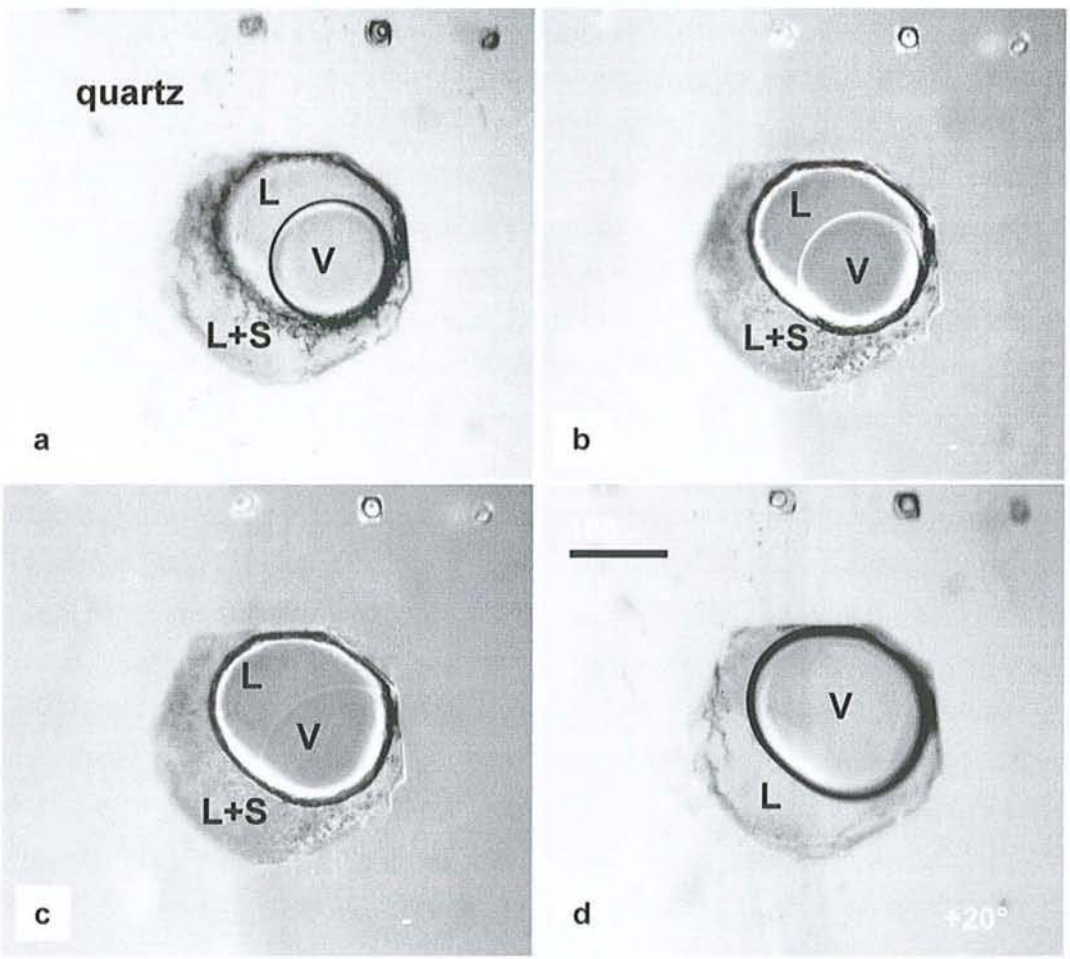

Figure B-12: Photomicrographs of inclusion Q21 from the Quebec Promontory nappe at different temperatures, showing the (L+S)+L+V —> L+V transition. L:liquid, S:solid, V:vapour, L(C):liquid near critical state, V(C):vapour near critical state.

6.4.1 Methane reference spectrum

A 200 µm long inclusion from Quebec City area (Q21) has been chosen for FT-IR analysis focussing the infrared beam into the vapour phase (Figure B-12). The vapour phase is in contact with the inclusion wall, such that the FT-IR analysis does not take into account the liquid phase of the inclusion. FT-IR measurements were done at low temperatures before (Figure. B-12a, b) and after (Figure B-12d) a (L+S)+L+V —> (L+S)+V transition observed at –65°C when liquid (L) and vapour (V) phases homogenise at critical state (Figure B-12c). Such partial miscibility at cryogenic state corresponds to a condensate gas behaviour (methane dominant with alkanes) (Luks et al., 1983). At –167°C, the FT-IR spectrum of the gas phase shows the presence of methane, with its P, Q and R narrow branches, corresponding to gas at low pressure (near atmospheric pressure) (Herzberg, 1968). CO_2 has disappeared from the vapour phase to be concentrated in the liquid phases. With increasing temperature, the bands become broader, indicating an increase of internal pressure (Figure B-13), and CO_2 partially migrates from liquid phases to the vapour phase. The full width at half maximum (FWHM) of the Q branch of methane rapidly increases up to the L+L+V —> L+V transition at –65°C, followed by a slow increase up to 100°C (Figure B-13, B-14a). The peak position decreases from 3018 to 3010 cm^{-1} from –167 to –50°C and seems to remain constant at high temperatures (Figure. B-14b). Small peak position oscillations between 3010 and 3012 cm^{-1} are probably due to the 4 cm^{-1} spectral resolution of the FT-IR microspectroscope. It appears that methane spectrum is affected by pressure only near atmospheric conditions, which are attained in the inclusion at low temperature. At higher pressure, the methane spectrum has constant FWHM and peak position such that the Quebec inclusion spectrum, recorded at room conditions, can be used as a reference. Nevertheless, the FT-IR spectrum is affected by alkane absorbance. With increasing temperature, methane – alkane partitioning between the gas and liquid phases in the L+V domain varies. Alkane concentration increases in the gas phase and its contribution must be subtracted from the methane peak. The methane spectrum is decomposed in 7 main contributions using the Opus software: the three P, Q, R branches of CH_4, and four symmetric and asymmetric CH_2 and CH_3 bands (Figure B-15). The remaining methane reference spectrum is similar to the FT-IR spectrum of pure methane inclusion described by Barrès et al. (1987), and was used for the quantitative studies.

This standard inclusion has been preferred to pure CH_4 natural or synthetic inclusion to give a FT-IR spectrum as similar as possible to the spectrum of methane in petroleum basin conditions. Pure CH_4 inclusions are created in different P, T, X conditions than oil inclusions. It is suspected that such differences are marked on the FT-IR spectrum, by shift of the wavenumber of the maximum of intensity and by modification of the relative intensity of the P, Q, R branches of the stretching band of methane.

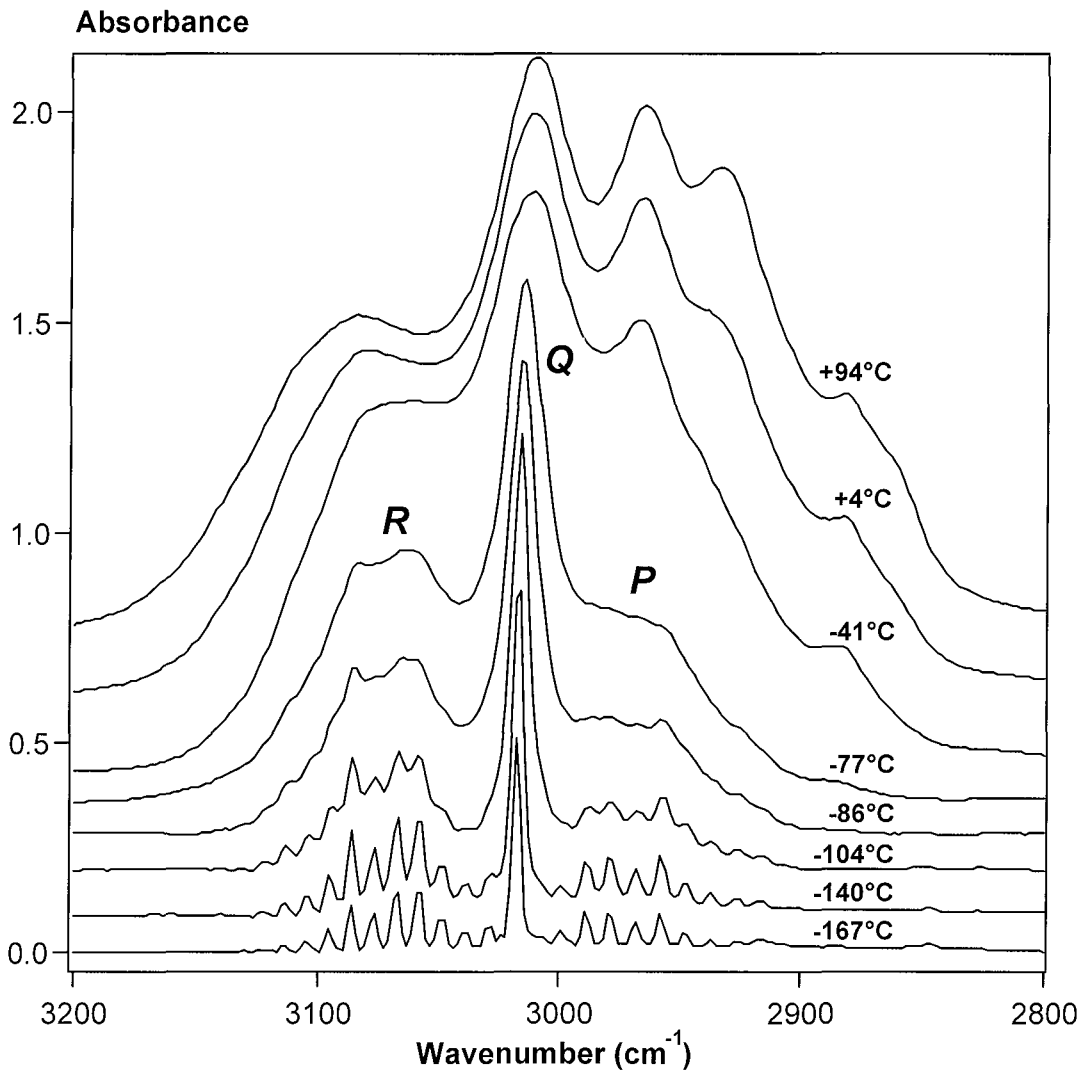

Figure B-13: FT-IR spectra of the gas phase of the Q21 inclusion from Quebec City area, recorded at different temperatures.

6.4.2 Methane, alkane and CO2 spectral area measurement

Spectral procedure for the quantification of methane, alkane and CO_2 in petroleum inclusions consists of:

- recording the whole inclusion FT-IR spectrum at 25°C;
- baseline subtraction, including removal of the water contribution;
- atmospheric CO_2 infrared spectrum subtraction;
- integration of the methane + alkane contribution between 3200 and 2800 cm^{-1} (A_X), and of CO_2 (A_{CO2});
- methane subtraction from the reference Q21 methane spectrum;

- area calculation of the remaining 3200-2800 cm^{-1} range (A_{alk}), and of the CH_2/CH_3 area ratio following Pironon & Barrès (1990);
- calculation of the methane area (A_{CH4}) by ($A_X - A_{alk}$) subtraction.

Steps 4 to 7 are summarised Fig. B-16.

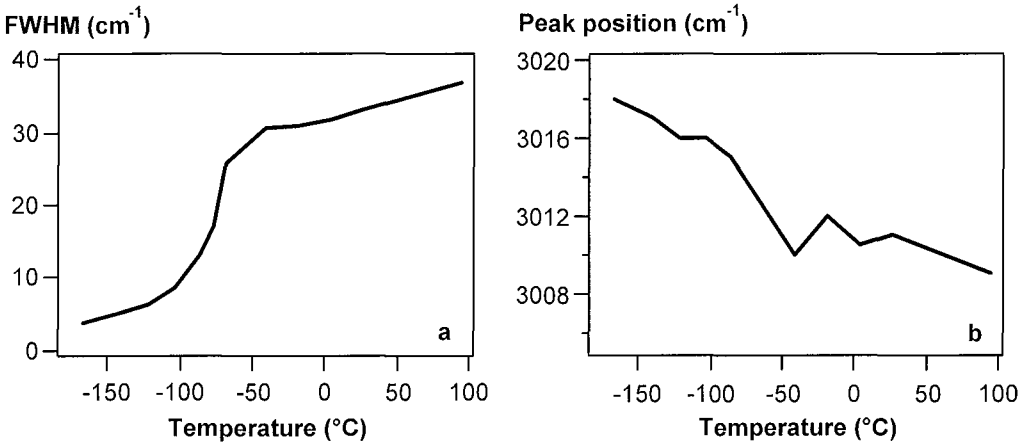

Figure B-14: Evolution of the full width at half maximum (FWHM) and of the position of the Q branch of methane for different temperatures. FT-IR spectra are recorded on the vapour phase of the Q21 inclusion from Quebec Promontory nappe.

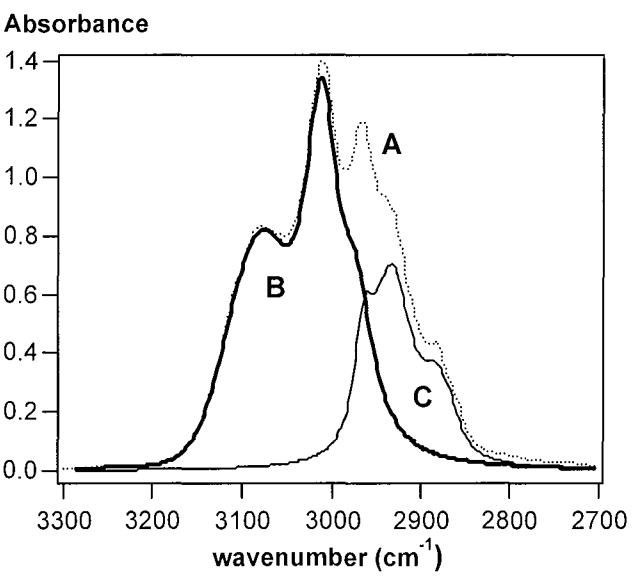

Figure B-15: FT-IR spectrum of methane (B) obtained after decomposition of the FT-IR spectrum of the gas phase (A) of the Q21 inclusion from the Quebec City Promontory nappe. Spectrum C corresponds to the presence of alkane.

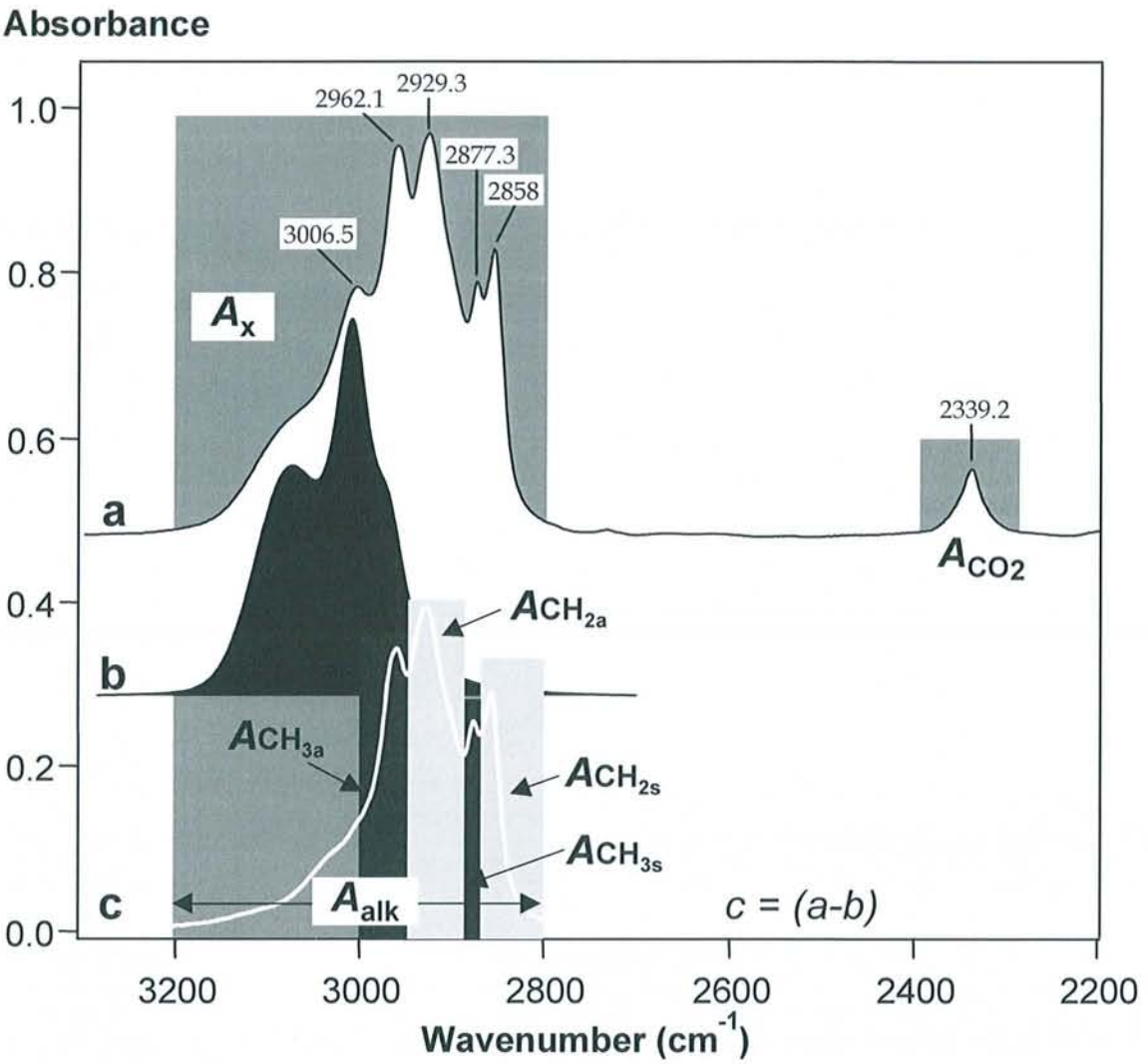

Figure B-16: Spectral procedure for the quantification of methane, alkane and CO_2 in petroleum inclusions. a: FT-IR spectrum of the bulk inclusion, b: reference spectrum of methane, c: (a-b) spectrum subtraction. 7 spectrum areas are calculated : $[A_x]$, $[A_{CO2}]$, $[A_{alk}]$, $[A_{CH3a}]$, $[A_{CH2a}]$, $[A_{CH3s}]$, $[A_{CH2s}]$.

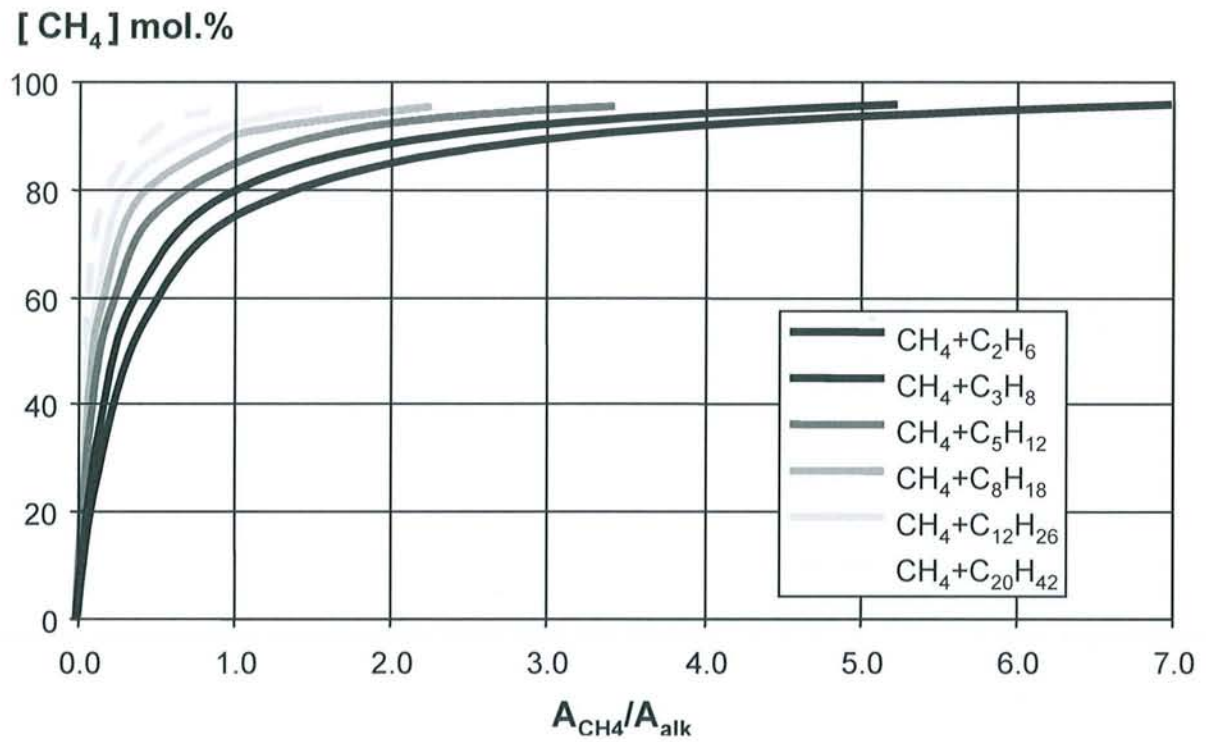

Figure B-17: Relations between measured infrared band area and methane concentration for some binary methane-alkane mixtures.

6.4.3 Calibration of quantitative FT-IR

Different authors have measured infrared intensities of methane, alkanes and carbon dioxide. Bode et al. (1980) and Gussoni (1982) have respectively proposed absolute absorption intensities of 65.5 and 67 km.mol^{-1} for methane. Gribov (1964) and Riley et al. (1982) give an absolute absorption intensity for carbon dioxide of 610 km.mol^{-1}. Kondo & Saëki (1973) give a value of 178 km.mol^{-1} for ethane and 192 km.mol^{-1} for propane. Jones & Sandorfy (1956) and Finkel (1966) show that absolute absorption intensities of alkanes increase with carbon number. From their observations, absorption values of 89 km.mol^{-1} for the methyl group and of 63 km.mol^{-1} for the methylene group can be used.

Beer-Lambert's law can be applied to our quantitative infrared measurement. The methane/alkane area ratio is related to the methane/alkane molar ratio by the following equation:

$$\frac{A_{CH_4}}{A_{alk}} = \frac{\varepsilon_1 . [CH_4] e}{\varepsilon_2 . [alk] e} \qquad (1)$$

where A_{CH4} and A_{alk} are the area of methane and alkane calculated from FT-IR spectrum, ε_1 and ε_2 are the absolute absorption intensities of methane and alkane respectively, $[CH_4]$ and [alk] are the molar concentrations of methane and alkane and e is the thickness of the inclusion.

Absolute absorption intensity of alkanes varies with carbon number and can be expressed by equation (2), where CH_2/CH_3 is the methylene/methyl ratio determined from the FT-IR spectrum.

$$\varepsilon_2 = 178 + 126\frac{CH_2}{CH_3} \qquad (2)$$

Considering a binary system, composed of only methane and alkanes, and an absolute absorption intensity of 67 km.mol^{-1} for methane, equation (1) becomes:

$$\frac{A_{CH_4}}{A_{alk}} = \frac{67.[CH_4]}{(178+126\frac{CH_2}{CH_3}).(100-[CH_4])} \qquad (3)$$

After development, equation (3) leads to the methane mole % of the petroleum inclusion by equation (4):

$$[CH_4] = \frac{100.A_{CH_4}\left(178+126\frac{CH_2}{CH_3}\right)}{67.A_{alk} + A_{CH_4}\left(178+126\frac{CH_2}{CH_3}\right)} \qquad (4)$$

Fig. B-17 shows the influence of the CH_2/CH_3 ratio on the methane mole % calculation for binary systems. FT-IR methane quantification is very sensitive to CH_2/CH_3 ratio for high methane concentration and to small CH_4/alkane area ratio variations at low methane concentration.

Concentration of CO_2, in mole %, will be calculated from the methane concentration, taking into account their relative absolute absorption intensities (equations (5) and (6)).

$$\frac{A_{CO_2}}{A_{CH_4}} = \frac{\varepsilon_3.[CO_2]e}{\varepsilon_1.[CH_4]e} \qquad (5)$$

$$[CO_2] = \frac{67.[CH_4]A_{CO_2}}{610.A_{CH_4}} \qquad (6)$$

Concentrations of methane, alkanes and carbon dioxide are therefore recalculated at 100 and given in mole %.

6.5 Results and discussion

Results of quantitative FT-IR analysis of six natural petroleum inclusions are summarised in Table 1. For each sample maximum and minimum values for CH_2/CH_3, $[CH_4]$, $[CO_2]$ and [Alk] parameters are reported because of the uncertainties on the CH_2/CH_3 measurement. The presence of a brine film around the oil phase inside an inclusion can create spectral deformations (pseudo-saturation effect), modifying infrared intensities of the alkane contribution (Pironon & Barrès, 1990, 1992). During routine FT-IR analysis of liquids in cells, quantification is limited by the difference between the refractive indices of the liquid and the window of the cell. It is recommended to regard with caution the results when refractive indices differ by more than 0.15 (Bertie & Apelblat, 1996). A fluid inclusion can be approximated as a liquid in a cell. Effects of brine and of refractive index are frequently more intense for oil trapped in NaCl or CaF_2 than in quartz, because the refractive indices of quartz and natural oils are more or less similar. The pseudo-saturation effect on FT-IR quantification decreases the alkane contribution in most cases (this effect could be observed on methane contribution only if methane contribution is higher than alkane contribution (i.e. $[CH_4]$>80%)). This effect is observed on the spectra from the two fluorite samples from Illinois and Tunisia, and, therefore, the highest alkane concentration is considered accurate (Table 1). For quartz samples, no or only slight pseudo-saturation effect is detected in the FT-IR spectra, such that the lower alkane value is considered accurate.

Although no standard petroleum inclusions, with a well-known composition, exist that can be used to validate FT-IR quantitative analysis and to provide measurement accuracy. Petroleum Inclusion Thermodynamic (PIT) modelling provides good argument to support the application of FT-IR quantitative analysis to petroleum inclusions. Modelling is based on homogenisation temperatures measured by microthermometry and on gas volume estimate at room temperature measured by CSLM. CO_2 concentration, estimated from FT-IR spectra, is taken into account for composition modelling. Data are given with an accuracy of 5%. A good correlation between PIT and FT-IR procedure is obtained (Figure B-18). The Illinois fluorite inclusion shows a higher concentration using FT-IR (Table B-4, Figure B-18). This result confirms the limit of FT-IR quantification for inclusions having FT-IR spectra affected by intense pseudo-saturation. It is recommended that this procedure not be applied where evidence of FT-IR spectral deformation is observed. The most important difference between FT-IR analysis and PIT modelling is observed for inclusion 3e in quartz. This is explained by the tiny size of the inclusion (8 µm), corresponding to the size limit for FT-IR spectroscopy. Such limitation causes the non-detection of CO_2.

n° inclusion	***(1)***	***(2)***	***(3a)***	***(3b)***	***(3c)***	***(3d)***	***(3e)***	***(3f)***	***(3g)***	***(4)***	***(5)***
CH_2/CH_3#1	**2.4**	**3**	1.7	1.9	2.3	1.8	1.8	2.1	1.7	2	2
CH_2/CH_3#2	4.3	6.1	**2.1**	**2.6**	**3.8**	**2.3**	**2.4**	**3.2**	**2.1**	**2.9**	**3**
[CH_4]#1 (mol.%)	**26.3**	**15.1**	48.6	44.3	13.2	23.8	29	24.7	17.3	62.7	60.9
[CH_4]#2 (mol.%)	33.9	21.6	**51.6**	**49**	**17.5**	**26.4**	**32**	**30.4**	**19.1**	**68.2**	**66.7**
[CO_2]#1 (mol.%)	**5.3**	**11**	1.9	1.3	4.1	0.6	-	0.2	0.7	4.3	1.2
[CO_2]#2 (mol.%)	6.8	15.7	**2**	**1.5**	**5.4**	**0.7**	**-**	**0.3**	**0.8**	**4.7**	**1.3**
[Alk]#1 (mol.%)	**68.4**	**73.9**	49.6	54.4	82.7	75.6	71	75.3	82.7	37.3	37.9
[Alk]#2 (mol.%)	59.3	62.7	**46.5**	**49.5**	**77.1**	**72.9**	**68**	**69.6**	**80.9**	**31.8**	**32**
[CH_4] (mol.%) PIT*	***18 ±5***	***16 ±5***	***48 ±5***	***47 ±5***	***14 ±5***	***24 ±5***	***36 ±5***	***29 ±5***	***20 ±5***	***71 ±5***	***71 ±5***
□ bulk (g/cm^3)*	***0.82***	***0.80***	***0.56***	***0.58***	***0.83***	***0.92***	***0.70***	***0.81***	***0.90***	***0.20***	***0.38***
Th (°C)	112.6	110.1	81.6	94.7	86.1	68.7	79.4	74.6	99.7	121	33
gas vol. %	9.0	9.5	21.8	25	6.3	3.1	9.0	5.8	5.8	80	40

*Table B-4: CH_2/CH_3, [CH_4], [CO_2], [Alk] parameters acquired by FT-IR measurements for eleven inclusions trapped in fluorite (1: Illinois, 2:Tunisia) and Quartz (3: Alwyn, 4: Haltenbanken, 5: Quebec). Parameters with * are calculated from PIT software, using Th, gas vol. %, and CO_2 approximation.*

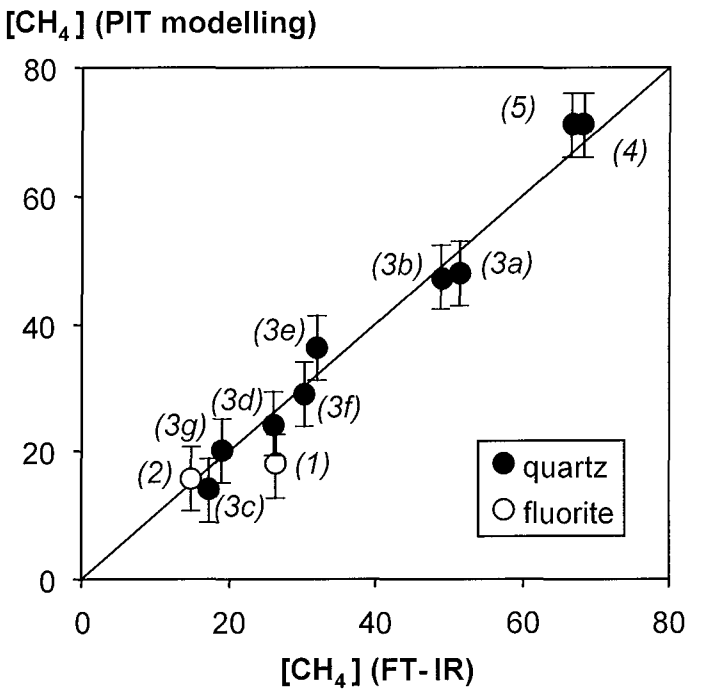

Figure B-18: Methane quantification (in mole %) by FT-IR and PIT modelling for 6 reference petroleum inclusions trapped in quartz and fluorite.

A good correlation between gas volume at room conditions and methane concentration is observed (Figure B-19a). Such correlation is explained by preferential methane partition in the gas phase. Inclusion bulk densities, computed with PIT modelling (Table B-4), display a good negative correlation with methane concentrations (Figure B-19b). Comparisons with proton NMR results can be made on Alwyn samples. Methane concentrations, varying from 24 to 41 mole %, have been deduced from NMR (Dereppe et al., 1994). Such variation is close to the variations observed from FT-IR analysis ranging from 17 to 50 mole %.

Limits of FT-IR quantification can be classified in two groups: 1) FT-IR intrinsic limitations, and 2) limitations due to the inclusion itself.

1) FT-IR intrinsic limitations:

- mid-infrared wavelengths preclude applications to inclusions smaller than 8 µm,
- selection rules of molecular spectroscopy precludes the FT-IR analysis of strictly symmetric molecules such as molecular nitrogen,
- absolute absorption intensity of H_2S is very low, such that this minor gas in petroleum inclusions cannot be detected,
- MCT detectors, used in FT-IR microscopy, have linearity in the C-H stretching range (2800-3200 cm^{-1}) limited to 1 or 1.3 in absorbance units. Large inclusions (more than 50 µm thick) will saturate the detector and the most intense bands of the FT-IR spectrum will be underestimated.

2) limitations due to the inclusions:

- absorption of the host mineral masks some infrared bands of the included oil. For instance, quartz absorption masks the aromatic C=C contributions, C=O and C-O groups, and CH bending vibrations, carbonate infrared absorption bands are superimposed to the all bands of oil,
- when the thickness of the preparation increases, the signal/background ratio of the FT-IR spectrum decreases,
- the shape of the inclusion can create diffraction and refraction of the infrared beam, inducing interference fringes or baseline deformations which can be difficult to delete by spectral processing,
- careful spectral subtraction of reference methane should avoid generation of negative absorbance values,
- differences between refractive indices of host mineral and oil should be less than 0.15,
- inclusions with high salinity aqueous liquid are not amenable to analysis because of interference between water film and oil phase. Salinity of the brine inside petroleum inclusion can be deduced from microthermometry of contemporaneous aqueous inclusions,
- the quantification procedure is not adapted for branched alkanes rich-oils. CH groups interfere with CH_2 and CH_3 groups and perturb the CH_2/CH_3 estimate,
- presence of CH aromatic groups can lead to the overestimate of methane.

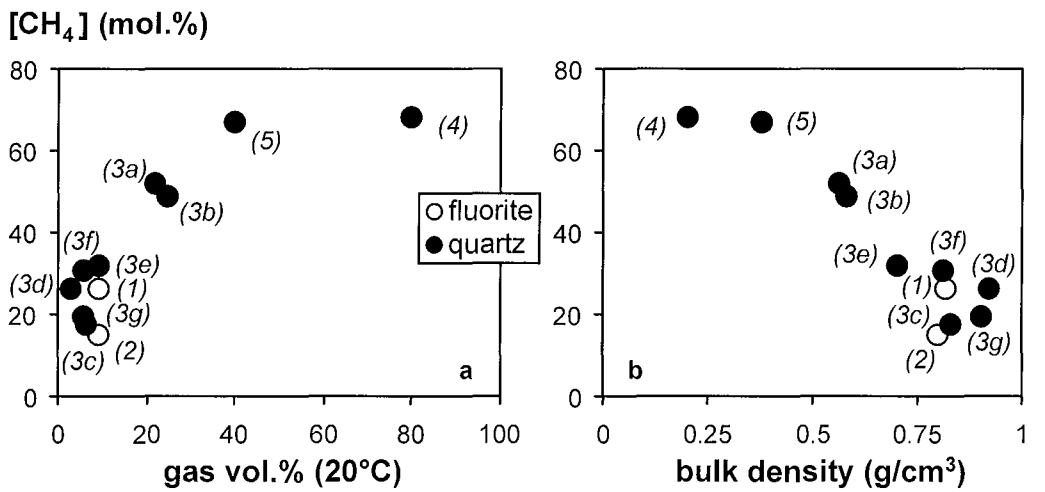

Figure B-19: Comparisons between methane concentration, determined by FT-IR quantification, and gas vol.% of the inclusion measured by CSLM at room temperature, and bulk density of the inclusion, determined by PIT modelling.

FT-IR analysis of petroleum inclusions is the only analytical technique to obtain individual quantitative analysis of oil trapped in inclusion. Raman signal is masked by fluorescence, and bulk analyses (GC-MS, NMR) produce an average composition that cannot reproduce the heterogeneity encountered in one sample. For instance, inclusions 3b and 3c belong to the same

fracture plane inside a detrital quartz grain from Alwyn. FT-IR and CSLM confirm the strong difference in methane concentration correlated with strong variations of volumetric properties. Such differences reveal variations of the petroleum reservoir evolution and give new insights about oil migration and trapping: loss of methane after unmixing, pressure regime variations, input of oils from different origins, oil alteration.

FT-IR quantitative analysis is a useful tool to characterise petroleum inclusions. It is the only technique that can yield a CO_2 molar content. Quantitative FT-IR provides good estimate on methane concentration, which is the main parameter that influences isopleth reconstruction. Isopleths limit the liquid and gas two-phase domain and provide the trapping pressure at the homogenisation temperature in the case of methane-saturated oil. In addition, petroleum inclusion PVTX data enable calculation of the methane concentration of water phase in equilibrium with the oil. Differences or agreement between these concentrations issued from calculation and results from methane analysis by Raman on aqueous inclusions (Dubessy et al., 2000) can help us to determine chronology between hydrocarbon and water inclusions.

6.6 Conclusion

PVTX characterisation of petroleum inclusions is of strategic interest to understand fluid migration. FT-IR quantitative analysis of methane, alkanes and carbon dioxide is feasible for individual inclusions taking into account limitations of this technique. The analytical procedure is based on 1) determination of a standard methane spectrum and 2) quantification of the spectral area of methane, alkanes and CO_2 by the absolute absorption intensities. Applications to natural inclusions from a variety of environments, show good agreement with the results of composition modelling. Coupled with microthermometry (homogenisation temperatures of petroleum inclusions), confocal scanning laser microscopy (gas vol.%), thermodynamic modelling and Raman microscopy (methane concentration in aqueous inclusion), FT-IR quantitative analysis is well adapted to determine methane and carbon dioxide content of petroleum inclusions coexisting with aqueous inclusions.

Results of FT-IR quantification of the oil in inclusions should give new arguments about pressure and temperature of fluid migration and about petroleum evolution between genesis and present time. Such quantification procedure is well adapted to “conventional oils and gases” produced during oil and gas windows, but is not adapted for the analysis of oils enriched in branched alkanes and/or aromatic rings. Fossil oil characterisation should be further enhanced by biomarker analysis, such as aromatic and heteroatom compounds.

ACKNOWLEDGEMENTS

The authors wish to thank C. Laplace-Builhe from Biorad and J. L. Coupier from Olympus for their help for 3D-image acquisition by confocal scanning laser microscopy.

REFERENCES

Aplin, A.C., Macleod, G., Larter, S.R., Pedersen, K.S., Sorensen, H. & Booth, T. (1999) Combined use of confocal laser scanning microscopy and PVT simulation for estimating the composition and physical properties of petroleum in fluid inclusions. *Marine and Petroleum Geology*, 16, 97-110.

Barrès, O., Burneau, A., Dubessy, J. & Pagel, M. (1987) : Application of micro-FT-ir spectroscopy to individual hydrocarbon fluid inclusion analysis. *Appl. Spectrosc.*, 41, 1000-1008.

Bertie, J. E. & Apelblat, Y. (1996) Infrared Intensities of liquids XIX: A simple and effective approximate method for the calculation of infrared optical constant spectra of liquids from transmission measurements. *Applied spectroscopy*, 50, 1039-1046.

Bode, J.H.G., Smit, W.M.A., Visser, T. & Verkruijsse, H.D. (1980) The absolute infrared intensities of propyne-d/sub 0/ and propyne-d/sub 3/. *J. Chem. Phys.*, 72, 6560-70.

Bouhlel, S., Fortuné, J.P., Guilhaumou, N. & Touray, J.C. (1988) Les minéralisations stratiformes à F-Ba de Hammam Zriba, Jebel Guébli (Tunisie nord orientale) : l'apport des études d'inclusions fluides à la modélisation génétique. *Mineral. Deposita,* 23, 166-173.

Bratus, M.D., Svoren, I.M., Danysh, V.V. (1975): Inclusions of hydrocarbons in "Marmorosh diamonds" from Carpathians as indicators of migration of oil fluids. Carbon and its compounds in endogenic processes of mineral formation. (abstract) *COFFI*, 8, 28.

Dereppe, J.M., Pironon, J. & Moreau, C. (1994) Characterization of the composition of fluid inclusion in minerals by ^{1}H NMR. *The American Mineralogist*, 79, 712-718.

Dubessy, J., Buschaert, S., Lamb, W., Pironon, J. & Thiéry, R. (2000) Methane-bearing aqueous fluid inclusions : Raman analysis, thermodynamic modelling and application to petroleum basins. *Chemical Geology* (in press).

Finkel, A.G. (1966) Experimental and theoretical study of absolute intensities in the infrared spectra of gaseous hydrocarbons. *Opt. And Spectrosc.*, 20, 432-435.

George, S.C., Krieger, F.W., Eadington, P.J., Quezada, R.A., Greenwood, P.F., Eisenberg, L.I., Hamilton, P.J. & Wilson, M.A. (1997) Geochemical comparison of oil-bearing fluid inclusions and produced oil from the Toro sandstone, Papua New Guinea. *Org. Geochem.*, 26, 155-173.

Greenwood, P.F., George, S.C. & Hall, K. (1998) Applications of laser micropyrolysis-gas chromatography-mass spectrometry. *Org. Geochem.*, 29, 1075-1089.

Gribov, L.A. (1964) *Intensity theory for infrared spectra of polyatomic molecules*, English translation by P.P. Sutton, Consultants Bureau, New-York, p. 106.

Guilhaumou, N., Dumas, P., Ingrin, J., Carr, G.L. & Williams, G.P. (1999) Synchrotron infrared microspectrometry applied to petrography in micron scale range. *The Internet Journal of Vibrational Spectroscopy*, 3, 14 p.

Guilhaumou, N., Szydlowskii, N. & Pradier, B. (1990) Characterization of hydrocarbon fluid inclusions by infrared and fluorescence microspectrometry. *Mineralog. Mag.*, 54, 311-324.

Guilhaumou, N., Touray, J.C. & Bouhlel, S. (1988) Stretching of hydrocarbon fluid inclusions in fluorite at 200 and 400 bars confining pressure. Application to low-pressure geobarometry. *Bull. Minéral.*, 111, 421-426.

Gussoni, M. (1982) Infrared intensities by parametric methods ; a guided tour. Chap. 5. In: *Vibrational intensities in infrared and Raman spectroscopy*. W.B. Person & G. Zerbi, Eds. Elsevier, Amsterdam. 466 p.

Herzberg, G. (1968) *Molecular spectra and molecular structure. II. Infrared and Raman spectra*. Van Nostrand, London, 632 p.

Horsfield, B. & Mc Limans, R.K. (1984) Geothermometry and geochemistry of aqueous and oil-bearing fluid inclusions from Fateh Field, Dubai. *Org.Geochem.*, 6, 733-740.

Jones, R.N. & Sandorfy, C. (1956) *Chemical Applications of Spectroscopy. IV Infrared and Raman spectrometry : applications*. Interscience. 432 p.

Kondo, S. & Saëki, S. (1973) Infrared absorption intensities of ethane and propane. *Spectrochimica Acta*, 29A, 735-751.

Levine, J.R., Samson, I.M. & Hesse, R. (1991) Occurrence of fracture-hosted impsonite and petroleum fluid inclusions, Quebec City Region, Canada. *AAPG Bulletin*, 75, 139-155.

Luks, K. D., Merrill, R.C. & Kohn, J.P. (1983) Partial miscibility behavior in cryogenic natural gas systems. *Fluid Phase Equilibria*, 14, 193-201.

Pang L.S.K., George S.C. & Quezada R. A. (1998) A study of the gross compositions of oil-bearing fluid inclusions using high performance liquid chromatography. *Org. Geochem.*, 29, 1149-1161.

Pironon, J. (1993) Estimation de la longueur de chaîne des hydrocarbures des inclusions fluides par spectrométrie Raman. *Compte-Rendus de l'Académie des Sciences, Paris*, t.316, Série II, 1075-1082.

Pironon, J., & Barrès, O. (1990) Semi-quantitative FT-IR microanalysis limits: Evidence from synthetic hydrocarbon fluid inclusions in sylvite:.*Geochim. Cosmochim. Acta,* 54, 509-518.

Pironon, J., & Barrès, O. (1992) Influence of brine-hydrocarbon interactions on FT-IR microspectroscopic analyses of intracrystalline liquid inclusions. *Geochim. Cosmochim. Acta*, 56, 169-174.

Pironon, J., Sawatzki, J., & Dubessy, J. (1991) Nir FT-Raman microspectroscopy of fluid inclusions: comparisons with VIS Raman and FT-ir microspectroscopies. *Geochim. Cosmochim. Acta*, 55, 3885-3891.

Pironon, J., Canals, M., Dubessy, J., Walgenwitz, F. & Laplace-Builhe, C. (1998) Volumetric reconstruction of individual oil inclusion by confocal scanning laser microscopy. *European Journal of Mineralogy*, 10, 1143-1150.

Poty, B., Leroy, J. & Jachimowicz, L. (1976) Un nouvel appareil pour la mesure des températures sous le microscope: l'installation de microthermométrie Chaixmeca. *Bulletin de la Société française de Minéralogie et Cristallographie*, 99, 182-186.

Riley, G., Susuki, S. & Orville-Thomas, W.J. (1982) Dipole moment parameters and infrared band intensities. Chap. 8. In: *Vibrational intensities in infrared and Raman spectroscopy.* W.B. Person & G. Zerbi, Eds. Elsevier, Amsterdam. 466 p.

Roedder, E. (1984) Fluid inclusions. *Reviews in Mineralogy*, 12, 644 p.

Thiéry, R., Pironon, J., Walgenwitz, F. & Montel, F. (2000) PIT (Petroleum Inclusion Thermodynamic): a new modelling tool for the characterisation of hydrocarbon fluid inclusions from volumetric and microthermometric measurements. *Journal of Geochemical Exploration*, 69-70, 701-704.

Wopenka, B., Pasteris, J. D. & Freeman, J. J. (1990) Analysis of individual fluid inclusions by Fourier transform infrared and Raman microspectroscopy. *Geochim. Cosmochim. Acta* 54, 519-533.

7 Article 3: FT-IR MICROSPECTROSCOPIC IMAGING : NEW INSIGHTS IN MINERALOGY

Un quartz des grès de la Mer du Nord et une émeraude ont été caractérisés en imagerie IR. Les expériences ont été réalisées sur un spectromètre ®Bruker Equinox 55 connecté à un microscope IR-scope II équipé d'un détecteur Hyperion. Des imprégnations d'huile ont été détectées dans des microfractures préexistantes de l'émeraude. La position et la distribution de l'huile indiquent la direction de propagation de la microfractures de l'émeraude. Pour le quartz, l'imagerie IR permet de visualiser spatialement et quantitativement la présence des groupements OH des minéraux argileux, l'eau constituant les inclusions et le minéral, les groupements C-H des hydrocarbures et la présence de CO_2. L'imagerie IR permet donc de localiser les différents minéraux et constituants organiques sur des sections de roche. Les résultats montrent que la recristallisation de quartz à basse température est marquée par la présence d'eau. L'imagerie du taux d'hydratation des minéraux semble être une bonne voie pour décrire les différentes étapes de croissance d'un cristal. La cartographie (mapping) des composés hydrocarbonés dans les espaces poreux, les inclusions ainsi que dans des microfissures peut nous aider à déterminer les paléo-fissures drainants les huiles lors de leur migration dans les bassins pétroliers. De plus, la distribution et la quantification des produits organiques sont désormais possibles.

FT-IR MICROSPECTROSCOPIC IMAGING: NEW INSIGHTS IN MINERALOGY

J. PIRONON[1], P., S. TEINTURIER[1] de DONATO[2], O. BARRES[2],

[1]*Laboratoire Environnement et Minéralurgie, UMR INPL et CNRS n° 7569, BP 40, 54 501 Vandœuvre-lès-Nancy, France*

[2]*UMR G2R-CNRS, Univ. H. Poincaré, BP 239, F-54506 Vandœuvre-lès-Nancy, France*

soumis à Bruker Report

ABSTRACT

FT-IR imaging have been used to characterise minerals through applications to natural quartz from sedimentary basin and emerald gem. Experiments have been conducted on a FT-IR spectrometer (®Bruker Equinox 55) in connection with an IR-scope I for IR analyses and an IR-scope II microscope (®Bruker) equipped with a Hyperion detector for FT-IR imaging. Experiments were carried out on natural emerald and quartz samples. Palm oil type-resin has been detected in pre-existing crack inside the emerald gem. The location and the distribution of the *resin-oil* interface indicate the direction of the breaking propagation through the gem. For the quartz samples from the North Sea basin, FT-IR imaging allows to visualise the presence of OH-groups from clay minerals, the presence of water as fluid inclusions or as mineral constituent, the C-H groups from hydrocarbons and the presence of CO_2. On the case of the analysis of a thin rock section, FT-IR imaging gives us the opportunity to locate the different mineral or organic constituents. It shows that quartz re-crystallisation at low temperature and pressure is marked by the presence of water. The imaging of the hydration rate of the minerals appears to be a good way to describe the different steps of crystal growth. The mapping of the hydrocarbon compounds, in the pore space, in inclusions or in residual cracks, can help us to determine the ancient drains for oil migration in petroleum basins or the presence of organic filler in gems. Moreover, distribution and quantification of such residual organic products is now available.

7.1 Introduction

Several applications of FT-IR micro-spectroscopy have been described since the beginning of the eighties. Interferometry coupled to Fourier transform and high sensitivity MCT detectors gave the opportunity to acquire spectra on samples with a spatial resolution limited by diffraction in the range of mid-infrared wavelength (10 µm at 1000 cm^{-1}). Rock samples, individual minerals or organic matters have been investigated with the objective of a better understanding of the rock and mineral formation and/or transformation with applications to geology, mining and petroleum industry, material sciences and gemmology (Barrès et al., 1987, Landais and Rochdi, 1990, Wopenka et al., 1990, Guilhaumou et al., 1990, Pironon et al., 1991, Charoy et al., 1996). Qualitative and quantitative (Pironon et al., 2001) molecular information is obtained at the micro-scale by transmission or reflection. High spatial resolution infrared spectra have been obtained using synchrotron radiation (Guilhaumou et al., 1999). Sequentially single point spectra can be acquired along a profile through the sample or along a grid covering a region of interest (ROI). This mapping technique induces the use of a motorised XY stage and is extremely time consuming. The number of single point spectra increases with the size of the ROI and with the spatial resolution. Long time acquisition can be an important limitation in the case of fragile samples. The 2-D mapping allows to obtain the cartography of molecules or molecular functional groups superimposed to the conventional image of the sample recorded by transmitted light with an optical microscope (Deneux-Mustin et al, .1997). False colours are used to represent the intensity variations of the chosen absorption infrared band.

Recently, infrared focal-plane array (FPA) detectors, issued from military applications, and composed by a series of detector elements have permitted to acquire 2-D molecular images at high spatial resolution in a short time. Applications to materials, solutions and biology have been described in the nineties coupling a FPA detector to a step-scan interferometer (Lewis et al., 1995, Oh and Koenig, 1998, Lasch and Naumann, 1998, Lasch et al., 2002). First applications to geological samples have been described by Pironon et al. (2001) and Ito and Nakashima (2002). Our goal is to show the feasibility of FT-IR imaging for the characterisation of minerals through applications to natural quartz from sedimentary basin and emerald gems.

7.2 Experimental

FT-IR micro spectroscopy

Experiments have been conducted on a FT-IR spectrometer (®Bruker Equinox 55) in connection with an IR-scope I microscope (®Bruker). This microscope is equipped with a narrow band, mercury-cadmium-telluride (MCT) detector with a 100µm-diameter window cooled at 77K. Using a series of diaphragms, the diameter of the beam can be reduced down to 20 µm with x15

objective magnification. Infrared spectra are the results of 200 accumulations with a 4 cm^{-1} spectral resolution.

FT-IR imaging

Experiments have been conducted on a FT-IR spectrometer (®Bruker Equinox 55) in connection with an IR-scope II microscope (®Bruker) equipped with a Hyperion detector. This detector (FPA) is a matrix of 4096 small MCT-type detectors arranged in a 64x64 grid. The spectral range is a part of the middle infrared (3800-950 cm^{-1}). Resolution has been choosen equal to 8 cm^{-1}. Some measurements were done with a resolution of 16 cm^{-1}. FT-IR analysis were done in transmission mode using a 15x objective. The measured area was a square of 270x270 micrometers with a spatial resolution equal to 4 micrometers.

All the spectra are presented in terms of absorbance versus wavenumbers (cm^{-1}). Air is used as a reference for absorbance calculation.

7.3 Samples

Natural emerald sample

A natural faceted emerald of 1.89 cts has been broken in two parts (a big one (A) and a small one (B)) during setting operation (Figure B-20). Specific infrared micro spectroscopy analysis reveals that the gem is originated from Colombia (Western zone: Coscuez Mine) (Cheilletz et al 2001a, Cheilletz et al 2001b) . In order to understand the reasons of this fracture, FT-IR imaging (transmission mode) have been conducted on the two pieces. Particular attention was given to the detection and the distribution of residual organic matter such as emeralds fillers (resin, oil). It must be remembered that such products are used to enhance quality of the emerald (transparency). Infrared beam was always in a direction perpendicular to the table of the gem.

Natural quartz from sandstones

A highly siliceous sandstone from the North Sea basin has been sampled. The rock fragment has been sawn and reduced to a thin section of 150 µm, polished in its two sides. Petrographical observations show the abundance of detrital quartz grains associated with quartz crystallisation in the form of overgrowths and fracture healing (Figure B-23A). These overgrowths are sometimes associated with clay minerals and have been created during diagenesis, reducing the porosity (i.e. inter-granular space) of the sample. Silica precipitation could be connected to the migration of fluids (water, gas or petroleum), responsible for economic accumulations. The knowledge of the diagenetic history is then a key parameter for the understanding of the formation of a natural fluid reservoir. The chronology and conditions of the formation of diagenetic minerals are deduced from

SEM-cathodoluminescence imaging, ion probe analysis, fission track analysis and fluid inclusion study (Pagel et al., 1997, Girard et al., 2001). FT-IR imaging could be a good way to acquire molecular information at the scale of the rock section.

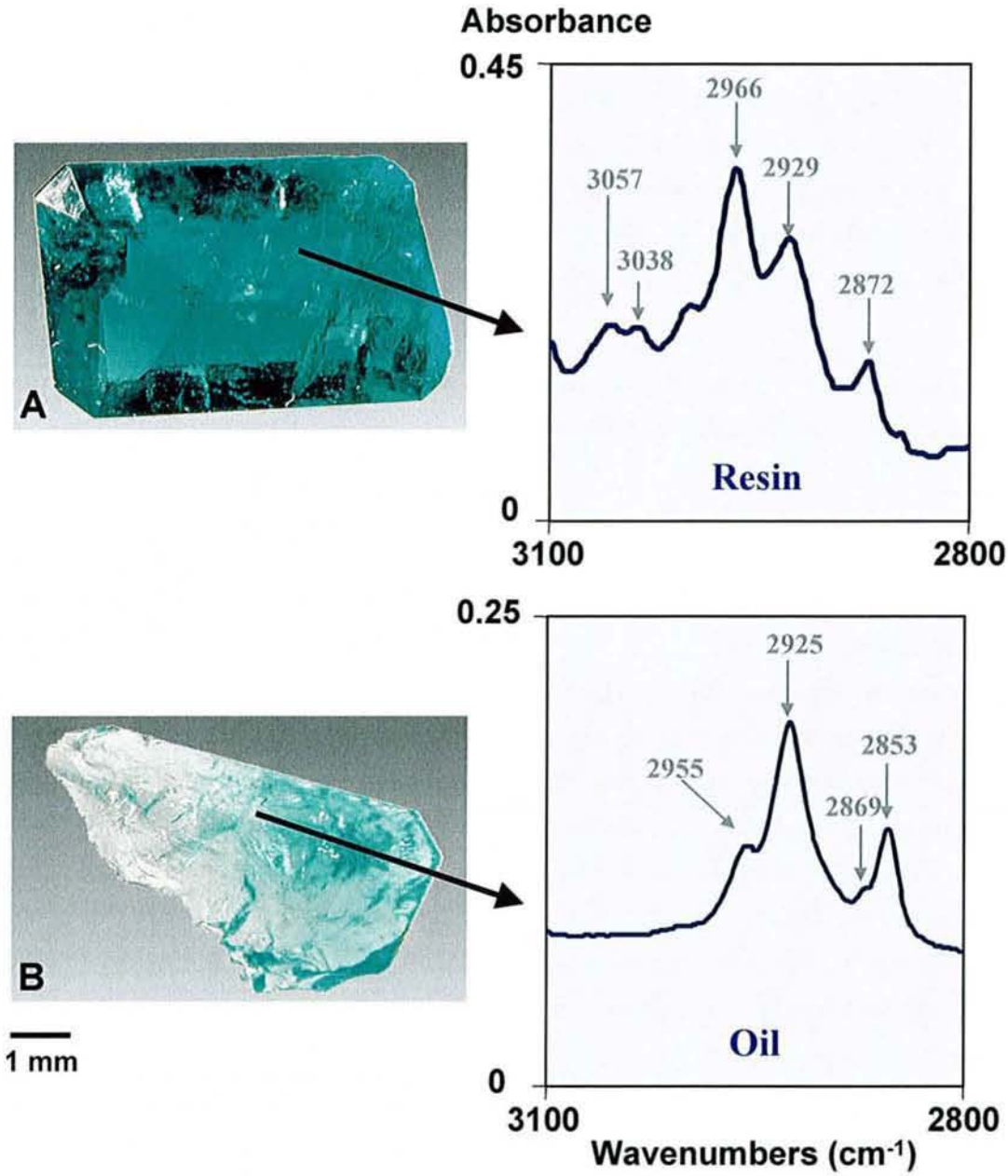

Figure B-20 : Faceted natural Colombian emerald fractured during setting operation. The μFT-IR analysis in transmission mode (diameter of the spot: 60 μm) reveals the presence of emerald fillers: resin on the big part (A) and oil on the small one (B).

7.4 Results and discussion

Emerald: part A and B

Figure B-20 exhibits the two parts of the initial emerald after fracturing during setting operation. As it can be observed, part A is the biggest (around 8 mm long and 4 mm thick) and part B is the smallest one (around 8 mm long and 0.05-3 mm thick). Conventional infrared micro analysis on part A (Figure B-20) mainly reveals the presence of resin. Corresponding absorption bands located at 3057, 3038, 2966, 2929 and 2872 cm^{-1} are mainly characteristic of palm oil or opticon. Position of the asymmetric stretching vibration of CH_2 groups (2929 cm^{-1}) argues in favour of palm oil type-resin. Zecchini and Maitrallet (1998) have shown a location at 2928 cm^{-1} for palm oil whereas the CH_{2as} stretching vibration is located at 2925 cm^{-1} for opticon. On the contrary, infrared microscopy spectra of part B indicate only the presence of oil (2955, 2925, 2869 and 2853 cm^{-1}). These observations prove that, at least, two different organic fillers have been used. In order to estimate their distribution in/on the emerald, FT-IR imaging was carried out. Figure B-21 presents the FT-IR imaging of the part A (270 x 270 µm) in the 3100-2800 cm^{-1} range in a combined 3-D and 2-D diagram. Red and blue colours indicate high and low amount of resin respectively. The major part of the investigated surface is covered with a high amount of resin (area values > 800 $AU.cm^{-1}$). Only a small part of the investigated surface (left part between 51200 and 51300 µm) is free of resin. On the contrary, the part B, which is directly superimposed to the part A is partially covered by oil, mainly on the left side : 100 µm large (27300 to 27400 µm) and 270 µm long (52680 to 552950 µm) (Figure B-22). More over, the amount of oil is less important than the amount of resin (maximum area < 20 $AU.cm^{-1}$). As its adhesion energy on emerald is weaker than those of resin, oil has been, with time, partially removed from this face of the gem. From these FT-IR images, it is obvious that the fracturing of the emerald produced by the setting operation is due to the presence of an important pre-existing crack inside the gem. Direction of propagation of the crack is easily visible on figure B-22 (red coloration), practically on the overall length of the emerald. Moreover, this crack has been defectively filled by resin resulting in a partial adhesion of the resin on only one face of the crack. Such conditions create the following interfaces system: *emerald-resin-oil-emerald* in the emerald. Propagation of the breaking has taken place along the *resin-oil* interface. Two hypotheses are available to explain the presence of this type of interface: 1) resin has been wrongly introduced in a clean crack, oil has then been added to fill up the residual gaps, or 2) resin has been introduced in a partially de-oiled crack producing a bad and heterogeneous adhesion of the resin on the two faces of the crack.

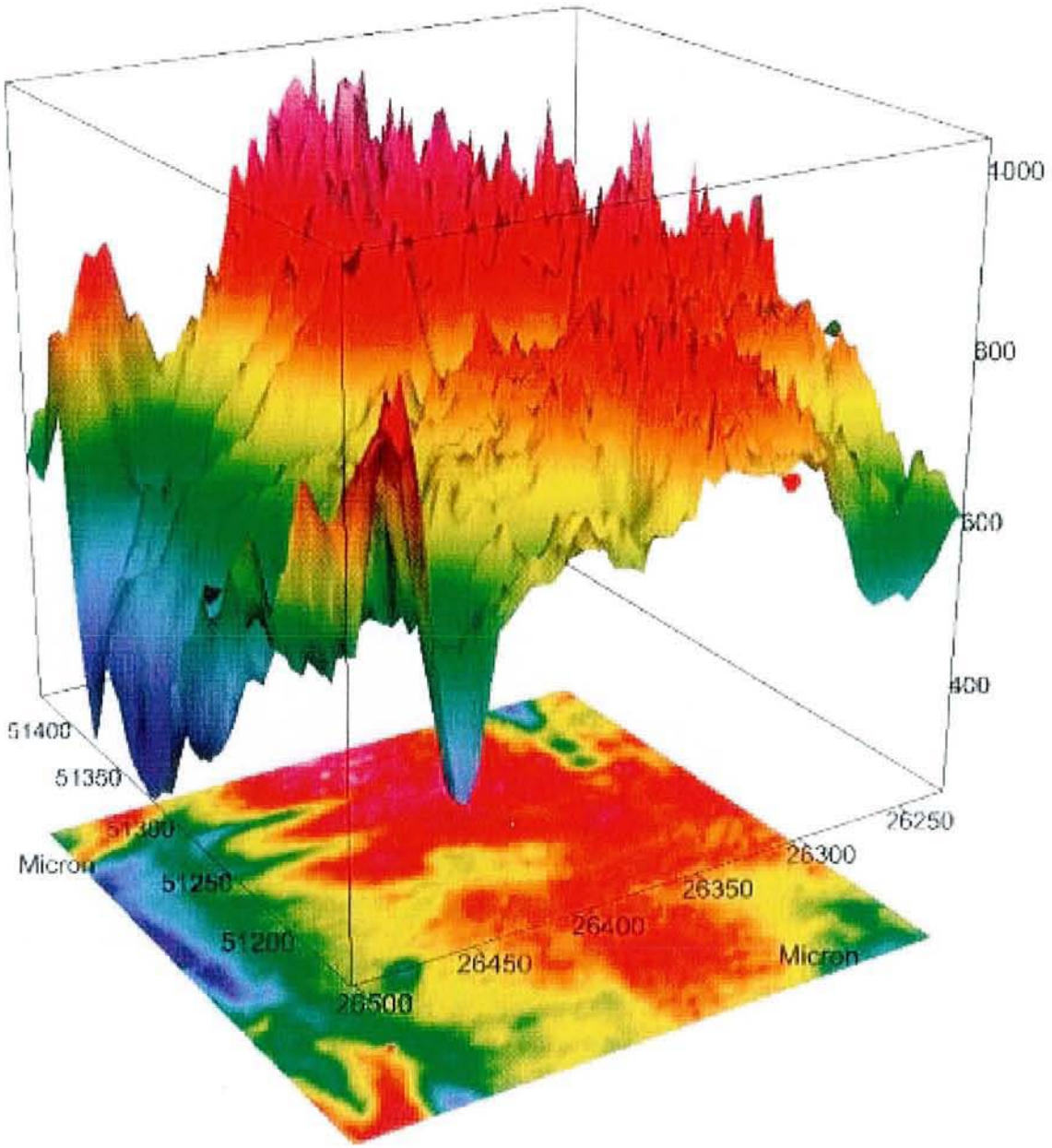

Figure B-21 : FT-IR imaging of the part A of the fractured emerald (270 x 270 µm). The 3-D diagram represents the intensity of the integrated wavenumber range (3100-2800 cm^{-1}) versus x-y co-ordinates of the sampling area. The 2-D image is the projection of the upper diagram, the red colour indicates a high amount of resin.

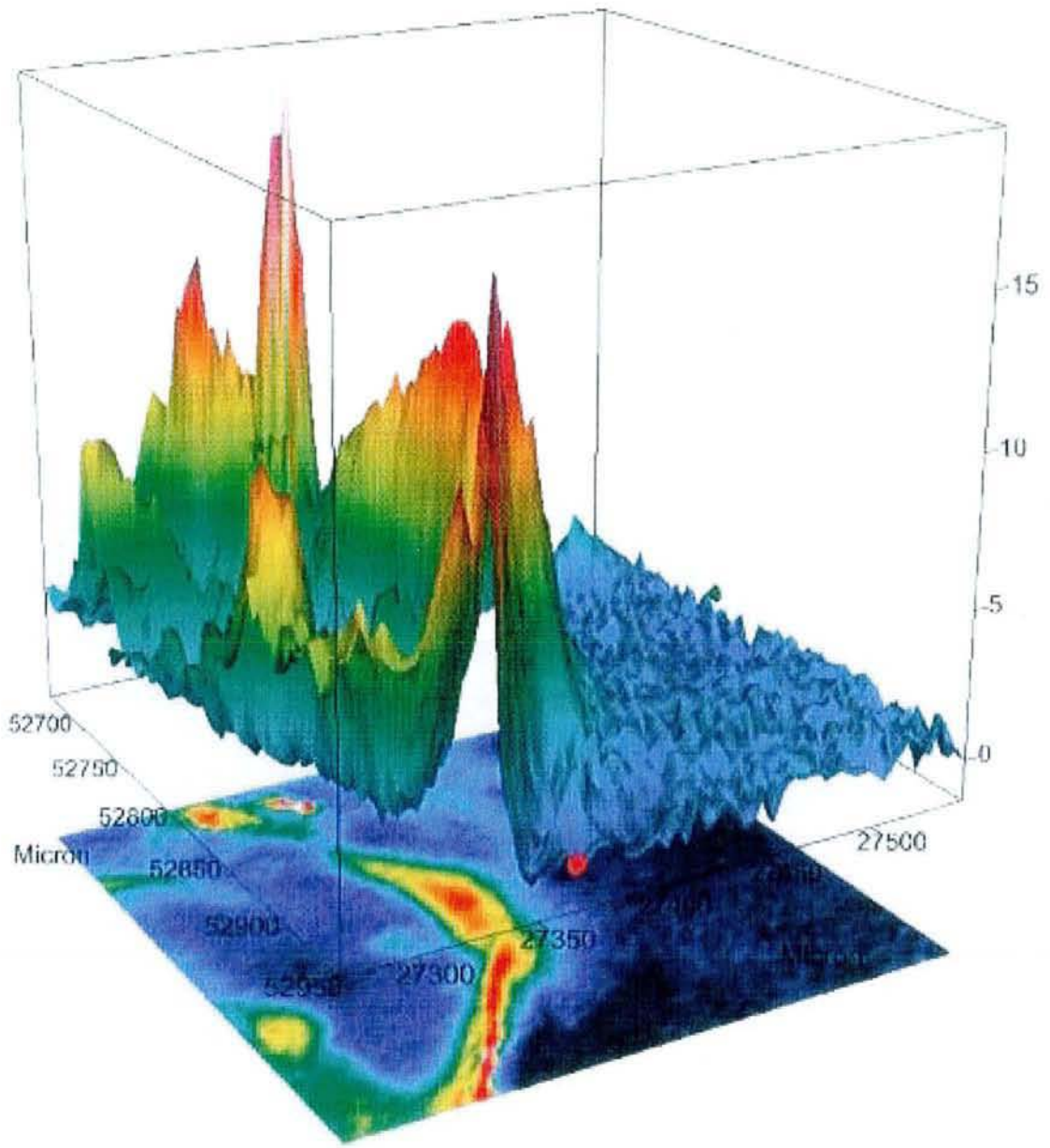

Figure B-22 : FT-IR imaging of the part B of the fractured emerald (270 x 270 µm). The 3-D diagram represents the intensity of the integrated wavenumber range (3100-2800 cm^{-1}) versus x-y co-ordinates of the sampling area. The 2-D image is the projection of the upper diagram, the red colour indicates a high amount of oil.

Natural quartz from sandstones

The scanned area of the sandstone sample takes into account the detrital quartz grain with petroleum inclusions, a micro-fracture, a quartz overgrowth located at the contact with a neighbouring detrital quartz grain and inter-granular spaces (Figure B-23B). The inter-granular space is filled with a dark material that is not clearly identified by observation in transmitted light. The FT-IR images are recorded with the Hyperion detector (Figure B-23C, D, E, F). At each pixel of the FT-IR images an infrared spectrum can be extracted. Three characteristic spectra are presented and four spectral ranges have been selected for the construction of the FT-IR images (Figure B-24): 1) the 3700-3600 cm^{-1} spectral range corresponds to the presence of OH-groups from clay minerals (kaolinite-illite), 2) the 3700-3100 cm^{-1} spectral range corresponds to the presence of water as fluid inclusions or as mineral constituent, 3) the 3100-2740 cm^{-1} spectral range is assigned to C-H groups from hydrocarbons and 4) the 2360-2320 cm^{-1} spectral range corresponds to CO_2. Absorption bands below 2000 cm^{-1} are due to the silicate absorption.

The 2-D image of the figure B-23C shows the presence of clay minerals. They are only located in the inter-granular space. Their fingerprint is also marked in the figure B-23D because the selected spectral range (3700-3100 cm^{-1}) overlaps the previous one (3700-3600 cm^{-1}). The difference between the figures B-23C and B-23D shows the presence of water in quartz : water is located inside the micro-fracture and the quartz overgrowth, it marks the re-crystallisation of quartz in low temperature and low pressure conditions (<150°C, <500 bar) of a petroleum basin.

The 2-D image of the figure B-23E corresponds to the location of the C-H molecular groups. They occur in the inter-granular space and in the fluid inclusions and correspond to bitumen impregnation of clays and liquid oil trapping respectively. The presence of bitumen confers the dark colour to the inter-granular space. No hydrocarbon has impregnated the micro-fracture that cannot be considered as a drain for oil migration. Petroleum inclusions are also clearly identified by the FT-IR imaging of CO_2 (Figure B-23F). CO_2 is dissolved in the oil trapped in the fluid inclusion. The colour intensity chart shows that CO_2 is detected at low concentration. Therefore, a signal of very low intensity does not prevent to build a 2-D molecular image using infrared focal-plane array detectors.

Some limitations can be deduced from this example: 1) north-east oriented structures with negative integrated intensities appear in the four FT-IR images. These values are due to the presence on the spectra of interference fringes, probably created by irregularities on the sample surface. Such defects are produced during the thin section preparation. 2) The 2-D FT-IR images are compared to the images recorded by conventional transmitted light. However, the 2-D FT-IR images are in fact the projections of the infrared information collected by transmission on the bulk rock section. FT-IR images differ from the observations acquired with surface techniques such as electronic or ionic microscopy. FT-IR surface imaging could be expected using FT-IR acquisition in reflection.

Users of FT-IR imaging will greatly benefit to carefully check the sample surface that must be free of contaminant (resins, glues, products of polishing), and the thickness of the sample that must be constant on the scanned area.

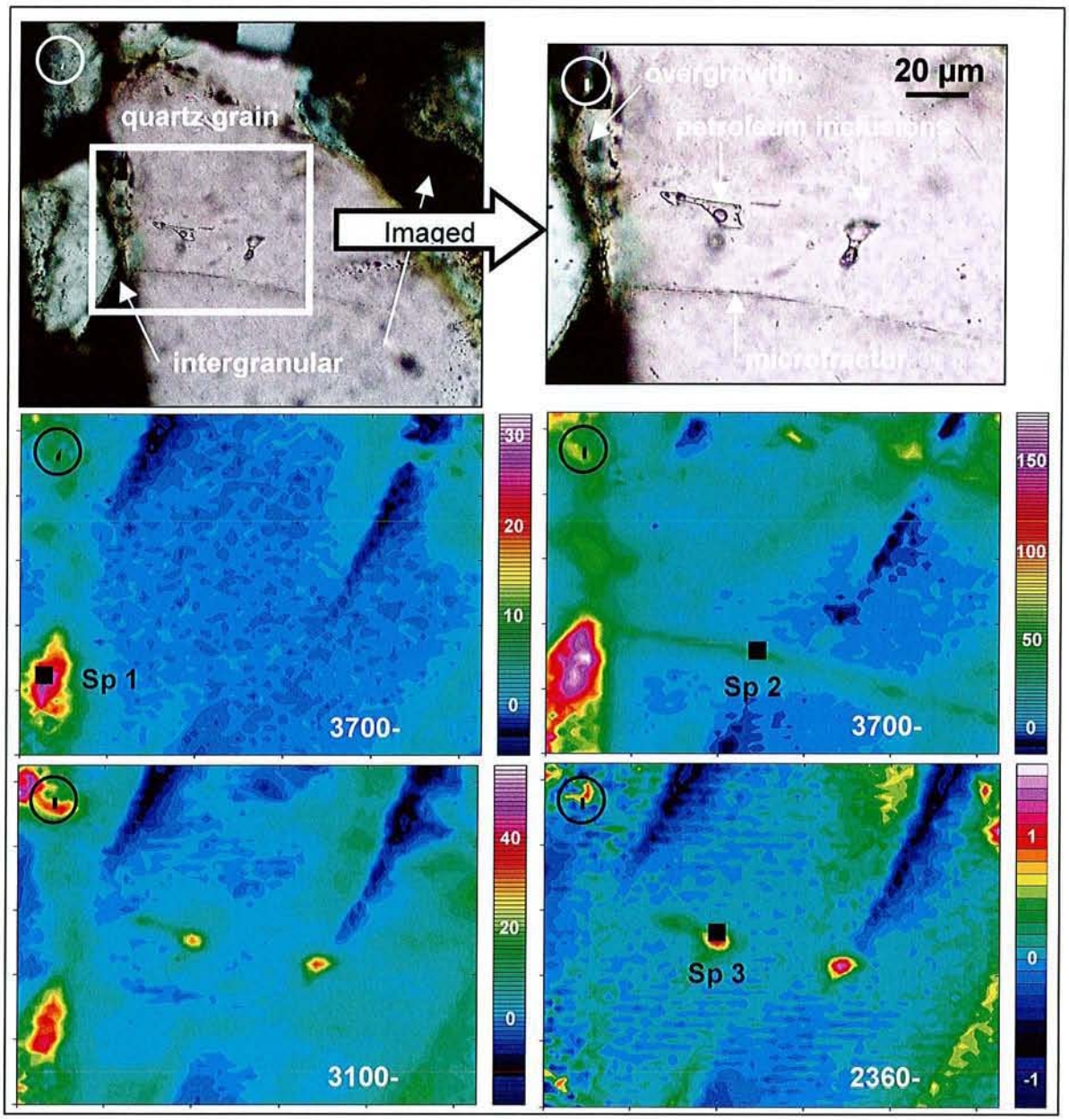

Figure B-23 : FT-IR imaging of a quartz grain from a Jurassic sandstone of the North Sea basin. A, B: scanned area observed in polarised transmitted white light; C, D, E, F: FT-IR imaging of the integrated intensities of the 3700-3600 cm^{-1}, 3700-3100 cm^{-1}, 3100-2740 cm^{-1} and 2360-2320 cm^{-1} ranges respectively, corresponding to the sample area B. Sp 1, 2 and 3 are the locations of the extracted spectra of the figure B-22.

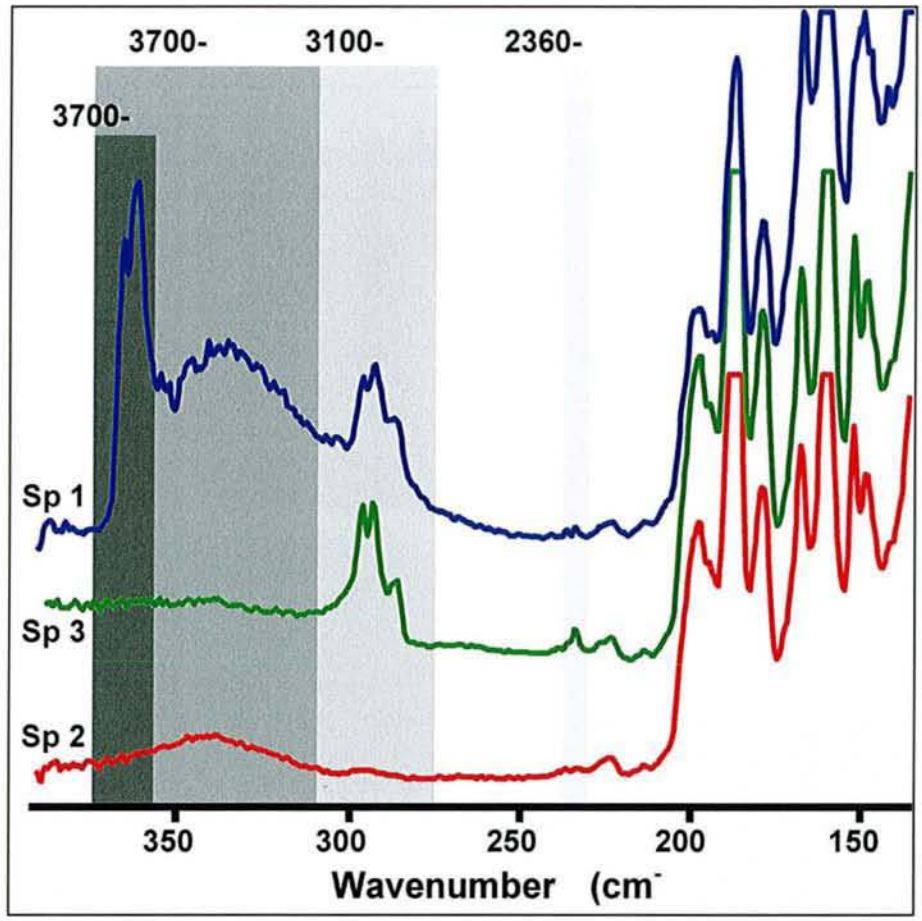

Figure B-24 : Extracted spectra of the FT-IR imaging of the figure B-21, with the chosen integrated intensity domains. Absorption bands located below 2000 cm^{-1} are mainly assigned to Si-O vibrations of quartz and clays.

7.5 Conclusion

FT-IR imaging is a complementary technique to the electron or ion techniques conventionally used for mapping in mineralogy. It is a fast and high resolution method allowing the acquisition of molecular information at the scale of 4 µm square-pixels. On the case of the analysis of a thin rock section, FT-IR imaging gives us the opportunity to locate the different mineral or organic constituents. It shows that quartz re-crystallisation at low temperature and pressure is marked by the presence of water. The imaging of the hydration rate of the minerals appears to be a good way to describe the different steps of crystal growth. The mapping of the hydrocarbon compounds, in the pore space, in inclusions or in residual cracks, can help us to determine the ancient drains for oil migration in petroleum basins or the presence of organic filler in gems. Moreover, distribution

and quantification of such residual organic products is now available. This is of first importance in gemmology for the expertise the gem. The knowledge of the origin and history of the gem will help us to better estimate its quality and value. On another hand, it is easy to extract an infrared spectrum from each pixel of the FT-IR image and then to control the molecular fingerprint in all parts of the sample, even a long time after the measurement session.

References

Barrès, O., Burneau, A., Dubessy, J. & Pagel, M. (1987) : Application of micro-FT-ir spectroscopy to individual hydrocarbon fluid inclusion analysis. *Appl. Spectrosc.*, 41, 1000-1008.

Charoy, B., de Donato, Ph., Barres, O. & Pinto-Coelho, C (1996): Channel occupancy in an alkali-poor beryl from serra branca (goias, brazil): spectroscopic characterization. *Am. Miner.*, 81, 395-403.

Cheilletz, A., de Donato, Ph., & Barres, O.(2001a) La traçabilité des émeraudes : une avancée décisive obtenue par microscopie infrarouge (μsirtf). *Revue de gemmologie*, a.f.g., n°141/142, 81-84.

Cheilletz, A., Barres, O., & de Donato, Ph. (2001b) L'emeraude : vers un génome minéral. *Le journal du cnrs*, n° 133, 12.

Deneux-Mustin, S., Lartiges, B., Villemin, G., de Donato, Ph., Bersillon, J.L., Thomas, F. & Snidaro, D (1997) Morpho-chemistry in secondary sludge filtration cakes: a case study. *Wat. Sci.Tech.*, 6, n°11, 93-99.

Girard J.-P., Munz I. A., Johansen H., and Hill S. (2001) Conditions and timing of quartz cementation in Brent reservoirs, Hild Field, North Sea: constraints from fluid inclusions and SIMS oxygen isotope microanalysis. *Chemical Geology* 176, 73-92.

Guilhaumou, N., Dumas, P., Ingrin, J., Carr, G.L. & Williams, G.P. (1999) Synchrotron infrared microspectrometry applied to petrography in micron scale range. *The Internet Journal of Vibrational Spectroscopy*, **3**, 14 p.

Guilhaumou, N., Szydlowskii, N. & Pradier, B. (1990) Characterization of hydrocarbon fluid inclusions by infrared and fluorescence microspectrometry. *Mineralog. Mag.*, 54, 311-324.

Ito Y. & Nakashima S. (2002) Water distribution in low-grade siliceous metamorphic rocks by micro-FTIR and its relation to grain size: a case from the Kanto Mountain region, Japan. Chemical Geology, 189, 1-18.

Landais P. and Rochdi A. (1990) Reliability of semiquantitative data extracted from transmission microscopy-Fourier transform infrared spectra of coal. Energy and Fuels, 4, 290-295.

Lasch P. and Naumann D. (1998) FT-IR microspectroscopic imaging of human carcinoma thin sections based on pattern recognition techniques. Cell. Mol. Biol., 44, 189-202.

Lasch P., Chiriboga L., Yee H., Boese M. and Diem M. (2002) A new tool in medical diagnostics: infrared microspectroscopic imaging. European Microscopy and Analysis, 77, 13-15.

Lewis E.N., Treado P.J., Reeder R.C., Story G.M., Dowrey A.E., Marcott C., and Levin I.W. (1995) Fourier transform spectroscopic imaging using an infrared focal-plane array detector. Analytical Chemistry, 67, 3377-3381.

Oh S.J. and Koenig J.L. (1998) Phase and curing behavior of polybutadiene/diallyl phtalate blends monitored by FT-IR imaging using focal-plane array detection. Analytical Chemistry, 70, 1768-1772.

Pagel M., Braun J.J., Disnar J.R., Martinez L., Renac C. and Vasseur G. (1997) thermal history constraints from studies of organic matter, clay minerals, fluid inclusions, and apatite fission tracks at the Ardèche paleo-margin (BA1 drill hole, GPF program), France. Journal of Sedimentary Research, **67**, 235-245.

Pironon J., Teinturier S., De Donato P. (2001) New developments in FT-IR measurements of petroleum fluid inclusions. International Meeting on Organic Geochemistry, Nancy, 10-14 septembre, Abstract, 2, 257-258.

Pironon J., Thiéry R., Ayt Ougougdal M., Beaudoin G. & Walgenwitz F. (2001) FT-IR measurements of petroleum fluid inclusions: methane, n-alkanes and carbon dioxide quantitative analysis. Geofluids, 1, 2-10.

Pironon, J., Sawatzki, J., & Dubessy, J. (1991) Nir FT-Raman microspectroscopy of fluid inclusions: comparisons with VIS Raman and FT-ir microspectroscopies. *Geochim. Cosmochim. Acta*, 55, 3885-3891.

Wopenka, B., Pasteris, J. D. & Freeman, J. J. (1990) Analysis of individual fluid inclusions by Fourier transform infrared and Raman microspectroscopy. *Geochim. Cosmochim. Acta* 54, 519-533.

Zecchini, P & Maitrallet, P.. (1998) : Les gisements d'émeraudes d'Inde. *in* "L'émeraude, connaissances actuelles et prospectives" D. Giard, G. Giuliani, A. Cheilletz, E. Fritsch, E. Gonthier, eds. Association Française de Gemmologie (AFG), C.N.R.S.-ORSTOM, Paris, 81-95.

C. SYNTHESE ET REPRESENTATIVITE DES INCLUSIONS FLUIDES DANS LES QUARTZ DIAGENETIQUES: INCIDENCE SUR LA COMPREHENSION DES MECANISMES DE CROISSANCE DES QUARTZ

SYNTHESE ET REPRESENTATIVITE DES INCLUSIONS AQUEUSES ET HYDROCARBONEES DANS LES QUARTZ DIAGENETIQUES: INCIDENCE SUR LA COMPREHENSION DES MECANISMES DE CROISSANCE DES QUARTZ

1 LA SILICE

La silice (SiO_2) est un des constituants majeurs du système terrestre. Il existe huit formes cristallisées de silice (Figure C-1) :

- **quartz-α** (*low-quartz*): forme stable de SiO_2 jusqu'à 573°C à pression atmosphérique.
- **quartz-β** (*high-quartz*): stable de 573 à 870 °C à pression atmosphérique.
- **tridymite-α**: forme de haute température et basse pression qui peut exister sous une forme métastable jusqu'à 117°C.
- **tridymite-β**: stable de 870 à 1470 °C.
- **cristobalite-α**: phase métastable jusqu'à 200-275°C.
- **cristobalite-β**: phase métastable de 200-275 à 1470°C mais est la forme stable de la silice de 1470 à 1713°C (point de fusion).
- **coesite**: stable de 21 à 81 kbar.
- **stishovite**: stable à des pressions supérieures à 81 Kbar.

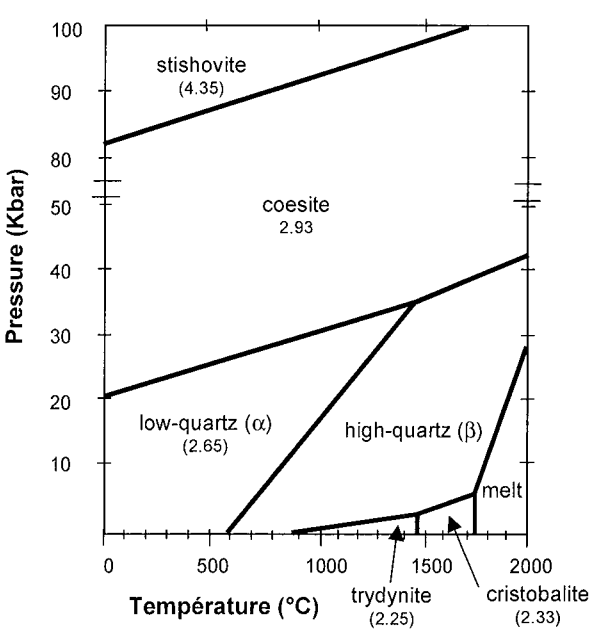

Figure C-1 : Diagramme de stabilité des espèces stables de silice (Swamy et al., 1994).

Le quartz est la forme de silice la plus stable rencontrée dans la croûte terrestre et en particulier dans les grès des bassins pétroliers. Ces environnements sédimentaires sont le siège de processus diagénétiques mettant en scène certaines étapes de transformations des différentes espèces de silice de basse température et pression (<200°C et 1Kbar). En particulier, le passage de la silice amorphe (opal-A) ou d'une silice d'origine biogénique en cristobalite (opal-CT) ou en quartz.

2 LES SOURCES DE SILICE

Les sources de silice des bassins pétroliers sont variées et encore très discutées (Hassouta, 1999; Worden and Morad, 2000, Giles et al, 2000). Les phénomènes les plus couramment invoqués pour expliquer les néoformations de quartz sont (1) les phénomènes de pression-dissolution (contact quartz-quartz), (2) les phénomènes de dissolution-cristallisation (contact quartz-micas), (3) les transformations smectite-illite, (4) les fluides sursaturés en silice, (5) la dissolution de la silice amorphe (silice biogénique et volcanique), (6) la dissolution des feldspaths.

3 CIMENTATION DE QUARTZ ET MIGRATION D'HYDROCARBURES

La cimentation du quartz est un processus diagénétique important puisqu'elle influence directement la qualité d'un réservoir pétrolier, notamment en régulant la porosité et donc son potentiel en huile ou en gaz. Cette cimentation de quartz correspond à la cicatrisation des fractures des grains et plus généralement à la croissance d'auréoles. Elle dépend en grande partie de la disponibilité de silice et du contrôle de son transport de sa source jusqu'à son site de précipitation (Worden and Morad, 2000). Les mécanismes physiques et chimiques de la croissance de quartz dans les environnements pétroliers sont encore mal connus. Dans les réservoirs naturels, les surcroissances de quartz sont observées aussi bien dans les niveaux aqueux que dans les niveaux à huile (Ramm, 1992; Saigal et al., 1992; Walderhaug, 1990). Cependant, de nombreux auteurs soutiennent le fait que la migration d'hydrocarbures puisse stopper ou du moins ralentir la cimentation de quartz, en se basant notamment sur des différences importantes de porosité entre les zones à eau et à huile de divers réservoirs pétroliers (Dixon et al., 1989; Gluyas et al., 1993; Marchand et al., 2001). Le degré d'inhibition devrait alors dépendre principalement de la saturation en eau restante, de la mouillabilité des quartz et de la pression fluide exercée sur les quartz (Worden and Morad, 2000). Si la venue d'hydrocarbures bloque effectivement la diagenèse, la présence d'inclusions hydrocarbonées dans les auréoles de croissance des quartz ne pourrait s'expliquer que par le remplissage tardif de leur porosité (Barclay and Worden, 2000; Larese and Hall, 1996; Meunier, 1992).

Les expériences réalisées dans cette étude montrent que la cimentation de quartz en présence d'hydrocarbures est possible même dans un milieu à forte saturation d'huile (chapitre C-§8 et 9). Des surcroissances de quartz ont été formées à 350°C-400 bar avec des rapports eau/huile (E/H) compris entre 10 et 50% à 25°C. Pour des rapports E/H inférieurs à 10%, des pyramides de quartz ont toutefois été observées (Tableau B-2). Dans l'hypothèse où l'eau est le seul agent de transport de la silice, il a notamment été démontré que la formation d'auréoles de croissance en système hydrocarboné nécessitait au moins la présence d'un film d'eau (eau irréductible) au contact du grain de quartz. En effet, la quasi-totalité de l'eau était dissoute dans la phase hydrocarbonée dans les conditions expérimentales. Les résultats de ces observations sont présentés et commentés dans les articles situés chapitre C-§8 et 9.

4 EQUILIBRE QUARTZ-FLUIDES

De nombreuses questions restent encore en suspens concernant l'origine des fluides qui vont transporter la silice, interagir avec le quartz et permettre la cimentation des microfractures ou la croissance d'auréoles des quartz. Cette redistribution de silice pourrait s'effectuer aussi bien à l'échelle locale par diffusion et recyclage du fluide (Aplin and Warren, 1994) qu'à grande échelle (Giles et al, 2000; Jourdan et al., 1987). Les données de la littérature montrent que les données isotopiques $\delta^{18}O$ des quartz diagénétiques sont souvent élevées, et souvent plus importantes dans les surcroissances que dans le grain détritique (Tableau C-3). En effet, les quartz de basse température ont un $\delta^{18}O$ élevé car le fractionnement isotopique entre l'eau et le quartz décroît avec la température (Matsuhisa et al., 1979; Zheng, 1993). Les hypothèses les plus couramment évoquées expliquant les fluctuations de $\delta^{18}O$ dans les surcroissances sont basées sur des fluctuations de températures et la présence de fluide d'origines différentes: un fluide chaud et profond et/ou météorique (Blanchet, 2002). Dans des ciments carbonatés de l'Oklahoma, Donovan et al (1974) ont également démontré que les valeurs de $\delta^{18}O$ sont importantes quand les ciments sont associés aux infiltrations d'hydrocarbures dans le réservoir. Ils suggèrent que ces valeurs de $\delta^{18}O$ soient le résultat de l'évaporation des eaux de surface causée par la dilatation du gaz naturel vers la surface.

Les compositions isotopiques en oxygène associées à des données de température, déterminées grâce aux inclusions fluides, sont classiquement utilisées pour discuter de l'origine des fluides à partir desquels précipitent les surcroissances de quartz (Girard et al., 2001; Hervig et al., 1995; Longstaffe, 2000; Longstaffe and Ayalon, 1987; Williams et al., 1997). Le fractionnement des isotopes lors de la cristallisation des minéraux est fonction du minéral considéré, de la composition isotopique initiale du fluide minéralisateur et de la température. Les mécanismes de fractionnement les plus couramment cités sont les processus de diffusion, de dissolution-précipitation et/ou les réactions chimiques lors des interactions des phases fluides avec le minéral

(Cole et al., 1983; Dennis, 1984; Doremus, 1998; Dubina and Lakshtanov, 1997; Elphick et al., 1986; Giletti and Yund, 1984; McConnell, 1995).

Les expériences réalisées dans cette étude montrent que la présence d'hydrocarbures peut fortement influencer les valeurs isotopiques en oxygène des surcroissances de quartz par rapport à un système exclusivement aqueux (chapitre C-§9). En effet, les valeurs de $\delta^{18}O$ des surcroissances des quartz synthétisées en milieu hydrocarboné ($\delta^{18}O \approx +9‰$) sont nettement supérieures à celles générées en milieu strictement aqueux ($\delta^{18}O \approx -2‰$) dans les conditions expérimentales (350°C-400 bar). Par ailleurs, la signature isotopique de l'oxygène de l'huile devrait varier selon le type d'huile. Les résultats de ces observations sont présentés et commentés dans l'article situé chapitre C-§9.

5 CROISSANCE DE QUARTZ ET SYNTHESE D'INCLUSIONS FLUIDES EN LABORATOIRE

5.1 Facteurs de croissance

La croissance de quartz en laboratoire est gouvernée par une cinétique de réaction très lente. Celle-ci est fonction des conditions P-T et redox du système, du degré de saturation en silice de la solution et des espèces ou minéraux additionnels présents en solution (Abercrombrie et al., 1994; Rimstidt and Barnes, 1980). La cristallisation et/ou la dissolution du quartz sont également contrôlées par les propriétés cristallographiques du quartz et sont plus importantes suivant la direction de croissance du cristal, l'axe c (Hurst, 1981).

Les courbes de solubilité de la silice amorphe à pression atmosphérique (Gunnarsson and Arnorsson, 2000) et à basse température (<350°C) mettent en évidence un faible gradient de solubilité (Figure C-2). Ce gradient est encore plus faible pour le quartz mais il augmente avec la pression (Tester et al., 1994), excepté dans la région comprise entre 340-550°C et 0-600 bars. Il se produit une rétrogradation de la solubilité liée aux changements des propriétés physiques de l'eau au voisinage de son point critique.

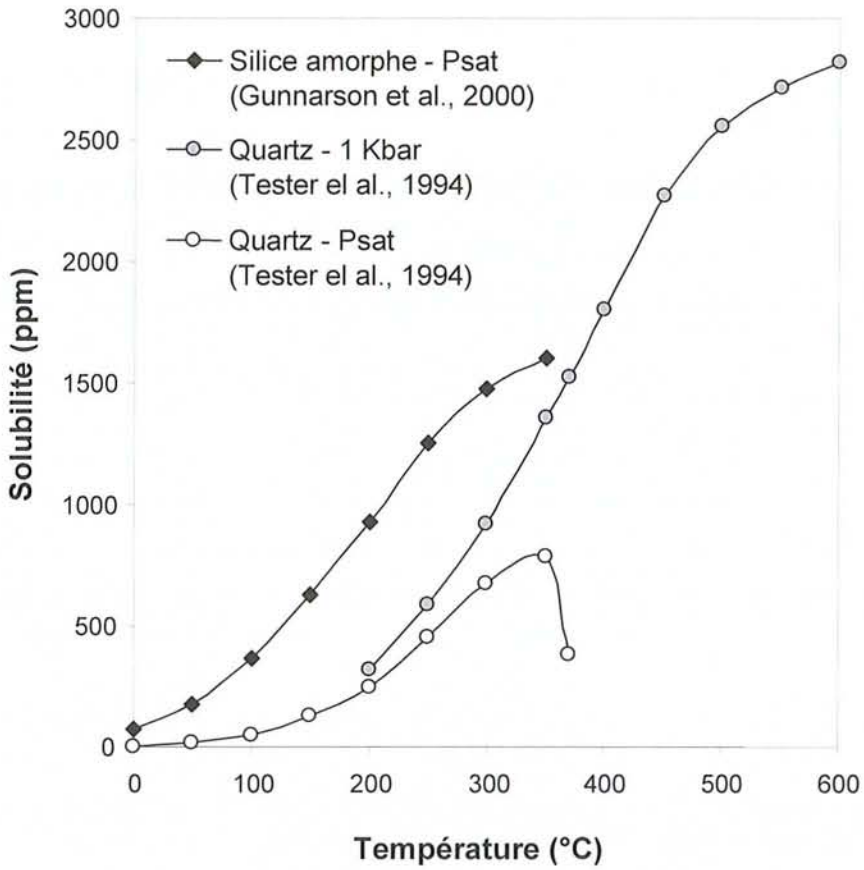

Figure C-2 : Solubilité de la silice amorphe et du quartz dans l'eau pure en fonction de la température et de la pression.

La température est le principal moteur et accélérateur du taux de réaction entre le quartz et la solution. En effet, la solubilité du quartz augmente plus en fonction de la température à une pression donnée qu'en fonction de la pression à une température donnée. SiO_2 (aq) est l'espèce stable pour des pH inférieurs à 9-9.5 ($SiO_2 + 2H_2O \leftrightarrow H_4SiO_4$). A des pH plus élevés, la dissociation de H_4SiO_4 en $H_3SiO_4^-$ et $H_2SiO_4^{2-}$ (Figure C-3) rend alors la solubilité du quartz dépendante du pH (Cassan et al., 1981). Plus le pH est important, plus la solubilité du quartz est grande (Figure C-4).

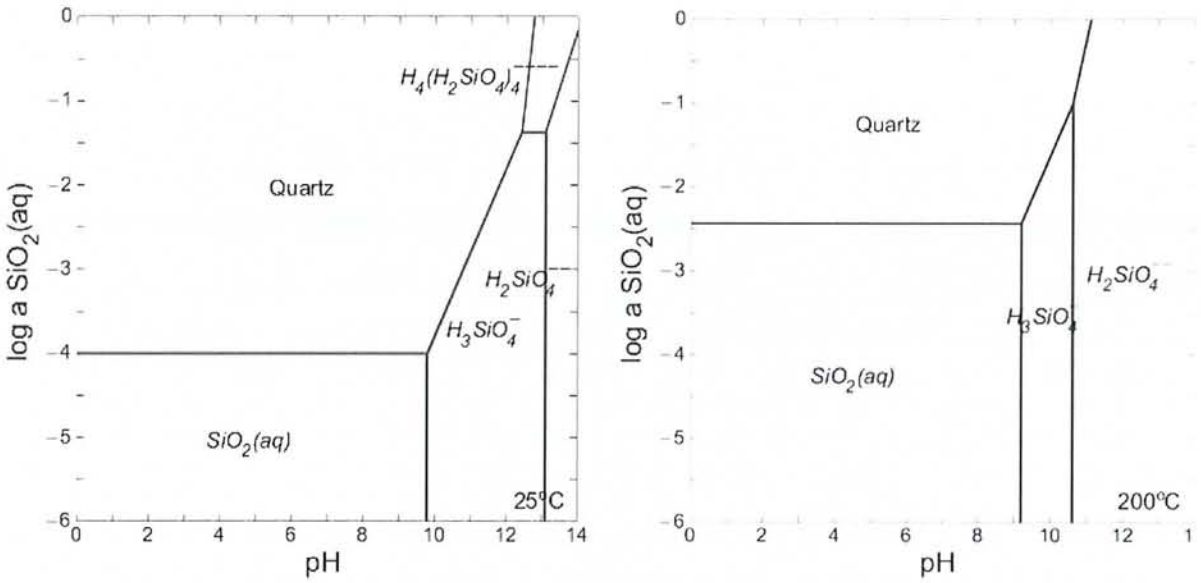

Figure C-3 : Diagramme de phase des espèces dissoutes de silice à 25°C et 200°C.

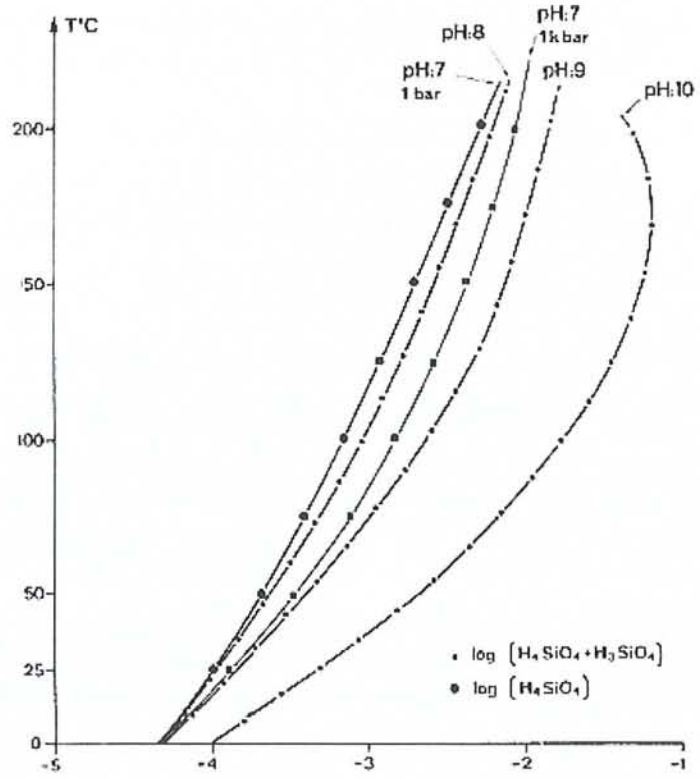

Figure C-4 : Solubilité du quartz en fonction de la température, de la pression et du pH (Cassan et al., 1981)

Les espèces minérales additionnelles dissoutes présentes en solution peuvent accentuer ou au contraire ralentir les processus de dissolution/recristallisation vis à vis du quartz. La solubilité de la silice augmente en présence d'anions tels que OH^- et CO_3^{2-} en formant des complexes chimiques. Une alcalinité importante (donc un pH élevé) favorisera le taux de coagulation de la silice ou de nucléation du quartz et réduira ainsi la silice concentrée en solution (Hinman, 1998). Selon Marshall (1980a, 1980b), la solubilité de la silice amorphe diminue à concentration égale dans cet ordre : $MgCl_2$ et $CaCl_2$ > LiCl > NaCl > KCl. Plus la concentration en sel dans la solution est importante, plus la solubilité de la silice amorphe à température constante (de 25 à 300°C) et à pression de vapeur saturante diminue. La solubilité du quartz en présence de NaCl semble être plus importante qu'en présence d'eau pure. Selon Xie et Walther (1993), NaCl augmenterait la solubilité du quartz à partir de 300°C à 0.5 kbar et au-dessus de 400°C à 1 kbar (Figure C-5).

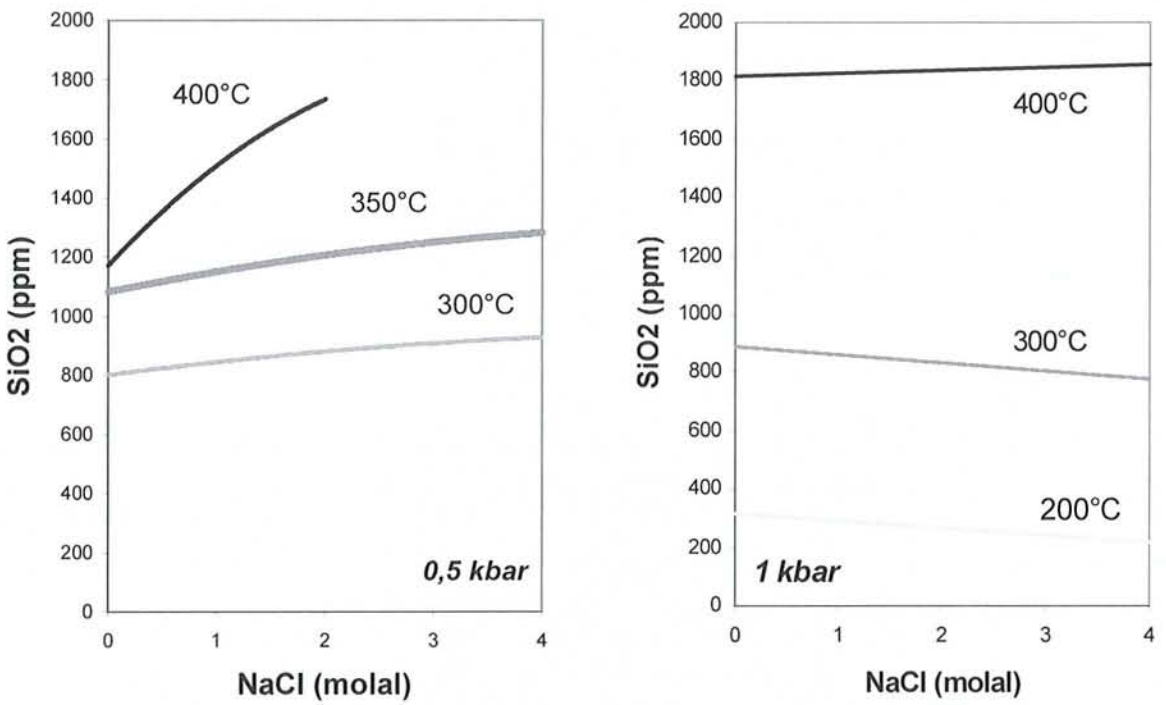

Figure C-5 : Solubilité du quartz en fonction de la température, de la pression et de la salinité (Xie and Walther, 1993)

5.2 Cristallisation de quartz en laboratoire

De nombreuses expériences de précipitation et/ou de croissance de quartz à partir de silice amorphe, de cristobalite, de quartz naturel ou synthétique ont été réalisées au cours de ces 40 dernières années. Outre des conditions expérimentales différentes (P-T, temps, pH, solution...), plusieurs voies protocolaires sont utilisées pour atteindre la sursaturation en silice de la solution et ainsi favoriser la précipitation de quartz. Deux types d'expérimentation sont à distinguer:

- les premières, généralement proches de la pression de vapeur saturante et dans des gammes de températures comprises entre 18 et 305°C (Tableau C-1). Les quantités de silice précipitées sont faibles et la croissance de quartz limitée. Ces quantités sont souvent obtenues par calcul indirect à partir des solutions extraites. A température stable, une partie de la solution est échantillonnée à intervalle plus ou moins régulier tout en injectant une quantité d'eau équivalente pour rééquilibrer la réaction et réguler la pression. La silice précipitée provient soit du quartz lui-même et/ou de silice dissoute en solution (gel de silice).
- les secondes se déroulent à pression de vapeur saturante et/ou haute pression (< 5 kbars), dans des gammes de températures comprises entre 80 et 900°C (Tableau C-2). Ces expériences, le plus souvent à vocation industrielle (Iwasaki and Iwasaki, 2002), sont réalisées en milieu oxydant (Na_2CO_3, NaOH...) et à pH élevé (>11). Les quantités de silice précipitées sont importantes et les croissances de quartz peuvent atteindre plusieurs dizaines de millimètres, voir plusieurs dizaines de centimètres. Les taux de croissance du quartz sont conditionnés par un certain nombre de critères techniques relatifs aux conditions expérimentales (Furong, 1995). En particulier, la surface spécifique et l'orientation du germe de croissance, la concentration du solvant, les fluctuations de température entre les zones de dissolution et de croissance (30-40°C) à l'intérieur de l'autoclave, et le remplissage de l'autoclave (Auvray and Regreny, 1973; Balitsky et al., 1998; Furong, 1995; Hosaka et al., 1995; Iwasaki et al., 1997; Lee et al., 1997). Ces types d'expériences utilisent différents gradients thermiques et paliers de température. Dans certaines, la température est amenée jusqu'à une température donnée (soaking temperature) puis rabaissée à différentes températures (quenching temperature) selon différents gradients thermiques, faibles au début (< 0.1°C/min) puis plus importants (> 5°C/s) jusqu'à température ambiante. Il semblerait que la croissance de quartz soit plus intense, principalement pendant ce refroidissement à faibles gradients thermiques (Hosaka et al., 1995).

En milieu hydrocarboné, les seules croissances de quartz réalisées en laboratoire sont associées à la synthèse d'inclusions hydrocarbonées (chapitre C-§5.3)

Matériel de départ	Granulométrie (µm)	Solution	pH	Température (°C)	Pression (bar)	Référence
Silice amorphe	-	Eau pure	neutre	18-305	P_{sat}	Rimstidt et Barnes (1980)
Silice amorphe	-	1 N NaCl	5-8	60-120	P_{sat}	Bohlmann et al. (1980)
Silice amorphe	-	0.1-1 m NaCl	4-8	25-50	P_{sat}	Fleming (1986)
Silice amorphe	-	NaOH, H_2S	7-10	60-90	P_{sat}	Bolt et van Santen (1997)
Silice amorphe	-	NaCl, NaOH, Molybdate, eau thermale	3-7	80-120	P_{sat}	Caroll et al. (1998)
Quartz naturel	100-1000	Eau pure	neutre	18-305	P_{sat}	Rimstidt et Barnes (1980)
Quartz naturel	90-125	Eau pure	neutre	123-221	P_{sat}	Bird et al. (1986)
Quartz naturel	100-200	Eau thermale	7-8	60-117	P_{sat}	Caroll et al. (1998)
Quartz naturel	50-125	Eau pure	5.7	200	P_{sat}	Gautier (1999)
Quartz de synthèse	50-100	Eau pure	3 et 7	200	P_{sat}	Gautier (1999)
Cristobalite	38-150	Eau pure	neutre	150-300	P_{sat}	Renders et al. (1995)
Cristobalite	100-1000	Eau pure	neutre	18-305	P_{sat}	Rimstidt et Barnes (1980)

Tableau C-1 : Conditions expérimentales des expériences de précipitation de quartz à basse température (<305°C) et pression de vapeur saturante.

Matériel de départ	Granulométrie (mm)	Solution	Temps (jours)	Température (°C)	Pression (bar)	Référence
Quartz naturel	-	0.1 - 1 m NaCl 0.1 - 1m KCl	-	300-500	P_{sat}	Hosaka et Tak (1981)
Quartz de synthèse	-	0.5 m NaCl	-	300-420	P_{sat}	Laudise (1961)
Quartz de synthèse	-	0.5-1 mNaOH	-	325-370	P_{sat}	Auvray et Regreny (1973)
Quartz de synthèse	15-220	NaOH Na_2CO_3	66-82	340	P_{sat}	Furong (1995)
Quartz de synthèse	3-70	Eau pure NaOH, K_2CO_3, NaCl, NH_4F, AlF_3, HF, Li_3PO_4	-	80-900	200-5000	Balitsky et al. (1998)
Quartz de synthèse	10-20	Na_2CO_3 NaOH, Li_2NO_3	-	340-345	-	Lee et al. (1997)
Quartz de synthèse	1-210	Na_2CO_3 Li_2CO_3	55-83	330-348	800-882	Iwasaki et al. (1997, 1998)
Cristobalite	0.5-1	2 m NaCl 1N NaOH	2-3	550-700	P_{sat}	Hosaka et al. (1995)
Quartz de synthèse	-	NaOH Na_2CO_3 - Li_2CO_3	≤ 60	100, 200 and 320	1, .7 and 320	Balitsky et al. (2002)

Tableau C-2 : Conditions expérimentales des expériences antérieures de croissance de quartz à hautes températures, à pression de vapeur saturante et hautes pressions

5.3 La synthèse d'inclusions aqueuses et hydrocarbonées

La réalisation et l'usage d'inclusions synthétiques aqueuses ou hydrocarbonées sont indispensables au calibrage des techniques analytiques et à la compréhension des phénomènes naturels complexes. Ces inclusions sont également utilisées pour les tests expérimentaux des données thermodynamiques et contribuent ainsi à améliorer les logiciels de modélisation thermodynamique basée sur les inclusions fluides tel que le logiciel PIT (Thiéry et al., 2000). Ce type de logiciel permet de reconstituer les conditions PTVX de piégeage des fluides aqueux et/ou pétroliers (chapitre B-§2.6).

Depuis les premiers essais de Roedder et Kopp (1975), de nombreuses synthèses d'inclusions aqueuses ont été réalisées dans divers systèmes, à des températures comprises entre 175 et 1000°C ainsi qu'à des pressions atteignant 7 kbar (Tableau C-1). La méthode de synthèse la plus communément utilisée se déroule dans des capsules d'or placées dans un autoclave à pression fluide similaire à celui décrit chapitre B-§1.2.2. D'autres synthèses ont également été effectuées dans un autoclave à pression gaz, identique à celui décrit chapitre B-§1.2.1 (Dubessy et al., 2000), ainsi que dans des autoclaves plus complexes permettant d'injecter du gaz dans des capsules (Lamb et al., 1996). Des synthèses d'inclusions fluides aqueuses ont même été réalisées dans des capsules placées dans des containers aux fonds d'un puits de 200 à 1485 m (Sawaki et al. 1997). La plupart de ces inclusions ont été synthétisées dans des plans de fractures et/ou dans des auréoles de croissance des quartz, ainsi que dans d'anciennes cavités. Les fractures sont généralement créees par choc thermique, plus rarement par ablation laser.

En ce qui concerne la synthèse d'inclusions hydrocarbonées dans du quartz, très peu d'expériences ont été réalisées (Tableau C-3). Larese et al (1996) ont synthétisé des inclusions hydrocarbonées dans des microfractures et des surcroissances de quartz, ainsi qu'en limite d'auréoles. Ces expériences ont été réalisées en utilisant divers rapports eau/huile (0 à 100%), à 150, 325 et 360°C avec une pression hydrostatique de 690 bar pendant 12 jours. En dépit d'une croissance significative d'auréole, les quelques rares inclusions hydrocarbonées observées en limite d'auréoles ont été mal cicatrisées. Néanmoins, cette interface perméable entre le grain et l'auréole constitue la preuve qu'un fluide postérieur aux surcroissances de quartz peut s'y infiltrer. Vityk et al (2001) ont également synthétisé des inclusions hydrocarbonées mais dans des carottes fracturées à 180°C et 480 bar pendant 10 jours. Leurs expériences suggèrent notamment que la saturation en huile semble jouer un rôle secondaire dans l'abondance et la distribution des inclusions hydrocarbonées. En dehors du quartz, d'autres travaux sur la synthèse d'inclusions hydrocarbonées ont été réalisés dans des cristaux de sels (Pironon, 1990; Stasiuk et al., 1997) à basse température (<200°C).

Matériel de départ	Granulométrie (mm)	Système	Durée (jours)	Température (°C)	Pression (kbar)	Localisation des inclusions	Référence
Quartz naturel	1.5-14	H_2O pure	0-3	600	2	fracture	Shelton et Orville (1980)
Quartz naturel	4.5-20	H_2O pure H_2O - NaCl , KCl, $CaCl_2$, CO_2, CH_4	3-87	200-850	0.5-7	fracture	Sterner et Bodnar(1984)
Quartz naturel	4.5-20	H_2O - KCl	10	300-700	1-3	fracture	Bodnar etSterner (1985)
Quartz naturel	4-30	H_2O - NaCl	-	500-1000	1-1.5	fracture	Bodnar et Sterner (1985)
Quartz naturel	2-10	H_2O - NaCl	-	300-700	1-3	fracture et auréole	Zhang et Frantz (1987)
Quartz de synthèse	-	H_2O - LiCl, KCl, CsCl	17-28	500-600	0.4-1	fracture	Dubois et al. (1994)
Quartz naturel	2-20	H_2O -NaCl - CH_4	4-19	400-600	1	fracture	Lamb et al. (1996)
Quartz du brésil, sable		H_2O - huile	12	150 - 360	0.69	Fracture et auréole	Larese and Hall (1996)
Quartz	-	H_2O pure, H_2O-NaOH	0-24	175-350	Psat-0.12	fracture	Sawaki et al. (1997)
Quartz naturel	5-15	H_2O -NaCl - CH_4	30	300	Psat	fracture	Dubessy et al. (2000)
Quartz (carotte)		H_2O - huile	10	180	0.48	-	Vityk et al. (2001)

Tableau C-3 : Conditions expérimentales des expériences de synthèse d'inclusions dans du quartz.

5.4 Résultats principaux de cette étude

Les résultats de croissance de quartz et de synthèse d'inclusions sont reportés dans les articles situés en fin de chapitre B-§5 et chapitre C-§7,8,9 et 10. Les principaux résultats sont les suivants:

- La formation d'inclusions et la croissance de quartz en laboratoire sont liées aux conditions pression-température, à la chimie du fluide hôte, à la nature et à la structure du quartz, au rapport eau/huile mais aussi à la mouillabilité en huile ou en eau des échantillons lors du remplissage de l'autoclave.
- La formation d'inclusion, la cicatrisation des fractures et la croissance de quartz sont des processus rapides (1 à 15 jours) dans les conditions expérimentales (150-400°C; 150-400 bar).
- La formation d'inclusions et la croissance de quartz secondaire sont plus importantes pour le quartz de synthèse que pour les quartz naturels brésiliens.
- La néoformation d'inclusions fluides et la croissance de quartz nécessite une solution sursaturée en silice. Il a été clairement observé qu'une baisse de température entraînait la sursaturation de la silice et favorisait la cimentation de quartz et la synthèse d'inclusions. Dans ces gammes de pression-température, l'effet de la pression sur la synthèse et la cimentation de quartz peut être considéré comme négligeable par rapport à la température, qui est le paramètre majeur.
- Les auréoles de croissance en milieux aqueux sont plus développées que celles réalisées en présence d'hydrocarbures.
- Des inclusions aqueuses ont été synthétisées dans des microfractures de grains de quartz, en présence de méthane dès 150°C-200 bar, en présence d'hydrocarbures à partir de 184°C-163 bar. Dans les surcroissances, des inclusions aqueuses en présence d'hydrocarbures ont été synthétisées à partir de 277°C-330 bar.
- Des inclusions hydrocarbonées ont été synthétisées avec différents rapports E/H, dans des microfractures de quartz (0<E/H<50%, 209-350°C; 175-400 bar), ainsi que dans des auréoles de croissance (10<E/H<50%, 289-350°C; 350-400 bar).
- La croissance de quartz et la formation d'inclusions fluides sont inexistantes si les quartz sont d'abord mouillés à huile. A l'inverse, quand le quartz est d'abord mouillé à l'eau, les expériences réalisées en présence d'hydrocarbures montrent que la croissance de quartz est possible même à forte saturation en huile. La croissance marquée de quartz n'a véritablement été observée qu'à partir d'un rapport E/H compris entre 10 et 50% à des températures et des pressions de 350°C et 400 bar respectivement. Toutefois, des pyramides de croissance ont été observées pour des rapports E/H inférieurs à 10%.

- La dissolution de la quasi-totalité de l'eau dans l'huile dans les conditions expérimentales tend à prouver qu'un film d'eau au contact du grain suffit à faire croître le quartz. Dans ce cas, l'eau est toujours considérée comme le transporteur et le vecteur de silice. Tout comme la croissance de quartz, la formation d'inclusion hydrocarbonée nécessite donc, au moins, la présence d'eau irréductible dans la structure ou au contact du quartz.

6 LA REPRESENTATIVITE DES INCLUSIONS FLUIDES DANS LES QUARTZ DIAGENETIQUES

Les inclusions fluides aqueuses ou hydrocarbonées sont à la base de nombreuses études diagénétiques visant à reconstituer les conditions PVTX de piégeage des fluides. Ces inclusions sont très souvent utilisées comme indicateur de température des auréoles de croissance des quartz, ainsi que des microfractures situées dans les grains détritiques. De part leurs localisations, leurs caractéristiques microthermométriques, morphologiques et compositionnelles, les inclusions fluides permettent dans certains cas, de différencier spatialement et temporellement les événements diagénétiques tel que la cimentation de quartz (fractures et/ou auréoles) et la migration d'hydrocarbures. Cependant, la plupart des études reposent sur l'hypothèse que les inclusions fluides ne subissent aucune déformation, aucun rééquilibrage post-piégeage. Or divers arguments tendent à prouver que ces processus de rééquilibrage existent bel et bien. Ainsi, Haszeldine et Osborne (1993) suggèrent un rééquilibrage probable (1) si les températures d'homogénéisation (T_h) maximales et les températures actuelles des formations sont similaires, (2) si d'importantes variations de T_h sont observées (3) si les données sont très dispersées et tendent vers des températures élevées, proches des températures maximales d'enfouissement. En revanche, ces auteurs considèrent que le rééquilibrage thermique des inclusions fluides n'affecte pas leur composition. Dans un second article, Osborne et Haszeldine (1993) ajoutent à leurs arguments l'existence d'une corrélation entre la taille, la forme et les T_h des inclusions, ainsi qu'une relation entre les salinités et les T_h, en affirmant qu'à une gamme de T_h correspond toujours une même salinité. A l'opposé, Robinson et al (1992) proposent des arguments contre de possibles rééquilibrages d'inclusions, notamment grâce à l'étude comparée des textures des quartz diagénétiques, des T_h des inclusions (en fonction de leur localisation dans le grain détritique ou au sein de la surcroissance) et les températures de formation des illites.

L'interface grain détritique-surcroissance est également sujette à discussion. Diverses expériences ont montré que cette interface pouvait être non seulement un site préférentiel de dissolution-précipitation (Meunier et al, 1992) mais également une interface poreuse et un site accessible aux fluides (chapitre C-§5.3) pendant, voir postérieurement à la formation de surcroissances (Larese et Hall). Dans ce cas, si les T_h des inclusions situées en bordure de grain

sont proches des températures actuelles, ces inclusions pourraient être issues d'infiltrations récentes. Par conséquent, les inclusions fluides localisées à la limite entre le grain détritique et l'auréole ne seraient pas représentatives du début de la silicification (Blanchet, 2002).

Au cours de cette étude, quelques tests de rééquilibrage d'inclusions fluides ont été effectués (hors articles) sur des quartz naturels brésiliens (chapitre C-§6.1) et sur des lames épaisses d'échantillons de Mer du Nord (chapitre C-§6.2). Ces rééquilibrages ont été effectués en appliquant une température toujours supérieure à la température initiale (ou à la T_h) de formation de ces inclusions. Les principaux résultats sur la représentativité des inclusions fluides de synthèse sont présentés chapitre C-§6.3.

6.1 Rééquilibrage d'inclusions fluides dans des quartz naturels brésiliens

Les quartz naturels brésiliens classiquement utilisés en laboratoire sont purs (>99% SiO_2) et généralement dépourvus d'inclusions. Or, quelques rares inclusions ont été observées sur certains grains. Ces inclusions ont des T_h comprises entre 83 et 98°C et les T_f de l'hydrohalite (NaCl, $2H_2O$) avoisinent +8°C. La T_f équivaut à une salinité de 27.4 %pds NaCl. Ces inclusions contiennent également de l'azote et du méthane en trace, détectés dans la phase vapeur par spectroscopie Raman.

	IF naturelles de départ	**IF re-équilibrées**	
		sans lithium (A)	*au lithium (B)*
CO_2	inexistant	inexistant	inexistant
CH_4	inexistant ou en trace en phase gazeuse (25°C) Jamais détecté à la T_h	inexistant ou en trace en phase gazeuse (25°C) Jamais détecté à la T_h	présent à partir d'une T_h >167°C (25°C et T_h)
N_2^*	1636 à 36033	1461 à 1612	57à 276
T_h	83 à 98°C	120 à 145°C	152 à 177.8°C
T_f	+7.5 à +8.4°C	+6.3 à +7.6°C	-21.7 à -12.5°C

*Tableau C-4 : Comparatif des données microthermométriques et compositionnelles des inclusions naturelles et rééquilibrées présentes dans les fractures des quartz brésiliens (Tableau B-2, expérience G2).*Aire du spectre Raman (unité arbitraire)*

Des rééquilibrages en sels, en méthane et en azote ont été réalisés dans des inclusions localisées dans des fractures des grains non chauffés et non décrépités. Ces rééquilibrages ont été réalisés en système H_2O-LiCl-CH_4 en faisant varier la température et la pression de 200-150°C et 200 bar - 170 bar respectivement (Tableau B-2, expérience G2).

Les T_h des inclusions A sont généralement comprises entre 120 et 145°C et les T_f mesurées entre +6.3 et +7.6°C. Il semble donc que ces inclusions aient localement re-piégé le même fluide salé mais à des températures supérieures à celles d'origine, lors de la montée en température de l'autoclave ou en fin d'expérience.

Les températures eutectiques proches de -70°C ont été mesurées dans les inclusions B et sont caractéristiques du système H_2O-LiCl. Les mesures de T_f de ces inclusions se situent autour de -21.7°C et -12.5°C. Les inclusions se sont donc rééquilibrées et enrichies en lithium par rapport à la solution de départ. Un mélange partiel entre un pôle en lithium et un pôle à hydrohalite est fort probable. La présence de méthane a été détectée par spectroscopie Raman dans les inclusions rééquilibrées au lithium et ayant une T_h supérieure à 167°C. La baisse de l'intensité du pic de l'azote des spectres Raman va également dans le sens d'une ouverture et d'un rééquilibrage de ces inclusions.

6.2 Rééquilibrage et/ou synthèse d'inclusions fluides dans des lames épaisses de Mer du Nord

Quelques tests de rééquilibrage et de synthèse d'inclusions ont été réalisés dans des lames épaisses polies de la zone d'Alwyn en Mer du Nord (3/14b9) dépourvues d'inclusions hydrocarbonées. Ces expériences ont été réalisées en présence d'huile, à des températures et des pressions comprises entre 250-150°C et 209-136 bar respectivement (Tableau B-2, expérience G9).

Les T_h des inclusions fluides présentes dans ces échantillons naturels sont comprises entre 97 et 103°C (Pironon et al, 2000). Après expérience, les T_h des inclusions aqueuses étudiées sont comprises entre 205 et 218°C. Les T_h des inclusions hydrocarbonées néoformées sont comprises entre 209 et 225°C. Ces inclusions aqueuses ou hydrocarbonées sont localisées dans les plans de fractures à l'intérieur et en limite des grains.

Les inclusions des quartz naturels brésiliens rééquilibrées précédemment (§6.1) ont été identifiées avant et après expériences. En revanche, l'absence de repérage et la forte densité d'inclusions des lames épaisses de Mer du Nord nous empêchent de différencier les inclusions rééquilibrées ou crées. Néanmoins, la présence d'inclusions hydrocarbonées, les T_h importantes des inclusions localisées dans les plans de fracture et en limite grain-auréole sont la preuve d'une infiltration des fluides aqueux et hydrocarbonées dans les quartz.

6.3 Représentativité des inclusions fluides de synthèse

La représentativité des inclusions fluides synthétiques dans les quartz des expériences est étudiée en détail et reportée dans les articles de ce chapitre C-§7,8,9,10 et 11. Les principaux résultats sont les suivants:

- La composition des inclusions hydrocarbonées est représentative de la composition du fluide parent jusqu'à des températures et pressions de 250°C et 212 bars respectivement. A 350°C-400 bar, des processus de cracking ont été mis en évidence aussi bien dans les inclusions fluides que dans l'huile parent.
- Dans les expériences réalisées avec un mélange eau-huile-gaz (CH_4), les inclusions aqueuses contemporaines des inclusions hydrocarbonées sont sous-saturées en méthane. L'huile semble jouer un rôle de barrière entre l'eau et le gaz en inhibant les processus de diffusion du méthane dans l'eau. La ségrégation et les variations locales de la colonne eau-huile-gaz pourraient ainsi expliquer les teneurs variables en méthane des inclusions aqueuses naturelles des basins pétroliers.
- Le modèle PIT (Petroleum Inclusion Thermodynamics) a été validé par les inclusions synthétisées à basse température (<250°C)
- Les propriétés PVTX des inclusions fluides hydrocarbonées sont modifiées par la présence d'eau à hautes températures (350°C).
- Les techniques de microscopie confocale et d'imagerie tridimensionnelle visant à reconstruire les volumes respectifs des phases des inclusions ne permettent actuellement pas de comparer précisément les rapports eau/huile/gaz des inclusions hydrocarbonées avec les rapports eau/huile/gaz utilisés lors du remplissage des autoclaves. En d'autres termes, il ne nous est pas encore possible de savoir précisément si la saturation en eau, en huile ou en gaz d'un bassin se reflète dans une inclusion.
- Aucun processus de rééquilibrage et d'infiltration post-auréole n'a été observé dans les auréoles des quartz lors d'une baisse continue de température. En revanche, quelques inclusions naturelles localisées dans des microfractures à l'intérieur ou en bordure des grains détritiques brésiliens dépourvus d'auréoles ont pu être rééquilibrées et marquées au lithium ou au méthane (chapitre C-§6.1 et 6.2). Ce rééquilibrage a été effectué à des températures expérimentales supérieures (150, 200 et 250°C) aux T_h des inclusions préexistantes (83 à 98°C).

7 Article 4: TIME FORMATION OF SYNTHETIC FLUID INCLUSION WITHIN MICROFRACTURES AND OVERGROWTHS

Des inclusions fluides aqueuses ont été synthétisées dans des microfractures situées dans des cristaux de fluorine (T=200°C, $P=P_{sat}$, t<30 jours), ainsi que dans des microfractures et des surcroissances de quartz (T=400 to 300°C, P= 400 bars, t<20 jours). La procédure expérimentale développée dans cet article permet de dater le temps de formation des inclusions fluides, à la minute dans la fluorine grâce aux températures de fusion de la glace (T_f) et au jour près dans le quartz grâce aux températures d'homogénéisation (T_h). Les temps de cicatrisation des microfractures et des surcroissances peuvent ainsi être estimés. Les résultats montrent que l'équilibre fluorine/H_2O-NH_4Cl est atteint en 82 heures. Pour les expériences réalisées sur du quartz, l'équilibre quartz/H_2O-NaCl est atteint plus rapidement dans le quartz de synthèse (1^{er} jour) que pour le quartz naturel brésilien ($6^{ème}$ jour). Cette différence est liée à l'hydratation différente des deux types de quartz. La baisse des T_h des inclusions de la limite grain-auréole vers les parties externes des auréoles est cohérente avec la baisse de température imposée par l'expérience. Par ailleurs, les résultats montrent que la croissance de quartz est un processus continu dans les conditions expérimentales. En revanche, la croissance de quartz nécessite une solution sursaturée en silice. Aucun processus de rééquilibrage et d'infiltration post-auréole n'ont été observés.

TIME FORMATION OF SYNTHETIC FLUID INCLUSION WITHIN MICROFRACTURES AND OVERGROWTHS

Stéphane TEINTURIER and Jacques PIRONON

UMR G2R (7566) and CREGU, Université Henri Poincaré, BP 239, 54506 Vandœuvre-lès-Nancy, France

Soumis à American Mineralogist (accepté)

ABSTRACT

Aqueous fluid inclusions have been synthesized within fluorite microfractures (T=200°C, P=P_{sat}, t<30 days), quartz microfractures and quartz overgrowths (T=400 to 300°C, P= 400 bars, t<20 days). The experimental procedures aim to date the time formation of the fluid inclusions, within the minute for fluorite experiment and within the day for quartz experiment. Therefore, the time needed to heal microfractures or create overgrowths can be estimated. The basic used analytical parameters are the melting temperature (T_m) of the inclusions for fluorite and the homogenization temperature (T_h) of the inclusions for quartz.

For the fluorite experiments, results show that the fluorite/NH_4Cl solution equilibrium has been reached in 82 hours. Moreover, the healing does not appear to be a regular process along the microfracture. For quartz experiments, the quartz/H_2O-NaCl solution equilibrium is faster reached for the synthetic quartz (1^{st} day) than for natural quartz (6^{th} day). This difference is linked to the hydration of the two types of quartz. The decrease of the T_h of synthetic fluid inclusions from the core-overgrowth boundary to the external part of the quartz overgrowth show that the growth of quartz is a progressive and constant process, which involve a silica sursaturated solution. No reequilibration process, no evidence of post-fluid infiltration after the quartz overgrowth formation have been observed.

Keywords: synthetic aqueous inclusions, fluorite, quartz, microfractures, overgrowths

7.1 Introduction

Fluid inclusions are often used to mark and separate diagenetic events (i.e. the growth of the mineral(s), the healing of microfractures) in time and space. Nevertheless, natural case studies often prevent to determine precise time formation of fluid inclusions especially if inclusions have been reequilibrated, re-filled or necked-down (Teinturier et al., 2002). The time to form fluid inclusions is mainly related to the pressure and the temperature of the system, but also by the fluid chemistry, the dimensions of the crack and the cementation rates of the host mineral (Brantley, 1992). Previous crack sealing on fluorite crystal have been realized in the H_2O-NaCl-CH_4 system during four weeks at a constant temperature of 200°C (Dubessy et al., 2000). For quartz, previous crack healing experiment have been realized between 200-600ºC and from vapor pressure up to 2kbar (Guillaume et al., 2002; Sawaki et al., 1997; Brantley, 1992; Smith and Evans, 1984). Sawaki et al. (1997) have shown that it took several hours to synthesize a small number of inclusions with a pH 13 solution at 300°C, and took 4 days at 200°C under saturated vapor pressures. With pure water and neutral pH conditions, it took two weeks to synthesize smaller inclusions in quartz around 300°C and vapor pressures (Sawaki et al., 1997).

This paper aims to date the fluid inclusion formation under laboratory conditions. Firstly, in fluorite microfractures (T=200ºC, $P=P_{sat}$, t<30 days) in the NH_4Cl-H_2O system. Secondly, in quartz microfractures and quartz overgrowths (T=400 to 300ºC, P= 400 bars, t<20 days) in the NaCl-H_2O system. Fluorite experiment has been conducted at constant P-T conditions and decrease of the salinities by induced leakage whereas quartz experiments have been carried out at constant pressure by varying the temperature of 10ºC per days. Petrographic observations coupled to microthermometric data allow us to give temporal and spatial information about inclusions sealing within fluorite microfractures and within quartz microfractures and quartz overgrowths. New experimental techniques have been developed in fluid and gas pressure autoclaves. They should permit to date the fluid inclusion formation, which can help us to determine the kinetic of mineral growth.

7.2 Samples

Fluorite crystals (®SOREM) have been thermally fractured by simple water soaking. Quartz experiments have been achieved using natural brazilian quartz fragments (<1cm) and synthetic quartz (sticks of 1cm in length and a square section of 0.3mm), which have been cut perpendicular to their growth c axis. Before run experiments, samples were heated at 700°C to eliminate eventual pre-existing inclusions. Quartz were then fractured by water soaking and dried for 6 hours at 80°C.

7.3 Experimental procedure

7.3.1 Fluorite experiment

Fluorite experiment were carried out in a gas-pressure autoclave (®Autoclave Engineer) of 150cm^3 in volume, which maintain the equilibrium between liquid and vapor phase at run conditions (Dubessy et al., 2000). Thus, it allows us to consider the homogenization temperature (T_h) of an inclusion equal to the trapping temperature of the fluid inside the inclusion.
Fluorite crystals and the NH_4Cl-H_2O solution (18 g/l NH_4) were mixed before the autoclave enclosure. The temperature of the autoclave was regulated at 200ºC in few hours. Experimental time was 720 hours. Non full clamping of the autoclave was carried out to provide minimum pressure leakage. This microleak of pressure is constant and linearly increases NH_4Cl content of the solution with time.

About 1-3 ml of solution was taken during each sampling period (1, 8, 15 and 30 days). All samples were extracted from the sample port (liquid phase) and trapped in an inox tube and frizzed into a liquid nitrogen dewar. Valves and tubes were heated at 200°C before using the N_2 dewar. At room condition, the solution was analyzed by ion chromatography to determine NH_4 concentration. Considering the small sampled volume of the solution, sampling does not affect the composition of the whole solution. Indeed, blank experiments have shown that the composition of the sample is equivalent to the composition of the remaining solution in the autoclave. Pressure and temperature were readjusted after each extraction.

Time formation of individual fluid inclusions within fluorite microfractures is determined using a correlation between the melting temperature (T_m) of the inclusions and the solution analyses. Indeed, T_m data are converted into NH_4Cl concentrations from literature tables (Linke, 1965). Thus, microthermometric and ion-chromatography data allow us to obtain a compositional-temperature-time relationship.

7.3.2 Quartz experiments

Quartz experiments were conducted into a fluid pressure autoclave (®Autoclave Engineer), inside gold capsules during 20 days (Landais et al., 1989). Each sample was mixed with an H_2O-NaCl (1M) solution and silica gel. Temperature and pressure were adjusted at 400°C and 400 bar respectively. However, the balance of the pressure and the temperature has involved a temporary overtaking of the experimental P-T conditions during the first 24 hours of the experiment. Pressure was maintained at 400 bar during all the experiments time while temperature was gradually reduced from 400 to 300ºC to enhance quartz precipitation and fluid inclusion formation.

NaCl solutions were used to increase the solubility of quartz and thus enhance the fluid inclusion formation (Xie and Walther, 1993). The trapping conditions are near the critical state of the NaCl-H_2O system.

7.4 Analytical techniques

7.4.1 Microthermometry

The T_h and T_m have been acquired on a ®Linkam MDS 600 stage for thin fluorite samples and on a ®USGS (Goldstein and Reynolds, 1994) for the thick natural and synthetic quartz samples. Stages are calibrated by pure CO_2 inclusion (T_m = -56.6°C) and poor salted water synthetic inclusion (T_m = -0.4°C) at low temperature, and by melting of organic crystals at positive temperatures. Phase transitions of the fluid inclusions were observed with ®Olympus x50 and x80 objectives.

For quartz experiment, T_h of fluid inclusion were corrected using Zhang and Frantz (1987) EOS with known pressure and molalities to give true trapping temperatures (T_t). Then, time formation of fluid inclusions within quartz overgrowth and/or microfractures can directly be read on the P-T-t diagram of the figure C-10. All positive temperatures mentioned in the text and figures are true T_t of the aqueous fluid inclusions.

7.4.2 Ion chromatography

Ion chromatography has been used to quantify NH_4^+ and Cl^- content of the solution in contact with fluorine. Measurements have been acquired at the CNRS analytical laboratory at Vernaison (France). A sampling device of 3 cm^3 has been adapted to the autoclave to collect the solution through the output valve. After collecting, the solution is quenched by rapid cooling into liquid nitrogen and stored at low temperature before analysis.

7.5 Results and discussion

7.5.1 Fluorite experiment

Numerous fluid inclusions have been formed within fluorite microfractures. Most of the inclusion sizes are lower than 10 µm (Figure C-6) but some of them reach 20-25µm. Figure C-7 shows the evolution of the T_m and the NH_4 concentration of each studied inclusion with time. Sampling periods are also represented on the curve. The induced leakage is constant and has been calculated around -0.008°C/h in term of T_m and around 0.045 g/l/h in term of concentration gain. The first sign of healing occurs at the 82nd hour with an inclusion that contains 21.67 g/l of NH_4Cl. This early inclusion is characterized by the lowest T_m at -4.1°C. At the opposite, the latest inclusion has been formed at the 665th hour. It contains 47.65 g/l of NH_4Cl and has a T_m of -8.7°C. Overall, microthermometric results show that the fluorite microfractures have mainly been healed between the 82nd and the 257th hours. It proves that, at 200°C, an aqueous solution of NH_4Cl needs 3 or 4 days to be equilibrated (saturated) with the fluorite allowing the sealing of inclusions.

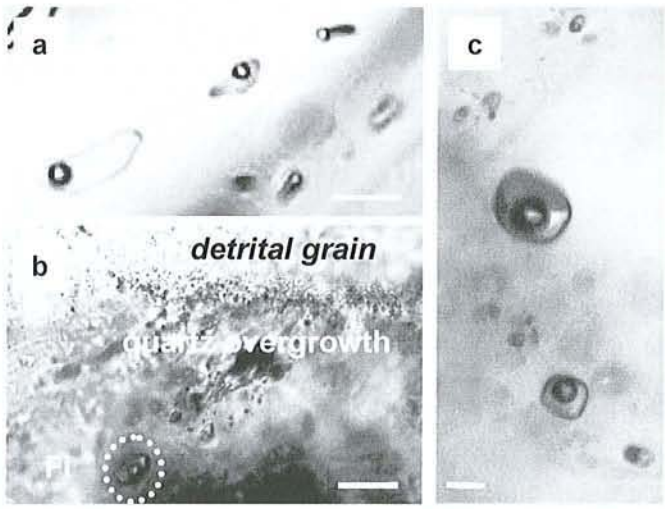

Figure C-6: Microphotography of synthetic fluid inclusions (a) inside fluorite microfractures, (b) inside brazilian quartz overgrowth and (c) within synthetic quartz microfractures. Bar scale = 10µm.

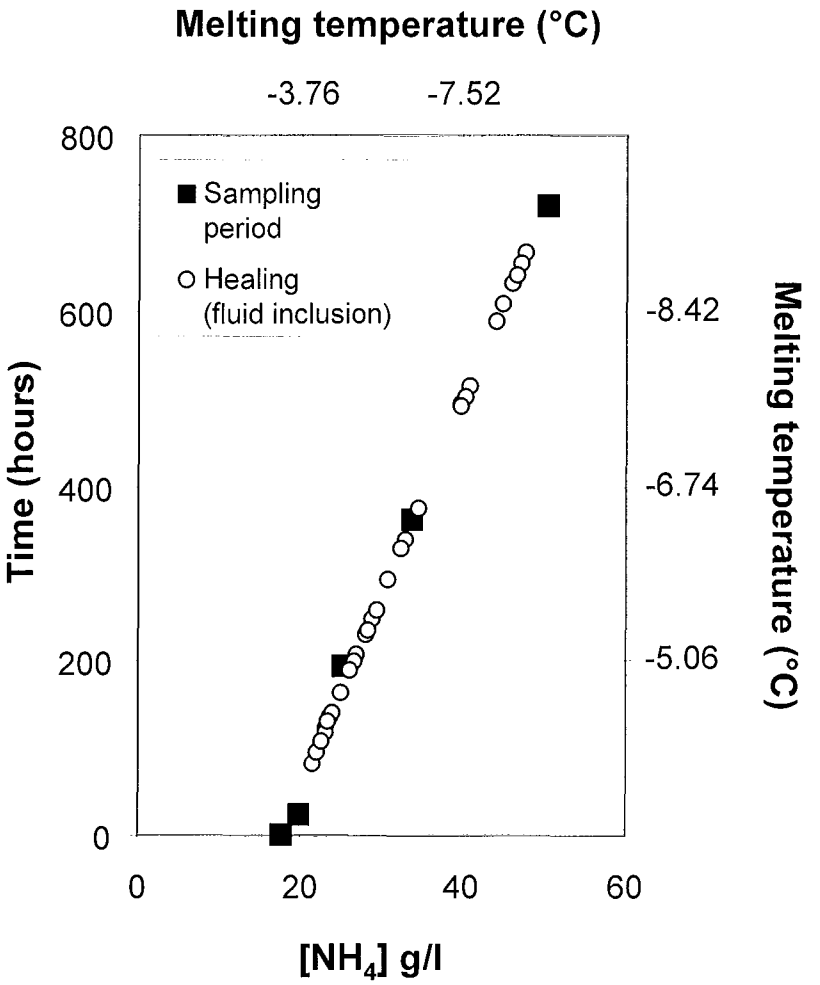

Figure C-7: Time formation of synthetic fluid inclusions inside fluorite microfractures.

In order to better understand and visualize the formation process of fluorite microfractures healing in time and space, 3-D continuous surfaces (Figure C-8) were constructed with GOCAD© software by triangulation and discrete smooth interpolation (Mallet, 1992). This surface intersects all inclusions that belong to this fracture plan. Each inclusion is characterized by its properties (i.e. T_m, NH_4 concentration, time and depth below the sample surface). Results show that these inclusions have been randomly sealed between the 117th to 513th hour of the experiment and that healing is not a continuous or linear process with time. In other words, the healing of each microfractures did not occur at one time. Indeed, the total cementation of a single microfracture can sometimes be completed within several days, sometimes up to 20 days. Therefore, local reequilibration of individual inclusions could occur in a same microfractures and could explain the range of T_h and T_m observed in one plane of inclusions for natural samples.

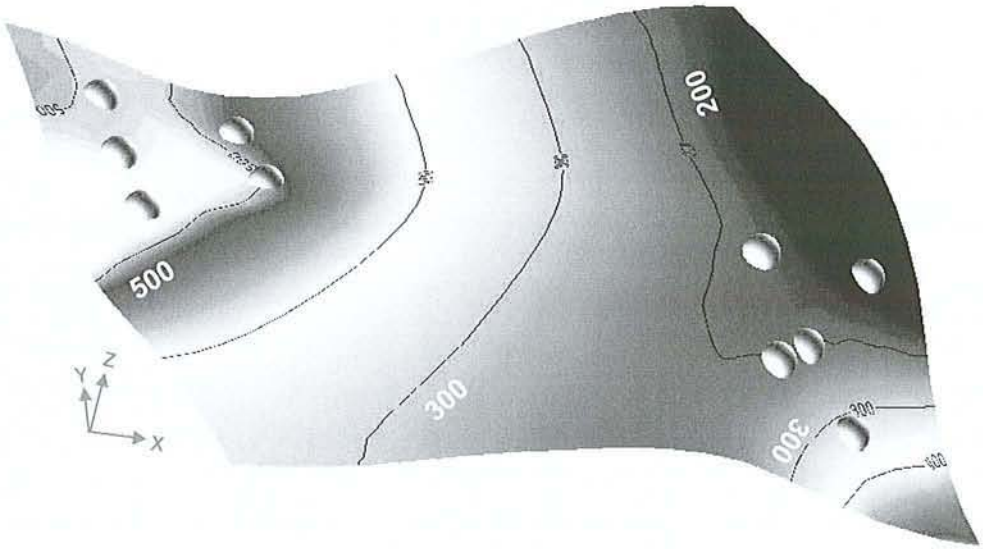

Figure C-8: Spatial and temporal evolution of fluid inclusions (white circles) sealing in a same fracture plan. Isochron time-lines are in hours (black lines)

7.5.2 Quartz experiments

Numerous fluid inclusions have been formed within healing microfractures, less inside quartz overgrowth. The inclusions located inside quartz microfractures have size rarely greater than 30µm in length (Figure C-6) and those inside overgrowths never exceed 8 µm in size.

In quartz microfractures, two types of fluid inclusions have been identified:

a) Fluid inclusions with variable gas filling (30-40% and 60-70%) and high T_t (between 385 and 418ºC) (Figure C-10). These inclusions are exclusively found in quartz microfractures (<15µm) and located near the surface of the synthetic quartz. These inclusions have a pseudo-critical behavior. Indeed, their P_t-T_t trapping conditions is near the critical temperature of 420ºC of a critical inclusion trapped in an H_2O-NaCl (1M) system (Bodnar and Vityk, 1994). These aqueous inclusions have been synthesized within the first 24 hours, during the balance of the P-T conditions at the beginning of the experiment.

b) Fluid inclusions with constant gas filling (around 25%), which have been trapped within larger microfractures (up to 30µm). These aqueous inclusions show a wide range of T_t: from 385 to 347°C in synthetic quartz and from 386 to 355°C in natural quartz. Healing of quartz microfractures have thus occurred within 12 days in synthetic quartz and 3 days natural quartz (Figure C-9).

Therefore, results a show that the synthetic quartz/H_2O-NaCl solution equilibrium has been reached within the 1st day whereas the natural quartz//H_2O-NaCl solution equilibrium has been reached after 6th day. This difference should be linked to the hydration of the two types of quartz.

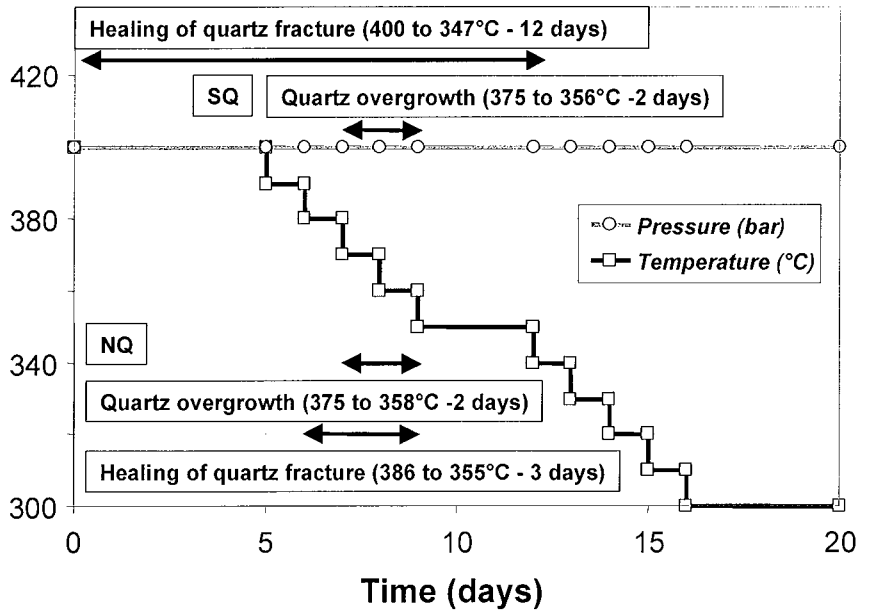

Figure C-9: Experimental conditions of natural (NQ) and synthetic quartz (SQ) experiments in the NaCl-H_2O system (400 bar - 400 to 300°C) for the healing of quartz fracture and the growth of quartz. Indicated temperatures are the corrected trapping temperatures (T_t) of the aqueous fluid inclusions.

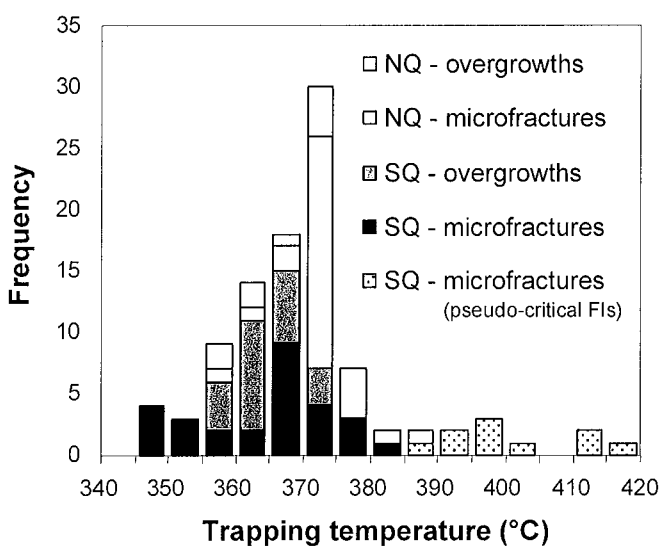

Figure C-10: Trapping temperatures (T_t) of synthetic fluid inclusions in synthetic quartz (SQ) and natural quartz (NQ) microfractures and overgrowths.

In quartz overgrowth, T_t of fluid inclusions localized in natural (from 375 to 358°C) and synthetic quartz (from 375 to 358°C) are very similar and coincide with the decrease of temperature during the experiment (Figure C-9 and C-10). Figure C-11 shows an example of the

evolution of a synthetic quartz overgrowth, which have growth during 2 days. Aqueous inclusions located inside quartz overgrowth are rare and small. Thus, few T_t have been measured. The core-overgrowth boundary is characterized by a relative large band (15-20µm) filled with numerous tiny inclusions, which have constant T_t of 368°C. Then, the T_t of aqueous inclusions decrease from the core-overgrowth boundary (368°C) to the external part of overgrowth (356°C). T_t from 368 down to 360 indicate that quartz have rapidly grown during the decrease of temperature. Therefore, and in our case, quartz growth mechanism is a progressive and constant process that has only been halted by the stopping of the silica supply. Moreover, the continuous decrease of the T_t is the proof that fluid has not accessed the inner part of overgrowth after the quartz growth.

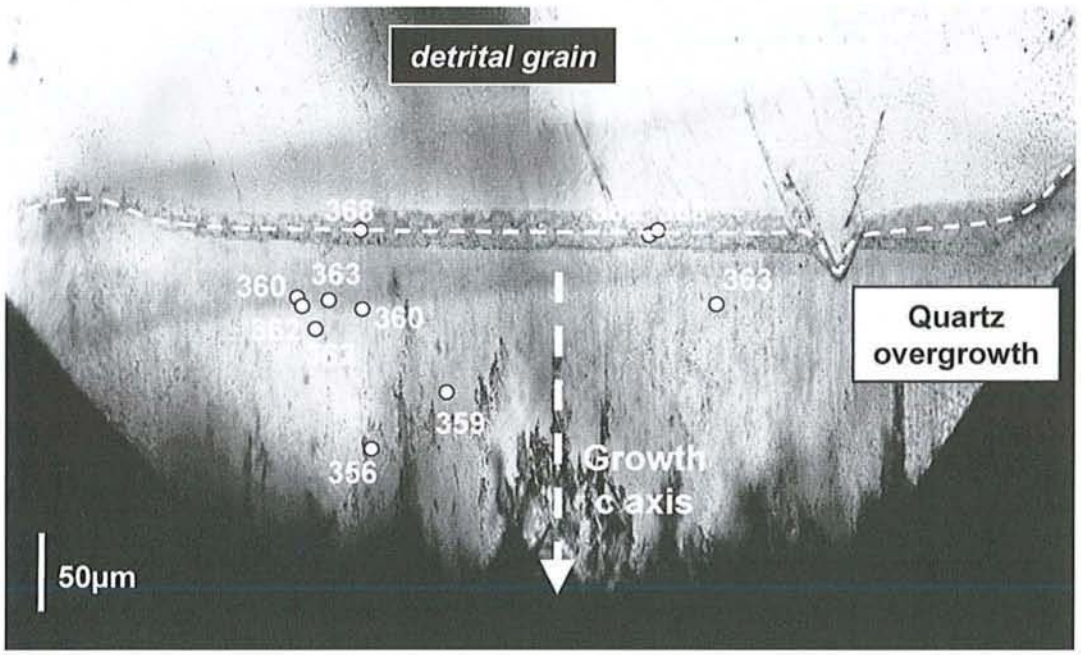

Figure C-11: 2-days evolution and characterization of a synthetic quartz overgrowth using corrected T_t of synthetic aqueous fluid inclusions (white circles).

In natural samples, T_t from microfractures and overgrowths are very similar, suggesting that the processes of healing and quartz growth have occurred in the same time. In some synthetic quartz samples, T_t of inclusions from microfractures are lower that the T_t of inclusions from the overgrowth. However, it does not prove that the aqueous solution could infiltrate the quartz microfractures after quartz overgrowth formation. Indeed, the morphology and the higher availability of water contained inside synthetic quartz compared to natural quartz should be taken into account. Moreover, most of studied inclusions are located at the quartz surface.

Besides the healing of synthetic quartz microfractures, all fluid inclusion formations seems to be halted just before the temperature step at 350°C (9^{th} day), suggesting that the solution were no more enough silica-sursaturated during and after this step.

7.6 Conclusion

Aqueous fluid inclusions have been synthesized within fluorite microfractures, quartz microfractures and quartz overgrowths. Two different experimental techniques and procedures have aimed to date the time formation of the fluid inclusions, within the minute for fluorite experiment using the T_m, and within the day for quartz experiment using the T_t. Thus, the time needed to heal cracks microfractures or create overgrowths can be estimated.

For fluorite experiments, results show that at temperature of 200°C, the fluorite/NH_4Cl solution equilibrium has been reached in 82 hours. Healing is a complex mechanism and does not appear to be linear or regular along the microfracture. Thus, it could explain the range of the T_m and the T_t range within a same fracture plan of natural samples.

For quartz experiments, the quartz/H_2O-NaCl solution equilibrium is faster reached for the synthetic quartz (1st day) than for natural quartz (6th day). This difference is linked to the hydration of the two types of quartz. The healing of quartz microfractures is overall prior to the quartz overgrowth formation and do not necessary need external silica supply as for quartz overgrowth. Therefore, it is likely possible that quartz microfractures of natural samples could be locally healed at low temperature as low as 50°C (Teinturier et al., 2002). The decrease of the T_t of synthetic fluid inclusions from the core-overgrowth boundary to the external part of the quartz overgrowth show that the growth of quartz is a progressive and constant process, which involve a silica sursaturated solution. No reequilibration process, any evidence of post-fluid infiltration after the quartz overgrowth formation has been observed.

References

Bodnar, R.J., and Vityk, M.O. (1994) Interpretation of microthermometric data for H_2O-NaCl fluid inclusions. In De Vivo, B. and Frezzotti, M.L. (eds.) Short Course of the Working Group (IMA) Fluid inclusions in minerals: Methods and Applications. Virginia Tech, Blacksburg, 117-130.

Brantley, S.L. (1992) The effect of fluid chemistry on quartz microcrack lifetimes. Earth and Planetary Science Letters, 113, 145-156.

Dubessy, J., Guillaume, D., Buschaert, S., Fabre, C., and Pironon, J. (2000) Production of synthetic fluid inclusions in the H_2O-CH_4-NaCl system using laser-ablation in fluorite and quartz. European Journal of Mineralogy, 12(6), 1083-1091.

Goldstein, R.H., and Reynolds, T.J. (1994) Systematics of fluid inclusions in diagenetic minerals. 212 p.

Guillaume, D., Teinturier, S., Dubessy, J., and Pironon, J. (2002) Calibration of methane analysis by Raman spectroscopy in H_2O-NaCl-CH_4 fluid inclusions. Validation using natural hydrocarbon and aqueous fluid inclusions. Chemical Geology (Special issues for XVIth ECROFI meeting), (in press).

Landais, P., Michels, R., and Poty, B. (1989) Pyrolysis of organic matter in cold-seal pressure autoclaves. Experimental approach and applications. Journal of Analytical and applied pyrolysis, 16, 103-115.

Linke, W.F. (1965) Solubilities of inorganic and metal-organic compounds. I and II, (4th edition). American Chemical Society, Washington, D. C.

Mallet, J.L. (1992) Discrete smooth interpolation in geometric modelling. Computer-Aided Design, 24, 178-191.

Sawaki, T., Sasada, M., Sasaki, M., Tsukimura, K., Hyodo, M., Okabe, T., Uchida, T., and Yagi, M. (1997) Synthetic fluid inclusion logging to measure temperatures and sample fluids in the Kakkonda geothermal field, Japan. Geothermics, 26(1), 281-303.

Smith, D.L., and Evans, B. (1984) Diffusional crack healing in quartz. Journal of Geophysical research, 89(b6), 4125-4135.

Teinturier, S., Pironon, J., and Walgenwitz, F. (2002) Fluid inclusions and PVTX modelling: Examples from the Garn Formation in well 6507 2/2, Haltenbanken, Mid-Norway. Marine and Petroleum Geology, *19(6), 755-765.*

Xie, Z., and Walther, J.V. (1993) Quartz solubilities in NaCl solutions with and without wollastonite at elevated temperatures and pressures. Geochimica et Cosmochimica Acta, 57, 1947-1955.

Zhang, Y.G., and Frantz, J.D. (1987) Determination of the homogenisation temperatures and densities of supercritical fluids in the system NaCl-KCl-CaCl2-H2O using synthetic fluid inclusions. Chemical Geology, 64, 335-350.

8 Article 5: EXPERIMENTAL DIAGENESIS OF QUARTZ IN PETROLEUM ENVIRONMENT. PART I: PROCEDURES AND FLUID TRAPPING

Un système expérimental silice-eau-huile-gaz a été mise au point dans le but de simuler la diagenèse siliceuse des réservoirs pétroliers naturels. Des inclusions aqueuses et hydrocarbonées ont été synthétisées dans des microfractures et des surcroissances de quartz dans divers rapport E/H (0; 5; 10; 20; 50 et 100%). Les expériences ont été réalisés dans un autoclave à pression de méthane jusqu'à des températures et pressions de 270°C et 212 bar et dans un autoclave à pression fluide jusqu'à 350°C et 400 bar. Ces conditions P-T relativement importantes ont permis de faire croître des auréoles dans un milieu à forte saturation d'huile (10 % < E/H < 50%). Des inclusions hydrocarbonées ont été synthétisées dans des microfractures de quartz (0<E/H<50%, 209-350°C; 175-400 bar), ainsi que dans des auréoles de croissance (10<E/H<50%, 289-350°C; 350-400 bar). Des inclusions aqueuses ont été synthétisées dans des microfractures de grains de quartz, en présence de méthane dès 150°C-200 bar, en présence d'hydrocarbures à partir de 184°C-163 bar. En présence d'hydrocarbures, dans les surcroissances, des inclusions aqueuses ont été synthétisées à partir de 277°C-330 bar. Les inclusions hydrocarbonées de synthèse sont représentatives de l'huile parent jusqu'à des températures et des pressions de 250°C-212 bar. A 350°C-400 bar, des processus de craquage ont été mis en évidence par spectroscopie IR. Par ailleurs, l'huile semble jouer un rôle de barrière entre l'eau et le gaz en inhibant les processus de diffusion du méthane dans l'eau.

EXPERIMENTAL DIAGENESIS OF QUARTZ IN PETROLEUM ENVIRONMENT. PART I: PROCEDURES AND FLUID TRAPPING

Stéphane TEINTURIER and Jacques PIRONON

**UMR G2R 7566 – (CREGU, CNRS, Université Henri Poincaré, INPL) BP239, F-54506 Vandœuvre-lès-Nancy Cedex, France.*

Soumis à Geochimica et Cosmochimica Acta

ABSTRACT

Silica-water-oil-gas system has been experimentally studied with the objective to simulate the diagenesis of siliceous petroleum reservoirs. Petroleum and aqueous inclusions in quartz microfractures and quartz overgrowths have been created in variable W/O proportions (0, 5, 10, 20, 50, 100%). Experiments were carried out in a gas-pressure autoclave under CH_4 pressure control, up to 250°C and 212 bar and in a fluid-pressure autoclave up to 350°C and 400bar. High p-T conditions have notably allowed the growth of quartz in high oil saturation level (10<W/O<50%). Petroleum inclusions have been synthesised inside quartz microfractures (0<W/O<50%, 209-350°C; 175-400 bar) and also inside quartz overgrowths (10<W/O<50%, 289-350°C; 350-400 bar). Aqueous inclusions have been synthesised in presence of oil inside quartz microfractures from 185°C-163 bar up to 400°C-400 bar and inside quartz overgrowth from 277°C-330 bar. Synthesised petroleum inclusions are representative of the parent oil up to 250°C. At 350°C, evidence of cracking process have been observed with the release of methane. On the other hand, it has been observed that the segregation of the oil/gas/water column inside the autoclave could prevent the methane diffusion into the water phase when oil is present. This experimental approach shows that an oil saturation of a reservoir should not prevent quartz diagenesis.

Keywords: experimental diagenesis, synthetic petroleum inclusions; quartz overgrowth

8.1 Introduction

In a quartz environment, petroleum and aqueous inclusions should be very useful to decipher the history of a natural petroleum reservoir. Unfortunately, quartz precipitation and fluid inclusions trapping are not always synchronous. The reequilibration, the necking of the fluid inclusions or the mode of trapping often prevents to separate or to determine precise relationship and chronology between the healing of fracture, the growth of quartz and the petroleum migration (Haszeldine and Osborne, 1993; Teinturier et al., 2002). Moreover, the eventual ability of petroleum emplacement to inhibit quartz cementation can be problematic. This question has been debated by many authors and depends mostly on the controls on silica transport from its source to precipitation (Worden and Morad, 2000). Petroleum inclusions inside quartz cements, similar homogenisation temperature ranges and/or relative similar volumes of cement or porosities between water and oil-saturated zones are the prime empirical arguments of authors who consider that oil emplacement does not halt quartz cementation (Dubina and Lakshtanov, 1997; Midtbo et al., 2000; Ramm, 1992; Saigal et al., 1992; Walderhaug, 1990). The concept that quartz cementation is inhibited by oil saturation is based on significant differences of porosity in some oil-bearing sandstones reservoirs (Dixon et al., 1989; Gluyas et al., 1993; Marchand et al., 2001). In that case, the presence of petroleum inclusions could be explained by possible quartz porosity filling after the formation of quartz overgrowths, especially at the core-overgrowth boundary (Barclay and Worden, 2000; Larese and Hall, 1996; Meunier, 1992).

Taking into account the numerous petroleum reservoirs studies, many problems or misunderstanding result from the lack of knowledge of the fluid inclusion formation processes when oil is present. In particularly, how the kinetic and chemical parameters control the fluid inclusion formation? What oil saturation is necessary to give rise to petroleum inclusions with or without aqueous inclusions during quartz cementation? Is the composition of petroleum inclusions representative of the original fluid composition? Are fluid inclusions inside quartz overgrowth representative of the growth of quartz? This paper aims to answer or argue these questions via an experimental approach with the objective of petroleum inclusions synthesis.

Since the first tests realised by Roedder and Kopp in 1975, numerous synthesis of fluid inclusions have been produced in quartz microfractures and/or quartz overgrowths (e.g. Shelton and Orville, 1980; Sterner and Bodnar, 1984; Bodnar and Sterner, 1985a;b; Zhang and Frantz, 1987; Dubois et al., 1994; Sawaki et al., 1997). These experiments have been carried out at different temperatures (175 to 1000°C) and pressures (P_{sat} to 7kbars) in different systems (pure H_2O, H_2O-NaCl, H_2O-NaOH, H_2O-LiCl, H_2O-CsCl, H_2O-KCl, H_2O-$CaCl_2$, H_2O-CO_2). The experimental time needed to form these aqueous inclusions was between 0 and 87 days. Other authors have synthesised fluid inclusions in the H_2O-NaCl-CH_4 system at temperatures from 150 to 600°C and pressures from 0.1 to 1kbar inside 30days (Lamb et al., 1996; Dubessy et al., 2000b; Guillaume et al., 2002). Regarding the synthesis of petroleum inclusions inside quartz, few

experiments have been realised. Larese and Hall (1996) have produced synthetic petroleum inclusions with a variety of pore fluids ranging from 100% aqueous to 100% oil, within quartz microfractures, dust rims and quartz overgrowth at 150, 325 and 360°C with a hydrostatic pressure of 690 bar over 12 days. Nevertheless, some of the rare dust-rims inclusions were sometimes incompletely sealed during the experiments, resulting in porous, permeable interfaces which were accessible to later pore fluids in spite of significant overgrowth formation. Vityk et al. (2001) have also produced synthetic petroleum inclusion but inside fractured core samples at 180°C and 480bar over 10 days. Their experimental observations notably suggest that oil saturation appears to play a secondary role in inclusion abundance and distribution. Beside quartz experiments, previous work on the synthesis of hydrocarbon inclusions have been also investigated in salt crystals (Pironon, 1990; Stasiuk and Snowdon, 1997) at low temperature (<200°C).

Through this study, we have tried to produce synthetic petroleum and aqueous fluid inclusions during quartz precipitation, i.e. the healing of microfracture and the quartz overgrowth. These fluid inclusions have been characterised by different techniques: microthermometry, confocal scanning laser microscope (CSLM), Raman & infrared microspectroscopies. They have been used to validate the modelling approach by PIT (Petroleum Inclusion Thermodynamics) software (Thiéry et al., 2000). This model leads to the PVTX reconstruction of the trapping conditions of petroleum fluid. Hence, the representativeness of fluid inclusions has been discussed.

8.2 Quartz samples

Experiments in autoclave have been realised on natural brazilian quartz fragments (<1 cm) and on synthetic quartz (sticks of 1 cm in length and a square section of 0.3 mm), which have been cut perpendicular to their growth c axis. Before run experiments, samples were heated at 700°C to eliminate eventual pre-existing inclusions. Quartz were then fractured by water soaking and dried for 6 hours at 80°C. After experiments, quartz were extracted from the aqueous and/or petroleum solution and cleaned with ethanol or dichloromethane. Quartz were manually and carefully polished to avoid quartz overgrowth and/or fluid inclusions destruction, especially near the quartz surface.

8.3 Dead oil

The dead oil used in the experiment comes from the Middle East. The oil is a paraffinic oil, which contains 44% of saturated hydrocarbon. The aromatic fraction is 32% and the polar fraction (asphaltenes and resins) is 24% (Teinturier et al., in review). Oil density is 878.5 Kg/m^3 at 15 °C. A large fraction of the dry and wet gas (C_2 à C_5) and especially the methane do not enter the oil

composition. Thus, the proportion of heavy alkanes is overestimated to its corresponding natural live oil.

8.4 Experimental procedure

The experimental cementation of quartz as well as the synthesis of fluid inclusions in the presence of variable proportions of petroleum or aqueous solution has been investigated at temperature and pressure up to 350°C and 400 bar on synthetic and natural Brazilian quartz crystals. Two types of autoclaves have been used, depending on the p-T conditions and autoclave limitations. Experiments with methane were carried out in a gas-pressure autoclave (GPA) up to 250°C and 212 bar. For higher temperature and pressure, experiments have been conducted into sealed gold bag, inside a fluid-pressure autoclave (FPA). Both types are ®Autoclave Engineering Closure trademarks.

8.4.1 Gas-pressure autoclave (GPA)

The experimental volume is connected to two tubes (Figure C-12): one tube extends into the liquid phase (V1) and the second ends in the vapour phase (V2). Additional gas pressure is given by a connected bottle of methane through V2. Temperature and pressure can be controlled and modified at any moment of the experiment. Previous works have shown that the major advantage of this autoclave is to maintain the equilibrium between liquid and vapour phases at run conditions (Dubessy et al., 2000b; Guillaume et al., 2002). Thus, it allows us to consider the homogenisation temperature (T_h) of an inclusion equal to the trapping temperature of the fluid inside the same inclusion (in an aqueous system). CH_4 is the only gas supplied to the aqueous solution and/or the dead oil.

Quartz samples are introduced into the autoclave with additional silica gel. When oil is present, the filling order can be modified (table C-5). Synthetic and natural quartz crystals are placed in the bottom of the autoclave. Some of the thicker synthetic quartz can bath both in the oil zone and the water zone. This last configuration allows to enhance the formation of aqueous and petroleum fluid inclusions in a same thick samples. Indeed, water and oil can access through the fracture network of the synthetic quartz. Methane is first introduced by the V1 tube entry to evacuate the air contained in the gas and liquid phase. Afterwards, the V2 tube is closed and the methane pressure is adjusted before the increase of temperature. The pressure inside the autoclave is thus higher than the saturated pressure in pure or chloride water.

At the end of the experiments, the autoclave is cooled to the ambient temperature in few hours and opened.

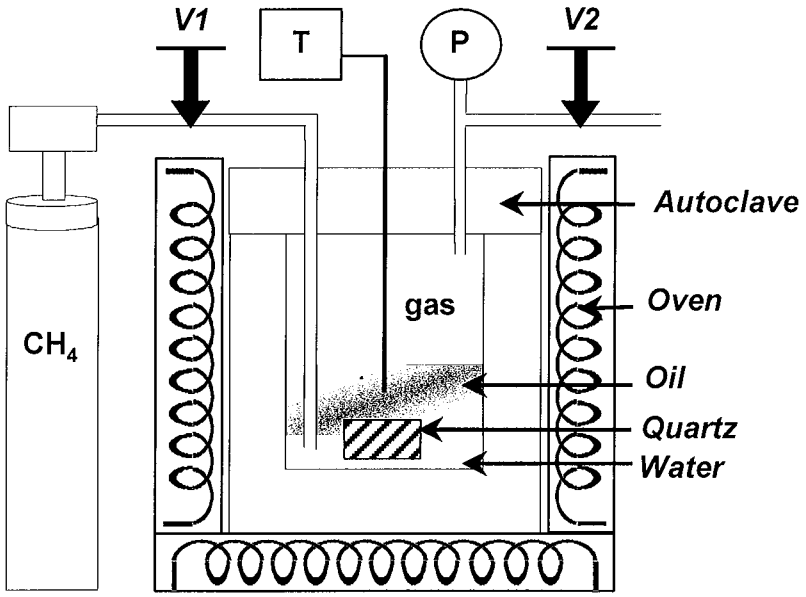

Figure C-12. Gas pressure autoclave (GPA).
V1: inlet valve, V2: outlet valve, T: thermocouple, P: manometer

8.4.2 Fluid-pressure autoclave (FPA)

In the fluid-pressure system, pressure is generated by a hydraulic pump and transmitted inside the autoclave by a water-oil mixture (®Hydraulub 16g/l) in a pressure line (Figure C-13). Quartz samples and the solution are put inside gold capsules (L=6 cm; i.d.=0.5 cm). Gold was chosen because it is chemically inert and has good thermal conductivity and malleability, which favours the temperature and pressure transfers. Temperature is controlled by two thermocouples. One is placed in the oven and the other one in the autoclave near the sample. Contrarily to the GPA system, no methane is supplied to the system. Fluid inclusions are synthesised in the monophasic liquid domain.

Gold tubes are welded at one end, then filled with the quartz samples, the silica gel and the solution. The other end is welded while the tube is cooled in liquid nitrogen in order to prevent any alteration or loss of the solution. When oil is present, this procedure is performed under inert argon atmosphere to avoid oxidation of oil during the capsule preparation and the experiments. Before loading the capsules into the autoclave, these ones are weighted before and after a short heat at 150°C for 2 hours. The capsules showing a weight difference of 0.2% are immediately removed. Temperature and pressure are reached and stabilised in few hours. P-T conditions can be controlled at any time of the experiments. At the end of the run, the autoclave is cooled in few hours. Capsules are cleaned with chloroform and weighted.

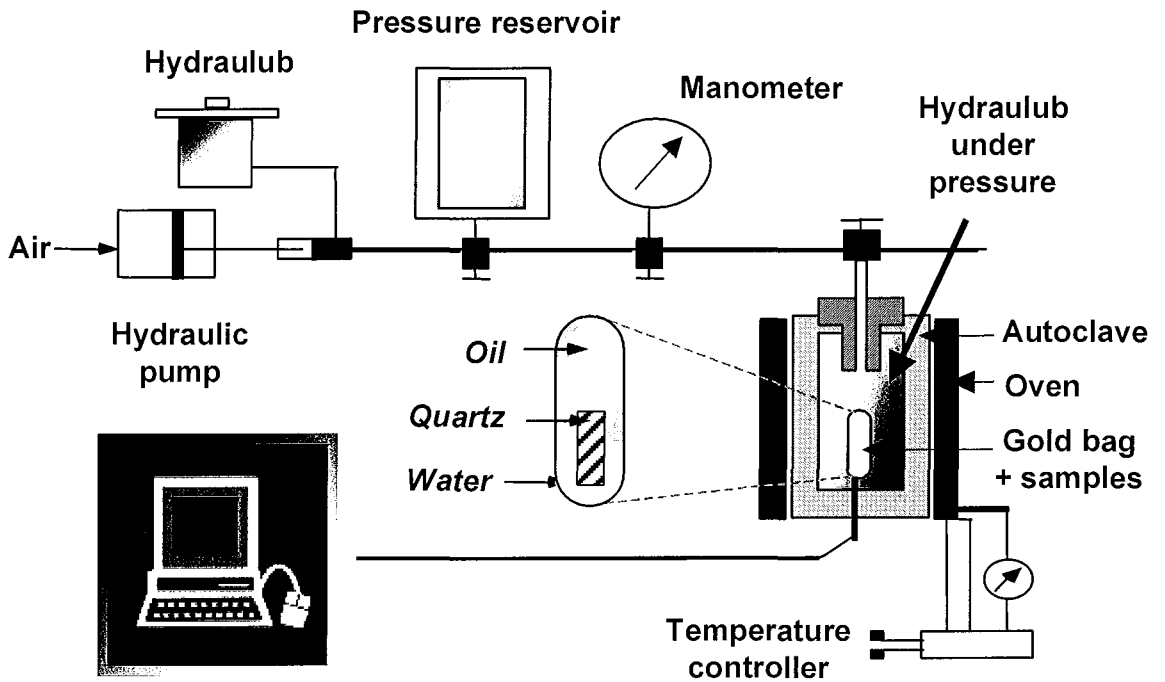

Figure C-13. Fluid-pressure autoclave (FPA).

8.4.3 Experimental conditions

Experimental conditions are shown in table C-5 for both type of autoclave. Experiments have been conducted in aqueous and/or petroleum system, with or without methane, with different ionic species such as NH_4^+, Cl^- or Na^+ and with silica gel. Different water/oil (W/O) ratio (0, 5, 10, 20, 50 and 100 wt% at 25°C) has been used and different order of filling of the autoclave has been tested. Thus, quartz samples are wetted with water or oil. For the most part of the experiments, the rate of quartz precipitation has been enhanced by varying the temperature and the pressure. Maximum pressure and temperature are maintained during 5 or 10 days to saturate the solution in silica. Then, temperature and pressure are gradually reduced step by step. This procedure aims to oversaturate the solution at each step and to thus enhance quartz precipitation and inclusion sealing. Experimental times are between 10 and 30 days. According to Tester et al. (1994), quartz solubility in pure liquid water increases with increasing pressure and temperature. For our p-T experimental condition range, the solubility of silica in NaCl solutions is higher than in pure water (Xie and Walther, 1993). The expected yield of quartz precipitation lies between 500 ppm at 250°C and 150 ppm at 150°C for the GPA experiments and around 1000 ppm at 350°C-400 bar for the FPA experiments. Thus, the formation of quartz overgrowth should be enhanced in the FPA system.

When oil is present, oxidation is partially avoided either by the evacuation of the air by a pressure transfer (GPA), either by a loading and a welding of gold capsules under inert

atmosphere (FPA). NH_4Cl have been sometimes used to maintain a redox potential thanks to the NH_4/N_2 equilibrium, which is similar to the hematite/magnetite buffer. Moreover, few amount of Fe^0 is always added to the solution to maintain a weak Eh at temperature around 250°C.

8.5 Analytical methods

All samples were inspected under a standard polarising microscope equipped with fluorescence accessories to locate and separate the aqueous inclusions from the petroleum inclusions. Petroleum inclusions were identified by their fluorescence under ultraviolet illumination. No barrier emission filter was used to enhance fluorescence detection.

8.5.1 Microthermometry

Microthermometric data have been acquired on a ®Chaix-Meca (Poty et al., 1976) for the melting temperatures (T_m), on an ®USGS (Goldstein and Reynolds, 1994) for the T_h and mainly on a ®Linkam MDS600 coupled to a PC video screen for the T_m and the T_h. Indeed, the measurement chamber of the ®Chaix-Meca and the ®USGS is enough large to contain thick samples, especially the synthetic quartz. Th measurement limit should be considered around +/- 5°C, which takes into account the potential thermal gradient between the thermocouple and the fluid inclusion area in thick quartz samples.

Stages were calibrated by pure CO_2 inclusions (T_m = -56.6°C) and low salinity synthetic aqueous inclusion (T_m = -0.4°C) at low temperature, and by melting of various crystals at positive temperatures. Phase transitions of oil and aqueous inclusions were observed with ®Olympus x50 and x80 objectives.

8.5.2 Raman microspectrometry

Methane detection and Raman quantitative analyses were performed on a ®Labram Dilor spectrometer using a 514.5 nm incident radiation produced by an argon laser coupled to an ®Olympus microscope equipped with a x80 objective and a ®Linkam heating stage. Methane concentration in the liquid phase at T_h was determined using the calibration of (Dubessy et al., 2000a; Guillaume et al., 2002). Accumulation time, laser power and confocal aperture were adapted for each inclusion measurement to obtain the best signal/background ratio.

8.5.3 Fourier transform infrared microspectrometry (FT-IR)

FT-IR spectra have been recorded using a ®Bruker Equinox 55 Fourier transform spectrometer equipped with a ®Bruker microscope. The mid-infrared range was reduced to 2000 cm^{-1} due to inclusion hosted quartz absorption. The infrared beam was narrowed to the bulk inclusion size with a variable diaphragm located in the image plane. The minimum aperture is 20 µm using a x15 objective and 8 µm using a x36 objective. The accumulation time is around 4 min and the spectral resolution is 4 cm^{-1}. Contributions of atmospheric H_2O and CO_2 were removed by subtraction of their independently recorded characteristic spectra. Before each inclusion measurement, a reference spectrum was recorded in the air. Quartz contribution was partially removed by subtraction of its FT-IR spectrum, recorded in an area neighbouring the inclusions, free of contaminants (fluid inclusions and organic matter). FT-IR spectra of dead oil have been obtained by placing small amount of oil between two CaF_2 slides polished sections. Analyses were made in transmission non-polarised mode.

Quantitative analysis of oils and petroleum inclusions was obtained according the method of Pironon et al. (2001) and only takes into account the alkanes, the CH_4 and the CO_2 content. CO_2 is detected at 2340 cm^{-1}, CH_4 at 2960, 3006 and 3050 cm^{-1}, alkanes (CH_2- and CH_3-) at 2860, 2877, 2930 and 2960 cm^{-1}.

8.5.4 Confocal Scanning Laser Microscopy (CSLM)

CSLM analyses were performed at the Institut de Biologie Moléculaire des Plantes (IBMP) of Strasbourg, using a ®Zeiss (LSM 510) apparatus. Spatial resolution of CSLM is near SEM resolution. Besides conventional transmission observations, two other modes of visualisation are used: (1) fluorescence mode using an incident laser radiation at λ_0=488nm and collecting emission of fluorescence at a longer wavelength of $\lambda>\lambda_0$. This mode is effective for liquid oil detection. (2) reflection mode using incident laser radiation and filter in front of the collecting photomultiplier, both at 637 nm. This mode is very sensitive to refractive index changes and is used for the detection of liquid water inside inclusions because oil and quartz have similar indices, higher than the liquid water index. Confocal planes are acquired with a 0.5 µm step and image processing was performed using Igor software (Pironon et al., 1998) for 3D reconstruction. Thus, the volume of the gas bubble (Fv), i.e the percentage of vapour inside the inclusion at a given temperature have been calculated. In some rare favourable cases, water phase has been estimated.

8.6 Results

8.6.1 Description of fluid inclusions

Synthetic petroleum, 3-phase petroleum and aqueous inclusions have been produced in synthetic quartz and natural brazilian quartz (Figure C-14 and table C-5). However, in the FPA system, few of them have been found in the Brazilian quartz compare to the synthetic quartz. Moreover, only very tiny and unsealed petroleum inclusions were found in the GPA system. Therefore, the study has been mainly focused on synthetic quartz, which seems to foster the quartz cementation.

Overall, petroleum inclusions have sizes between 5 and 30µm and often appear to be larger than aqueous inclusions. The largest petroleum inclusion has a maximum size of around 75 µm. Vapour-liquid (-water) ratio of fluid inclusions are almost constant, but more accurate data will be detailed further in the text (i.e. §8.6.5.).

Petroleum inclusions are located within healed microfractures (GPA and FPA experiments) and inside quartz overgrowth (FPA experiments only). Despite the absence of water in the F1 experiment (350°C-400 bar; W/O = 0%), rare and tiny petroleum inclusions have been observed within microfractures. It is not the case in the G4 experiment (250°C-200 bar; W/O = 0%). When quartz samples are first wetted by oil (G3 experiment), petroleum inclusions are very rare. Petroleum inclusions emplacement inside quartz overgrowth are mostly parallel (Figure C-14a,b) to the growth c axis of the quartz. According to the experiment, the W/O ratio and the degree of cementation, petroleum inclusions located within healed microfractures are often flat (Figure C-14d). It is noticeable by the darkness and the non-sphericity of their gas bubble at 25°C. Necking-down have been sometimes observed between a 2-phase and a 3-phase petroleum (containing water) inclusions and between aqueous and 3-phase petroleum inclusions. The smallest necked inclusions are depleted of a gas bubble.

Aqueous inclusions are mainly localised within healed microfractures (Figure C-14e), especially when samples are first wetted by water. Synthetic aqueous inclusions from the quartz overgrowth are sometimes tiny and monophasic.

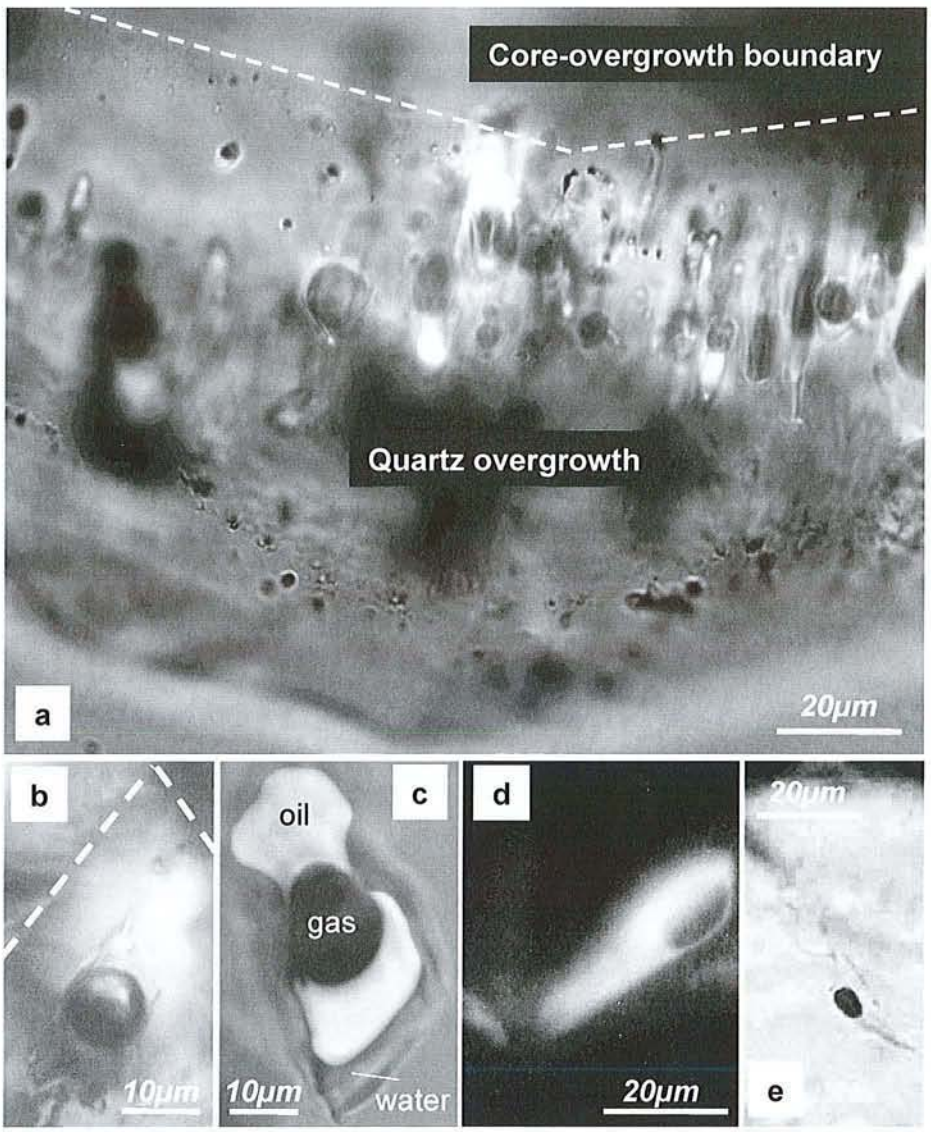

Figure C-14. Synthetic fluid inclusions in quartz (table C-5). a, b: petroleum inclusions inside quartz overgrowth, F3 experiment, W/O ratio = 10%, c: petroleum inclusions inside quartz microfractures F5 experiment, W/O ratio = 50% d,e: petroleum (d) and aqueous (e) inclusions within healed fractures, F2 experiment, W/O ratio = 10% All quartz are synthetic quartz except (b), which is a natural brazilian quartz

	Exp.	System[2]	Autoclave/bag filling order[3]	p-T conditions		Duration	W/O ratio	Quartz cementation		Fluid inclusions			CH_4
				Maximum	Minimum	(days)	(%)	HF[4]	QO[5]	Aqueous	Petroleum	Triphasic	aq. Inclusion[6]
Gas-pressure autoclave	G1[1]	CH_4+H_2O+NaCl	S-W	250°C-200bar	150°C-100bar	20	100	yes	pyr.	yes	-	-	saturated
	G2	HC+CH_4+H_2O+NH_4Cl	S-W-HC	250°C-212bar	150°C-141bar	30	10	yes	pyr.	yes	yes	-	undersaturated
	G3	HC+CH_4+H_2O+NH_4Cl	S-HC-W	250°C-209bar	150°C-136bar	30	20	yes	pyr.	yes	yes	-	not detected
	G4	HC+CH_4+H_2O+NH_4Cl	S-HC	250°C-200bar	150°C-200bar	25	0	no	no	no	no	-	-
	G5	HC+CH_4+H_2O+NaCl	S-W-HC	270°C-200bar		30	5	yes	pyr.	yes	yes	-	not detected
Fluid-pressure autoclave	F1	HC+H_2O+NaCl	S-W-HC	350°C-400bar		25	0	yes	pyr.	no	yes	-	-
	F2	HC+H_2O+NaCl	S-W-HC	350°C-400bar		25	5	yes	pyr.	yes	yes	-	not detected
	F3	HC+H_2O+NaCl	S-W-HC	350°C-400bar		25	10	yes	yes	yes	yes	yes	not detected
	F4	HC+H_2O+NaCl	S-W-HC	350°C-400bar		25	20	yes	yes	yes	yes	yes	not detected
	F5	HC+H_2O+NaCl	S-W-HC	350°C-400bar		25	50	yes	yes	yes	yes	yes	not detected
	F6	H_2O+NaCl	S-W	350°C-400bar		20	100	yes	yes	yes	-	-	-

Table C-5: General experimental conditions of the experiments realised in the gas-pressure autoclave and inside gold capsules (Fluid pressure autoclave). [1]Guillaume et al., (in press); [2]HC: dead oil; [3]S: quartz sample, W: aqueous solution, HC: dead oil; [4]HF: healing fracture; [5]QO: quartz overgrowth, pyr.: pyramidal quartz (weak growth); [6] Raman detection.

8.6.2 Microthermometry

Th diagrams are displayed on the figure C-15 for the GPA and the FPA experiments. Results show that for most of the experiments, Th values of synthetic aqueous and petroleum fluid inclusions are not homogeneous. Indeed, the spreading of Th mainly result from the p-T conditions drop imposed inside the GPA and the cooling of the FPA at the end of the experiments.

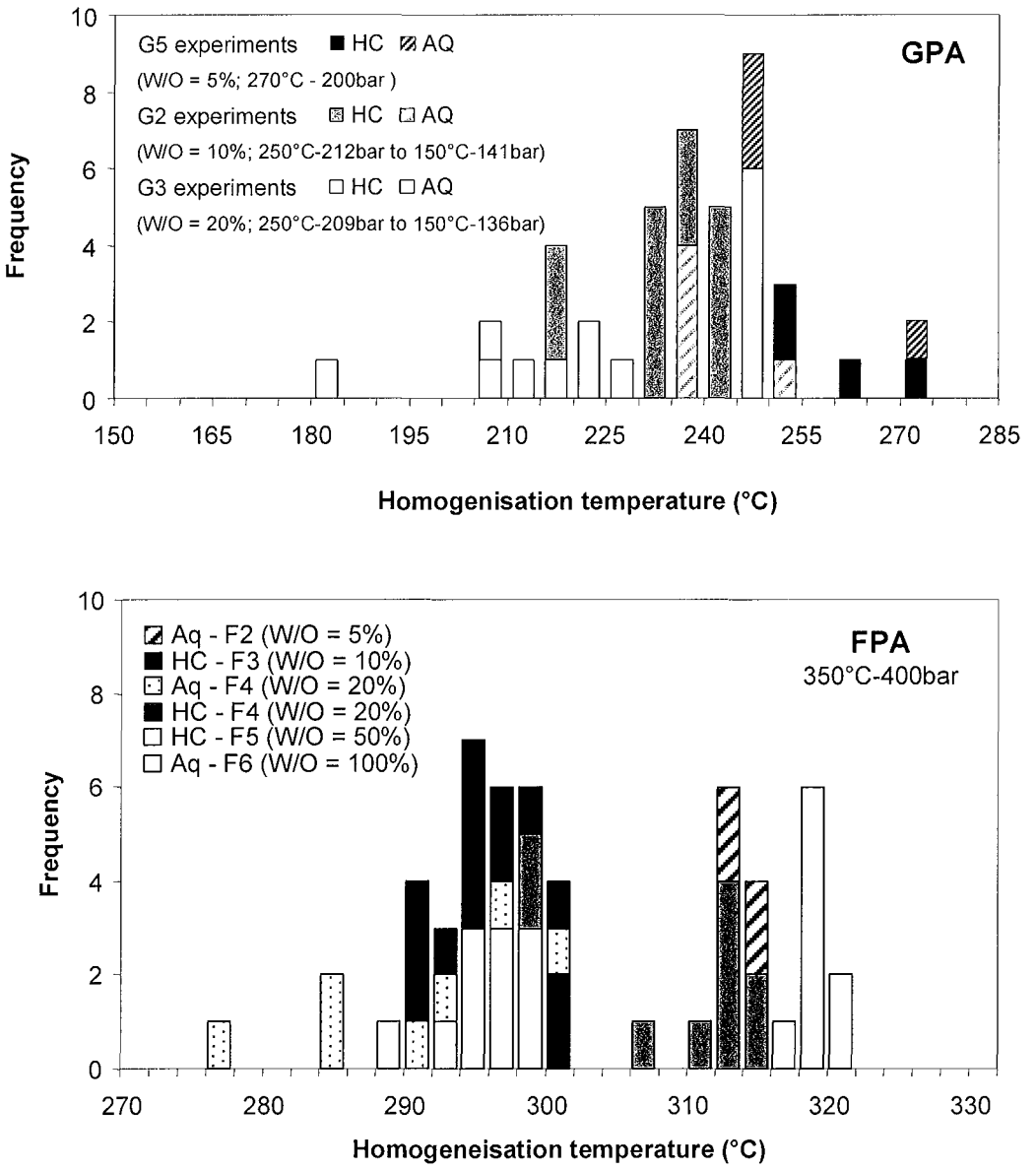

Figure C-15. Homogenisation temperatures

In the GPA experiments, the lowest and the highest measured T_h are respectively 209 (G5) and 274.6°C (G3) for synthetic petroleum inclusions and 184.6 (G3) and 270°C (G5) for synthetic aqueous inclusions.

In the FPA experiments, the maximum p-T trapping conditions of fluid inclusion are be at 350°C and 400 bar in the monophasic liquid domain. According to the EOS of Brown et al. (1989) and Zhang and Frantz (1987), the maximum T_h of our synthetic aqueous fluid inclusions should be respectively between 320 and 332°C with a NaCl salinity of 1 molal. Our maximal Th values are around 320°C. They belong to aqueous fluid inclusions trapped inside microfractures and quartz overgrowths (F6 experiments). Overall, aqueous or petroleum inclusions from quartz fracture have usually the highest T_h.

No evident correlation between the W/O ratio and the Th of aqueous and petroleum inclusions have been found for both type of experiments.

Few T_m have been measured for each experiment to verify the salinity of the aqueous fluid. T_m values are between -3.8 and -3°C, which correspond to the NaCl molality of the starting aqueous solution, around 1 molal.

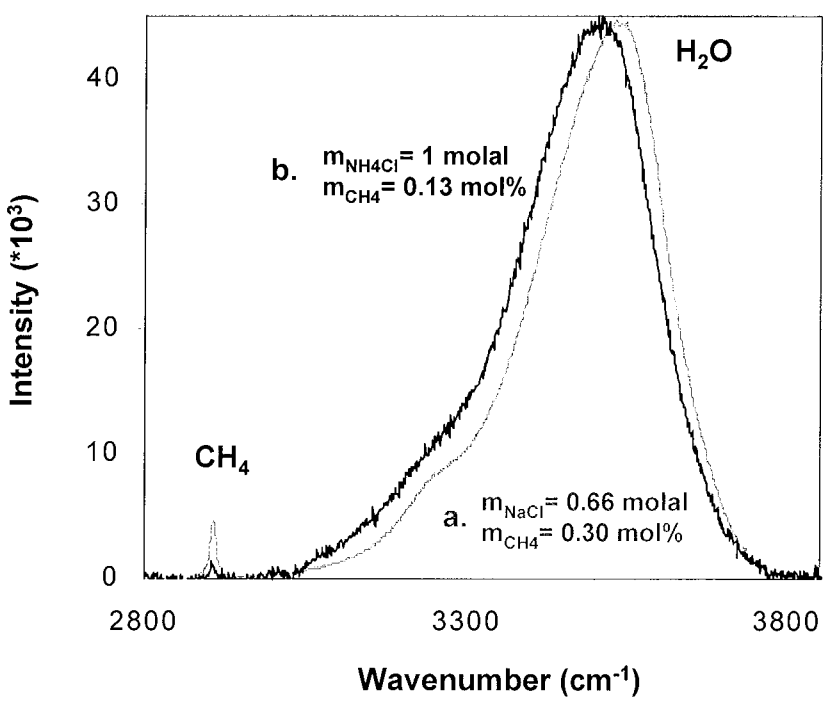

Figure C-16. Raman spectrum of synthetic aqueous inclusions in the liquid phase at T_h. Both have been trapped in the GPA with methane adjunction a. aqueous inclusion without petroleum oil A1 experiment, P-T_h = 234°C, 200bar b. aqueous inclusion coexisting with petroleum inclusions. A2 experiment, W/O = 10%, P-T_h = 237.3°C, 201bar

8.6.3 Raman microspectrometry

Methane of aqueous inclusions has only been detected within few samples. Figure C-16 shows two Raman spectra of two synthetic aqueous inclusions, which have been trapped inside quartz fracture inside the GPA (G1 and G2 experiments) with methane adjunction. Both have similar p-T trapping conditions but the inclusion a has been trapped in the H_2O-(NaCl)-CH_4 system and the aqueous inclusion b has been trapped in the H_2O-NH_4Cl-CH_4 system with petroleum. The presence of different ions explains the shift of the wavenumber of the maximum of intensity of the water stretching band. CH_4/H_2O ratio and thus methane concentration is lower when oil is present (mCH_4 = 0.13) than when oil is absent (mCH_4 = 0.30). Except for the G2 experiment, no methane has been detected inside aqueous inclusion when oil is present.

		Dead oil		Petroleum inclusions	
	before exp.	**G2 exp. (250°C-212bar)**	**F1 to F5 exp. (350°C-400bar)**	**G2 exp. 250°C-212bar**	**F1 to F5 exp. 350°C-400bar**
CH_2/CH_3	5.4 ±0.2	5.6 ±0.2	4.4 ±0.2	5.8 ±0.2	3.1±0.5
$[CH_4]_m$	0	-	-	30 ±5	20 ±5
$[CO_2]_m$	0	-	-	0	0.4 ±0.3
$[Alk]_m$	100	-	-	70 ±5	80 ±8

Table C-6: Mean values of the dead oil and petroleum inclusions composition from FT-IR data. Values are in mol%.

8.6.4 FT-IR

FT-IR analysis has been realised on individual petroleum inclusion and also on the original dead oil, before and after experiments (table C-6).

In the GPA experiments, results show that FT-IR spectra of petroleum inclusions (250°C-212 bar) are very similar to those obtained on the dead oil before and after the corresponding experiments. Indeed, they are characterised by similar mean CH_2/CH_3 ratios around 5.4. No water and no CO_2 have been found inside petroleum inclusions. Accurate analysis of spectra suggests that the starting oil has lost some sulphur compounds during the experiment.

In the FPA experiments, calculated CH_2/CH_3 ratios are different and non-constant. Mean CH_2/CH_3 ratios for the F1 to F5 experiments (350°C-400 bar) have been calculated around 3.1±0.5

for petroleum inclusion and around 4.4±0.2 for residual dead oil. This difference should be related to cracking processes during the experiments. Indeed, methane has been detected within the gas and the liquid phase inside synthetic petroleum inclusions, although methane has not been added to these experiments (Figure C-17). FT-IR spectrum of methane inside the gas phase of the inclusion shows its P, Q, R branches which are characteristic of gas at very low pressure. CO_2 content has been calculated around 0.4 ± 0.3 mol%, proving that oil have lost some C-O or C=O compounds. On the other hand, water (vapour and/or liquid) inside petroleum inclusion was difficult to quantify because of the absorption of the thick quartz samples.

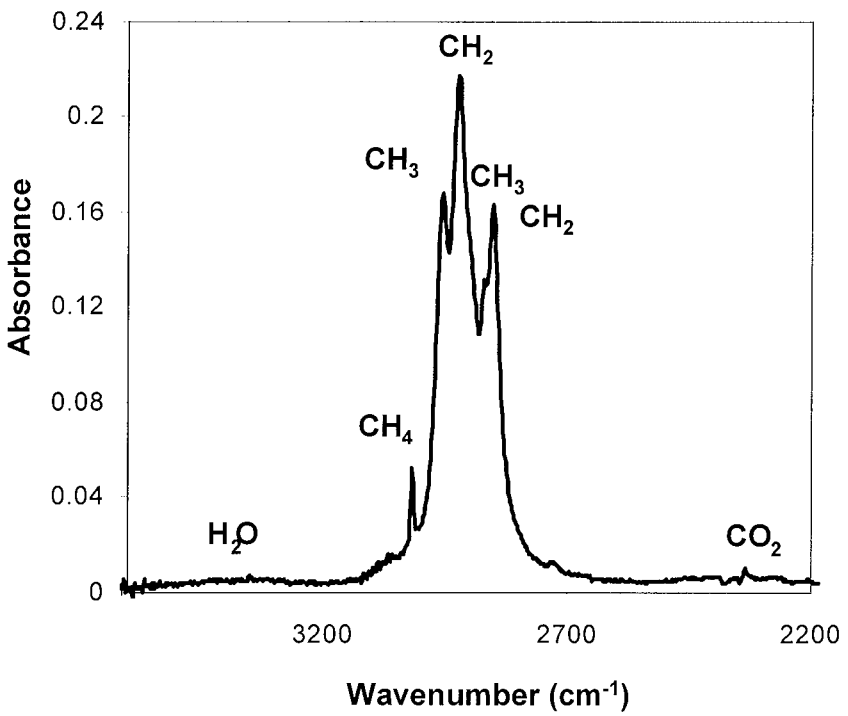

Figure C-17. FT-IR spectrum of a synthetic petroleum inclusion in the gas phase at 25°C showing the presence of methane and traces of CO_2. F3 experiment, W/O = 10%, P, T_{max} = 350°C- 400bar, T_h = 295°C.

8.6.5 CSLM

Some petroleum inclusions created with different W/O ratios (10, 20, 50) were analysed (Figure C-21). Maximum-recorded inclusion volume (oil and gas) is around 14000 μm^3 (F5 experiment, W/O = 50%) and minimum is 55 μm^3 (F3 experiments, W/O = 10%). Vapour percentage at 20°C for liquid petroleum inclusions varies from 10.1% to 29.5% for GPA experiments. CSLM observations or photomicrographs obtained in reflection mode reveals water inside petroleum inclusions that cannot be observed by conventional optical microscope (Figure

14c and C-20). Water proportion inside petroleum inclusion has been estimated in few inclusions. Values are between 27% (F4 experiments, W/O = 20%) and 35% (F5 experiment, W/O = 50%).

Volumetric calculations obtained from CSLM analysis clearly show a positive evolution of the F_v with the W/O ratio at 25°C imposed by the experimental conditions (Figure C-21). The more the water is present, the more the F_v is large.

8.7 Discussion

8.7.1 Effect of the W/O ratio on quartz cementation and fluid inclusion formation

Data from the literature show that water is always soluble in hydrocarbon whatever the nature of the hydrocarbon (Pironon et al., 2000). The concentration of water in hydrocarbon phase exponentially increases with temperature. Experimental data are very variable at high temperature and reaches about 1 wt% of the hydrocarbon phase at 150°C, 1.5 wt% at 200°C, 6 wt% at 250°C, 10 to 40 wt% at 300°C, 20 to 80 wt% at 350°C (Guerrant, 1964; Guillaume et al., 2001; Heidman et al., 1985; Kertes, 1989; Tsonopoulos and Wilson, 1983). Thus, in the GPA system, the dissolved water into oil will evolve with temperature from about 1 to 6 wt% of water. In the FPA system, all the water contained inside the capsules can be dissolved into a complex petroleum phase. This system should operate in a monophasic liquid domain.

Experiments carried out in the FPA (350°C-400bars) have partially answered the question of the (eventual) inhibition of quartz cementation with high oil saturation. Indeed, the quartz cementation process has been observed from a limited stage of growth, i.e. the healing of quartz microfractures (0% < W/O ratio < 50%), to the ultimate step of quartz growth, i.e. the formation of quartz overgrowth (10 % < W/O ratio < 50%). Larger overgrowths have reached up to 100 µm. Therefore, a high oil saturation (≤100%) does not prevent the quartz cementation to be formed at these p-T conditions.

The formation of petroleum inclusions is mainly related to the quartz cementation, to the wettability of the quartz samples, the p-T conditions and the W/O ratio. When quartz are first wetted or partially wetted by water, quartz cementation and thus the fluid inclusion formation are enhanced. Indeed, petroleum inclusions are very rare (G3 and F1 experiments) or non-existent (G4 experiments) when quartz samples are first wetted by oil. Most of petroleum and aqueous fluid inclusions have been synthesised just after the maximum p-T condition stage, during the decrease of temperature and pressure. Regarding the effect of the W/O ratio, what is the minimum water saturation that can yield petroleum inclusions during quartz cementation? Petroleum inclusions have been synthesised with a W/O from 5 to 20% in the GPA and from 0 to 50% in the FPA experiments. Nevertheless, when the W/O ratio is 0%, we cannot assert that water is totally absent. First, we think that the dead oil could contain very weak amount of dissolved water.

Second, synthetic quartz can contain irreducible water trapped inside its structure or inherited from the thermal fracturation of quartz during the water soaking.

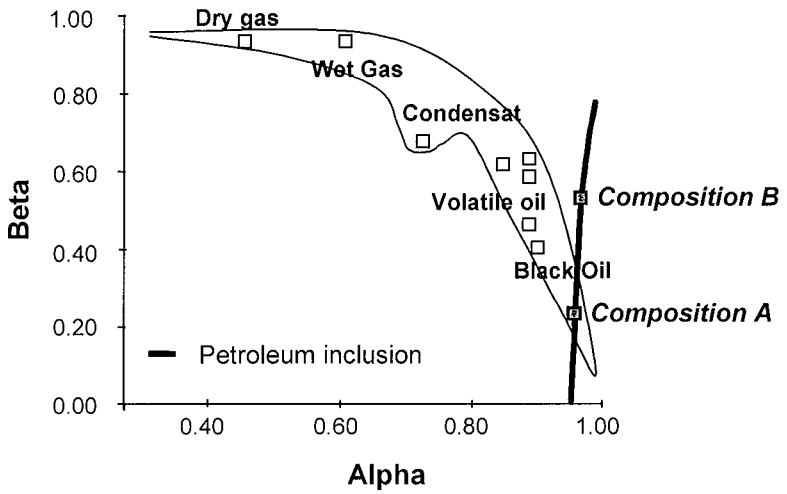

Figure C-18: α and β compositional diagram showing the trend of natural fluids from the dry gas to the black oil. PIT has modeled a α-β curve (black curve) for a synthetic petroleum inclusion.

8.7.2 PVTX reconstruction modelling

The aim of the PVTX reconstruction is (1) to restore the trapping P-T conditions of the oil inside the inclusion, (2) to generate a petroleum composition modelling which is consistent with the composition of the oil trapped inside the inclusion and then (3) to validate the model.

According to the experiments, oil trapped inside the petroleum inclusion could have different composition. For the GPA experiments, the petroleum should correspond to a mixture of heavy alkanes (the dead oil) with dry gas (methane). For the FPA experiments, the methane issued from the cracking processes is taken into account. Methane contents generated by the model are compared to those obtained in FT-IR. Note that PIT software does not take into account the presence of water inside petroleum inclusions. Therefore, PIT modelling results are only valid on GPA petroleum inclusions because they contain less than 1% of water whereas those from the FPA experiments contains a lot of water, which can modify the isochore of petroleum inclusion (Pironon et al., 2000).

The PIT (Petroleum Inclusion Thermodynamics) software (Thiéry et al., 2000) have then been used to reconstruct the trapping conditions of synthetic petroleum fluid and oil composition. Two approaches have been used.

The first approach uses the data from the synthetic petroleum inclusions as input parameters, i.e. the T_h, acquired by microthermometry and the F_v acquired by CSLM. In that case,

the P-T-X reconstruction modelled by PIT software is based on two parameters: α and β, which respectively represent the heavy fraction compounds (≥ C_{10}) and the methane plus the light alkanes. PIT modelling produces for each inclusion a series of α, β solutions intersecting the natural oil and gas trend (Figure C-18). First, α and β have been chosen at the intersect at point A. The isopleth issued from the α_A, β_A modelling does not fit with the experimental conditions of trapping (242°C -204 bars), the cricondenbar is located at 87 bar (Figure C-19). The related modelled composition is methane depleted. These results show that modelling A does not reproduce the experimental conditions and the oil composition. Second, in order to simulate the experimental isopleth, another α, β solution has been chosen (point B, figure C-18). It is located out of the natural oil and gas trend. In this case, the composition modelling gives a methane concentration of 26 mol%. This methane concentration is in good accordance with the methane concentration determined from infrared analyses (around 30 mol%). The composition B can be assimilated to a mixing of two fluids, one rich in methane and the other one rich in heavy compounds. It mimics the experimental fluid composition.

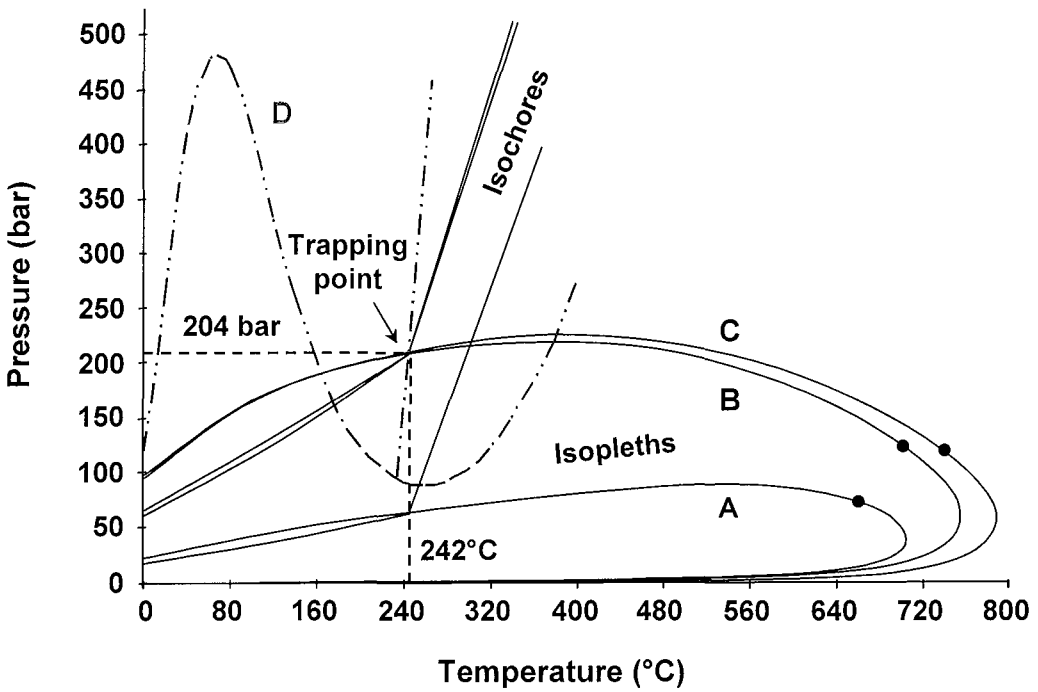

Figure C-19: P-T-X relationships from aqueous and petroleum systems. Isopleths and isochores of the petroleum fluids (A, B, C) are issued from PIT modelling whereas isopleth of the contemporaneous aqueous fluid (D) are drawn using Duan EOS. PIT modelling showing isopleths and isochores for an α-β chosen on the natural oil trend (A), out of the trend (B) and for the modified starting dead oil adjusted with 35 mol% of methane (C). B and C fit with the trapping conditions of the synthetic petroleum inclusion.

The second approach is based on a known oil composition. The dead oil composition is progressively enriched with methane until the P-T experimental conditions are reached. The necessary methane concentration appears to be 35 mol%. It is near the methane concentration measured by FT-IR.

The oil composition issued from modelling B is different to the composition of the experimental system (C). This is explained by the presence of more C_2-C_5 fraction in the modelling than in the experiment. Although the composition of B and C are different, both isopleths (B, C) are very similar up to 300°C. The approach by PIT modelling has been validated whatever the petroleum composition is. It can be used for mature oils, as for mixing of gas and oils.

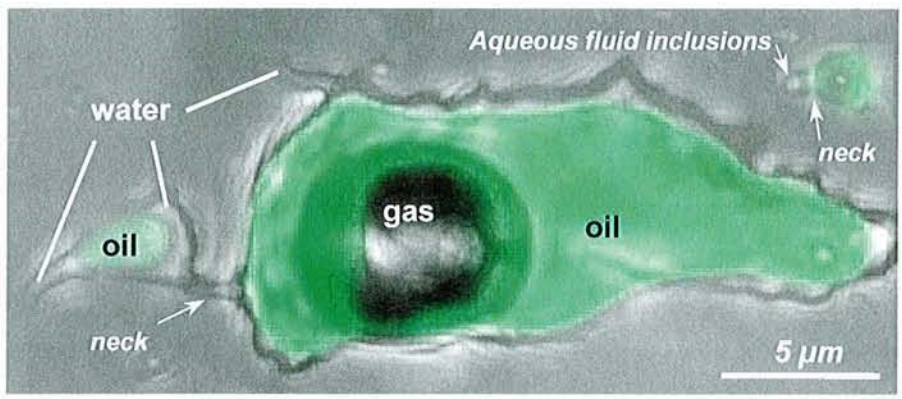

Figure C-20. CSLM microphotograph in transmission and fluorescence mode of two necked synthetic petroleum inclusions trapped inside a quartz microfracture.
F4 experiment, 350°C-400bar, W/O ratio = 20%

8.7.3 Representativeness of petroleum fluid inclusions

8.7.3.1 With the quartz cementation?

In complex natural petroleum reservoir, fluid inclusions from a same zone or a same quartz overgrowth often display variable T_h, variable composition, gas filling and morphologies, even if they are close to each other (Teinturier et al., 2002). According to the burial reservoir history, this difference should be explained by the combination of one or several processes: heterogeneous trapping or homogeneous trapping of different fluid migration at different times, necking down or reequilibration processes. Contrarily to the natural system, fluid inclusions from a same experiment have similar morphology, composition and oil/vapour ratio. Thus, our synthetic fluid inclusions should be representative of the quartz cementation on one p-T path. On the other hand, rare necking-down processes have been observed inside microfractures or inside quartz overgrowths (parallel to the c axis of growth) in the FPA system (Figure C-20). Indeed, when a 3-phase

petroleum inclusion is necked, the disconnected small inclusion, which usually contained water, seems to have migrated whereas its mother inclusion does not move. Unfortunately, the rarity of the necking-down process prevents to conclude if these inclusions migrate to the outer part or the inner part of the quartz overgrowth or during the cooling of the autoclave. Anyway, this hypothesis could explain the presence of tiny monophasic aqueous inclusions in the last part of the overgrowth, whereas petroleum inclusions are usually localised near the core-overgrowth boundary (Figure C-14a,b). The thermomigration of fluid inclusion have already been clearly observed in various KCl and NaCl crystals (Anthony and Cline, 1974; Muller, 1985) and in various crystals with oil (Kalyuzhny, 1982a). Liquid-filled inclusions can migrate up an imposed thermal gradient by dissolution at the hot inclusion wall and reprecipitation at the cold wall. Even this process cannot be visualised in real time in quartz, it could happen at high temperature and pressure (350°C-400 bar). Further investigations should be undertaken in that way.

8.7.3.2 With the starting oil composition?

The comparison of the FT-IR spectra of the oil before and after the experiments with the associated petroleum inclusions shows that in an experimental system, fluid inclusion composition is very similar to the initial oil composition up to 250ºC and 212 bar (GPA experiments). The PIT modelling of the oil inside synthetic petroleum inclusions based on the known composition of the starting dead oil goes in the same way. At higher temperature, i.e. at 350ºC-400 bar (FPA experiments), extracted dead oil and the oil inside the petroleum inclusions has evolved, notably during cracking process. Indeed, the composition and the distribution of oil have evolved to a relatively lighter oil, generating light alkanes and CH_4. Moreover, solid dark residues or bitumen have been formed since they are found in gold capsules after FPA experiments.

8.7.3.3 With the experimental W/O ratio?

Theoretical curve of the F_v evolution with the T_h has been drawn on the figure C-21, for the GPA (G2) and the FPA (F3, F4, F5) experimental conditions. This curve has been obtained using PIT software with the modelled composition of the oil of the petroleum inclusions from the GPA experiments. It does not take into account the presence of water and thus correspond to a W/O ratio of 0%. Overall, most of the measured F_v are higher than the theoretical F_v. This should be related to the presence of dissolved water in the petroleum phase and possibly to the methane enrichment with temperature or issued from cracking (only in the FPA system).

For the GPA system, measured F_v values of each petroleum inclusion lie between 10 and 16 vol%. They are in good accordance with the predictive data. Nevertheless, values of Fv at high T_h are higher than the modelling values. As seen before, the amount of dissolved water in the

petroleum phase drastically increases between 200 and 250°C, from 1 to 6 wt%. Therefore the more the temperature increase, the more the Fv will move off the modelling tendency.

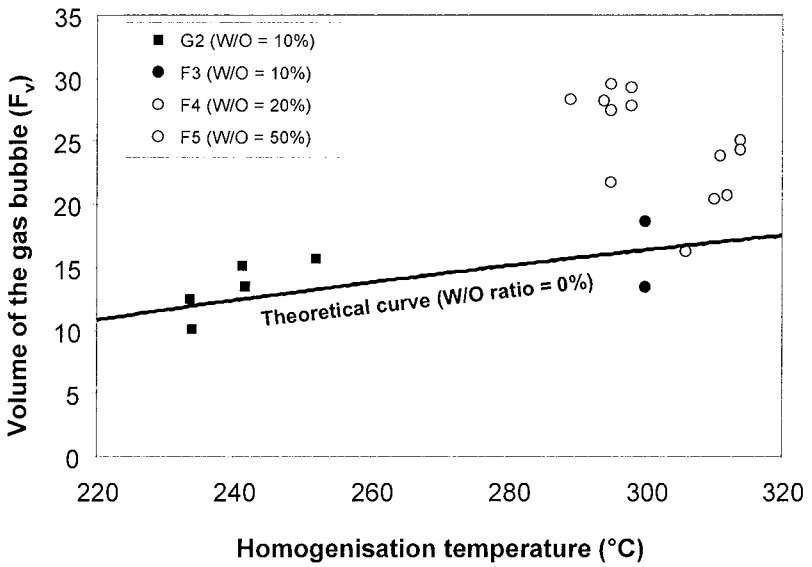

Figure C-21. F_v-T_h diagram of synthetic petroleum inclusions created in the GPA and in the FPA system for different W/O ratio (10, 20 and 50%). F_v values increase with increasing W/O ratio

For the FPA system, the variance of the measured Fv and the theoretical Fv increase with the W/O ratio. It is about ±2.6% with a W/O of 10%, from -0.8% to 8% with a W/O ratio of 20% and from 12.1 to 13.5% with a W/O ratio of 50%. In other terms, a W/O ratio of 10% corresponds to a measured F_v of 13 to 18%; a W/O ratio of 20% corresponds to a F_v of 16 to 25%; a W/O ratio of 50% corresponds to a F_v of 27 to 30%. Regarding the F3, F4 and F5 experiments, it seems that the W/O ratio plays a primary role in the evolution of the F_v compare to the temperature effect. Indeed, studied petroleum inclusions from the F5 experiments have lower T_h but higher F_v values. Bearing in mind that these experiments have been realised at high p-T conditions, water (vapour) can also be present in the gas phase. Unfortunately, FT-IR analysis of gas bubble is not enough sensitive to certify the presence of water vapour at low density and then low pressure.

Is the experimental W/O ratio representative of the F_v of the petroleum inclusions? At these p-T conditions and if we do not take into account the Th variation for a same population and taking mean measured F_v, we can say that a W/O ratio of 10 and 20% does not affect a lot the corresponding F_v of the petroleum inclusions. It is not true for a W/O ratio of 50%.

Is the W/O ratio imposed at the beginning of the experiment representative to the W/O ratio inside the trapped petroleum inclusions? To answer this key question, we should be able to precisely measure the W/O ratio inside the petroleum inclusions. However, at this time, it is not totally the case. The CSLM technique prevents to determine accurate water volume in reflection mode and our models do not take into account the water for the reconstruction of the isopleth, the

isochore and the oil composition, especially at these high p-T conditions. Moreover, observed necking-down and possible thermal migration of fluid inclusions could drastically modify the W/O.

8.7.4 The methane: where, when, why and how?

Regarding to the CH_4 and its concentrations inside synthetic aqueous and petroleum inclusions, singular phenomena have been observed. In the GPA experiments, aqueous inclusions are methane undersaturated or absent when oil is present. It seems like if oil plays a barrier role between the gas (upper) and the water (bottom) zones. In the FPA experiments, CH_4 has been produced during the experimental time. Indeed, CH_4 has been identified and quantified by FT-IR analysis inside synthetic petroleum inclusions although it was absent at the beginning of the experiments. A weak CH_4 content (around 20 mol%) has been calculated inside petroleum inclusions (FT-IR) whereas no methane have been detected inside aqueous inclusions (Raman) of corresponding experiments.

The absence or the under-saturation of methane inside aqueous inclusions should be related to the incomplete or the non-diffusion of methane into the aqueous phase. In other words, it seems possible that CH_4 diffusion inside water is limited, reduced or stopped by the presence of oil. If the convection processes inside the GPA system prevent to reach the equilibrium, the oil phase may be stratified from a heavy pole (at the water/oil interface) to a light pole (at the oil/gas interface). In this case, the water phase at the bottom of the autoclave should be equilibrated with the heaviest oil phase and not with the gas phase. In a p-T diagram, such behaviour should be characterised by the shifting of the aqueous isopleth to lower pressure as oil isopleth depleted with methane. However, the isochore of the aqueous inclusions should cross the trapping point of the contemporaneous petroleum inclusions (Figure C-19). In contrast, if the aqueous system was at the equilibrium with the petroleum system, the isopleth of the aqueous system should cross this trapping point. However, at these p-T conditions, the isopleth of the aqueous system reach its minimum values. The CH_4 molality of the aqueous inclusions in equilibrium with petroleum inclusions should be equal to 0.3 mol%.

The eventual effect of petroleum on methane diffusion into water phase could explain the variable methane content of aqueous inclusions in natural petroleum reservoir. Indeed, the segregation and the local variation of the oil/gas/water column could increase the possible inhibition of petroleum on gas diffusion into the water phase.

8.8 Conclusion

Silica-water-oil-gas system has been experimentally studied with the objective to simulate the diagenesis of siliceous petroleum reservoirs. Petroleum inclusions have been synthesised with different water/oil ratio (W/O) inside quartz microfractures (0<W/O<50%, 209-350°C; 175-400 bar) and also inside quartz overgrowths (10<W/O<50%, 289-350°C; 350-400 bar). Aqueous inclusions have been synthesised in presence of oil inside quartz microfractures from 185°C-163 bar up to 350°C-400 bar and inside quartz overgrowth from 277°C-330 bar. Synthesised petroleum inclusions are representative of the parent oil up to 250°C. At 350°C, evidence of cracking process have been observed with the release of methane. Moreover, observed necking-down and possible thermal migration of fluid inclusions could drastically modify the W/O of the inclusions.

Several implications to natural reservoir or case studies can be relevant. The presence of oil does not prevent quartz cementation from 185°C-163 bar up to 350°C and 400 bar for the duration of the experiment (<25days). It can be expected that similar conclusions could be formulated for P,T conditions of a natural petroleum reservoir and geological times. Moreover, high p-T conditions have notably allowed the growth of quartz in high oil saturation level (10%< W/O ratio < 50%). Therefore, a high oil-saturated petroleum reservoir can still evolve during burial history and petroleum migration can be reactivated from a reservoir to another with quartz growth. On the other hand, if the role of the petroleum barrier is valuable and justified, most of the aqueous inclusions associated to petroleum inclusions should be methane-undersaturated. The eventual effect of petroleum on methane diffusion into water phase could thus explain the variable methane content of aqueous inclusions in natural petroleum reservoir.

Such preliminary study could be the first step of new further developments on the studies of the siliceous diagenesis in petroleum environments. The presence of water in the petroleum phase has an incidence on the modelling of the isopleth and the isochore of petroleum inclusion, especially above 250°C where the solubility of water into the petroleum phase increases. The effect of the W/O ratio on the fluid inclusions PVTX properties should be further studied and integrated into thermodynamic model, especially if fluid inclusions are synthesised at high temperature. On the other hand, such approach could also be used to simulate and characterise the cracking process of the organic matter (Teinturier et al., in review). Finally, the interaction between oil, water and quartz, the physical and chemical mechanisms of quartz growth in high oil saturation could be studied. This will be developed in part II of this investigation.

Acknowledgements

We would like to express our special thanks to Frédéric Walgenwitz from TotalFinaElf for his helpful support. Jérôme Mutterer from IBMP (Strasbourg, France) is thanked for his active participation to CSLM analyses.

References

Anthony T. R. and Cline H. E. (1974) Thermomigration of liquid droplets in salt, 4th Symposium on Salt. *Northern Geological Society* 1, 313-321.

Barclay S. A. and Worden R. H. (2000) Effects of reservoir wettability on quartz cementation in oil fields. In *Quartz cementation in sandstones. Special publication of the International Assocation of Sedimentologists*, Vol. 29 (ed. W. R. H. a. M. S.), pp. 103-117.

Dixon S. A., Summers D. M., and Surdam R. C. (1989) Diagenesis and prservation of porosity in Norphlet Formation (Upper Jurassic), southern Alabama. *AAPG Bulletin* 73, 707-728.

Duan Z., Moller N., and J.H. W. (1992) An equation of state (EOS) for CH4, CO2 and H2O. *Geochimica et Cosmoschimica Acta* 56, 2605-2618.

Dubessy J., Buschaert S., Lamb W., Pironon J., and Thiery R. (2000a) Methane-bearing aqueous fluid inclusions: Raman analysis, thermodynamic modelling and application to petroleum basins. *Chemical Geology* 173(1-3), 193-205.

Dubessy J., Guillaume D., Buschaert S., Fabre C., and Pironon J. (2000b) Production of synthetic fluid inclusions in the H_2O-CH_4-NaCl system using laser-ablation in fluorite and quartz. *European Journal of Mineralogy* 12(6), 1083-1091.

Dubina E. O. and Lakshtanov L. (1997) A kinetic model of isotopic exchange in dissolution-precipitation processes. *Geochimica et Cosmochimica Acta* 61(11), 2265-2273.

Gluyas J. G., Robinson A. G., Emery D., Grant S. M., and Oxtoby N. H. (1993) The link between petroleum emplacement and sandstone cementation. *Petroleum Geology of Northwest Europe: Proceedings of the 4th Conference. J.R. Parker Ed.*, 1395-1402.

Goldstein R. H. and Reynolds T. J. (1994) *Systematics of fluid inclusions in diagenetic minerals.*

Guerrant R. P. (1964) Hydrocarbon-water solubilities at high temperatures under vapor-liquid-liquid equilibrium conditions, Pennsylvania State University.

Guillaume D., Teinturier S., Dubessy J., and Pironon J. (2002) Calibration of methane analysis by Raman spectroscopy in H2O-NaCl-CH4 fluid inclusions. Validation using natural hydrocarbon and aqueous fluid inclusions. *Chemical Geology* (Special issues for XVIth ECROFI meeting), (in press).

Guillaume D., Tkachenko S., Dubessy J., and Pironon J. (2001) High-temperature and high-pressure water solubility in ethylbenzene to 200°C and 1 kbar and the acetic acid effect. *Geochimica et Cosmochimica Acta* 65(19), 3319-3324.

Gunnarsson I. and Arnorsson S. (2000) Amorphous silica solubility and the thermodynamic properties of H_4SiO_4 in the range of O° to 350°C at P_{sat}. *Geochimica et Cosmochimica Acta* 64(13), 2295-2307.

Haszeldine R. S. and Osborne M. (1993) Fluid inclusion temperatures in diagenetic quartz reset by burial: implications for oil field cementation. *AAPG* 36, 35-46.

Heidman J. L., Tsonopoulos C., Brady C., and Wilson G. M. (1985) High-temperature mutual solubilities of hydrocarbons and water. Part II: ethylbenzene, ethylcyclohexane, and n-octane. *AIChE J.* 31, 376-384.

Kalyuzhny V. A. (1982a) *Principles of knowledge about mineral-forming fluids*.

Kertes A. S. (1989) Hydrocarbons with water and seawater. Part II: C8 to C36. *Pergamon Press, New York* 38.

Larese R. E. and Hall D. L. (1996) Studying Petroleum migration with fluid inclusions: results from hydrothermal burial simulation experiments. *PACROFI VI*, 74-75.

Marchand A. M. E., Haszeldine R. S., Smalley P. C., Macaulay C. I., and Fallick A. E. (2001) Evidence for reduced quartz-cementation rates in oil-filled sandstones. *Geology* 29(10), 915-918.

Meunier J. D. (1992) Precipitation of minerals between detrital quartz and quartz overgrowths in sandstones. *European Journal of Mineralogy* 4, 1401-1406.

Midtbo R. E. A., Rykkje J. M., and Ramm M. (2000) Deep burial diagenesis and reservoir quality along the eastern flank of the Viking Graben. Evidence for illitization and quartz cementation after hydrocarbon emplacement. *Clay Minerals* 35, 227-237.

Muller E. (1985) The transportation of brine inclusions in rock salt in a temperature field of a heat source. *Cryst. Res. Technol.* 20(5), 677-682.

Pironon J. (1990) Synthesis of hydrocarbon fluid inclusions at low temperature. *American Mineralogist* 75, 226-229.

Pironon J., Canals M., Dubessy J., Walgenwitz F., and Laplace-Builhe C. (1998) Volumetric reconstruction of individual oil inclusions by confocal scannig laser microscopy. *Eur. Journal Mineral.* 10, 1143-1150.

Pironon J., Thiéry R., Teinturier S., and Walgenwitz F. (2000) Water in petroleum inclusions: evidence from Raman and FT-IR measurements, PVT consequences. *Journal of Geochimical Exploration* 69-70, 663-668.

Poty B., Leroy J., and Jachimowicz L. (1976) Un nouvel appareil pour la mesure des températures sous le microscope: l'installation de microthermométrie Chaixmeca. *Bull. Soc. fr. Minéral. Cristallogr.* 99, 182-186.

Ramm M. (1992) Porosity-depth trends in reservoir sandstones: theoretical models related to Jurassic sandstones, offshore Norway. *Marine and Petroleum Geology* 9, 324-327.

Roedder E. and Kopp O. C. (1975) A check on the validity of the pressure correction in inclusion geothermometry, using hydrothermally grown quartz. *Fortschr. Mineral.* 52(Special), 431-446.

Saigal G., Bjorlykke K., and Larter S. (1992) The effects of oil Emplacement on diagenetic processes - Examples from the Fulmar reservoir sandstones, Central North Sea. *American Association of Petroleum Geologists Bulletin* 76(7), 1024-1033.

Stasiuk L. D. and Snowdon L. R. (1997) Fluorescence micro-spectrometry of synthetic and natural hydrocarbon fluid inclusions: crude oil chemistry, density and application to petroleum migration. *Applied Geochemistry* 12, 229-241.

Teinturier S., Elie M., and Pironon J. (in review) Evidence of oil cracking using synthetic petroleum inclusion. *Journal Of Geochimical Exploration.*

Teinturier S., Pironon J., and Walgenwitz F. (2002) Fluid inclusions and PVTX modelling: Examples from the Garn Formation in well 6507 2/2, Haltenbanken, Mid-Norway. *Marine and Petroleum Geology, 19(6), 755-765.*

Tester J. W., W.G. W., Robinson B. A., Grigsby C. O., and Feerer J. (1994) Correlating quartz dissolution kinetics in pure water from 25 to 625°C. *Geochimica et Cosmochimica Acta* 58(11), 2407-2420.

Thiéry R., Pironon J., Walgenwitz F., and Montel F. (2000) PIT (Petroleum Inclusion Thermodynamic): a new modeling tool for the characterization of hydrocarbon fluid inclusions from volumetric and microthermometric measurements. *Journal of Geochimical Exploration* 69-70, 701--704.

Tsonopoulos C. and Wilson G. M. (1983) High-temperature mutualsolubilities of hydrocarbons and water. Part I: benzene, cyclohexane and n-hexane. *AIChE J.* 61, 815-817.

Vityk M. O., Pottorf R. J., Gray G. G., Larese D., and Hall D. (2001) Application of synthetic fluid inclusions to hydrocarbon system analysis. *ECROFI XVI*, 455-456.

Walderhaug O. (1990) A fluid inclusion study of quartz-cemented sandstones from offshore mid-norway - possible evidence for continued quartz cementation during oil emplacement. *Journal of Sedimentary Petrology* 60(2), 203-210.

Worden R. H. and Morad S. (2000) Quartz cementation in oil field sandstones: a review of the key controversies. In *Special Publication Number 29 of the International Association of Sedimentologists* (ed. R. H. Worden, Morad, S.). Blackwell Science.

Worden R. H., Oxtoby N. H., and Smalley P. C. (1998) Can oil emplacement prevent quartz cementation in sandstones? *Petroleum Geoscience* 4, 129-137.

Xie Z. and Walther J. V. (1993) Quartz solubilities in NaCl solutions with and without wollastonite at elevated temperatures and pressures. *Geochimica et Cosmochimica Acta* 57, 1947-1955.

Zhang Y. G. and Frantz J. D. (1987) Determination of the homogenisation temperatures and densities of supercritical fluids in the system NaCl-KCl-CaCl2-H2O using synthetic fluid inclusions. *Chemical Geology* 64, 335-350.

9 Article 6: EXPERIMENTAL DIAGENESIS OF QUARTZ IN PETROLEUM ENVIRONMENT. PART II: SOLID-LIQUID (DIS)-EQUILIBRIUM

Le système expérimental silice-eau-huile-gaz a été étudiée avec l'objectif de simuler la diagenèse siliceuse des réservoirs pétroliers naturels. Les expériences ont été effectuées sur des quartz synthétiques et des quartz naturelles brésiliens. Des surcroissances de quartz ont été crées dans un système aqueux et également dans un milieu à forte saturation d'huile avec des quartz mouillés à l'eau. Les expériences menées dans un système H_2O-NaCl ont été effectuées de 400 à 300°C et 400 bar durant 20 jours. Les expériences menées dans un système H_2O-NaCl-huile ont été effectuées 350°C et 400 bar durant 25 jours. Ces dernières ont été réalisées dans des capsules d'or placées dans un autoclave à pression fluide. L'imagerie IR montre que pour les deux types de quartz, les surcroissances sont enrichies en eau par rapport aux grains. Des profils de $\delta^{18}O$ obtenus par sonde ionique ont été tracés à travers le grain et les surcroissances. Les résultats montrent que les valeurs de $\delta^{18}O$ obtenus dans les surcroissances crées dans un milieu eau-huile sont supérieures à celles crées dans un milieu strictement aqueux. Ces résultats sont reliés aux processus de fractionnement entre l'huile et l'eau au cours de la dissolution de l'eau dans l'huile. Dans un milieu à forte saturation en huile (E/H = 10%) et dans les conditions expérimentales (350°C -400 bar), la dissolution de la quasi-totalité de l'eau dans l'huile tend à prouver qu'un film d'eau (voire de l'eau irréductible) au contact du grain suffit à faire croître le quartz. Cette hypothèse n'est bien sûr valable que si l'eau reste le seul transporteur et vecteur de silice.

EXPERIMENTAL DIAGENESIS OF QUARTZ IN PETROLEUM ENVIRONMENT. II SOLID-LIQUID (DIS)-EQUILIBRIUM

Stéphane TEINTURIER[1], Jacques PIRONON[1], C. FRANCE LANORD[2]

[1]UMR G2R 7566 – (CREGU, CNRS, Université Henri Poincaré, INPL) BP239, F-54506 Vandœuvre-lès-Nancy Cedex, France

*** CRPG,15 rue Notre Dame des Pauvres 54501 Vandoeuvre lès Nancy France*

Geochimica et Cosmochimica Acta (en préparation)

ABSTRACT

Silica-water-oil-gas system has been experimentally studied with the objective to simulate the diagenesis of siliceous petroleum reservoirs. The experiments have been carried out on synthetic and natural Brazilian quartz. Quartz overgrowths have been created in an aqueous system and also in a high oil saturation system when quartz are water-wet. Experiments in H_2O-NaCl were carried out from 400 to 300°C and 400 bar during 20 days. Experiments in the H_2O-NaCl-petroleum system were carried out at 350°C and 400 bar during 25 days. All the experiments have been carried out in a fluid pressure autoclave. FT-IR imaging have shown that for both type of quartz, quartz overgrowths are enriched in water and silanol boundaries versus the quartz grain. SIMS $\delta^{18}O$ profiles have been obtained across the quartz grain and its overgrowth. Results show that $\delta^{18}O$ obtained in the overgrowth created in high oil saturation shows higher values that those created exclusively in a water system. This should be linked to fractionation processes between oil and water, during the dissolution of water into oil. In a high oil saturation (W/O = 10%) and in the experimental conditions (350°C-400 bar), results show that a simple water film is enough to give rise to quartz overgrowth. Indeed, water solubility should be extremely high at these p-T conditions. In this case, the water still remains.

Keywords: experimental diagenesis, oxygen isotope, IR imaging, water-oil fractionation, quartz overgrowth

9.1 Introduction

The physical and chemical mechanisms of quartz growth in petroleum environment still remain misunderstood. In natural reservoirs, quartz overgrowths are found both in water and petroleum zones (Ramm, 1992; Saigal et al., 1992; Walderhaug, 1990), depending on the silica availability and the controls on silica transport from its source to precipitation (Worden and Morad, 2000). However, some authors support the eventual ability of petroleum emplacement to inhibit quartz cementation, notably on the basis of significant differences of porosity in some oil-bearing sandstones reservoirs (Dixon et al., 1989; Gluyas et al., 1993; Marchand et al., 2001). In that case, the presence of petroleum inclusions inside quartz overgrowths could be explained by possible quartz porosity filling after the formation of quartz overgrowths, especially at the core-overgrowth boundary (Barclay and Worden, 2000; Larese and Hall, 1996; Meunier, 1992).

A way to study the mechanisms of quartz growth and silica transport concerns the oxygen (O) isotope analysis of diagenetic quartz. Data from literature show that $\delta^{18}O$ values of diagenetic quartz from reservoir sandstones are usually high and often higher in the overgrowth than its corresponding detrital quartz (table C-7). Indeed, low-temperature quartz should have high $\delta^{18}O$ values because the fractionation factors decrease with increasing temperature (Matsuhima et al., 1979; Zheng, 1993). Quartz overgrowths with high $\delta^{18}O$ values are usually assumed to precipitated from ^{18}O-rich basinal waters or at low temperature from meteoric waters. It has been notably assumed that the smectite-illite transformation occurring at depths between 2 and 4 km could increase the $\delta^{18}O$ of the formation fluid(s) up to positive values (Wilkinson et al., 1992). On the other hand, Aplin and Warren (1994) claimed that redistribution of silica could occurred on a local scale by both diffusion and local recycling of fluid, and not in response to large-scale episodes of fluid flow. In carbonate cements, Donovan et al. (1974) demonstrated that $\delta^{18}O$ values are extremely high when cements are spatially associated with seeping petroleum reservoirs (in Oklahoma). He suggests that the extremely high $\delta^{18}O$ values were the result of evaporation of groundwater due to natural gas expansion near the surface.

In diagenetic studies, the fractionation of O isotopes during crystal growth is commonly assumed to be an equilibrium process. However, some authors have shown that differences in $\delta^{18}O$ values between sectors along the same growth zone cannot result from variations in the O isotope composition of the fluid and strongly suggest disequilibrium partitioning of O isotopes between fluid and the growing crystal (Onasch and Vennemann, 1995). The variance between the $\delta^{18}O$ values from the detrital grain and its overgrowth strongly depends to the origin and the isotopic signature of the detrital quartz (Blatt, 1987) and the fluid(s) from which quartz overgrowth precipitated. Isotope compositions are however strongly affected by the mechanism of isotopic (re-) equilibration or fractionation. The usual cited mechanisms are the diffusion, the chemical reactions and/or the dissolution-precipitation processes occurring during the interaction of the fluid

phase with the mineral at a given p-T conditions (Cole et al., 1983; Dennis, 1984; Doremus, 1998; Dubina and Lakshtanov, 1997; Elphick et al., 1986; Giletti and Yund, 1984; McConnell, 1995). However, although these processes have been largely studied and discussed for a water-silica system, similar studies or experimental works in a water-silica-petroleum system are comparatively rare or non-existent at this time.

Sandstones or Formation	$\delta^{18}O$ values (‰) of quartz		References
	Detrital quartz	Quartz overgrowth (or cement)	
Glenelg, North Sea	12-17	20-23	Blanchet ,2002
Elgin, North Sea	5-12	20-21	Blanchet ,2002
Dunbar, North Sea	8-17	23-28	Blanchet ,2002
North Alwyn, North Sea	7-13	20-24	Blanchet ,2002
Rotliegende, North Sea	-	23	Lee et al., 1985
Brent, North Sea	-	17-21	Hogg et al., 1995; Aplin et al., 1993; Brint et al., 1991
Garn, Haltenbanken, Norwegian North Sea	6-24	13 to 28	Williams et al., 1997
Piper, UK North Sea	11	21-26	Lyon et al., 2000
South Brae, North Sea	-	21-25	Macaulay et al., 2000
Miller , UK North Sea	-	17 to 24	Marchand et al., 2000
Hill Field, North Sea	-	17-27	Girard et al., 2001
Penrith, northern England	11-14	26-31	Lyon et al., 2000
Frio, Gulf Coast	-	30-34	Milliken et al., 1981
Wilcox, Gulf Coast	-	23-31	Fisher and Land, 1986
Norphlet, Gulf Coast	13	18	McBride et al., 1987
Travis Peak, Gulf Coast	-	20-24	Dutton and L.S., 1988
Offshore, Gulf Coast	-	34	McBride, 1989
St Peter, Wisconsin Arch and Michigan basin	5-13	12 to 32	Graham et al., 1996
Spiro, Arkoma basin	10	18 to 22	Spotl et al., 2000
Belly River, Canada	-	13-18	Ayalon and Longstaffe, 1988
Kiskatinaw, Canada	5-25	20-34	Hervig et al., 1995
Viking, Alberta	-	16-27	Longstaffe and Ayalon, 1987
Falher and Cadomin, Alberta	-	15-18	Tilley and Longstaffe, 1989

Table C-7: Isotopic data from detrital and quartz overgrowth from (potential) petroleum reservoir.

This paper aims to better understand the mechanism of quartz growth in a relative simple experimental aqueous and petroleum system. Has the type of quartz an influence on the growth of quartz? Is the core-overgrowth accessible to later fluid after quartz growth? What are the interactions between the water, the oil phases and the quartz during its growth? Does the quartz contain any isotopic signature of the presence of the oil or the water during its growth?

Experimental approach developed in the Part I of our investigation of the diagenesis of quartz in petroleum environment (Teinturier and Pironon, in prep) has allowed to synthesised petroleum inclusions with different water/oil ratio (W/O) inside quartz microfractures (0<W/O<50%, 209-350°C) and also inside quartz overgrowths (10<W/O<50%, 289-350°C). Results have shown that the oil emplacement did not prevent the microfractures to be healed and the aqueous fluid inclusion formation between 185-350°C; 165-400 bar. Moreover, high p-T conditions of 350°C-400 bar have notably allowed the observation of relative large quartz overgrowths (<80µm). In this study, detrital quartz and quartz overgrowths from previous experiments (Teinturier and Pironon, in prep; Teinturier and Pironon, in review) were analysed by Fourier transform infrared microscopy imaging (FT-IR imaging), secondary ion mass spectrometry (SIMS) and cathodoluminescence (CL). These preliminary results should allow to propose a model of quartz growth and oxygen isotope fractionation (coefficient) in our water-petroleum system.

9.2 Material and experimental procedure

Quartz growth experiments were realised in an aqueous and in a high oil saturation system. All the experiments have been carried out inside gold capsules placed inside a fluid pressure autoclave. The experimental procedure and the fluid pressure autoclave system have already been described previously in the Part I of this investigation (Teinturier and Pironon, in prep) for the synthesis of petroleum inclusions in quartz microfractures and overgrowths. Experiments were realised on natural brazilian quartz fragments (NQ) and on synthetic quartz (SQ). The dead oil used in the experiment comes from Abu Dhabi, in the United Arab Emirates (Teinturier et al., in review).

Experiments in H_2O-NaCl on quartz samples (Q_{Aq}) were carried out during 20 days. Pressure was maintained at 400 bar during all the experiment time while temperature was gradually reduced from 400 to 300ºC to enhance quartz precipitation and fluid inclusion formation (Teinturier and Pironon, in prep; Teinturier and Pironon, in review). Experiments in H_2O-NaCl-oil on quartz samples (Q_{HC}) were carried out at 350°C and 400 bar during 25 days with a W/O ratio of 10%. During the capsule loading, quartz samples were first wetted by the aqueous solution, then by oil. The loading and the closure of gold capsules were performed under inert atmosphere to avoid the oxidation of the oil during the experiment. Moreover, few amount of Fe^0 was always added to the solution to maintain a weak Eh at elevated temperature.

9.3 Analytical procedure

All quartz samples were observed with conventional optical microscope in transmission and reflection mode and under ultra-violet (UV). Q_{Aq} were analysed by FT-IR imaging, SIMS and CL, whereas Q_{HC} were only analysed by SIMS and CL. FT-IR imaging is always acquired before SIMS because the resin coating of the studied Q_{HC} samples required for SIMS analyses prevent any further FT-IR imaging analysis without contamination of the overgrowths.

9.3.1 FT-IR imaging

FT-IR imaging is still a new technique applied for the understanding of the diagenetic history of petroleum rock samples (Pironon poster, PiroDonaTeintu, in prep). The conventional approach to analyse two-dimensional samples by FT-IR is to acquire sequentially single point spectra at defined locations from the sample. However, for the study of larger samples at a high spatial resolution this mapping technique is extremely time consuming. To overcome this hindrance, new FT-IR imaging instrumentation has been based on focal plane array detection systems. ®Bruker has equipped the ®IRscope II with the HYPERION™ detector. A sample area of 250 x 250 µm can be analysed simultaneously at a spatial resolution of 4 µm. Signal intensities at IR-frequencies, characteristic for certain functional groups can be plotted in 2-D-false colour plots versus the imaged sample area.

9.3.2 Oxygen isotope microanalysis by SIMS

In situ oxygen isotope microanalysis of quartz overgrowths was performed by secondary ion mass spectrometry (SIMS). This work was carried out on the Cameca IMS1270 at the Centre de Recherches Pétrographiques et Géochimiques (CRPG) of Nancy (France), following the approach by Hervig et al. (1995) and Girard et al. (2001). Quartz fragments were first mounted into an alumina ring filled with Araldite® resin and carefully polished to avoid any quartz overgrowth destruction. Measurements were then done on the polished mounted samples coated with gold by use of a ≈ 0.5 nA defocused primary ion beam of Cs+ (impact energy 20 keV) producing sub-circular ablation craters of ≈ 10–20 µm diameter. Positive charge build-up on the sample was neutralised by use of the Cameca normal-incidence electron flood gun. Oxygen isotope profiles were made across several overgrowths and their host detrital grains.

Determination of oxygen isotope ratios was performed as described in Mahon et al. (1998) and Girard et al. (2001) at a mass resolving power (M/ΔM) of about 5000. The secondary $^{16}O^-$ ions were measured on a Faraday cup (counting time = 4s) and the $^{18}O^-$ ions were counted on an

electron multiplier (counting time = 5s). Counting rates were corrected for deadtime and background. Instrumental mass fractionation (IMF) was corrected by repeated analysis of international (NL615 and BOG1) and laboratory (QZ-CWRU and QZ-BRA; Fouillac and Girard, 1996) standards. Measured ^{18}O values were corrected for IMF using the average IMF recorded by the analyses of standards before and after the SIMS profiles inside quartz overgrowth and grain. The standard deviation is between 0.1 and 0.6‰. Other results that overtake this deviation were rejected. Analyses of the quartz samples were performed within 3 days, over two analytical sessions, the 31/01, 01/02-2002 and the 03-05-2002.

9.3.3 Differentiation of quartz overgrowths from detrital quartz grains by CL-MEB and reflected light

The differentiation of quartz overgrowths from detrital quartz grains was performed using a classical reflected light microscope and also using a cathodoluminescence (CL) ®Oxford mono-CL detector mounted on a scanning electron microscope *(SEM)*. Samples were coated with carbon and observed using an accelerating voltage of 20-25kV and a probe current of 6 nA. Images were acquired at the Laboratoire commun d'analyses from the Nancy UHP University.

9.4 Results

9.4.1 FT-IR imaging

One SQ_{Aq} and one NQ_{Aq} samples have been investigated by FT-IR imaging. Only one infrared band has been selected from the transmission spectra and corresponds to the stretching vibrations of water and the hydroxyls groups. The corresponding wavelength range is located between 3000-3730 cm^{-1}. False colours are used to represent the intensity variations of the chosen absorption IR band.

For both type of quartz, quartz overgrowths are enriched in water and silanol boundaries versus the quartz grain (Figure C-22). For NQ_{Aq} sample, intensity variations of the water and silanol IR band is well marked from the inner to the outer part of the overgrowth. In contrast, the transition from the core to the quartz overgrowth of the SQ_{Aq} sample is more continuous. However, these interpretations should be related to the type, the geometry of quartz overgrowth with depth and to the scale of observation. Although the polishing of quartz samples do not prevent any quartz overgrowth destruction and that silica gel supply can differ from a capsule to another, SQ_{Aq} overgrowths (144 to 365µm) are always larger than NQ_{Aq} overgrowths (81 to 180µm) in a same capsule (Figure C-23). The reason is that SQ_{Aq} is basically more hydrated and have higher silanol

concentration than NQ_{Aq} (Giletti and Yund, 1984). Therefore, larger SQ_{Aq} overgrowths allow a large-scale observation. Second, regarding the geometry of the SQ_{Aq} overgrowth on figure C-25b.

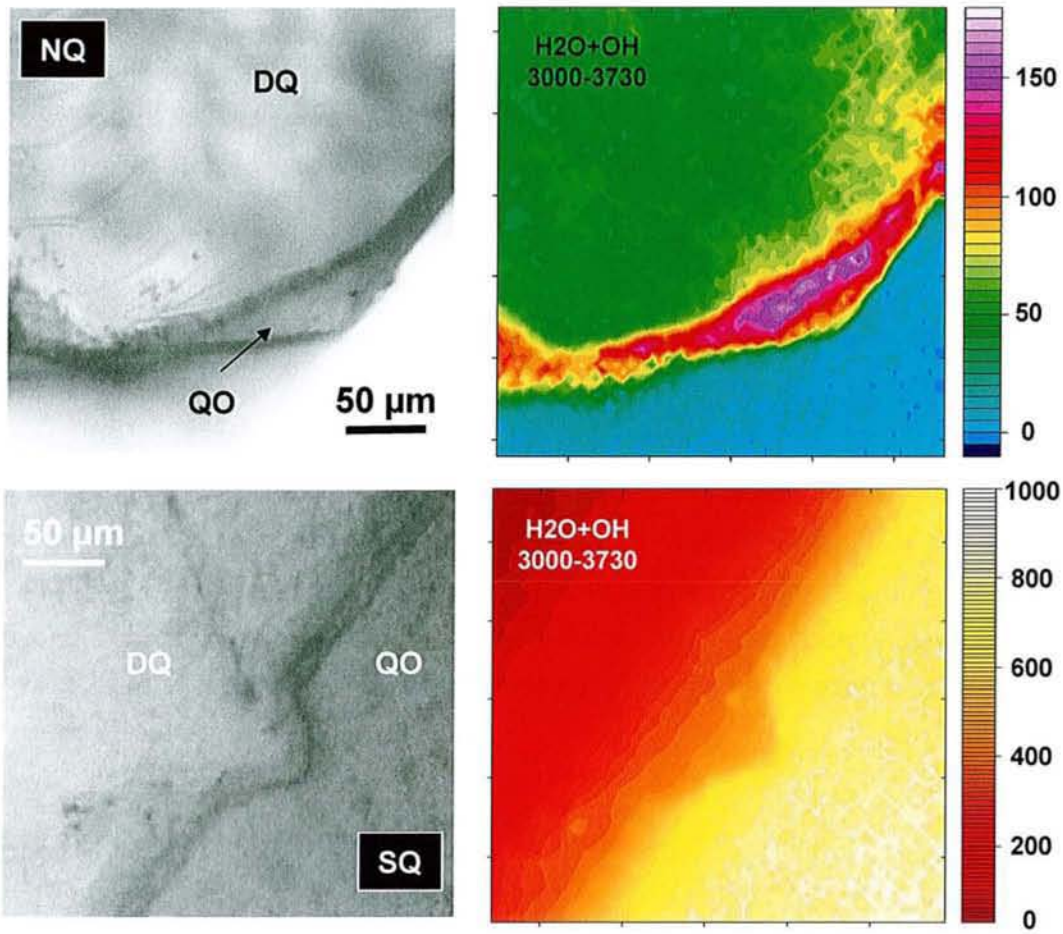

Figure C-22: FT-IR imaging,of the core-overgrowth boundary of a synthetic (SQ_{Aq}) and natural brazilian (NQ_{Aq}) quartz T=400 to 300°C; P=400 bar; W/O ratio = 100%

9.4.2 SIMS analyses

9.4.2.1 Water system

Four SQ_{Aq} and four NQ_{Aq} $\delta^{18}O$ profiles were respectively obtained across a detrital grain and its overgrowth (Figure C-24 and C-25). Histograms of the figure C-27 display the whole $\delta^{18}O_{SMOW}$ values obtained in the aqueous system for the two different experimental p-T conditions, at 400-300°C, 400 bar (Figure C-27a) and at 350°C-400 bar (Figure C27b). The $\delta^{18}O$ of the aqueous solution before the experiment is -7.8±0.1‰.

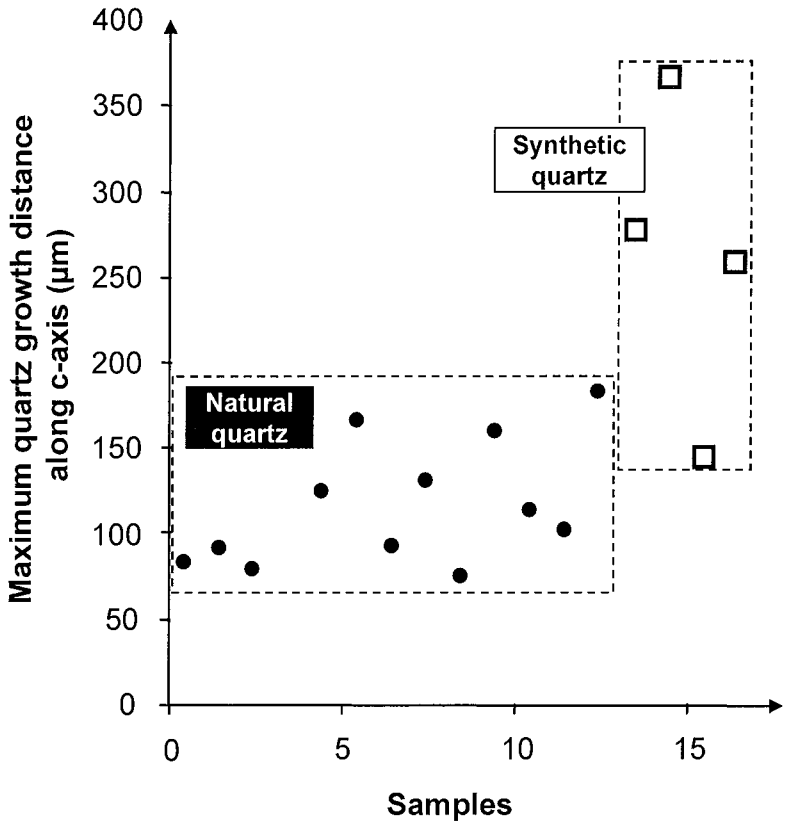

Figure C-23: Maximum quartz growth distance along c-axis (µm) Variable values are due to polished steps of the samples T=400 to 300°C; P=400 bar; W/O ratio = 100%.

Regarding the experiment carried out at 400-300°C and 400 bar, the mean $\delta^{18}O$ value (Figure C-27a) obtained from the SQ_{Aq} profiles is -0.3‰ for the detrital grain and -3.02‰ for the quartz overgrowth. The mean $\delta^{18}O$ value (Figure C-27a) obtained from the NQ_{Aq} profiles is +16.7‰ for the detrital grain and -1.1‰ for the quartz overgrowth. Contribution of the grain-overgrowth overlapping is clearly identified for SIMS craters located at the core-overgrowth boundary. This phenomenon is observed on the figure C-24a with $\delta^{18}O$ at +7.79‰. Regarding the profiles obtained for the both type of quartz, there is no evidence of a continuous decrease of the $\delta^{18}O$ from the core-rim to the external part of overgrowth. However, in most cases, the minimum $\delta^{18}O$ compositions are usually reported in the external part of quartz overgrowth. These extreme $\delta^{18}O$ values are -5.64‰ for SQ_{Aq} and -2.48‰ for NQ_{Aq}. For the experiment carried out at 350°C and 400 bar, the mean $\delta^{18}O$ value (Figure C27b) obtained from the NQ_{Aq} profiles is +17.1‰ for the detrital grain and +0.4‰ (minimum value is -1.2‰) for the quartz overgrowth. No $\delta^{18}O$ values have been obtained for SQ_{Aq} at 350°C-400 bar. However, there is few difference between the experiment A and B, indeed, they are similar experimental temperature, same pressure and aqueous fluid.

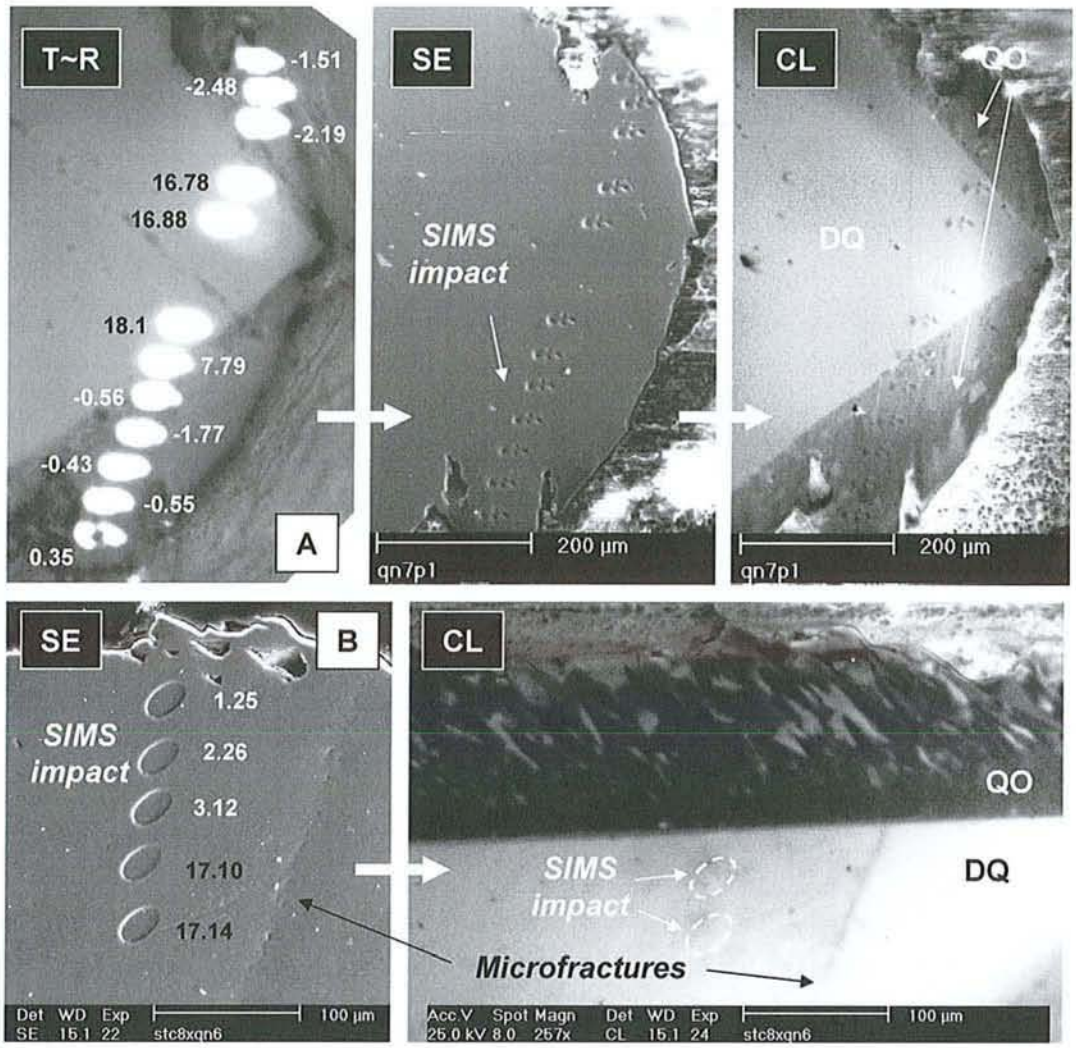

Figure C-24: Photomicrographs of two natural brazilian (NQ_{Aq}) quartz and their overgrowths (QO) under a mixing of transmitted (T) and reflected (R) light, in cathodoluminescence (CL) and in a secondary electron (SE) mode. SIMS craters are here printed on the quartz gold coating.

A - $\delta^{18}O_{SMOW}$ values are maximum in the quartz grain (~+17.25‰) and minimum in the overgrowth (~-1‰). T=400 to 300°C; P=400 bar; W/O ratio = 100%

B - $\delta^{18}O_{SMOW}$ values are maximum in the quartz grain (~+17.12‰). Positive values of the $\delta^{18}O_{SMOW}$ inside overgrowth (~+2.21‰) should be correlated to the geometry of the overgrowth and/or the contribution of the detrital isotopic signature of the natural quartz.

T=350°C; P=400 bar; W/O ratio = 100%

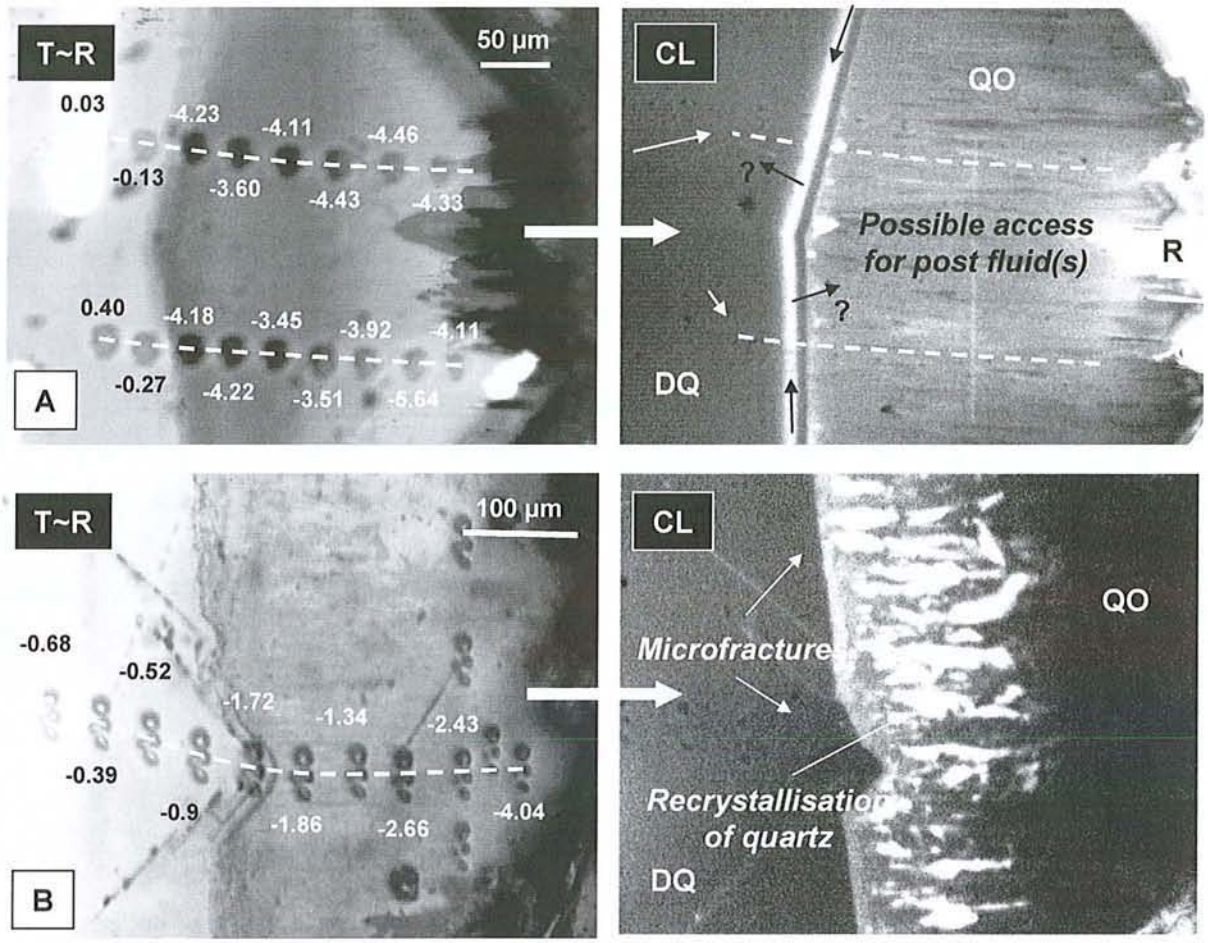

Figure C-25: Photomicrography of a synthetic quartz and its overgrowth under a mixing of transmitted (T) and reflected (R) light, and in cathodoluminescence (CL). SIMS craters are here printed on the quartz gold coating.

A - $\delta^{18}O_{SMOW}$ values are lower at the core-overgrowth boundary (~-4.2‰) and in the external part of quartz overgrowth (~-4.8‰). $\delta^{18}O$ values are around 0‰ in the detrital grain. CL image suggests that the core-overgrowth boundary is a possible porous transit for fluids or post-fluids. Indeed, the luminescence of this core-overgrowth boundary is similar to the resin (R) luminescence.

B - $\delta^{18}O_{SMOW}$ values are maximum in the quartz grain (DQ) (~-0.6‰) and minimum in the overgrowth (~-2.4‰). CL image suggests possible quartz re-crystallisation near the core-overgrowth boundary (white textures), resulting in the heterogeneous values of $\delta^{18}O_{SMOW}$ due to the re-equilibration of detrital and fluid/overgrowth isotopic signature.

T=400 to 300°C; P=400 bar; W/O ratio = 100%

9.4.2.2 Water-petroleum system

Two $\delta^{18}O$ profiles from SQ_{HC} were obtained across a detrital grain and its overgrowth (Figure C-26). Histogram of the figure C-27b displays the whole $\delta^{18}O$ values obtained in the petroleum system at 350°C-400 bar with a W/O ratio of 10%. Quartz overgrowths of the NQ_{HC} samples are smaller than the NQ_{Aq} samples, therefore, SIMS profiles cannot be performed.

The mean $\delta^{18}O$ values (Figure C27b) obtained from the SQ_{HC} profiles are +0.36‰ for the detrital grain and +8.69‰ (maximum 9.17%) for the quartz overgrowth (Figure C-26). Values inside quartz overgrowth are fairly homogenous. SIMS impact overlapping the overgrowth and the core grain has an intermediate $\delta^{18}O$ value equal to +4.43‰.

9.4.3 CL observations

9.4.3.1 Water system

The luminescence of NQ_{Aq} and SQ_{Aq} overgrowths is mostly darker than its corresponding detrital grains (Figure C-24 and C-25). NQ_{Aq} and SQ_{Aq} overgrowths texture is characterised by an alternate bedding of relative thin white or grey slots parallel to the c-axis. CL images of SQ_{Aq} samples of the figure 4 show two continuous core-overgrowth boundaries of 10--20µm width, which, in figure C-25b, goes rounds a junction of two microfractures extending in the core grain via a triangle shape. The luminescence of the core-overgrowth boundary of figure 4-A is fairly similar to the luminescence of the resin (R) luminescence, suggesting possible fluid or post-fluids circulation along this boundary. On the other hand, the texture of the overgrowth is often heterogeneous near the core-overgrowth boundary (Figure C-25b), suggesting lattice defect during the growth with possible infiltration of fluid from the core-overgrowth boundary, or local recrystallisation of quartz.

9.4.3.2 Water-petroleum system

The luminescence of SQ_{HC} overgrowths is lighter than its corresponding detrital grains (Figure C-26). CL images of the SQ_{HC} samples do not show evidence of the alternation of dark or grey slots like in the water system. However, SE and CL images show that the overgrowth can carries few holes or pits, which can be identified as petroleum inclusions. Moreover, microfractures crossing the core grain and a part of the overgrowth can be observed, assuming the possibility of oil to reach inner part of the core grain.

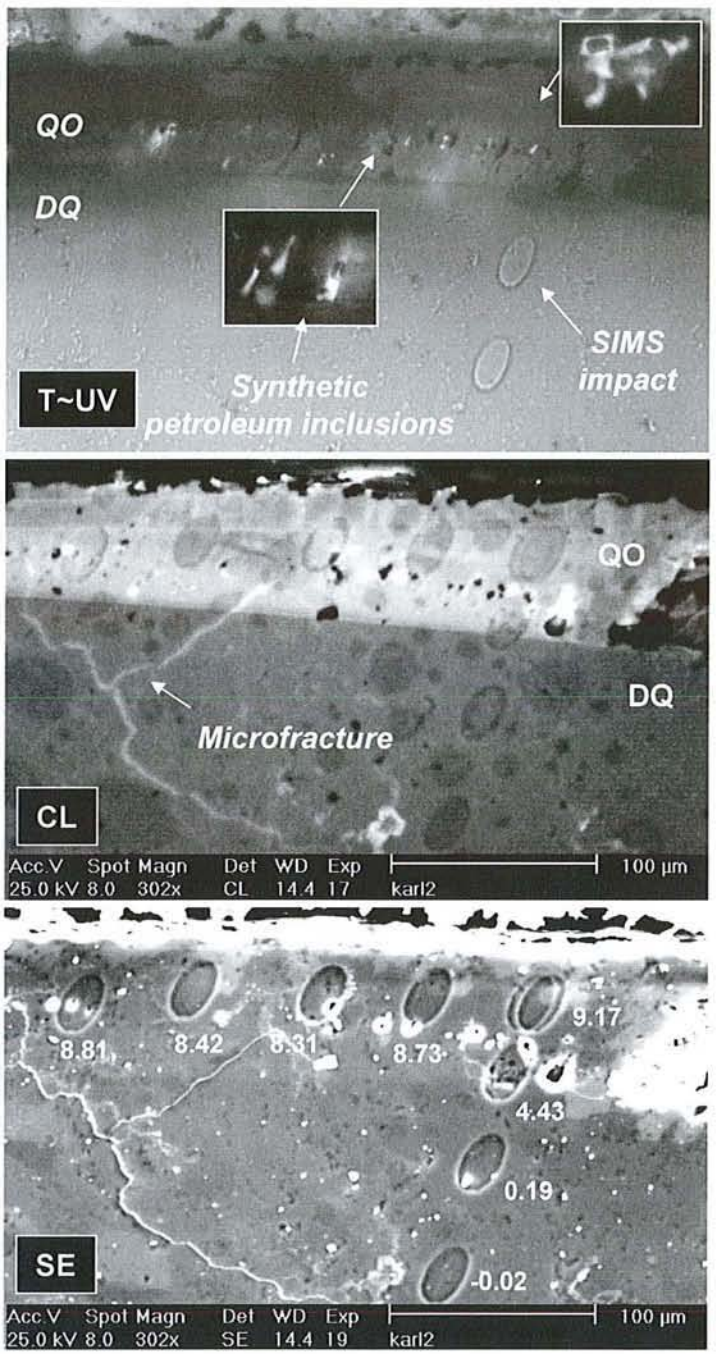

Figure C-26: Photomicrographs of synthetic quartz (DQ) and its overgrowth (QO) under a mixing of ultra-violet (UV) and transmitted (T) light, in cathodoluminescence (CL) and in a secondary electron (SE) mode. $\delta^{18}O$ are constant inside the quartz overgrowth (~+8.7‰) and inside the detrital quartz (~0‰). Most of the synthetic petroleum inclusions containing in the quartz overgrowth are located at the core-overgrowth boundary. T=350°C; P=400 bar; W/O ratio = 10%

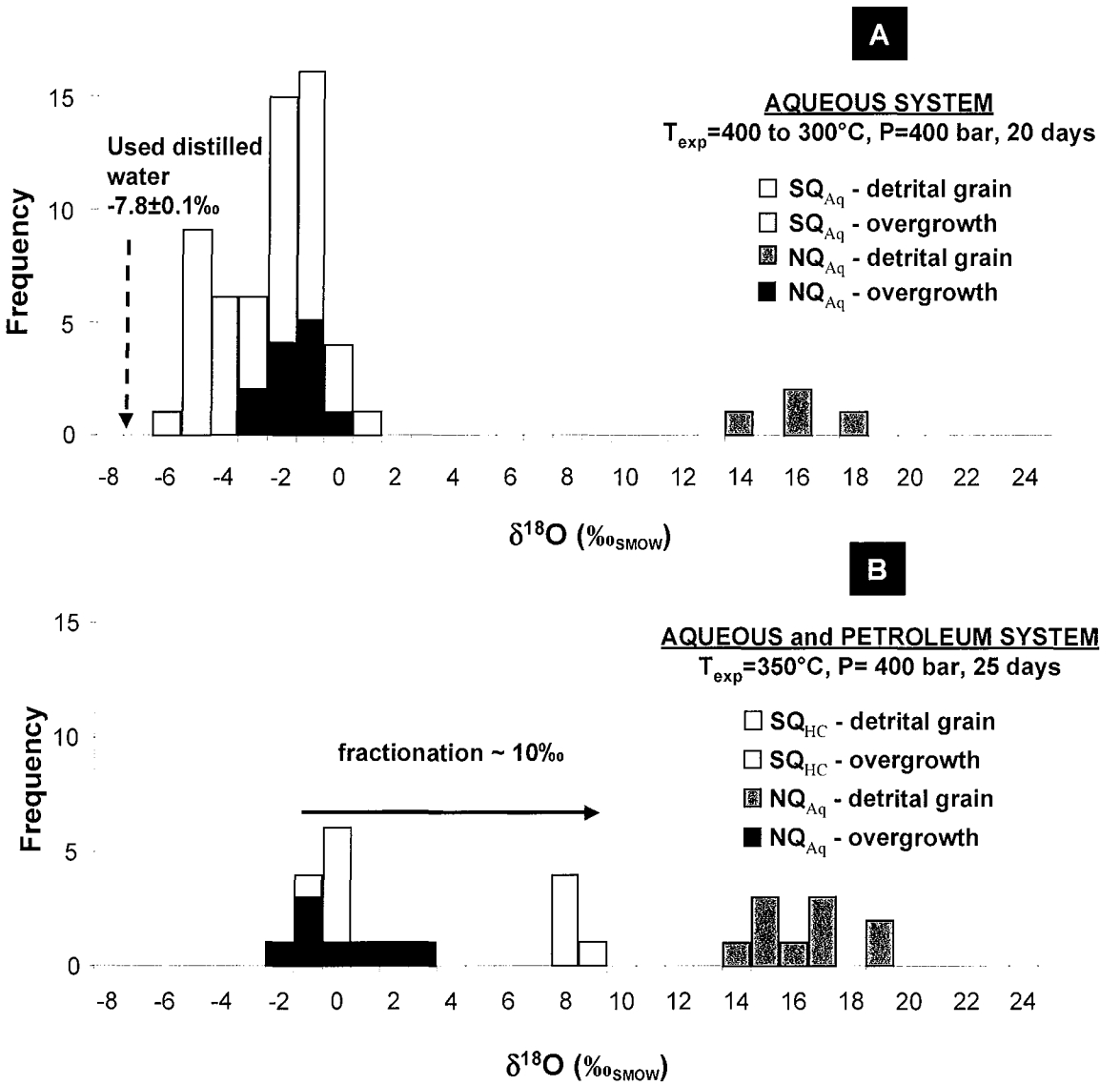

Figure C-27: Results of SIMS oxygen isotope microanalyses performed on synthetic (SQ_{Aq}) and natural Brazilian quartz (NQ_{Aq}) for two FPA experiments.

A. Aqueous system: evolution of the $\delta^{18}O_{Q\text{-}AQ}$ during the crystallisation of secondary SQ_{Aq} and reequilibration of Q_{Aq} with the starting water.

B. Aqueous (on NQ_{Aq}) and petroleum (on SQ_{HC}, W/O ratio = 10%) system.

9.5 Discussion

Oxygen isotopic fractionations have been experimentally determined or calculated between quartz and water (Matsuhima et al., 1979; Sharp and Kirschner, 1994). The mean fractionation factors obtained by these authors are around 4.3‰ at 400°C, 5.5‰ at 350°C, 6.9‰ at 300°C and 15.4‰ at 150°C. Application of these fractionation factors is only valid between water and the neogenic quartz. In contrast, our experiments have been realised in a more complex system, which include the detrital quartz, the neogenic quartz, the silica gel and the water with or without oil.

9.5.1 Water system

Theoretical $\delta^{18}O$ values of neogenic overgrowths of our experiments should be around -2‰, considering a fractionation factor of about 6 with a mean experiment temperature of 350°C and an initial $\delta^{18}O$ of water of -7.8‰. The measured $\delta^{18}O$ values of experimental overgrowths are near the value of -2‰ but are generally higher for natural core-quartz and lower for synthetic core-quartz. The $\delta^{18}O$ data of the overgrowths are affected by the nature of the detrital quartz. The high $\delta^{18}O$ values of the overgrowth of NQ_{Aq} are probably due to a phenomenon of self-diffusion of oxygen between the quartz grain and the overgrowth. Moreover, dissolution of NQ_{Aq} at the beginning of the experiment can contribute to increase the initial $\delta^{18}O$ of the water. The lower value $\delta^{18}O$ of the overgrowth from SQ_{Aq} cannot be explained by a self-diffusion process of oxygen between the grain and the overgrowth. The initial $\delta^{18}O$ value of the SQ_{Aq} is equal to 0‰ and cannot contribute to decrease the $\delta^{18}O$ of the overgrowth below the theoretical value of -2‰. The hypothesis of the presence of residual liquid water (as it is observed by FT-IR) inside the quartz lattice, taken into account by SIMS analysis, could explain the lowest value of $\delta^{18}O$ and the dispersion of the data observed for SQ_{Aq}.

Heterogeneity of the overgrowths is clearly shown by CL. Luminescence colour varies and bedded structures oriented along the c-axis of quartz are observed. Such structures could be possible channels enhancing oxygen diffusion during crystal growth. Heterogeneity are more pronounced for SQ_{Aq} than for NQ_{Aq}. The crystallography of the quartz overgrowth seems to be affected by the nature of the crystallography of the detrital quartz. Fractionation of oxygen isotopes during crystal growth is commonly assumed to be an equilibrium process. Onash and Vennemann present evidence that large variations in $\delta^{18}O$ values in a zoned vein quartz crystal are the result of disequilibrium partitioning between fluid and crystal (Onasch and Vennemann, 1995). These authors show that differences in $\delta^{18}O$ values between sectors along the same growth zone cannot result from variations in the O isotope composition of the fluid and strongly suggest disequilibrium partitioning of oxygen isotopes between fluid and the growing crystal.

The presence of a continuous core-overgrowth boundary is sometimes observed on SQ_{Aq} as on NQ_{Aq} in literature (Blanchet, 2002). Such fragile porous zones could be a possible access for post-overgrowth fluids. The experimental approach of quartz synthesis gives results in good accordance with the expected values from fractionation equations. However, detailed observations show heterogeneity in the overgrowths, redistribution of water and oxygen diffusion between the core and the overgrowth. The role of the detrital quartz is then demonstrated and should be taken into account in the case of basinal applications.

9.5.2 Water-petroleum system

Quartz overgrowths created in presence of oil have trapped petroleum inclusions and show extremely different $\delta^{18}O_{Q\text{-}HC}$ values (+8.7‰) in contrast with $\delta^{18}O_{Q\text{-}Aq}$ values (≈ -2‰) of the overgrowths created in absence of oil. This mean $\delta^{18}O$ value of +8.7‰ is far from the mean expected value of -2‰ (at 350°C). SIMS profiles show that $\delta^{18}O_{Q\text{-}HC}$ composition is fairly constant inside a same quartz overgrowth and this homogeneity is confirmed by a homogeneous luminescence of the overgrowth under CL. Although data from literature are extremely variable above 250°C, they show that around 350°C, 10 to 100wt% of water dissolve into the hydrocarbon phase, whereas under 150°C, this value falls below 1wt% (Guerrant, 1964; Pironon et al., 2000). Therefore, in our samples synthesised with a W/O ratio of 10%, the total amount of water should be dissolved into the petroleum phase. The hypothesis of an oxygen fractionation between liquid water and the water-oil mixture can then be formulated. Water dissolved in oil should be ^{18}O depleted and a residual liquid water film wetting the quartz edges should be ^{18}O enriched. Quartz overgrowths created from the liquid water film would have a high $\delta^{18}O$. In that case, the calculated $\delta^{18}O$ of the water film should be around +3‰. This hypothesis, however, requires the presence of a residual water film whereas literature data predict the entire water dissolution in oil in the experimental conditions (Guerrant, 1964; Pironon et al., 2000). If no remaining liquid water is present, the high $\delta^{18}O$ of the overgrowth should be produced by oxygen exchange with the oil itself. Oxygen of the oil would play an important role during quartz precipitation. This second mechanism cannot be retained because oil is known to be ^{18}O depleted (Tissot and Welte, 1984). Therefore, high positive value of $\delta^{18}O_{Q\text{-}HC}$ inside quartz overgrowth can be only explained by a fractionation during oxidation process between the water and the asphaltenes, which are known to be the most plausible petroleum compounds to exchange oxygen with water during maturation (Michels et al., 1996).

9.6 Conclusion

Silica-water-oil-gas system has been experimentally studied with the objective to simulate the diagenesis of siliceous petroleum reservoirs. Quartz overgrowths have been created in an aqueous system and also in a high oil saturation system when quartz are water-wet. Experiments in H_2O-NaCl were carried out from 400 to 300°C and 400 bar during 20 days. Experiments in the H_2O-NaCl-petroleum system were carried out at 350°C and 400 bar during 25 days. FT-IR imaging have shown that for both type of quartz, quartz overgrowths are enriched in water and silanol boundaries versus the quartz grain. It could be assumed that natural reservoir quartz are mostly hybrid between our synthetic quartz (wet) and our natural brazilian quartz (dry).

The fractionation of O isotopes during crystal growth is commonly assumed to be an equilibrium process. The O isotopic composition of authigenic quartz in sandstones is assumed to reflect both the temperature and isotopic composition of the fluid from which it precipitated. SIMS $\delta^{18}O$ profiles have been obtained across the quartz grain and its overgrowth. In a water system, results show that the composition of the fluid has evolved during quartz crystallisation. In the water-petroleum system, results show that $\delta^{18}O$ obtained in the overgrowth created in high oil saturation shows higher values that those created exclusively in a water system. This should be linked to fractionation processes between oil and water, during the dissolution of water into oil. In a high oil saturation and in the experimental conditions (350°C-400 bar, W/O = 10%), results show that a simple water film is enough to give rise to quartz overgrowth. Indeed, water solubility should be extremely high at these p-T conditions. In this case, the water still remains.

Several implications to natural reservoir or case studies can be relevant. The fluid, which has precipitated quartz overgrowth, is usually assumed to be originated from meteoric water and/or deep fluids. However, our results suggest that if petroleum have migrated close to the quartz environment, high $\delta^{18}O$ values of diagenetic quartz could be correlated to the fractionation partitioning of the water fluid with petroleum during the dissolution of water into oil. In this case, the highest $\delta^{18}O$ values should indicate maximum oil saturation and thus a potential oil migration.

Acknowledgements

We would like to express our special thanks to Frédéric Walgenwitz from TotalFinaElf for helpful support. Special thanks are expressed to Michel Champenois, Claire Rollion-Bard and Denis Mangin from CRPG, Nancy, for the Cameca IMS1270 ion microprobe analyses and Etienne Deloule for helpful discussions.

References

Aplin A. C., Warren E. A., Grant S. M., and Robinson A. G. (1993) Mechanisms of quartz cementation in North Sea reservoir sands: constraints from fluid compositions. *AAPG Studies in Geology*, Vol. 36 (ed. A.D. Horbury, Robinson, A.G.), pp. 7-22.

Ayalon A. and Longstaffe F. J. (1988) Oxygen isotope studies of diagenesis and porewater evolution in the western Canada Sedimentary basin: Evidence from the Upper Cretaceous basal Belly River sandstone. *Journal of Sedimentary Petrology* 58, 489-505.

Barclay S. A. and Worden R. H. (2000) Effects of reservoir wettability on quartz cementation in oil fields. In *Quartz cementation in sandstones. Special publication of the International Assocation of Sedimentologists*, Vol. 29 (ed. W. R. H. a. M. S.), pp. 103-117.

Blanchet A. (2002) Origine, conditions et processus de la silification diagénétique de reservoirs gréseux en Mer du Nord, Université Paris XI.

Blatt H. (1987) Oxygen isotopes and the origin of quartz. *J. Sediment. Petrol.* 57, 373-377.

Brint J. F., Hamilton P. J., Haszeldine R. S., Fallick A. E., and Brown S. (1991) Oxygen isotopic analysis of diagenetic quartz overgrowths from the Brent sands: a comparison of two preparation methods. *Journal of Sedimentary Petrology* 61(4), 527-533.

Carpenter S. J. and Lohmann K. C. (1997) Carbon isotope ratios of Phanerozoic marine cements: Re-evaluating the global carbon and sulfur systems. *Geochimica et Cosmochimica Acta* 61(22), 4831-4846.

Dutton S. P. and L.S. L. (1988) Cementation and burial history of a low-permeability quartzarenite, Lower Cretaceous Trabis Peak Formation, east Texas. Geological Society of American Bulletin 100, 1271-1282.

Cole D. R., Ohmoto H., and Lasaga A. C. (1983) Isotope exchange in mineral-fluid systems. I. Theoritical evaluation of oxygen isotope exchange accompanying surface reaction and diffusion. *Geochimica et Cosmochimica Acta* 47, 1681-1693.

Dennis P. F. (1984) Oxygen self-diffusion in quartz under hydrothermal conditions. *Journal of Geophysical Research* 89(B6), 4047-4057.

Dixon S. A., Summers D. M., and Surdam R. C. (1989) Diagenesis and prservation of porosity in Norphlet Formation (Upper Jurassic), southern Alabama. *AAPG Bulletin* 73, 707-728.

Donovan T. J., Friedman I., and Gleason D. (1974) Recognition of petroleum-bearing traps by unusual isotopic compositions of carbonate-cemented surface rocks. *Geology* 2, 351-354.

Doremus R. H. (1998) Diffusion of water and oxygen in quartz: reaction-diffusion model. *Earth and Planetary Science Letters* 163, 43-51.

Dubina E. O. and Lakshtanov L. (1997) A kinetic model of isotopic exchange in dissolution-precipitation processes. *Geochimica et Cosmochimica Acta* 61(11), 2265-2273.

Elphick S. C., Dennis P. F., and Graham C. M. (1986) An experimental study of the diffusion of oxygen in quartz and albite using an overgrowth technique. *Contributions to Mineralogy and Petrology* 92, 322-330.

Fisher R. S. and Land L. S. (1986) Diagenetic hystory of Eocene Wilcox sandstones, south-central Texas. Geochimica et Cosmochimica Acta 50, 551-561.

Giletti B. J. and Yund R. A. (1984) Oxygen diffusion in quartz. *Journal of Geophysical Research* 89(B6), 4039-4046.

Girard J.-P., Munz I. A., Johansen H., and Hill S. (2001) Conditions and timing of quartz cementation in Brent reservoirs, Hild Field, North Sea: constraints from fluid inclusions and SIMS oxygen isotope microanalysis. *Chemical Geology* 176, 73-92.

Gluyas J. G., Robinson A. G., Emery D., Grant S. M., and Oxtoby N. H. (1993) The link between petroleum emplacement and sandstone cementation. *Petroleum Geology of Northwest Europe: Proceedings of the 4th Conference. J.R. Parker Ed.*, 1395-1402.

Graham C. M., Valley J. W., and Winter B. L. (1996) Ion microprobe analysis of $^{18}O/^{16}O$ in authigenic and detrital quartz in the St. Peter Sandstone, Michigan Basin and Wisconsin Arch, USA: Constrasting diagenetic histories. *Geochimica et Cosmochimica Acta* 60(24), 5101-5116.

Guerrant R. P. (1964) Hydrocarbon-water solubilities at high temperatures under vapor-liquid-liquid equilibrium conditions, Pennsylvania State University.

Hogg A. J. C., Pearson M. J., Fallick A. E., and Hamilton P. J. (1995) An integrated thermal and isotopic study of the diagenesis of the Brent Group, Alwyn South, U.K. North Sea. *Applied Geochemistry* 10, 531-546.

Hervig R. L., William L. B., Kirkland I. K., and Longstaffe F. (1995) Oxygen isotope microanalyses of diagenetic quartz: possible low temperature occlusion of pores. *Geochemica et Cosmochimica Acta* 59, 2537-2543.

Kraishan G. M., Rezaee M. R., and Worden R. H. (2000) Significance of trace element composition of quartz cement as a key to reveal the origin of silica in sandstones: an example from the Cretaceous of the Barrow Sub-basin, Western Australia. In *Quartz Cementation in Sandstones. Special Publication of the International Association of Sedimentologists*, Vol. 29 (ed. R. H. Worden and S. Morad), pp. 317-331. Blackwell Science.

Lee M. and Savin S. M. (1985) Isolation of diagenetic quartz overgrowths on sand grains for oxygen isotopic analysis. Geochemica et Cosmochimica Acta 49, 497-501.

Longstaffe F. J. and Ayalon A. (1987) Oxygen-isotope studies of clastic diagenesis in the Lower Cretaceous Viking Formation, Alberta: Implication for the role of meteoric water. In The diagenesis of sedimentary sequences. Geological Society of London Special Publication, Vol. 36 (ed. J. D. Marshall), pp. 277-296.

Lyon I. C., Burley S. D., McKeever P. J., Saxton J. M., and Macaulay C. (2000) Oxygen isotope analysis of authigenic quartz in sandstones: a comparison of ion microprobe and

conventional analytical techniques. In Quartz Cementation in Sandstones. Special Publication of the International Association of Sedimentologists, Vol. 29 (ed. R. H. Worden and S. Morad), pp. 299-316. Blackwell Science.

Marchand A. M. E., Haszeldine R. S., Smalley P. C., Macaulay C. I., and Fallick A. E. (2001) Evidence for reduced quartz-cementation rates in oil-filled sandstones. *Geology* 29(10), 915-918.

Matsuhima Y., Goldsmith J. R., and Clayton R. N. (1979) Isotopic fractionation in the system quartz-albite-anorthite-water. *Geochimica et Cosmochimica Acta* 43, 1131-1140.

McBride E. F. (1989) Quartz cementation in sandstones: *Earth-Science Reviews* 26, 69-112.

McBride E. F., Land L. S., and Mack L. E. (1987) Diagenesis of eolian and fluviatil feldspathic sandtones, Norphlet Foramtion (Upper Jurassic), Rankin Country, Mississippi, and Mobile County, Alabama. *AAPG Bulletin* 71, 1019-1034.

McConnell J. D. C. (1995) The role of water in oxygen isotope exchange in quartz. *Earth and planetary Science Letters* 136, 97-107.

Meunier J. D. (1992) Precipitation of minerals between detrital quartz and quartz overgrowths in sandstones. *European Journal of Mineralogy* 4, 1401-1406.

Michels R., Langlois E., Ruau O., Mansuy L., Elie M., and Landais P. (1996) Evolution of asphaltenes during artificial maturation: A. Record of the chemical processes. *Energy & Fuels* 10(39-48).

Milliken K. L., Land L. S., and Loucks R. G. (1981) History of burial diagenesis determined from isotopic geochemistry, Frio Formation, Brazoria County, Texas. *AAPG Bulletin* 65, 1397-1413.

Onasch C. M. and Vennemann T. W. (1995) Disequilibrium partitioning of oxygen isotopes associated with sector zoning in quartz. *Geology* 23(12), 1103-1106.

Pironon J., Thiéry R., Teinturier S., and Walgenwitz F. (2000) Water in petroleum inclusions: evidence from Raman and FT-IR measurements, PVT consequences. *Joumal of Geochimical Exploration* 69-70, 663-668.

Ramm M. (1992) Porosity-depth trends in reservoir sandstones: theoretical models related to Jurassic sandstones, offshore Norway. *Marine and Petroleum Geology* 9, 324-327.

Saigal G., Bjorlykke K., and Larter S. (1992) The effects of oil Emplacement on diagenetic processes - Examples from the Fulmar reservoir sandstones, Central North Sea. *American Association of Petroleum Geologists Bulletin* 76(7), 1024-1033.

Sharp Z. D. and Kirschner D. L. (1994) Quartz-calcite oxygen isotope themometry: a calibration based on natural isotopic variations. *Geochimica et Cosmochimica Acta* 58, 4491-4501.

Spotl C., Houseknecht D. W., and Riciputi L. R. (2000) High-temperature quartz cement and the role of stylolites in a gas reservoir, Spiro Sandstone, Arkoma Basin, USA. In *Special Publication Number 29 of the International Association of Sedimentologists* (ed. R. H. Worden, Morad, S.), pp. 281-297

Teinturier S., Elie M., and Pironon J. (in review) Evidence of oil cracking using synthetic petroleum inclusion. *Journal Of Geochimical Exploration.*

Teinturier S. and Pironon J. (in prep) Experimental diagenesis of quartz in petroleum environment. Part I: Fluid phases - Procedures and fluid trapping. *Geochimica et Cosmochimica Acta.*

Teinturier S. and Pironon J. (in review) Time formation of individual fluid inclusion within fluorite crystal in H_2O-NH_4Cl and quartz in H_2O-NaCl system. *American Mineralogist.*

Tilley B. J. and Longstaffe F. J. (1989) Diagenesis and isotopic evolution of porewaters in the Alberta Deep Basin: The Falher Member and Cadomin Formation. *Geochimica et Cosmochimica Acta* 53, 2529-2546.

Tissot B. P. and Welte D. H. (1984) *Petroleum formation and occurrence, 2nd ed.*

Walderhaug O. (1990) A fluid inclusion study of quartz-cemented sandstones from offshore mid-norway - possible evidence for continued quartz cementation during oil emplacement. *Journal of Sedimentary Petrology* 60(2), 203-210.

Wilkinson M., Crowley S. F., and Marshall J. D. (1992) Model for the evolution of oxygen isotope ratios in the pore fluids of mudrocks during burial. *Marine and Petroleum Geology* 9, 98-105.

Williams L. B., Hervig R. L., and Bjorlykke K. (1997) New evidence for the origin of quartz cements in hydrocarbon reservoirs revealed by oxygen isotope microanalyses. Geochimica et Cosmochimica Acta 61(12), 2529-2538

Worden R. H. and Morad S. (2000) Quartz cementation in oil field sandstones: a review of the key controversies. In *Special Publication Number 29 of the International Association of Sedimentologists* (ed. R. H. Worden, Morad, S.). Blackwell Science.

Worden R. H., Oxtoby N. H., and Smalley P. C. (1998) Can oil emplacement prevent quartz cementation in sandstones? *Petroleum Geoscience* 4, 129-137.

Zhang Y., Stolper E. M., and Wasserburg G. J. (1991) Diffusion of a multi-species component and its role in oxygen and water transport in silicates. *Earth and Planetary Science Letters* 103, 228-240.

10 Article 7: OIL CRACKING PROCESSES: EVIDENCE FROM SYNTHETIC PETROLEUM INCLUSIONS

Une étude couplée entre les inclusions hydrocarbonées synthétisées dans du quartz avec l'huile parente et résiduelle a été entreprise jusqu'à des températures et des pressions de 350°C et 400 bar. La spectroscopie IR, les fractions organiques extraites et les analyses GC-MS ont mis en évidence des processus de craquage de l'huile durant l'expérience. Les résultats montrent que jusqu'à des températures et des pressions de 250°C-212bar, les inclusions hydrocarbonées synthétiques, l'huile parente et résiduelle ont des spectres IR et des rapports CH_2/CH_3 similaires. Bien que la distribution des hydrocarbures saturés et aromatiques des huiles soient similaires, le rapport asphaltène/résine s'est inversé au cours de l'expérience. Une telle inversion implique un craquage précoce des asphaltènes durant la maturation de l'huile. A 350°C et 400 bar, les spectres IR et les rapports CH_2/CH_3 sont variables. De plus, du CO_2 et du CH_4 ont été détectés dans la phase liquide et gazeuse des inclusions hydrocarbonées. Les résultats montrent que le craquage secondaire de l'huile est important à cette température. La quantité relative de composé NSO baisse. Les analyses GC-MS révèlent que le craquage des composés les plus instables thermiquement ainsi que les processus de désalkylation des hydrocarbures aromatiques sont plus prononcés. De plus, l'huile est enrichie en saturés. La formation d'inclusions hydrocarbonées de synthèse permet donc un échantillonnage de l'huile à un instant t caractéristique d'une condition P-T et sont par conséquent, des témoins non négligeables de l'évolution d'une huile lors d'une maturation thermique.

OIL CRACKING PROCESSES: EVIDENCE FROM SYNTHETIC PETROLEUM INCLUSIONS

Stéphane TEINTURIER, Marcel ELIE and Jacques PIRONON

**UMR G2R 7566 – (CREGU, CNRS, Université Henri Poincaré, INPL) BP239, F-54506 Vandœuvre-lès-Nancy Cedex, France.*

Soumis à Journal of Geochemical Exploration

ABSTRACT

A correlated study of petroleum inclusions synthesised in quartz with the parent and the residual oil has been performed up to 350°C and 400bar. FT-IR, extracted fractions and GC-MS analysis have shown evidence of oil cracking processes during the experiments. Results show that up to 250°C-212 bar, synthetic petroleum inclusions, the parent oil and the residual oil have very similar FT-IR spectra and CH_2/CH_3 ratio. Although saturate and aromatic-HC distributions of oils are similar, the asphaltene/resin ratio has been inverted. Such an inversion indicates that asphaltenes are cracked first during thermal maturation of oil. At 350°C and 400 bar, FT-IR spectra, CH_2/CH_3 ratio are variable. Moreover, CO_2 and methane has been detected within the gas and the liquid phase of synthetic petroleum inclusions. Results show that the oil secondary cracking is effective at this temperature. The relative amount of NSO compounds decreases. GC-MS analysis reveal that the cracking of the most thermally labile saturates and the dealkylation processes of aromatic hydrocarbons are more pronounced. Contemporaneous with these variations, the oil is enriched in saturates. Synthetic fluid inclusions act as a sampling of the oil at one p-T conditions and are thus the useful witnesses of the oil cracking during the experiments.

10.1 Introduction

Natural petroleum inclusions are known to be the witness of the petroleum migration and are often used as the starting point for the PVTX reconstruction of the petroleum migration (Teinturier et al., 2002). Beside fluid inclusions post-trapping modifications (necking down, leakage...), petroleum inclusions are generally assumed to be representative to the parent oil reservoir (or source). But is it really the case? And up to which p-T ranges? To answer these questions, several experiments have been carried out in the water-petroleum system to produce fluid inclusions in quartz. A correlated study of the synthetic fluid inclusions with the parent and the residual oil was thus performed.

The synthesis of fluid inclusions in the presence of variable proportions of petroleum or aqueous solution has been investigated at temperature and pressure up to 350°C and 400 bar on synthetic and natural brazilian quartz crystals. Two distinct types of autoclaves have been used, depending on the p-T conditions and autoclave limitations. Experiments were carried out in a gas-pressure autoclave (GPA) up to 250°C and 212 bar during 30 days and conducted into sealed gold bag, inside a fluid-pressure autoclave (FPA) at 350°C and 400 bar during 25 days. Both types are ®Autoclave Engineering Closure trademarks. The dead oil used in the experiment comes from the Middle East and is depleted in methane and C_2-C_5 fraction.

For the characterisation of the initial and residual oil composition, the samples were deasphaltened with *n*-heptane. The aliphatic, aromatic and polar fractions were then separated from deasphaltening oils by liquid chromatography on activated alumina and silica columns with successive elution by solvents of different polarities (pentane, pentane/dichloromethane, dichloromethane/methanol). The different fractions were concentrated and then weighted. The GC-MS analyses of the aliphatic, aromatic and polar (asphaltene and resins) fractions were performed using a HP6890 GC coupled to a HP 5971A mass spectrometer, using a split/splitless injector, a 60m DB-5 J&W, 0.25mm id and a 0.1µm film fused silica column. The temperature program was 40-130°C at 15°C/min, then 130-300°C at 3°C/min, followed by an isothermal stage at 300°C during 15 min (constant helium flow of 1ml/min). Samples were analyzed in the full data acquisition mode (fullscan) by scanning from 50 to 550 a.m.u. at 1 cycles/s. Individual petroleum inclusions and parent dead oil were analysed by Fourier transform infrared microspectrometry (FT-IR).

10.2 Results and analyses

FT-IR analysis has been realised on individual petroleum inclusions and also on the original dead oil, before and after experiments (Teinturier and Pironon, in prep). Results show that up to 250°C-212 bar (GPA experiments), FT-IR spectra of petroleum inclusions are very similar to those obtained on the dead oil before and after the corresponding experiments. CH_2/CH_3 ratios are

around 5.4. No CO_2 has been found inside petroleum inclusions. Accurate analysis of the FT-IR spectra show that the starting oil has lost some sulphur compounds during the experiment. At 350°C and 400 bar (FPA experiments), calculated CH_2/CH_3 ratios are different and non-constant. Mean CH_2/CH_3 ratios have been calculated around 3.1±0.5 for petroleum inclusion and around 4.4±0.2 for residual dead oil. Moreover, methane has been detected within the gas and the liquid phase inside synthetic petroleum inclusions and calculated around 20 ± 5mol% according Pironon et al. (2001) method. CO_2 content has been calculated around 0.4 ± 0.3mol%, proving that oil have lost some C-O or C=O compounds. A weaker CH_2/CH_3 ratio of the residual oil and of the oil inside petroleum inclusions compare to the parent oil, the release of CH_4 and CO_2 are evidences of oil-cracking processes during the experiments.

	Oil composition				GC-MS parameters						
					Saturates					Aromatics	
Dead oil	Asphaltenes (wt%)	Resins (wt%)	Aromatics (wt%)	Saturates (wt%)	CPI	Pr/nC_{17}	Ph/nC_{18}	Pr/Ph	P/ΣP	MPI1	MDR
Before experiments.	11	13	32	44	1.01	0.31	0.50	0.74	0.14	0.56	1.56
GPA (250°C-212bar)	4	20	34	42	1.00	0.32	0.47	0.78	0.14	0.54	1.37
FPA (350°C-400bar)	4	12	28	56	1.00	0.19	0.27	0.82	0.27	0.95	2.28

Table C-8: Evolutions of oil composition, of Pr/n-C17, Ph/n-C18, Pr/Ph ratios from saturated hydrocarbons and MPI1, P/ΣP, MDR indices from aromatic hydrocarbons.
MPI1=1.5(2MP+3MP)/(P+1MP+9MP); MDR=4MDBT/1MDBT;*
PΣP=P/(P+1MP+2MP+3MP+9MP).
MP = methylphenanthrene and MDBT = methyldibenzothiophene.

The table C-8 shows the changes in oil composition during heating experiments. At 250°C-212 bar, the relative amounts of saturated and aromatic compounds seem stables when comparing to the dead oil. The observed differences are ranged in the analytical uncertainty (± 4). On the other hand, the oil is enriched in resins whereas the percentage of asphaltenes decreases. No significant change in the relative amount of asphaltenes can be noticed between 250°C-212 bar and 350°C-400 bar. The percentages of aromatics and resins drop, while the saturate yield drastically increases in the oil recovered from the highest temperature experiment. Aromatic and saturated-HC gas chromatograms are unaffected at 250°C-212 bar whereas the differences are pronounced at 350°C-400 bar comparatively to the initial dead oil (Figure C-28).

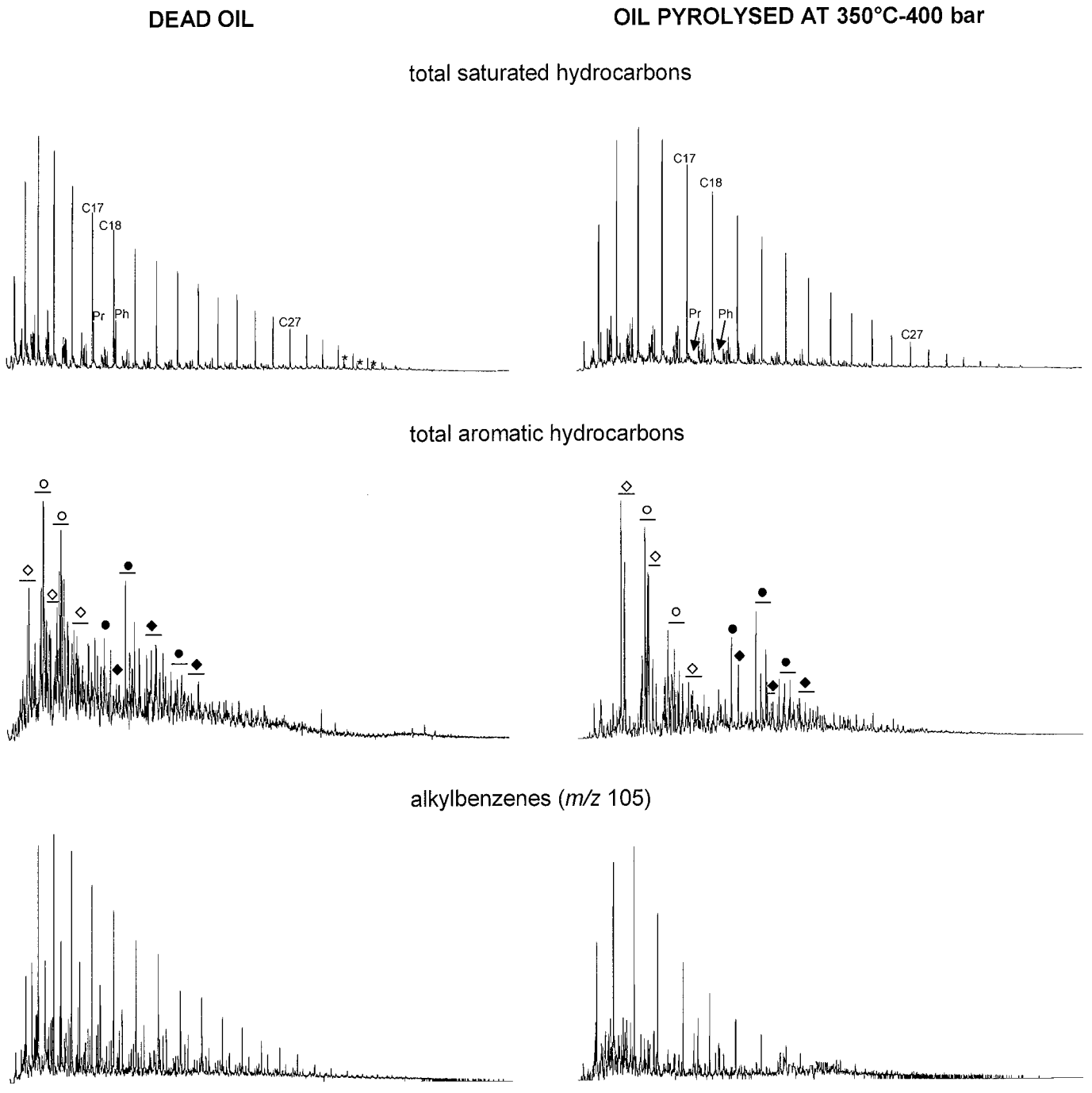

Figure C-28: Comparison of the total saturated-HC, total aromatic-HC and alkylbenzene distributions between dead oil and FPA experiment oil (350°C-400 bar).
(= hopanes, ◇ = naphthalenes,*
◆ =phenanthrenes, ● = dibenzothiophenes, =○ benzothiophenes).

It can be noted that the C_{15+} saturates distribution is shifted toward low molecular weight *n*-alkanes and the hopanes have almost disappeared. GC-MS parameters such as Pr/*n*-C_{17}, Ph/*n*-C_{18} and Pr/Ph indicate that oil is at a higher thermal maturity (Table C-8). Aromatic-HC and alkylbenzene (m/z 105) gas chromatograms (Figure C-28) show an increase in the relative contribution of the lighter species in the 350°C-400 bar oil. Similarly, phenanthrene and dibenzothiophene indices (MPI-1 and MDR, Table C-8) consistently indicate a higher maturity level, and the increase in the P/ΣMP ratio suggests that the dealkylation process is effective.

10.3 Discussion and conclusions

Data from literature show that the p-T range and the overall rate of oil cracking processes highly depend on the oil composition (Huang, 1999; Huang and Otten, 2001). The observed transformations follow a scheme of secondary cracking reactions depending on the involved energy during heating experiments (Bjoroy et al., 1988; Horsfield et al., 1992, Behar et al., 1992). Asphaltenes that is the most thermally labile compounds in oil start to crack at 250°C-212 bar giving NSO compounds, while the aromatic and saturated-HCs are not significantly affected. The effect of temperature can be clearly seen on gas chromatograms of the pyrolysis products. At 350°C-400 bar, the proportion of isoprenoids pristane (Pr) and phytane (Ph) decreases relative to their adjacent *n*-paraffins and hopanes have almost disappear since cyclic and branched components require less energy for cracking than straight chain alkanes. So the longer linear alkanes are more readily cracked inducing a displacement of the saturate distribution toward low molecular weight species. Aromatic-HC gas chromatogram seems to indicate that the dealkylation process is effective. Contemporaneous with these molecular transformations, the oil is enriched in saturates, while the relative amounts of resins and aromatics decrease. The analysis of oil is in good agreement with the analysis of inclusions which shows a decrease of the CH_2/CH_3 ratio of the saturate fraction.

Assuming that the composition of the oil inside the synthetic petroleum inclusion is similar to a live oil due to the oil-cracking processes during the experiment, we have generated an oil composition using PIT software (Thiéry et al., 2000). The homogenisation temperature and the volume of the gas bubble of the inclusion were the two parameters used for the PIT modelling. The modelled composition corresponds to the redistribution of the hydrocarbon-saturated fraction during oil cracking (Figure C-29). The methane concentration is similar to the concentration calculated from FT-IR. The oil composition mimics a black oil composition.

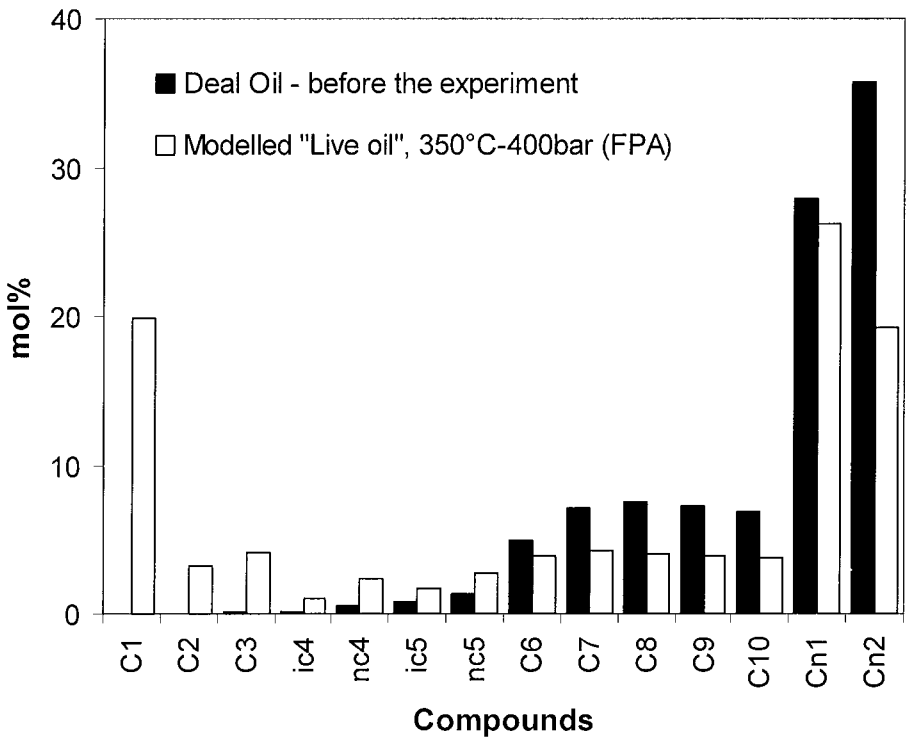

Figure C-29: Composition in mole% of the original dead oil and the live oil at 350°C-400 bar modelled by PIT software. Cn1= C_{11}-C_{15}; Cn2 = C_{15+}.

Synthetic fluid inclusions correlated to the study of the parent and the residual oil can be a new way to study oil-cracking processes because synthetic inclusions can memorise an oil or gas composition at a single p-T condition. Moreover, the effect of aqueous on oil cracking processes can be envisaged. The effects of ionic content of water could be also checked. Similar experiments with different oil types could be developed in order to characterise the effects of oil composition on the secondary cracking.

Acknowledgements

We would like to express our special thanks to Frédéric Walgenwitz from TotalFinaElf for providing the dead oil.

References

Behar, F., Kressmann, S., Rudkiewicz, J.L., Vandenbroucke, M. 1992. Experimental simulation in a confined system and kinetic modelling of kerogen and oil cracking. Organic Geochemistry. 19, 173-189.

Bjoroy, M., Williams, J.A., Dolcater, D.L., Winters, J.C. 1988. Variations in hydrocarbon distribution in artificially matured oils. Organic Geochemistry. 13, 901-913.

Horsfield, B., Schenk, H.J., Mills, N., Welte, D.H. 1992. An investigation of the in-reservoir conversion of oil to gas: compositional and kinetic findings from closed-system programmed-temperature pyrolysis. Organic Geochemistry. 19, 191-204.

Huang, D., 1999. Advances in hydrocarbon generation theory (I) Generation and evolution model for immature oils and hydrocarbon. Journal Of Petroleum Science & Engineering, 22: 121-130.

Huang, W.-L. and Otten, G.A., 2001. Cracking kinetics of crude oil and alkanes determined by diamond anvil cell-fluorescence spectroscopy pyrolysis: technique development and preliminary results. Organic Geochemistry, 32: 817-830.

Pironon J., Thiery R., Ayt Ougougdal M., Teinturier S., Beaudoin S., and Walgenwitz F. (2001) FT-IR measurements of petroleum fluid inclusions: methane, n-alkanes and carbon dioxide quantitative analysis. *Geofluids* 1(1), 2-10.

Teinturier, S. and Pironon, J., in prep. Experimental diagenesis of quartz in petroleum environment. Part I: Procedures and fluid trapping. Geochimica et Cosmochimica Acta.

Teinturier, S., Pironon, J. and Walgenwitz, F., 2002. Fluid inclusions and PVTX modelling: Examples from the Garn Formation in well 6507 2/2, Haltenbanken, Mid-Norway. Marine and Petroleum Geology *19(6), 755-765.*.

Thiéry, R., Pironon, J., Walgenwitz, F. and Montel, F., 2000. PIT (Petroleum Inclusion Thermodynamic): a new modeling tool for the characterization of hydrocarbon fluid inclusions from volumetric and microthermometric measurements. Journal of Geochimical Exploration, 69-70: 701--704.

11 Article 8: WATER IN PETROLEUM INCLUSIONS. EVIDENCE FROM RAMAN AND FT-IR MEASUREMENTS, PVT CONSEQUENCES

Les inclusions fluides hydrocarbonées ne peuvent être dépourvues d'eau. De nouvelles expériences réalisées en spectroscopie IR et Raman ont permis de suivre la solubilité de l'eau dans les hydrocarbures piégés dans les inclusions, dans des conditions de température et de pression similaires aux réservoirs pétroliers. Contrairement au spectre Raman de l'eau liquide entre 3250-3450 cm^{-1}, le spectre Raman de l'eau dissoute dans la phase hydrocarbonée se marque par une bande fine à 3630 cm^{-1}. L'évolution de la solubilité de l'eau avec la température a été suivie grâce à un spectromètre Raman couplé à une platine microthermométrique. Cependant, dans la majorité des cas, les analyses Raman ne peuvent pas être appliquées aux inclusions hydrocarbonées car leur fluorescence masque le signal Raman. Des expériences similaires ont donc été réalisées en utilisant un spectromètre IR sur des inclusions naturelles et synthétiques. L'intensité de la bande IR de l'eau liquide baisse avec l'augmentation de température, ce qui est cohérent avec la solubilisation de l'eau dans la phase hydrocarbonée. La T_h globale d'une inclusion hydrocarbonée est ainsi obtenue lorsque la bande de l'eau liquide, centré à 3400 cm^{-1} disparaît du spectre IR. Si l'on considère que les inclusions aqueuses sont associées aux inclusions hydrocarbonées, les T_h des deux types d'inclusions devraient être similaires. Dans ce cas, les interprétations PVTX des inclusions hydrocarbonées doivent être reconsidérées.

WATER IN PETROLEUM INCLUSIONS. EVIDENCE FROM RAMAN AND FT-IR MEASUREMENTS, PVT CONSEQUENCES

J. PIRONON*, R. THIERY**, S.TEINTURIER* AND F. WALGENWITZ***

*UMR G2R 7566 – (CREGU, CNRS, Université Henri Poincaré, INPL) BP239, F-54506 Vandœuvre-lès-Nancy Cedex, France.

**Université B. Pascal, Département des Sciences de la Terre, 2-5 rue Kessler, 63038 Clermont-Ferrand, France

***ELF, CSTJF, Avenue Larribau, 64018 Pau Cédex, France

Journal of Geochemical Exploration (2000), Vol 69-70, pp.663-668

ABSTRACT

Petroleum inclusions cannot be considered as water-free inclusions. Raman and FT-IR new experiments have shown solubility of water in hydrocarbons trapped in inclusions for temperature conditions of natural petroleum reservoirs. Water dissolved in hydrocarbon phase appears at 3630 cm^{-1} on the Raman spectrum and its Raman fingerprint is totally different than the Raman signature of liquid water in the 3250-3450 cm^{-1} range. Raman microscope has been coupled with a heating stage to follow water solubility with the temperature increase. However, Raman analyses cannot be applied to petroleum inclusions: their fluorescence masks the Raman signal. Similar experiments have been made using FT-IR microspectroscopy on synthetic and natural inclusions. Intensity of the liquid water infrared band decreases with temperature increase that is due to solubility of water in the oil phase. Therefore, bulk homogenisation temperature of a petroleum inclusion is obtained when the liquid water band, centred at 3400 cm^{-1}, disappears from the FT-IR spectrum. When aqueous inclusions are associated with petroleum inclusions, homogenisation temperatures of the two inclusion types should be similar. PVTX interpretations of petroleum inclusions should be then reconsidered.

Keywords: petroleum inclusions, Raman microspectroscopy, FT-IR microspectroscopy, water solubility in hydrocarbons, homogenisation temperature.

11.1 Introduction

Hydrocarbon in petroleum environments can be trapped in aqueous inclusions or in petroleum inclusions. Aqueous inclusions are frequently enriched in methane gas, which can be quantified by Raman microspectroscopy (Dubessy et al., 2000). Other hydrocarbons (ethane, propane) or gases (CO_2, N_2, H_2S) should be present in inclusions but have concentrations below the detection limit of the Raman method. Petroleum inclusions in salt or fluorite are often filled with an oil-water immiscible mixture. The water phase is rarely observed inside petroleum inclusions from sandstones in deep oil reservoirs. It is supposed to be present as a non-visible liquid film, wetting the inclusion walls. P,V,T,X interpretations of oil migration consider neat hydrocarbon inclusions and do not take into account the presence of water.

Data from literature show that water is always soluble in hydrocarbon whatever the nature of the hydrocarbon (Figure C30). The concentration of water in hydrocarbon phases exponentially increases with temperature and reaches about 1% at 150°C.

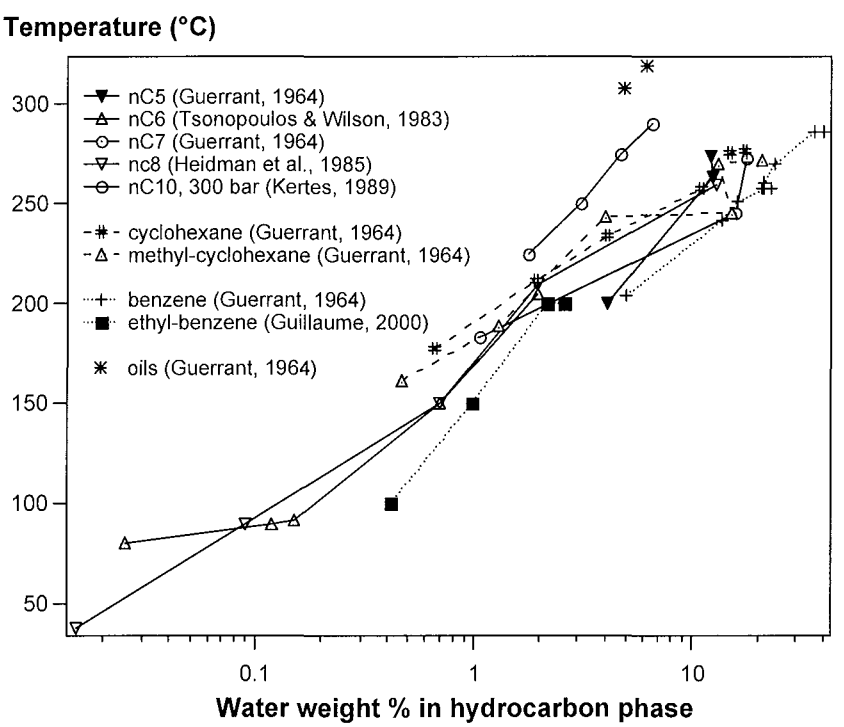

Figure C-30: Weight percent of water in hydrocarbon phase vs. temperature for five n-alkanes, two cycloalkanes, two aromatics and one oil.

The objective of this work is to show 1) the ubiquitous presence of water in petroleum inclusions and its solubility at high temperature and 2) the consequences on pressure-temperature reconstruction and understanding of oil migration phenomenon.

11.2 Methods and material studied

Natural petroleum inclusions from MVT deposit (Illinois, USA) and synthetic oil inclusions have been used. Natural sample has two main advantages: 1) inclusions are trapped in fluorite that is transparent in mid-infrared range, and 2) inclusions with variable water/oil volumetric ratios (from water dominant to oil dominant) are associated in same planes. Synthetic inclusions have been created in KCl crystals following Pironon's method (Pironon, 1990), from n-dodecane and natural degassed oil.

Raman spectra have been acquired with a Labram ©Dilor microspectrometer linked to an Argon laser with an incident radiation of 514.5 nm. Microspectrometer is coupled with a Chaixmeca microthermometric stage to follow the evolution of the Raman spectra with temperature. FT-IR spectra have been recorded at LEM laboratory (Nancy, France) with an IFS 55 Bruker spectrometer linked to an infrared microscope coupled with a Linkam heating stage.

OH and CH molecular groups from water and oil respectively are detected in Raman and FT-IR spectra by their characteristic stretching and bending vibration areas. For this study, stretching bands have been considered and their integrated intensities (i.e. band areas) have been measured.

11.3 Results and analyses

Evidence of water in hydrocarbon inclusions has been shown using Raman backscattering on synthetic non-fluorescent inclusions. Spectra are recorded focusing the laser beam inside the hydrocarbon phase of a three-phase inclusion (liquid water, liquid hydrocarbon, and vapour). Contribution of surrounding water phase is rejected decreasing the confocal hole of the Labram microspectrometer.

Spectra recorded between 25 and 300°C at saturated vapour pressure are plotted in Figure C-31. Presence of dissolved water is clearly observed for the first time at 3630 cm^{-1}. This water contribution is totally different than the liquid water Raman band, which is bimodal with two maximums at 3250 and 3450 cm^{-1}. This band location is coherent with isolated water molecules like water vapour. No hydrogen bonding is detected. The $[H_2O]/[CH]$ band area ratio increases with temperature (Figure C-32) with similar exponential evolution than in Figure C-30.

Raman analysis of hydrocarbon cannot be applied to natural petroleum inclusions because of fluorescence. Emission of fluorescence is induced by laser excitation of aromatic molecules and masks the Raman signal.

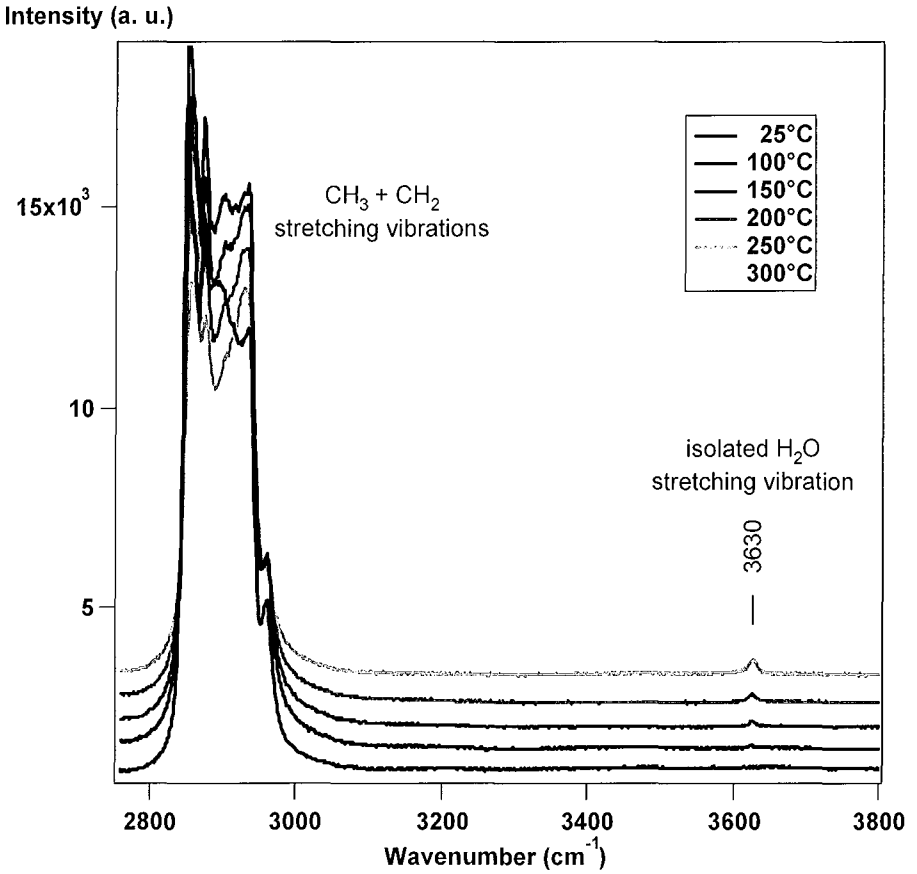

Figure C-31: Raman spectra at different temperatures of an n-dodecane inclusion synthesised in KCl.

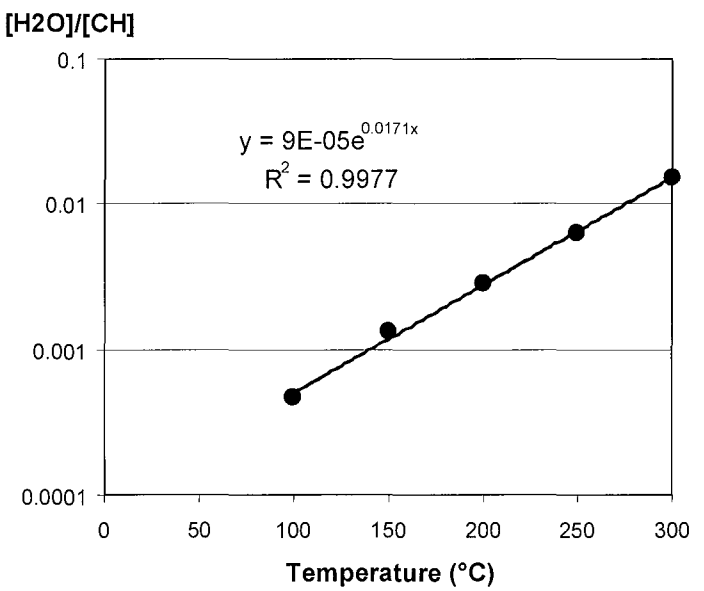

Figure C-32: Evolution of the H_2O/CH band area ratio measured on Raman spectra with temperature for an n-dodecane synthetic inclusion in KCl.

In the case of natural inclusions, FT-IR spectroscopy will be more efficient than Raman spectroscopy because it is not affected by fluorescence. It can also detect the presence of water in petroleum inclusions but has lower spatial resolution; minimum analytical spot size is 10 µm instead of 1 µm for Raman. The IR beam is reduced to the size of the bulk inclusion. Liquid water stretching vibrations are located at 3200 and 3400 cm^{-1}. They are clearly detected on the spectrum of a synthetic oil inclusion at room temperature. Their intensity decreases with temperature (Figure C-33). The volume of the liquid water phase inside inclusion decreases. This phenomenon is related to the increase of water solubility in oil.

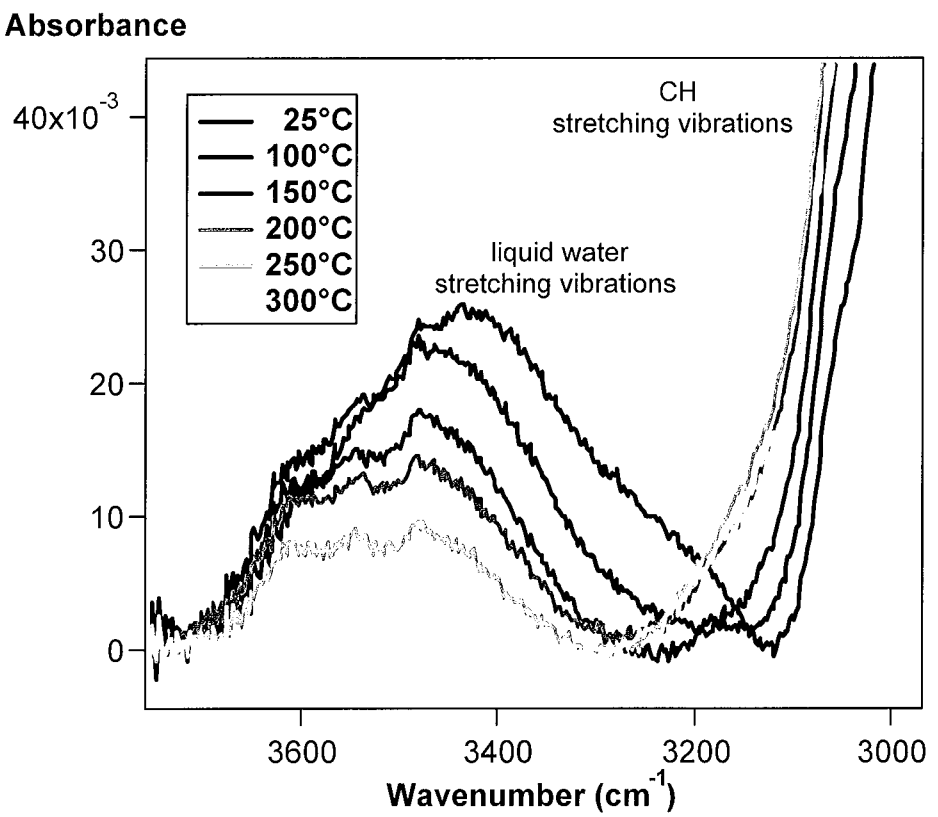

Figure C-33: Evolution of the FT-IR spectra with temperature of a synthetic petroleum dominant inclusion in KCl. Intensity of liquid water stretching bands decreases with temperature increase.

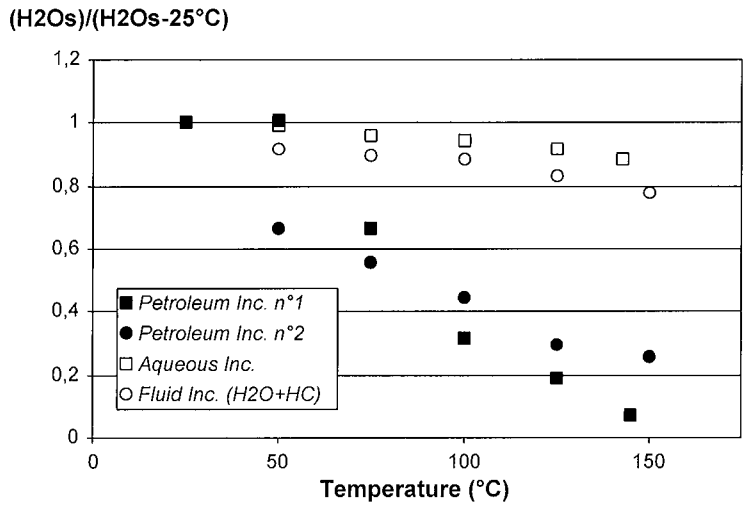

Figure C-34: Evolution with temperature of the FT-IR band area ratio between liquid water at experiment temperature and liquid water at 25°C for natural inclusions in fluorite from Illinois (USA). open squares : aqueous inclusion, open circles : aqueous inclusion with oil droplet, filled circles : oil inclusion with visible liquid water meniscus, filled squares : oil inclusion without visible water.

Liquid water band area has been measured at 25°C and at different temperatures for different natural inclusion types from MVT fluorite deposit (Illinois): aqueous inclusion, aqueous inclusion with oil droplet, oil inclusion with visible liquid water meniscus and oil inclusion without visible water. FT-IR band area of liquid water [H_2O] at a given temperature has been normalised to the liquid water band at 25°C [H_2O(25°C)]. The [H_2O]/[H_2O(25°C)] ratio is equal to 1 at 25°C and to 0 at the bulk homogenisation temperature of the inclusion. Aqueous inclusions from Illinois show a slight decrease of the liquid water band area with temperature, which can be explained by a decrease of the infrared absorption with temperature (Figure C-34). When hydrocarbons are present in the water phase (fluid inclusion with oil and water immiscible phases) a more important decrease of the liquid water band area is observed: a water fraction has been dissolved in oil. For oil dominant inclusions the decrease of the liquid water band area is important and the slope of the trend increases when the water content decreases. Inclusion with no visible water phase has been probably trapped in homogeneous state. Its normalised liquid water band area gives the bulk homogenisation temperature (150°C) when it becomes equal to zero. This temperature is higher to the homogenisation of the oil phase (120°C) and is similar to the homogenisation temperature of the aqueous inclusions (143°C).

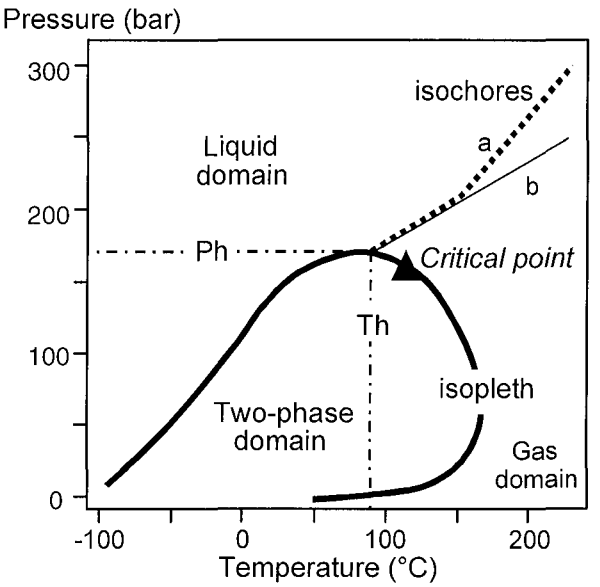

Figure C-35: P-T diagram for a model oil inclusion with a homogenisation temperature (Th) of 90°C and a homogenisation pressure (Ph) of 170 bar. a : isochore for oil + 10 mole% of water, b : isochore for pure oil system.

11.4 Discussion and conclusions

Coupled with a heating stage, FT-IR analysis allows us to determine the bulk homogenisation (water in oil) temperature of petroleum inclusions. Bulk homogenisation is never measured by conventional microthermometric studies, which only take into account the homogenisation of the oil phase. These new data should help us to reconsider PVTX interpretations of petroleum inclusions. The "water effect" on isochore has been tested using Daridon (1992) equation of state on a model inclusion with homogenisation temperature at 90°C. Two different ways of calculation have been chosen taking (a) or not taking (b) into account the presence of 10 mole % of water (Figure C-35). At low temperature, between 90 and 150°C, the isochore is linear and is superimposed to the isochore of a pure oil system (b). At high temperature (> 150°C) the isochore shows a curvature and differs from the isochore of the pure oil system (b).

It appears from this simulation that the presence of water in hydrocarbon does not drastically modify P,T properties of the inclusion. Therefore, when petroleum and contemporary aqueous inclusions are present, trapping pressure and temperature could be obtained by intersection between hydrocarbon and aqueous isochores.

Nevertheless, when petroleum inclusions are not associated with contemporary aqueous inclusions, bulk homogenisation should be measured by FT-IR spectroscopy and could be interpreted as trapping temperature and pressure. The bulk homogenisation temperature of an oil inclusion, containing liquid water, liquid and vapour oil, may be some tens of degrees higher than the homogenisation temperature of its oil phase.

References

Daridon, J.L., 1992. Mesure et représentation des équilibres de phases sous pression de mélanges d'eau, de paraffines et de dioxyde de carbone. Thesis, University of Pau, France, 177 p.

Dubessy J., Buschaert S., Lamb W., Pironon J., and Thiery R. (2000). Methane-bearing aqueous fluid inclusions: Raman analysis, thermodynamic modelling and application to petroleum basins. *Chemical Geology* 173(1-3), 193-205.

Guerrant, R.P., 1964. Hydrocarbon-water solubilities at high temperatures under vapor-liquid-liquid equilibrium conditions. Ph.D. Thesis, Pennsylvania State University, 124 p.

Guillaume, D., Tkachenko, S., Dubessy, J., Pironon, J., (2001). High temperature and high pressure water solubility in ethylbenzene to 200°C and 1kbar and the acetic acid effect. *Geochimica et Cosmochimica Acta* 65, 3319-3324.

Heidman, J.L., Tsonopoulos, C., Brady, C., Wilson, G.M., 1985. High-temperature mutual solubilities of hydrocarbons and water. Part II : ethylbenzene, ethylcyclohexane, and n-octane. AIChE J. 31, 376-384.

Kertes, A.S., 1989. Hydrocarbons with water and seawater. Part II: C8 to C36. Pergamon Press, New-York, vol.38.

Pironon, J., 1990. Synthesis of hydrocarbon fluid inclusion at low temperature. The American Mineralogist 75, 226-229.

Tsonopoulos, C., Wilson, G.M., 1983. High-temperature mutualsolubilities of hydrocarbons and water. Part I : benzene, cyclohexane and n-hexane. AIChE J. 61, 815-817.

D. RELATIONS ENTRE LA DIAGENÈSE DU QUARTZ ET LA MISE EN PLACE DES HYDROCARBURES: EXEMPLE DES GRÈS DU GARN, HALTENBANKEN, NORVÈGE

RELATIONS ENTRE LA DIAGENÈSE DU QUARTZ ET LA MISE EN PLACE DES HYDROCARBURES: EXEMPLE DES GRÈS DU GARN, HALTENBANKEN, NORVÈGE.

La diagenèse siliceuse et la migration des fluides aqueux et hydrocarbonés des grès de la formation du Garn de la zone d'Haltenbanken de Mer du Nord ont été caractérisées par une approche multi-techniques basée sur l'étude des inclusions fluides et des surcroissances de quartz. Les résultats de cette étude sont présentés dans l'article situé dans ce chapitre D-§4. Les résultats principaux, ainsi que les résultats additionnels obtenus en sonde ionique sont présentés et discutés ci-après.

1 ETUDE DES INCLUSIONS FLUIDES

De très nombreuses inclusions hydrocarbonées ont été repérées en limite grain-auréole et à l'intérieur des auréoles de croissance des quartz. Les inclusions aqueuses sont essentiellement localisées dans des plans de fracture, plus rarement dans les auréoles. Les inclusions hydrocarbonées ont des remplissages gazeux variables et appartiennent à trois familles distinctes : des inclusions à fort remplissage gazeux (≥70 %) (HC_G), des inclusions à fort remplissage liquide (≤40 %) (HC_L) et des inclusions triphasiques (eau-huile-gaz) à 25°C. Les inclusions HC_L et HC_G sont parfois reliées par de fins canaux témoignant de phénomènes de necking-down ou étranglements.

L'étude microthermométrique montre des transitions de phase LLG-LG vers –60°C pour les inclusions HC_L et vers –50°C pour les inclusions HC_G. Les températures d'homogénéisation en phase liquide des inclusions HC_L varient entre 100-135°C. L'homogénéisation des inclusions HC_G s'effectue en phase vapeur autour de 130°C. Une homogénéisation en phase critique a été mesurée à 131°C. L'homogénéisation des inclusions aqueuses peu salées varie de 105 à 150°C.

Les analyses quantitatives Raman et infrarouge montrent un fort enrichissement en méthane des inclusions HC_G. Le faible rapport CH_2/CH_3, l'abondance de méthane et de CO_2 sont caractéristiques d'un fluide de type gaz à condensat. Les inclusions aqueuses analysées dans les fractures sont pauvres en méthane, entre 0,01 et 0,05 molal, celles des auréoles sont beaucoup plus riches et leur teneur est comprise entre 0,05 et 0,16 molal.

L'étude des inclusions hydrocarbonées par microscopie confocale à balayage laser a permis de calculer des pourcentages en gaz des inclusions HC_L entre 0,9 et 20,8% et ceux des inclusions HC_G autour de 87%.

2 ETUDE DES AUREOLES DE CROISSANCE DES QUARTZ

2.1 Cathodoluminescence

Les images obtenues en CL révèlent une diagenèse siliceuse très développée avec cinq, voir six stades de croissance (Figure D-1 et D-5). Les limites des zones internes de croissance sont caractérisées par une bande luminescente blanche. Les stades terminaux des auréoles sont le plus souvent dépourvus d'inclusions hydrocarbonées (zones E et F). Dans ce cas, les zonations internes des auréoles sont bien marquées. En revanche, lorsque les zones de croissance sont riches en inclusions (zones A, B), les zonations sont irrégulières et disparaissent même dans les premières zones de croissance situées en bordure du grain (zones A et B). La limite entre les zones B, C et D est relativement floue suivant la position dans l'auréole. Dans la partie droite de la figure D-1b, la zone C est clairement postérieure à B. Entre les deux profils de sonde, la partie B semble être directement en contact avec les deux parties D (droite) et C (gauche).

Lorsque les inclusions hydrocarbonées sont situées en limite grain-auréole, celle-ci est irrégulière et corrodée, ce qui est probablement dû à des phénomènes de dissolution du quartz (Figure D-1). La présence de necking-down, de zones irrégulières de croissance, de limite grain-auréole corrodée peut être considéré comme un marqueurs de dissolution ou de recristallisation du quartz. Les fractures situées à l'intérieur du grain sont en contact avec la limite grain-auréole mais ne se poursuivent pas dans l'auréole.

2.2 Isotopes de l'oxygène

Des mesures de $\delta^{18}O_{SMOW}$ ont été obtenues dans les grains détritiques et les auréoles de croissance des quartz. L'ensemble quartz-auréole de la Figure D-1 est un exemple très représentatif des auréoles de la zone d'Haltenbanken. La configuration du grain et de l'auréole, ainsi que la taille relativement importante de l'auréole ont permis de tracer deux profils de sonde traversant le grain et les différentes zones de l'auréole. Les valeurs de $\delta^{18}O_{SMOW}$ oscillent entre 9.28 et 12.16‰ dans le grain détritique et entre 19.3 et 25.8‰ dans les auréoles de croissance des quartz (figure D-1). Les valeurs $\delta^{18}O$ sont relativement hétérogènes à l'échelle de l'auréole. Il n'y a pas d'évidence d'augmentation ou de réduction constante des valeurs en $\delta^{18}O$ de la limite grain-auréole vers l'auréole externe. La zone interne B des auréoles enrichies en inclusions hydrocarbonées a des valeurs de $\delta^{18}O$ maximales, entre 21 à 26‰. Les zones C, D, E, F, dépourvues en inclusions ont des valeurs de $\delta^{18}O$ minimales, entre 17 et 21‰. Les zones de silicification A et F, qui spatialement correspondent à la première et à la dernière étape de silicification, ont des $\delta^{18}O$ moyens autour de 20‰. Contrairement à la zone F, la zone A, située en limite de grain, est riche en inclusions hydrocarbonées.

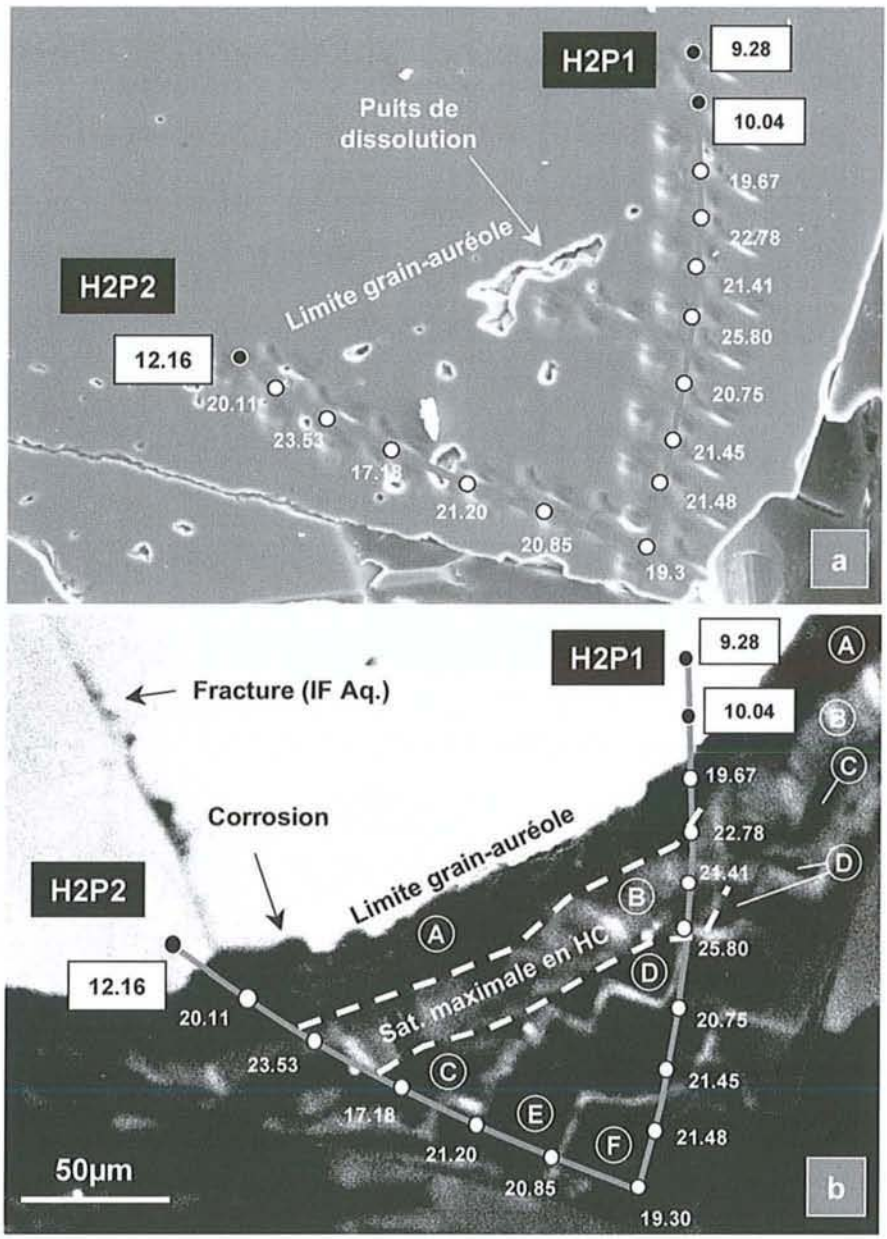

Figure D-1: Auréole de croissance de quartz de la zone d'Haltenbanken, puits 6507/2-2. Deux profils H2P1 et H2P2 ont été dessinés. Les valeurs associées aux points d'impact de sonde ionique ®IMS 1270 correspondent aux valeurs isotopiques du $\delta^{18}O$ dans le quartz.
a: Image en électrons secondaires, b: image en cathodoluminescence.

3 EVOLUTION DU OU DES FLUIDE(S) EN EQUILIBRE AVEC LES SURCROISSANCES DE QUARTZ

Lors des processus de cristallisation, le fractionnement des isotopes est fonction du minéral considéré, de la composition isotopique initiale du fluide minéralisateur et de la température. Les données de fractionnement des isotopes de l'oxygène entre le quartz et l'eau (Matsuhisa et al, 1979; Zheng, 1993) sont le plus souvent utilisées pour tracer les courbes d'équilibres entre les surcroissances de quartz et "les fluides" des bassins. La composition isotopique du fluide au moment de la précipitation du quartz est estimée si le fractionnement et la température sont connus. Les T_h des inclusions peuvent être considérées comme des températures minimales de silicification. A partir des $\delta^{18}O$ du fluide, des paléo-compositions et des compositions actuelles, des hypothèses peuvent ensuite être émises sur l'origine des fluides et leur circulation. Les hypothèses les plus souvent évoquées sur l'origine des fluides en Mer du Nord portent sur la venue d'un fluide riche en $\delta^{18}O$ d'origine météorique, éventuellement en contact avec de l'eau marine ou provenant de formations argileuses plus profondes (Girard et al, 2001;Wilkinson et al, 1992; Blanchet, 2002). Ces fluides auraient migré, circulé ou infiltré les grès.

L'objectif ici est de confronter la démarche et les hypothèses classiquement utilisées et émises sur l'origine des fluides avec les résultats expérimentaux développées et illustrées chapitres B et C. Pour illustrer notre démarche, l'exemple du quartz de la figure D-1 est utilisé.

3.1 Approche conventionnelle

Les six zones internes de l'auréole ont des signatures isotopiques relativement différentes. Les zones A, B, C, D, E, F ont respectivement un $\delta^{18}O$ moyen de 19.9, 23.4, 17.2, 20.8, 21.1 et 20.6‰. Les courbes de fractionnement ont été tracées figure D-2 en fonction de la température. Pour plus de clarté, les courbes D, E et F ont été groupées sur une seule courbe de fractionnement de 21‰ . La contrainte thermique apportée par les T_h des inclusions fluides est comprise entre 111 et 134°C en bordure de grain (zone A et B). L'écart de fractionnement entre une température de 111 et 134°C est d'environ 2.7 (Matsuhisa et al, 1979) et est différent de l'écart mesuré de 8.6 entre les valeurs extrêmes de $\delta^{18}O$ des auréoles des grès d'Haltenbanken.

Les sédiments de la formation du Garn d'Haltenbanken étudiés se sont déposés au Jurassique. Le mélange d'une composition isotopique d'une eau marine ($\delta^{18}O$ = -1.2‰) et d'une eau météorique ($\delta^{18}O$ = -7‰) en Mer du Nord au Jurassique est estimé entre -7 et -1‰. Les $\delta^{18}O$ des eaux de formation actuelles de la Mer du Nord se situent dans une fourchette de +2 à +5‰ (Egeberg et Aagaard, 1989; Wilkinson et al, 1992). Ces valeurs sont reportées sur la figure D-2.

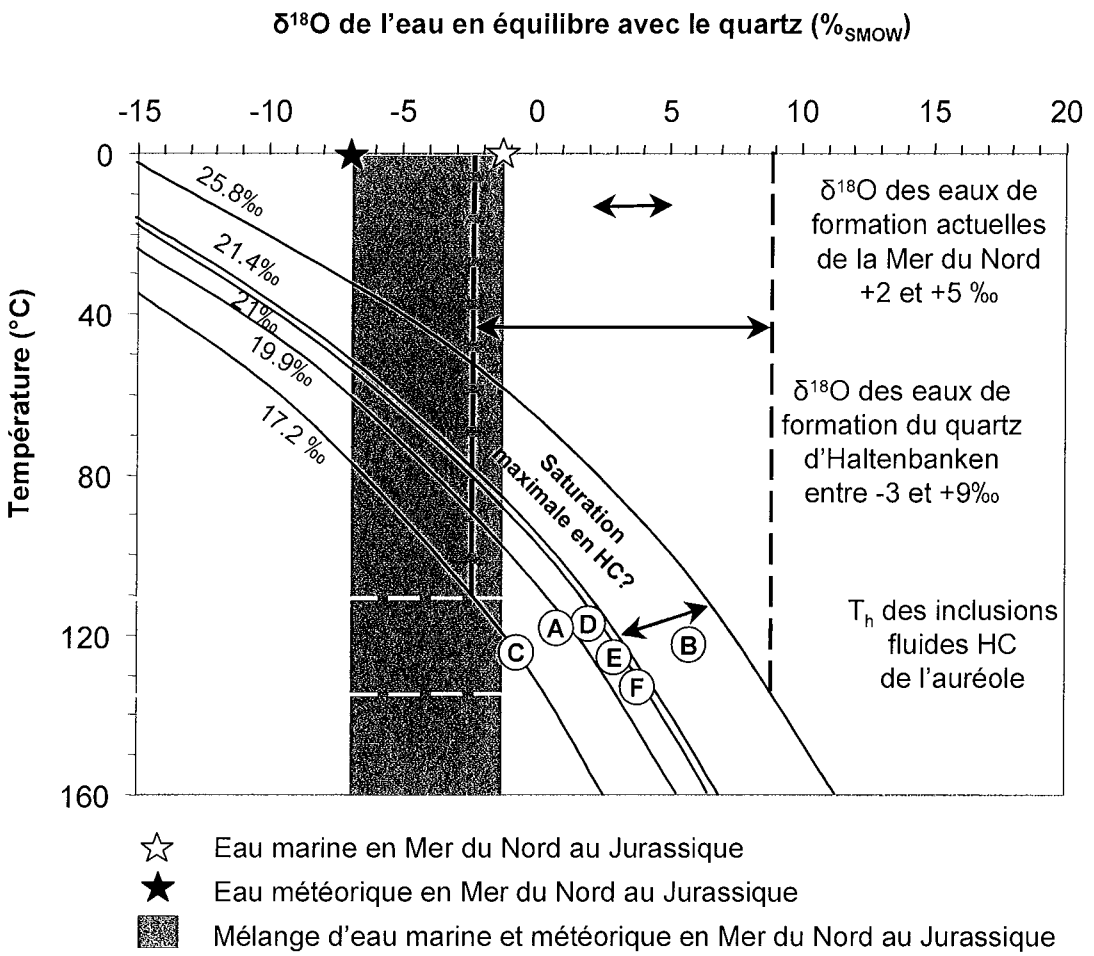

Figure D-2: Courbes de fractionnement des isotopes de l'oxygène du quartz du puits 6507/2-2 de la zone d'Haltenbanken dans une auréole de croissance d'un quartz (Figure D-1).

Les valeurs $\delta^{18}O$ de l'auréole sont hétérogènes. Le manque d'indicateurs thermiques (inclusions) empêche de déterminer avec précision les valeurs en $\delta^{18}O$ du fluide en équilibre avec les zones de silicification C, D, E, F.

Le $\delta^{18}O$ du fluide en équilibre le plus bas est obtenu dans la zone C. Il est estimé à -3‰ (Figure D-2) pour une température minimale de silicification de 111°C. Il correspond à une signature isotopique d'eau météorique fortement mélangée à une eau de mer. La zone A est spatialement la première zone de silicification. Le fluide en équilibre avec cette zone A est compris entre +1 à +3‰. Le fluide en équilibre avec les dernières zones de croissance (D, E, F) est estimé entre +1 et +4‰ avec une légère diminution du $\delta^{18}O$ dans le dernier stade. Le fluide en équilibre avec les zones de silicifications B est de +2 à +9‰.

L'écart de fractionnement entre des températures minimales de piégeages des inclusions entre 111 et 134°C est d'environ 2.7. Cette valeur ne peut donc pas expliquer à elle seule les variations isotopiques dans l'auréole, entre 25.8 et 17.2‰, soit un écart de 8.6. La région d'Haltenbanken est connue comme une zone de surpression et de transit de fluides (Karlsen et al,

1995). Les roches mères sont les shales de la formation de Spekk (fin Jurassique) et les charbons et les shales de la formation du Åre (Odden et al, 1998). Les huiles et les gaz à condensat porteraient la signature plus ou moins prononcée d'une origine à la fois marine et terrestre de ces deux formations (Karlsen et al, 1995; Odden et al, 1998).

Les différentes zones de croissance de la zone d'Haltenbanken (Figure D-1) semblent donc avoir précipité à partir de fluides dont les compositions isotopiques évoluent d'un pôle eau marine (avec éventuellement une influence météorique) vers un pôle enrichis en $\delta^{18}O$. L'hypothèse d'un fluide profond riche en $\delta^{18}O$ n'est donc pas écartée.

3.2 Apport des données expérimentales

Les données expérimentales obtenues en SIMS sur les auréoles de croissance des quartz en présence d'eau et d'hydrocarbures ont montré que les auréoles générées en présence d'huile avaient des $\delta^{18}O$ supérieures, d'environ 10‰ par rapport à celles crées en milieu strictement aqueux dans les conditions expérimentales à 350°C et 400 bar (chapitre C-§9). Il est donc clair que la présence d'huile a une influence directe sur les valeurs de $\delta^{18}O$ des auréoles. Il est envisageable que les valeurs de $\delta^{18}O$ puissent alors varier d'une huile à l'autre et ainsi faire varier les $\delta^{18}O$ au sein même d'une auréole. Cet aspect est d'autant plus important que les huiles d'une zone naturelle comme Haltenbanken peuvent provenir de différentes roches mères (Karlsen et al, 1995; Odden et al, 1998).

Les zones internes des auréoles enrichies en inclusions hydrocarbonées de la zone d'Haltenbanken (Figure D-1) ont des valeurs en $\delta^{18}O$ maximales, entre 21 et 26‰. Si l'on fait le parallèle entre l'étude des auréoles naturelles de cette zone avec les auréoles expérimentales, il est fort probable que les valeurs maximales en $\delta^{18}O$ des auréoles de croissance des quartz d'Haltenbanken puissent correspondre à une forte saturation en huile du réservoir. Dans ce cas, les hypothèses d'un fluide météorique ou profond ne suffiraient plus à elles seules pour expliquer les fortes valeurs isotopiques en $\delta^{18}O$ des quartz diagénétiques.

4 CROISSANCE DE QUARTZ ET MIGRATION DES HYDROCARBURES

4.1 Apport des données expérimentales

Les expériences réalisées dans cette étude ont montré que la mouillabilité des quartz vis à vis de l'eau et/ou des hydrocarbures était un paramètre très important. En effet, quand le quartz est d'abord mouillé à huile, la croissance de quartz et la formation d'inclusions fluides sont inexistantes. A l'inverse, quand le quartz est d'abord mouillé à l'eau, les expériences réalisées en présence d'hydrocarbures montrent que la croissance de quartz est possible même à forte

saturation en huile (E/H = 10% à 25°C). Dans les conditions expérimentales à 350°C-400bar, la dissolution de la quasi-totalité de l'eau dans l'huile tend à prouver qu'un film d'eau (voire de l'eau irréductible) au contact du grain suffit à faire croître le quartz. Cette hypothèse n'est bien sûr valable que si l'eau reste le seul transporteur et vecteur de silice.

4.2 Scénario de croissance de quartz et migration des hydrocarbures

La région d'Haltenbanken est connue comme une zone de surpression et de transit de fluides (Karlsen et al, 1995; Odden et al, 1998). Malgré la complexité du système, les données d'inclusions fluides, de CL, de sonde ainsi que les données expérimentales (chapitre C) permettent de contraindre le système et d'élaborer un scénario sur l'histoire de la silicification des auréoles en présence d'hydrocarbures. Il est fort probable que les stades décrits ci-après soit plus le fait d'une fluctuation de la colonne eau/huile/gaz appartenant à un même fluide plutôt qu'à des stades différents de migration ou de croissance. Un piégeage hétérogène des inclusions aurait pu être ainsi produit par un seul et unique type de fluide hydrocarboné. Pour illustrer notre démarche, l'exemple du quartz de la figure D-1 est utilisé.

4.2.1 Stade 1

La zone A des auréoles croît dans un milieu à forte saturation en huile en présence d'eau et d'hydrocarbures (Figure D-1). Les grains sont corrodés. Des inclusions hydrocarbonées sont piégées dans le domaine à deux phases (liquide et gaz). La quasi-absence d'inclusions aqueuses dans ces zones tend à prouver que le peu d'eau restant a été en grande partie incorporé au quartz néoformé. L'observation d'un film d'eau mouillant les parois des inclusions hydrocarbonées suggère que les quartz étaient mouillés à l'eau et confirme bien l'existence d'un film d'eau autour des grains.

4.2.2 Stade 2

Une deuxième phase d'arrivée d'hydrocarbures et de croissance de quartz conduit à la formation de la zone B. La saturation en huile est supérieure à la précédente, l'extension de la zone B est réduite. Cette phase de forte saturation en huile est accompagnée de phénomènes de necking-down, d'infiltrations des précédentes zones de croissance par les hydrocarbures et l'eau. La texture CL des zones A et B est alors perturbée et des phénomènes de dissolution et de cristallisations se produisent. Des infiltrations au contact grain-auréole sont possibles.

4.2.3 Stade 3

L'huile se retire. La texture des auréoles de croissance des quartz et l'absence d'inclusion hydrocarbonée de la zone C, D, E, F indiquent une reprise de la croissance en milieu exclusivement aqueux.

5 Article 9: FLUID INCLUSIONS AND PVTX MODELLING: EXAMPLES FROM THE GARN FORMATION, HALTENBANKEN, MID-NORWAY

La diagenèse siliceuse et la migration des fluides aqueux et hydrocarbonés des grès de la formation du Garn de la zone d'Haltenbanken de Mer du Nord ont été caractérisées par une approche multi-techniques basée sur l'étude des inclusions fluides et des surcroissances de quartz. Des changements de phase de basses températures des inclusions hydrocarbonées ont été mis en évidence et sont caractéristiques des gaz à condensat riche en méthane et alcanes lourds. L'hypothèse d'un piégeage dans le domaine biphasique des hydrocarbures explique la diversité des inclusions fluides hydrocarbonées. Un tel piégeage hétérogène serait à l'origine de l'abondance des figures d'étranglement (necking-down). Ainsi, la grande variété des inclusions aurait pu être produite par un seul et unique type de fluide hydrocarboné riche en gaz. Trois épisodes de piégeage ont été distingués. Le premier correspond au piégeage d'un fluide aqueux dans les fractures des grains de quartz, autour de 50°C et 50 bar. Le second correspond à l'arrivée du fluide hydrocarboné supercritique, autour de 100-120°C et 190-230 bar. Enfin, le piégeage principal des inclusions hydrocarbonées, autour de 110-160°C et 230-280 bar s'est produit durant la recristallisation des ciments de quartz au cours d'un enfouissement rapide produit lors des cinq derniers millions d'années.

FLUID INCLUSIONS AND PVTX MODELLING: EXAMPLES FROM THE GARN FORMATION, HALTENBANKEN, MID-NORWAY

S. TEINTURIER [a], J. PIRONON [a] and F. WALGENWITZ [b]

[a] *CREGU-UMR G2R-7566, BP23 F-54506 Vandoeuvre-lès-Nancy, France*
[b] *CSTJF, TotalFinaElf, Avenue Larribau, F-64018 Pau, France*

Marine and Petroleum Geology (2002), Vol 19 (6), p755-765

ABSTRACT

Fluid inclusions study and multi-techniques quantitative analyses have been coupled to reconstitute PVTX conditions of aqueous and petroleum fluid entrapment of a local Haltenbanken area from the Garn Formation. Unusual low temperature behaviour showing the liquid portion separates into two liquids have been described. This behaviour is typical of a gas condensate/volatile mixture with high methane content and heavy alkanes. The variable liquid-vapour ratio, compositions and morphologies of all petroleum inclusions can be interpreted as a result of a combination of heterogeneous trapping and necking down. Thus, all petroleum inclusions can be related to a single petroleum source. Three main episodes of fluid entrapment can be distinguished. The first one corresponds to the water trapped within detrital quartz microfractures, at around 50°C and 50 bar; the second to the petroleum fluid arrival in the biphase field of a critical system around 100-120°C and 190-230 bar. The third one to the main trapping of present-day petroleum inclusions during the recrystallisation of quartz cements (around 110-160°C and 230-280 bar) within the last few million years of a short and relatively rapid burial.

Keywords: Fluid inclusion; PVT modelling; Haltenbanken; Hydrocarbon; Petroleum; Quartz cementation

5.1 Introduction

Fluid inclusion studies are a powerful tool in understanding and deciphering the diagenetic history of petroleum reservoirs. Microthermometry, confocal scanning laser microscopy (CSLM), Raman and FT-IR spectroscopies coupled with thermodynamic modelling, allow the reconstruction of accurate PVT conditions of aqueous and petroleum fluid entrapment occurring in sedimentary basins (Pironon, Canals, Dubessy, Walgenwitz & Laplace-Builhe, 1998; Aplin, MacLeod, Larter, Pedersen, Sorensen & Booth, 1999; Pironon, Thiéry, Ayt Ougougdal, Teinturier, Beaudoin & Walgenwitz, 2001). Nevertheless, this approach must take into account the relationships between quartz cementation and oil migration to clearly define diagenesis events and chronology. The presence of petroleum inclusions within quartz cement is not conclusive evidence that these inclusions represent the initial petroleum fluid composition and that they were simultaneously formed at the same time that quartz cementation.

The ability of petroleum emplacement to inhibit quartz cementation has been debated by many authors and depends mostly on the controls on silica transport from its source to precipitation (Worden & Morad, 2000). Oil inclusions inside quartz cements, similar homogenisation temperature ranges and/or relative similar volumes of cement or porosities between water and oil-saturated zones are the prime empirical arguments of authors who consider that oil emplacement does not halt quartz cementation (Walderhaug, 1990; Ramm, 1992; Saigal, Bjorlykke & Larter, 1992). The concept that quartz cementation is inhibited by oil saturation is based on significant differences of porosity in some oil-bearing sandstones reservoirs (Gluyas, Robinson, Emery, Grant & Oxtoby, 1993).

The purposes of this paper are (1) to describe unusual microthermometric behaviour and new analytical data derived from fluid inclusion studies and quantitative spectroscopic analyses (2) to propose a PVTX model for aqueous and petroleum fluid entrapment and (3) to discuss the relationships between quartz cementation, petroleum migration and emplacement in the Garn Formation in the Haltenbanken Mid-Norway area.

Previous fluid inclusion studies in the Haltenbanken region argue for a continuous process of quartz cementation at temperatures between 89-141°C (Ehrenberg, 1990; Walderhaug, 1990; Grant & Oxtoby, 1992, Walderhaug, 1994a; Walderhaug, 1994b; Williams, Hervig & Bjorlykke, 1997) and a trapping pressure for the petroleum fluid around 200 and 260 bar (Swarbrick & Edwards, 1993). Migrating petroleum is assumed to have entered the reservoir at temperatures around 100°C in the last 3-5 Ma. The main source rocks of the Haltenbanken offshore Mid-Norway area are the marine shales of the Late Jurassic Spekk Formation and the coals and paralic shales of the Early Jurassic Åre Formation (Odden, Patience & Graas, 1998). According to Odden et al. (1998), oil and gas-condensates from the Alve and the Norne field to the east of this area mostly originated from the Spekk Formation with variable Åre contribution, minor for Alve, significant for

Norne. Karlsen et al. (1995) stated that the C15+ fraction from Alve originated from a mixed marine/terrestrial input from the Spekk Formation.

5.2 Sample material

The studied sandstones belong to the Middle Jurassic Garn Formation and are located in the Haltenbanken area offshore mid-Norway (Bjorlykke, Aagaard, Dypvik, Hastings & Harper, 1986), (Figure D.-3). This area is overpressured and known as a migration route for petroleum fluids (Karlsen et al., 1995). Seven samples were cored from 3685m to 3925m. The samples were made into double-sided polished rock sections around 200-300µm thick, suitable for observation by the different analytical techniques we applied. These sandstones are subarkosic arenites with more than 90% quartz, other minerals include kaolinite, muscovite and a small amount of illite and pyrite. They contain numerous fluid inclusions and have a highly developed siliceous diagenesis with marked quartz overgrowths and quartz-filled microfractures inside and at the edge of the detrital quartz grains.

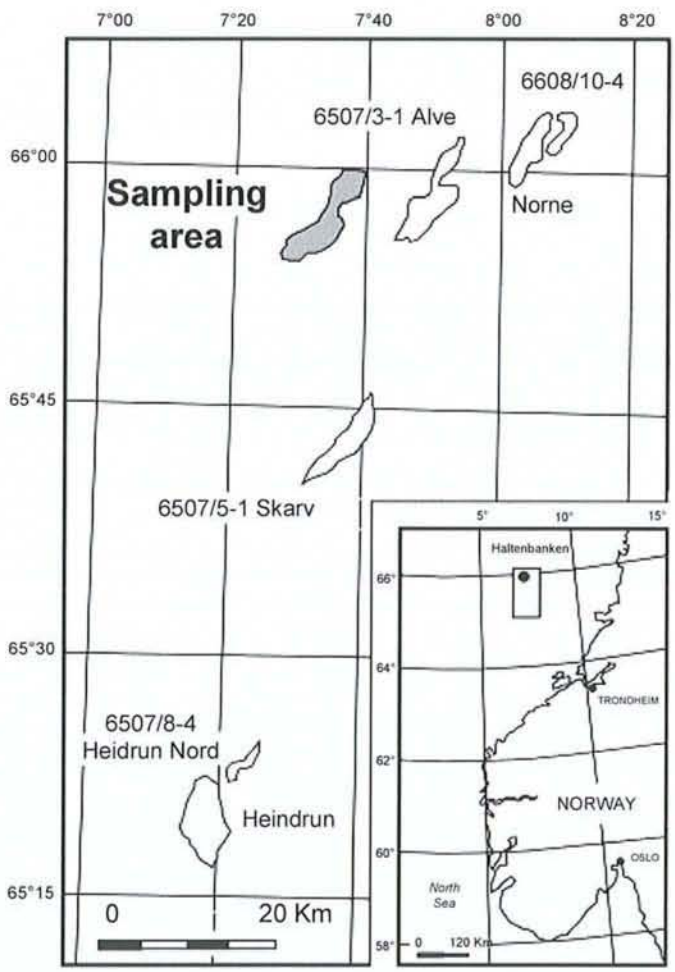

Figure D-3: Location map of the Haltenbanken, offshore mid-Norway.

5.3 Analytical methods

All samples were inspected under a standard polarising microscope equipped with fluorescence accessories to locate and separate the aqueous inclusions from the petroleum inclusions. Petroleum inclusions were identified by their fluorescence (blue to yellow) under ultraviolet illumination. No barrier filter was used to enhance fluorescence detection. This system allows detection of small amount of liquid oil within gas inclusions.

5.3.1 Cathodoluminescence

The differentiation of diagenetic overgrowths from detrital quartz grains was performed using a cathodoluminescence (CL) detector on a scanning electron microscope *(SEM)* ®Oxford mono-CL. Samples were coated with carbon and observed using an accelerating voltage of 20-25kV and a probe current of 6 nA. Images were acquired at the Laboratoire commun d'analyses from the Nancy UHP University.

5.3.2 Microthermometry

Microthermometric data were acquired both on ®Chaix-Meca (Poty, Leroy & Jachimowicz, 1976) and ®USGS (Goldstein & Reynolds, 1994) equipment. Stages were calibrated by pure CO_2 inclusions (Tm = -56.6°C) and low salinity synthetic aqueous inclusion (Tm = -0.4°C) at low temperature, and by melting of various crystals at positive temperatures. Phase transitions of oil and aqueous inclusions were observed with ®Olympus x40 and x80 objectives.

5.3.3 Raman microspectrometry

Raman quantitative analyses were performed on a ®Labram Dilor spectrometer using 514.5 nm incident radiation produced by an argon laser. A ®Chaix-Meca and a ®Linkam heating stage were coupled to an ®Olympus microscope equipped with x80 objectives. Methane concentration in the liquid phase at homogenisation temperature was determined using the calibration of Guillaume et al. (in press) and Dubessy et al. (2001). Accumulation time, laser power and confocal aperture were adapted for each inclusion measurement to obtain the best signal/background ratio.

5.3.4 Fourier transform infrared microspectrometry

Infrared spectra were recorded using a ®Bruker Equinox 55 Fourier transform spectrometer equipped with a ®Bruker microscope. The mid-infrared range was reduced to 2000 cm^{-1} due to inclusion hosted quartz absorption. The infrared beam was narrowed to the bulk inclusion size with a diaphragm in the image plane. The minimum aperture was 20 µm using a x15 objective and 8µm using a x36 objective. The accumulation time was around 4 min and the spectral resolution was 4 cm^{-1}. The contribution of atmospheric H_2O and CO_2 was removed by subtraction of their independently recorded characteristic spectra. Before each inclusion measurement, a reference spectrum was recorded in the air. The quartz contribution was partially removed by subtraction of its FT-IR spectrum, recorded in an area neighbouring the inclusions, free of contaminants (minerals, fluid inclusions and organic matter). Analyses were made in transmission non-polarised mode.

The content of methane, CO_2 and alkanes in inclusions was obtained according to the method of Pironon et al. (2001): CO_2 is detected at 2340 cm^{-1}, CH_4 at 2960, 3006 and 3050 cm^{-1}, alkanes (CH_2- and CH_3-) at 2860, 2877, 2930 and 2960 cm^{-1}.

5.3.5 Confocal Scanning Laser Microscopy

CSLM analyses were performed using a number of microscopes through the course of this study: from ®Zeiss (LSM 510), ®Bio-Rad (Radiance 2000) and ®Olympus (FV 300) companies. The spatial resolution of CSLM is near SEM resolution. Besides conventional transmission observations, two other modes of visualisation were used. Firstly, in fluorescence mode using an incident laser radiation at λ=488nm and collecting emission of fluorescence at a longer wavelength of $\lambda > \lambda_0$. This mode is effective for liquid oil detection. However, volume estimates can rarely be made on gas-rich inclusions because of the irregular bubble morphology and the small liquid oil content. Secondly, in reflection mode using incident laser radiation and filter in front of the collecting photomultiplier, both at 637 nm. This mode is very sensitive to refractive index changes and is used for the detection of liquid water inside inclusions because oil and quartz have similar indices, higher than the liquid water index. Confocal planes are acquired with a 0.5 µm step and image processing was performed using Igor software (Pironon et al., 1998) for 3D reconstruction.

5.4 Results

5.4.1 Description of fluid inclusions

Both aqueous and petroleum inclusions are found in all samples, except in 3770.8 m where only aqueous inclusions are present. The inclusion shapes are extremely variable. Some of the more irregular shapes are those expected from necking down (Figure D-4.).

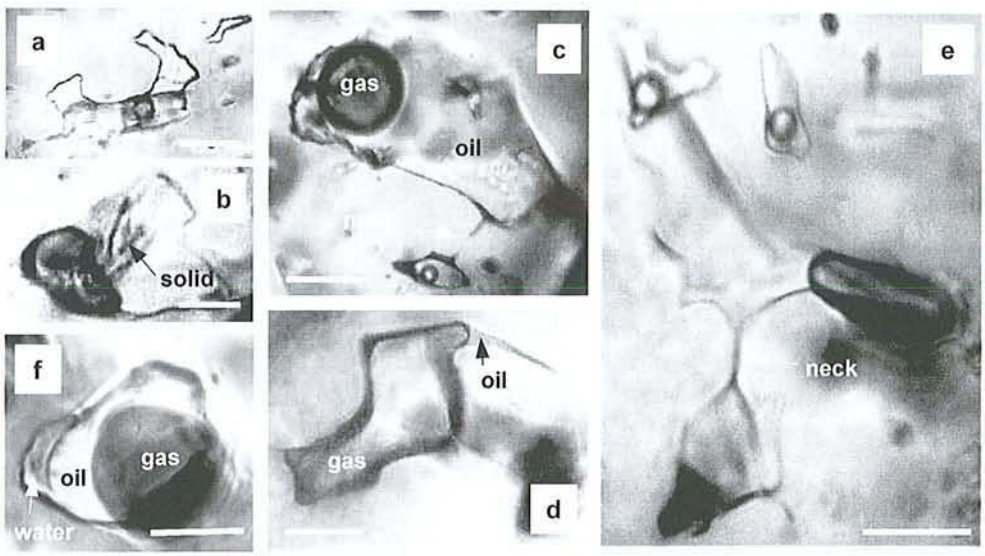

Figure D-4: Photomicrographs of fluid inclusions. a) aqueous inclusions. b) petroleum inclusions with solids. c, d, e) hydrocarbon inclusions showing necking-down effects. (f) three phase inclusion. Bar scale = 10µm.

Aqueous inclusions are two-phase or single-phase and are mainly localised within healed microfractures inside quartz grains, or along dust rims between detrital quartz grains and quartz overgrowths. Most of these inclusions have sizes lower than 10 µm but some reach 30 µm in length. Two-phase and single-phase aqueous inclusions are often observed in the same healed microfracture at room temperature. At 3687.6 m, 3691.7 m, 3770.8 m and 3921.25 m, no aqueous inclusions were detected in quartz overgrowths. Samples at 3685.9 m, 3694 m and 3925.75 m contain aqueous inclusions inside quartz overgrowths coexisting with petroleum inclusions.

The numerous petroleum inclusions dominantly occur at the boundary between quartz grains and quartz overgrowths and inside quartz overgrowths. No petroleum inclusions were found within microfractures. They often appear to be larger than aqueous inclusions but are rarely greater than 25 µm in length. The largest petroleum inclusions have a maximum size of around 50 µm. Petroleum inclusions have variable liquid-vapour ratio in both quartz overgrowths and at the

boundary between detrital quartz and quartz overgrowths. Two distinct families have been observed: (1) HC_G inclusions with dominant vapour fill (vapour vol. % > 70 %) and (2) HC_L inclusions with dominant vapour fill (vapour vol. % < 30) at 25°C. Variations of their fluorescence colour in UV and intensity depend on the type and the filling of petroleum inclusions: pale-yellow to intense yellow for the HC_L inclusions and various shades of brown for the HC_G inclusions. HC_G inclusions and HC_L inclusions are found in similar proportion in all samples except at 3687.6 m where the number of HC_G inclusions with more than 90% of vapour is clearly higher in quartz overgrowths than the number of HC_L inclusions. Both petroleum families are randomly distributed in the overgrowths. Petroleum inclusions are often connected by thin channels attesting to the phenomenon of necking down (Figure D-4). It observed between HC_G and HC_L inclusions, HC_L and HC_L inclusions but not between HC_G and HC_G inclusions. Many HC_L inclusions contain one or several solids.

3-phase inclusions (water-petroleum-gas) were found inside quartz overgrowths at 3685.9 m. They are often large but do not exceed 30 µm in length. The volumetric water/petroleum percentage has been visually estimated between 10 and 30%.

5.4.2 Cathodoluminescence

CL images reveal up to five or six growth zones in the quartz cements (Figure D-5b) and show that outer (later) growth zones are sometimes depleted in petroleum inclusions (Figure D-5a). Zoning is clearly marked in the external part of the overgrowth depleted of inclusions but disappear in the earliest growth zones rich in petroleum inclusions. In addition to necking down, these features should be considered as a marker of quartz recrystallisation. When these petroleum inclusions are located at the boundary between detrital quartz and the overgrowth, the detrital grain shows irregular limits with corrosion pits, probably due to a dissolution process (Figure D-5). Microfractures within quartz grains do not cross the overgrowths.

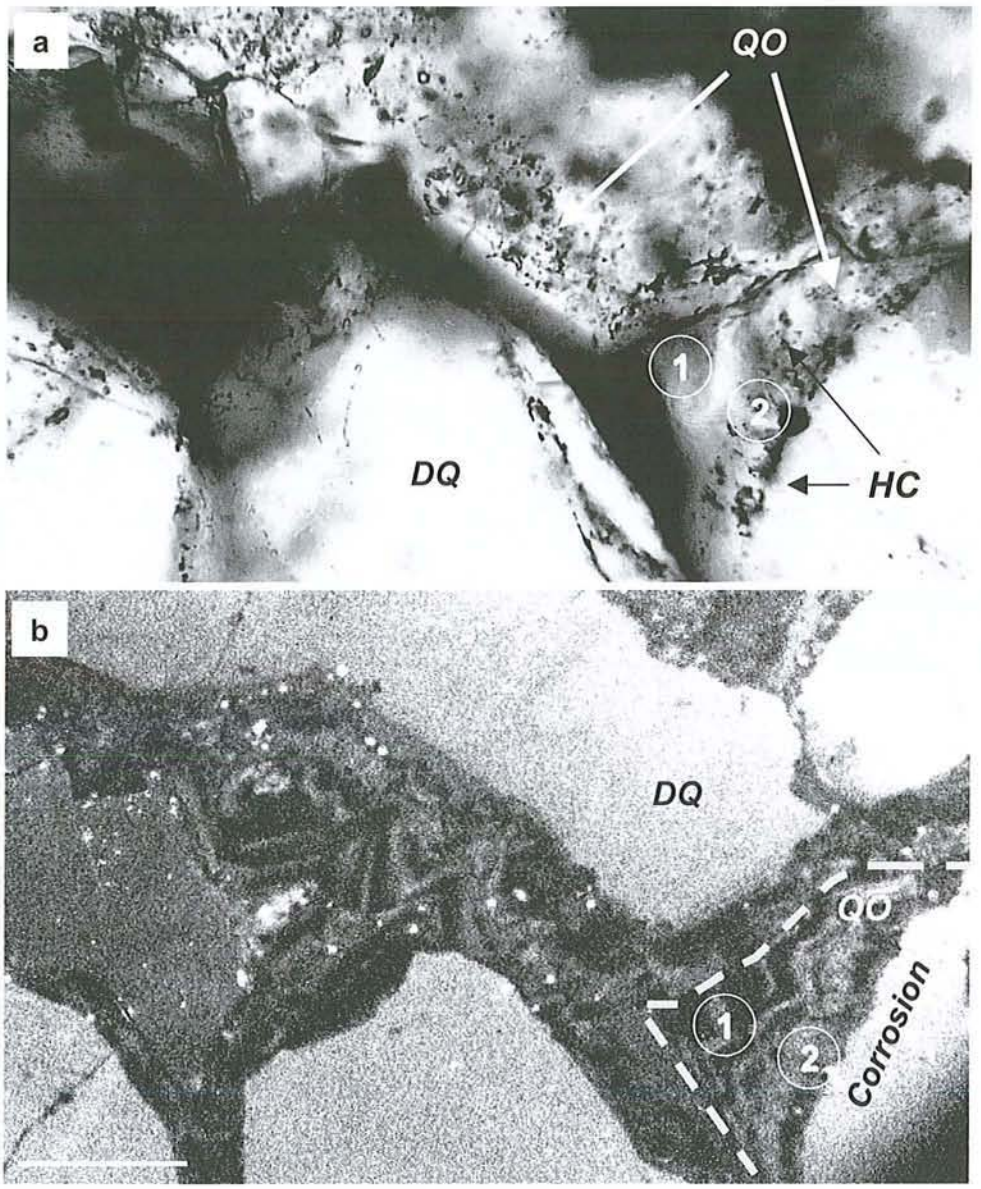

Figure D-5: Detrital quartz (DQ), quartz overgrowths (QO) and petroleum inclusion emplacement (HC) from the Haltenbanken area. Bar scale = 100µm.

(a) Optical photomicrograph showing typical distribution of inclusions: 1. the outer parts of the overgrowth is depleted of hydrocarbon inclusions. 2. The inner part of the overgrowth is rich in hydrocarbon inclusions.

(b) CL/SEM photomicrograph showing zonation in overgrowth episodes, quartz corrosion occurs at the boundary between detrital quartz and overgrowth when oil is present.

5.4.3 Microthermometry

The microthermometric study of the fluid inclusions was subject to two main limitations: (1) homogenisation temperatures for HC_G inclusions could not be accurately measured (2) it was not always possible to obtain both melting and homogenisation temperatures on aqueous inclusions.

Homogenisation temperatures for 3685.9 m to 3694 m, 3770 m and 3921.25 m to 3925.75 m are summarised in the histogram of figure D-6. The frequency of measurements approximately reflects the number and the proportion of each type of inclusion. Petroleum inclusions are much more numerous than aqueous inclusions for all depths, except at 3925.75 m and 3770 m.

The main range of homogenisation temperatures for both aqueous inclusions (102 to 137°C and measurements above 155ºC) and petroleum inclusions (87.2 to 138°C with two measurements above 157ºC) is very similar. The "3685.9 m to 3694 m" histogram shows one major peak between 105°C and 120ºC. Temperatures between 85 and 95ºC have been measured inside quartz overgrowths at 3694 m and 3685.9 m. The homogenisation temperatures of HC_G inclusions mainly range between 115°C and 130°C and are slightly higher than the homogenisation temperature of the HC_L inclusions. Critical homogenisation at 131°C has been measured at 3685.9 m in a quartz overgrowth, with a vapour-liquid ratio of about 40% at 20ºC. At 3770 m, homogenisation temperatures of aqueous inclusions are between 115-130ºC. Histograms from hydrocarbon inclusion bearing depths (Figure D-6a and 6c) are similar. Homogenisation temperatures of aqueous inclusions between 130 and 140°C are only observed in the deeper samples. Homogenisation temperatures for aqueous inclusions located inside quartz overgrowths and at the boundary between quartz grain and quartz overgrowth are similar and sometimes lower than those located within healed microfractures (Table D-1). Some aqueous inclusions inside quartz overgrowths have temperatures close to petroleum inclusions temperatures around 110ºC. Results of table D-1 suggest that there may be a systematic increase in both maximum and minimum homogenisation temperatures with depth for the aqueous inclusions. These data are consistent with Grant & Oxtoby (1992). No evident correlation between homogenisation temperature values and depths has been found for petroleum inclusions.

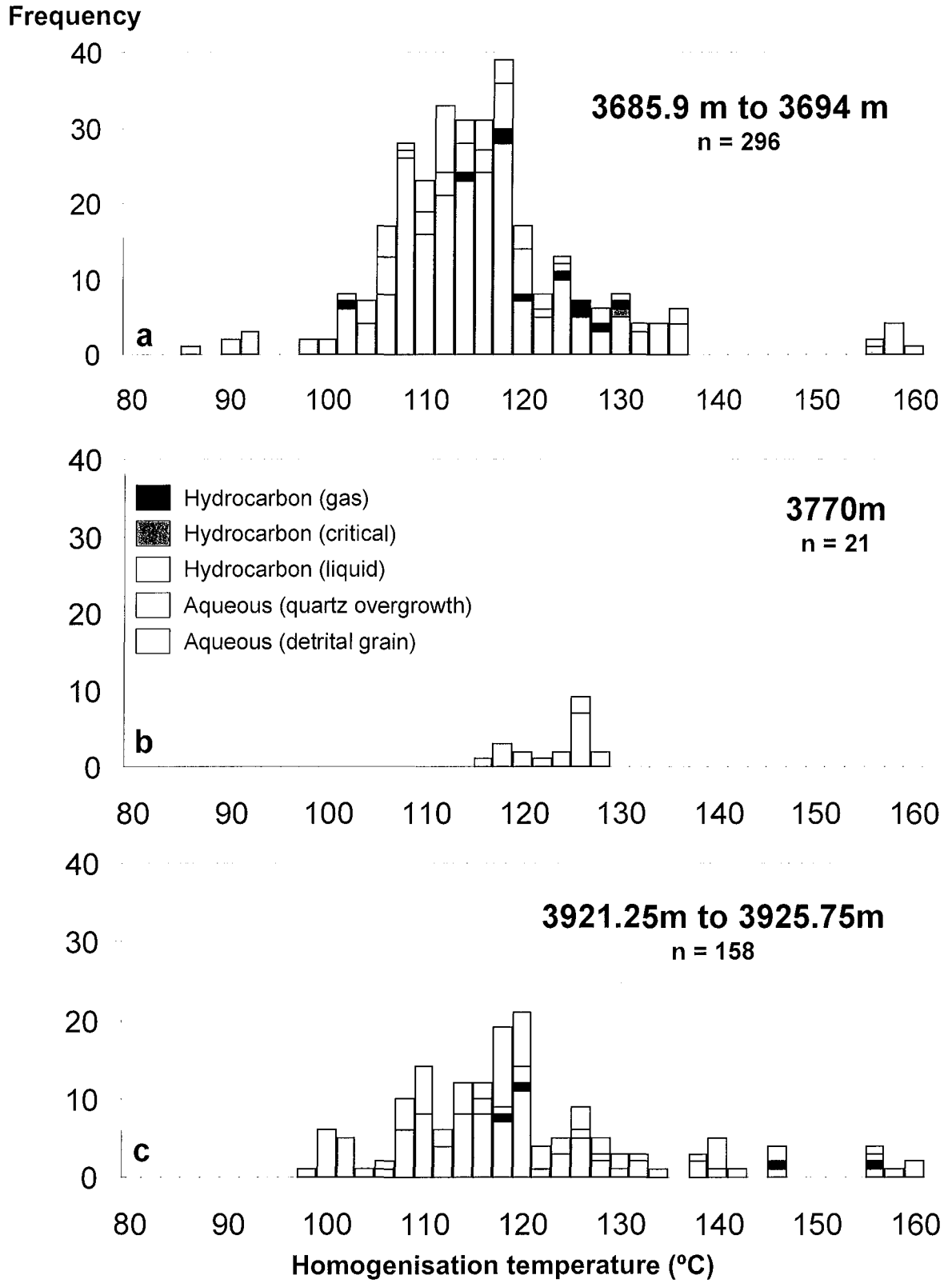

Figure D-6. Homogenisation temperature histograms for aqueous and hydrocarbon inclusions at different depths for this Haltenbanken area.

During cooling of the most of the petroleum inclusions (up to -150°C), an unusual phase transition is observed and this seems to depend on the degree of vapour fill (Table D-2). An LLV → LV transition occurs between -52°C and -48°C for HC_G inclusions (Figure D-7) and between -59°C and -56°C for HC_L inclusions (Figure D-8). This behaviour is typical of gas condensates with a high methane content mixed with heavy alkane compounds (Luks, Merrill & Kohn, 1983). Although a few inclusions were found which did not show such behaviour, the lower temperature LLV → LV transition occurs for all petroleum inclusions with a homogenisation temperature between 90-160°C.

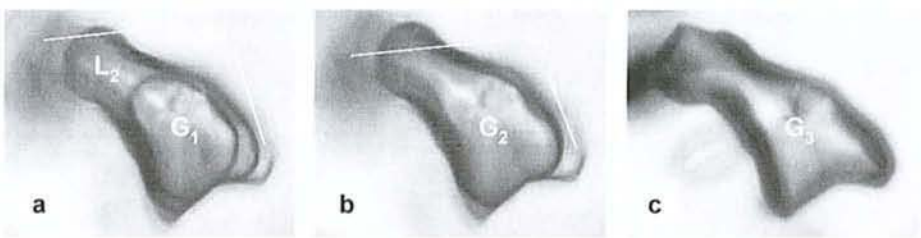

Figure D-7. Photomicrographs showing the microthermometric behaviour of an HC_G inclusion: (a) -60°C: three equilibrium phases (L_1, L_2, G_1) (b) -51.7°C: homogenisation of the liquid (L_2) and gas (G_1) fractions (c) 124°C: total homogenisation to vapour (G_3). Scale bar = 10µm.

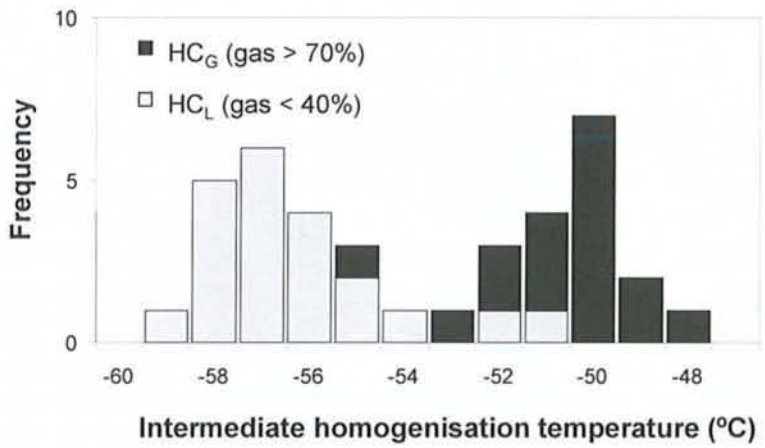

Figure D-8. Histograms of partial homogenisation temperatures of the LLG → LG transition for hydrocarbon inclusions according to their vapour fill at room temperature.

Core depth m RKB	Aqueous inclusions						Petroleum inclusions			
	healed fractures		quartz-overgrowth boundary		inner overgrowth		quartz overgrowth			
							HC_L inclusions		HC_G inclusions	
	Th range	*Th mode*	*Th range*	*Th mode*	*Th range*	*Th mode*	*Th range*	*Th mode*	*Th range*	*Th mode*
3685.9	104-137	118	102-124	110	107-113	111	87-156	118	114-130	124
3687.6	120-158	121	112-118	115	-	-	108-135	109	102	102
3691.7	107-160	120	-	-	-	-	106-160	116	-	-
3694	106-132	118	113-114	114	106-113	112	90-126	114	-	-
3770.8	119-128	124	123-127	125	-	-	-	-	-	-
3921.25	107-142	117	127-131	129	-	-	99-156	118	118-156	135
3925.75	130-160	133	117-141	123	118-129	122	111-124	119	-	-

Table D-1: *Summary of homogenisation temperatures (°C) for aqueous and petroleum inclusions.*

Petroleum composition	Inclusion type	Phase present		
		-100°C	25°C	Bulk homogenisation
Dry gas	HC_{G1}	G	G (100%)	"G"
Wet gas	HC_{G2}	L-G	L-G (> 80%)	G
Gas condensate	HC_{G3}	L-L-G	L-G (> 70%)	G
Gas condensate	HC_{C}	L-L-G	L-G (≈ 30%)	C
Gas condensate	HC_{L1}	L-L-G	L-G (< 30%)	L
Oil	HC_{L2}	L-G	L-G (< 30%)	L

Table D-2: *Petroleum inclusion types after microthermometric behaviour. G: gas C: critic L: liquid.*

Ice melting temperatures between –2°C and -4°C in aqueous inclusions translates to moderate salinities around 2.5 to 6 %wt NaCl (Figure D-9). For some of these inclusions, melting temperatures are overestimated because they are measured at the L-S equilibrium, without vapour phase. Melting temperatures obtained for inclusions inside quartz overgrowths and on the edge of it are sometimes positive. Other inclusions found at 3925.75 m along the core-overgrowth boundary reveal a $CaCl_2$ fluid enrichment with an observed eutectic temperature below –40°C and melting temperature of -8 to -12°C. For these, melting temperatures can always be measured at the L-V-S equilibrium.

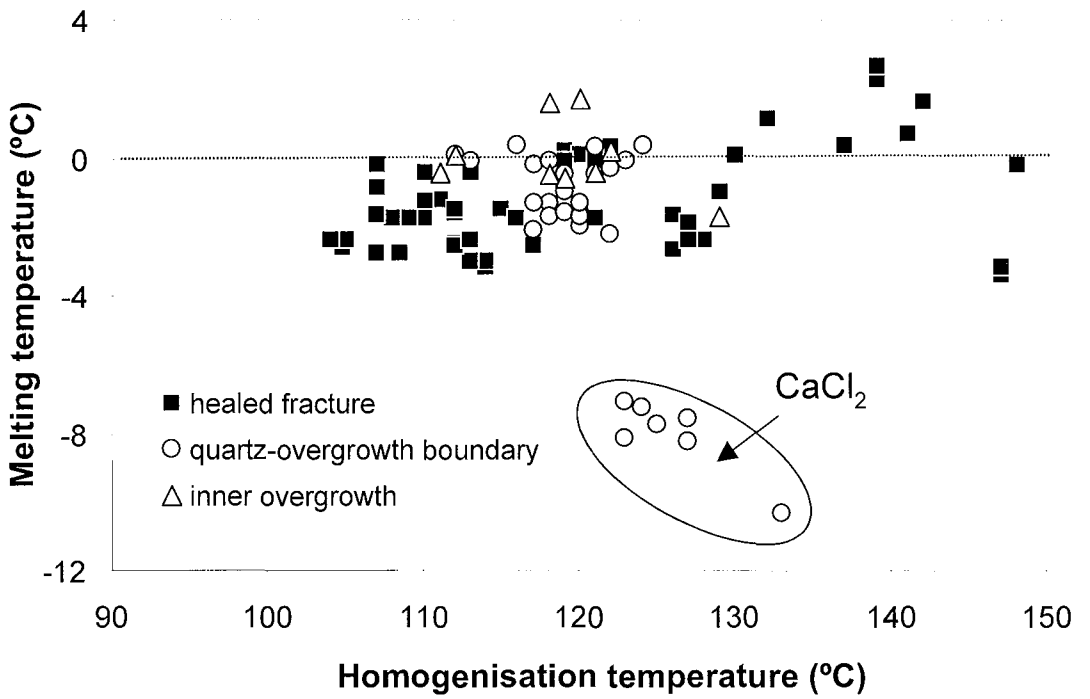

Figure D-9. Crossplot of homogenisation and melting temperature of aqueous inclusions according to their location(3685.9 m to 3925.75 m).

5.4.4 Raman and FT-IR spectroscopy

Quantitative analyses using Raman spectroscopy show that the aqueous inclusions have variable methane contents depending on their position (Table D-3). Methane content is low for aqueous inclusions from quartz microfractures (0 to 0.05 molal); higher for aqueous inclusions located at the core-overgrowth boundary and inside quartz overgrowths (0.05 to 0.16 molal). The Raman signal has also been recorded inside the water phase of a 3-phase inclusion, giving a CH_4 molality around 0.18. No H_2S, N_2, CO_2 or light alkanes have been detected.

	Aqueous inclusions			3 phase inclusions (water phase)
	Healed fractures	Core-overgrowth boundary and overgrowth	Overgrowth (vapour inclusions)	Overgrowth
CH_4 molality (moles%)	0 - 0.05	0.05 - 0.16	0.8 - 1.64	0.18

Table D-3: *CH_4 molality for aqueous inclusions and the water phase of 3-phase petroleum inclusions calculated from Raman data.*

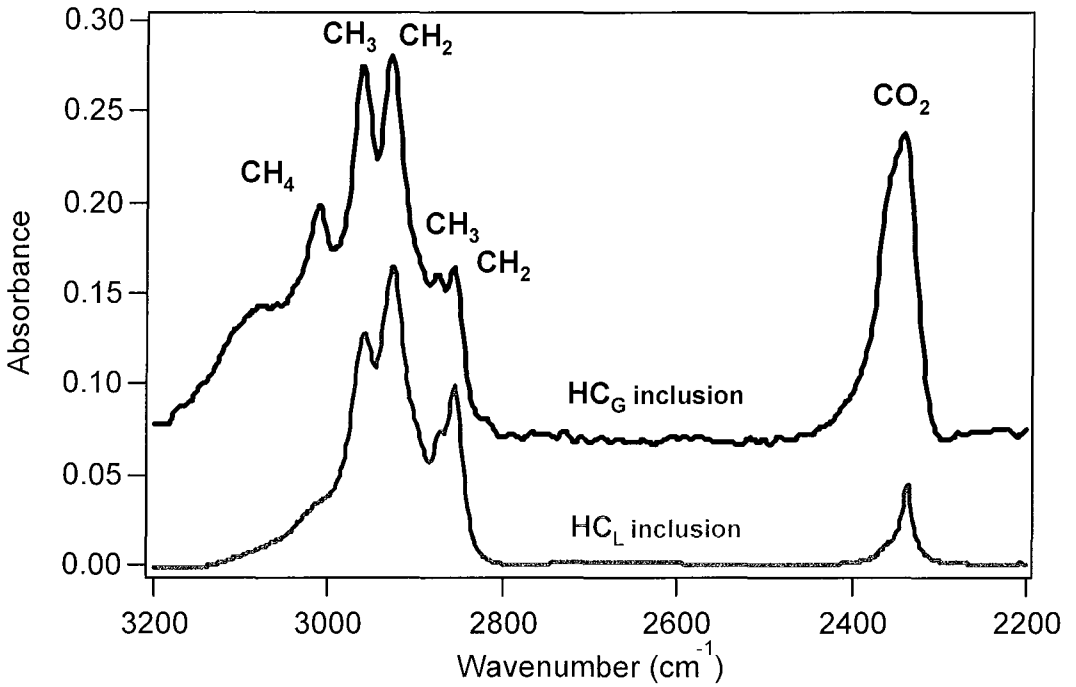

Figure D-10. Typical FT-IR spectra of HC_G and HC_L petroleum inclusions.

FT-IR spectra of two representative petroleum HC_G inclusions and HC_L are shown on figure D-10. Both contain CO_2 but the HC_G inclusion has a higher methane content. Quantitative analyses of petroleum inclusions display a continuous trend from a CH_4-poor (9 mol%) to a CH_4-rich (85 mol%) fluid (Figure D-11). Inclusions with solid phases have lower methane content. HC_G inclusions contain between 52 to 85 mol% CH_4, 2 to 12 mol% CO_2, and a mean CH_2/CH_3 alkane ratio around 0.82. Two subgroups associated to cooling microthermometric behaviour (table D-2) can be described: (a) HC_{G1} inclusions with CH_4 content from 84 to 85 mol% and CO_2 content around 4 mol% (b) HC_{G3} inclusions with CH_4 content from 52-82 mol%. The highest CO_2 enrichment occurs in inclusions which have 52-60 mol% of CH_4. On the other hand, no values between 65-74 mol% of methane are found but this may be a sampling issue. HC_L inclusions contain 9 to 54 mol% of CH_4, up to 6 mol% of CO_2 and high CH_2/CH_3 ratios around 2.6. No relation between methane content and homogenisation temperatures has been found for any of the types of petroleum inclusions

Analyses have not been performed on other minor petroleum inclusions such as dry gas and heavier oil due to inclusions and FT-IR limitations: rarity, size, contamination...

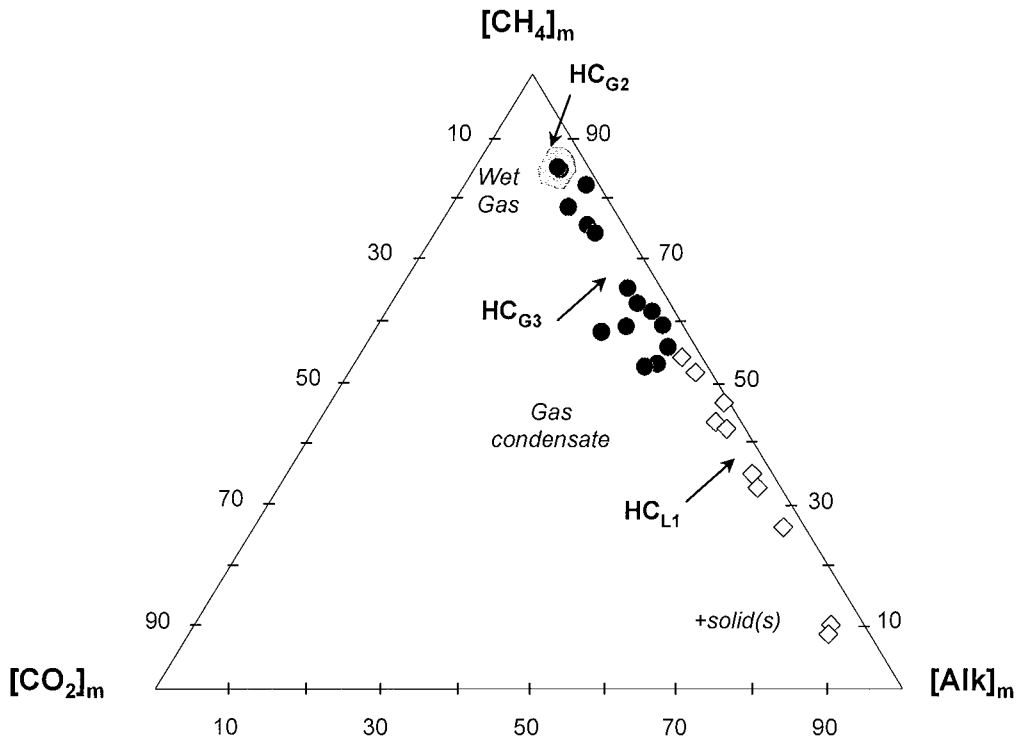

Figure D-11. Ternary diagram showing content of $[CH_4]_m$, $[CO_2]_m$ and $[alkanes]_m$ for petroleum inclusions obtained from FT-IR data. HC_G inclusions (black circles) HC_L inclusions (grey diamond).

5.4.5 Confocal Scanning Laser Microscopy

In view of the large number of inclusions and gas filling and composition, only a few representative petroleum inclusions were analysed. The maximum recorded inclusion volume is 2600 μm^3 and minimum is 85μm^3. The vapour percentage for HC_L inclusions varies from 0.9% to 20.8% (Table D-4). Only one measurement of gas volume for HC_G inclusions could be measured, at 87 %. CSLM photomicrographs obtained in reflection mode reveal water inside HC_G and HC_L inclusions within quartz overgrowths. When a water film wets the wall of a HC_G inclusion (Figure D-12), water is always detected in the narrow asperities of the inclusion, which undergoes necking down.

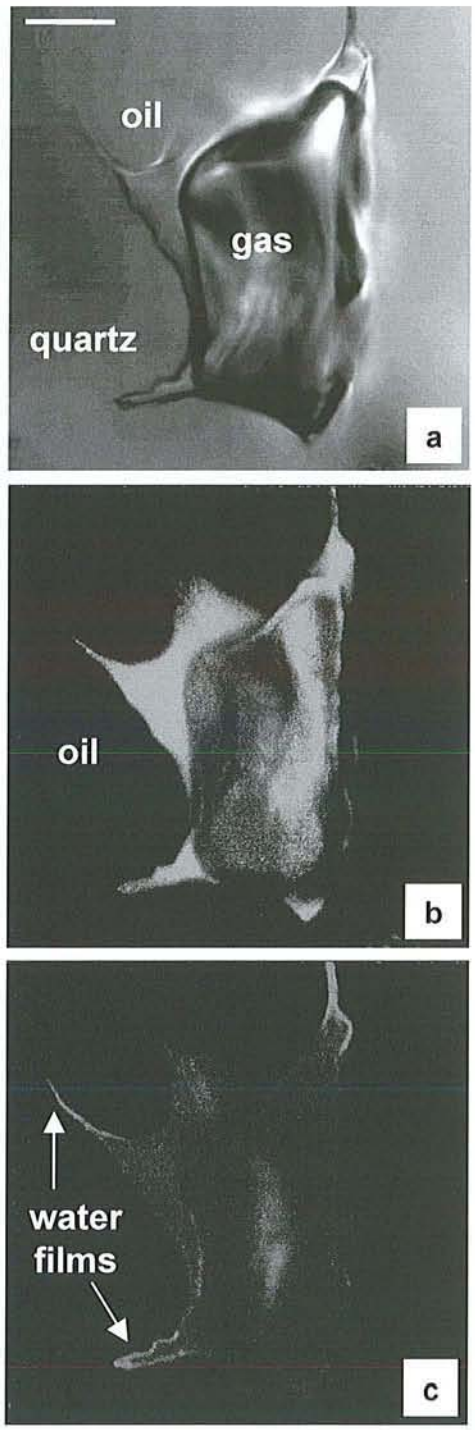

Figure D-12. CSLM photomicrographs of petroleum inclusions in (a) transmission mode (b) fluorescence mode and (c) reflection mode. A water film is trapped between the hydrocarbon liquid phase and inner wall of the inclusion. Scale bar = 10µm. Thickness of inclusion=39µm.

5.5 Discussion

5.5.1 One or multiple petroleum fluid episodes?

Highly variable compositions in closely associated petroleum inclusions may arise in a number of ways: 1) multiple fluids at different times; 2) heterogeneous trapping at different times; 3) post-trapping modification (necking down, re-equilibration, cracking inside the inclusion) of the above or of a single fluid composition.

Most of the reservoir petroleum in the Haltenbanken area is gas-condensate. Microthermometric and petrographic data indicate that gas-condensate inclusions are common in the overgrowths and thus probably represent a similar fluid to bulk reservoir petroleum. Dry gas and black oil inclusions have also been recorded (types HC_{G1} and HC_{L2} respectively, see table D-2), but they are in very low abundance, and probably result from delayed entrapment or necking down. The highly variable character of the inclusions could conceivably be explained by the emplacement and trapping of multiple petroleum charges, but the close proximity of liquid-rich and vapour-rich inclusions would then be generated from heterogeneous trapping, i.e. a combination of phase separation of a single petroleum fluid into oil and gas and subsequent trapping. The shapes and mutual proximity of different types of inclusions indicate that necking down was important in closing the inclusions. While heterogeneous trapping offers the most plausible explanation of our observations, it is necessary to evaluate the importance of necking down and quartz recrystallisation (suggested by the irregular CL patterns in the inner overgrowth) to the results. The similar homogenisation temperature ranges of both liquid-rich and vapour-rich inclusions and the range itself (largely 100-130°C), which is relatively narrow, suggest that, remarkably, there has been almost equilibrium trapping of the oil and gas fractions, with little mixing or cross-contamination. This further suggests that necking down only had a minor effect on phase behaviour. Some inclusions with very high homogenisation temperatures are present and these could have been generated from cross-contamination or necking down. A similar argument may be proposed for recrystallisation, i.e. the evidence for near-equilibrium phase trapping suggests that recrystallisation was of relatively minor importance in controlling phase ratios, with the added implication that recrystallisation was the trapping mechanism.

In view of these complexities, have any inclusions representing the original charge been preserved? The short answer is that none would be recognisable as such. However, the composition of the original charge is likely to be combination of the extreme vapour-rich and liquid-rich types. Accordingly, this could be close to the inclusion containing critical petroleum, but it is not possible to be certain - a critical petroleum could form during the process of phase separation. The critical petroleum does, however have the highest bubble point p and T, and serves to constrain maximum p-T conditions, as discussed in the next section.

Component	Petroleum fluid composition (moles %)						
	Liq. 1	**Liq. 2**	**Liq. 3**	**Critic**	**Gas 1**	**Gas 2**	**Gas 3**
CO_2	-	-	2.6	-	3.1	9.2	10.0
C_1	11.6	24.4	38.5	56.9	79.4	72.5	65.9
C_2	1.7	4.7	7.5	8.9	6.8	6.7	7.5
C_3	2.7	5.4	6.5	6.3	3.4	3.5	4.2
iC_4	0.7	1.3	1.4	1.2	0.5	0.5	0.7
nC_4	1.6	3.0	3.2	2.8	1.1	1.2	1.6
iC_4	1.3	2.2	2.1	1.7	0.5	0.6	0.8
nC_5	2.0	3.5	3.3	2.7	0.8	0.9	1.3
nC_6	3.8	4.7	3.8	2.7	1.0	1.0	1.3
nC_7	4.1	5.1	4.1	2.9	1.1	1.1	1.4
nC_8	4.0	4.7	3.7	2.5	0.8	0.8	1.1
nC_9	3.9	4.4	3.4	2.2	0.6	0.6	0.9
nC_{10}	3.9	4.1	2.9	2.0	0.4	0.5	0.7
Cn_1	29.3	23.9	14.1	9.1	0.6	0.9	2.4
Cn_2	29.4	8.6	3.0	1.8	0.0	0.0	0.2
Th (°C)	*87.2*	*122*	*127*	*131*	*100*	*115*	*125*
Fv (%)	*3.2*	*10.4*	*19.9*	*30*	*90*	*87.1*	*70.1*

Table D-4: *Mole percent composition of representative petroleum inclusions obtained by PIT modelling. Th: homogenisation temperatures (°C), Fv: gas volume percentage at 23°C (%), Cn_1: C11 to C15, Cn_2: C15+.*

5.5.2 P-V-T-X reconstruction

PVTX simulation was performed using PIT modelling software (Thiéry, Pironon, Walgenwitz & Montel, 2000). Accurate volumetric measurements and bulk homogenisation temperature are used by the model to reconstitute the paleo-thermobarometric trapping conditions of the petroleum system. FT-IR spectroscopy data also allow to refine the model especially regarding the CO_2 content. Aqueous isopleths have been drawn using Duan EOS (Duan, Moller, Greenberg & J.H., 1992).

P-T phase diagram shows multiple isopleths and isochores, representing the main petroleum inclusion populations found from this Haltenbanken area (Table D-4). Different isopleths for aqueous inclusions are drawn in figure D-13: aqueous inclusions that have been trapped within quartz microfractures (Aq. 1), at the core-overgrowth boundary (Aq. 2) and inside quartz overgrowths (Aq. 3). The isopleth of the aqueous phase of the 3-phase inclusions corresponds to the highest methane concentration and is in the upper part of the P-T diagram (Aq. 4). Isochores of the aqueous inclusions have not been drawn for legibility.

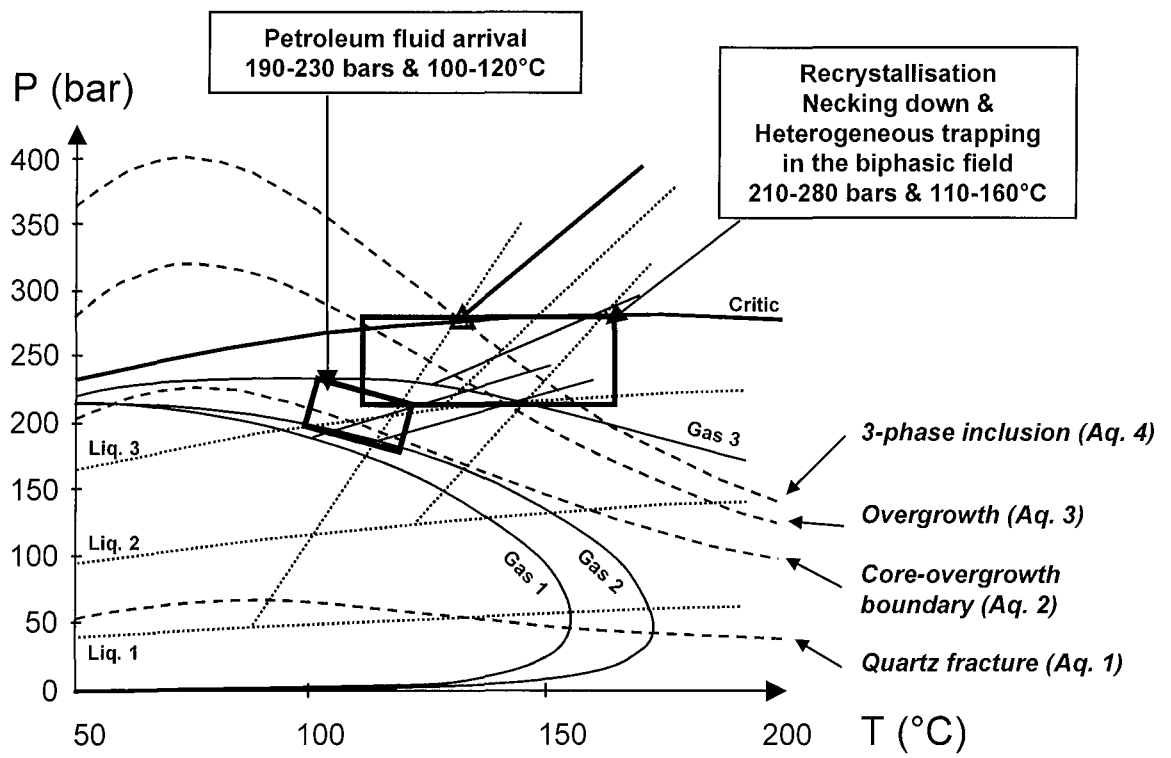

Figure D-13. P-T-X relationships from aqueous and petroleum systems. Isopleths and isochores of the petroleum fluids are issued from PIT modelling whereas isopleths of the aqueous fluids are drawn using Duan EOS.

The shifting of the aqueous inclusions isopleths to the highest-pressures (Aq.2, Aq.3, Aq. 4) results in the methane enrichment of these aqueous inclusions from the quartz-overgrowth boundary to the inner part of the overgrowth. Thus, if these aqueous inclusions are methane-saturated, their entrapment has occurred between 190-280 bar at around 110°C. The petroleum system entrapped inside quartz overgrowths should be correlated to the aqueous system entrapment during burial. With some reservations (as discussed earlier), the critical petroleum inclusion may represent the mean composition of the petroleum charge, even if its entrapment occurs in the latest stage of burial. In any case, however, isochore and isopleth intersection of the critical petroleum with Aq. 4 gives a maximum p-T of approximately 280 bar and 160°C for the system. The intersection of Gas 1 (isochore) with the Aq. 2 (inclusions at the grain-overgrowth boundary) isopleth give the p-T conditions of the first petroleum charge as 190-230 bar and 100-120°C. Subsequently, the main trapping of present-day petroleum inclusions has occurred in the biphase field of this critical system. The heterogeneous trapping of the majority of the petroleum inclusions, made up of both liquid-rich and vapour-rich populations, includes elements of necking down and possible recrystallisation of the inner overgrowths. Bearing in mind that the reservoirs are currently overpressured, it is possible that phase separation was generated by temporary overpressure loss. On the other hand, Liq 1 and Liq 2 isopleths and isochores should correspond to the heavy fraction segregation induced by necking-down and possible recrystallisation. Petroleum emplacement and subsequent processes thus occurred at temperatures between 100-160°C and 190-280 bars. The comparison with the burial history models of neighbouring fields (Bjorlykke, Aagaard, Dypvik, Hastings & Harper, 1986; Walderhaug, 1994b) indicates that these events occurred in the last 5 Myr during a phase of rapid burial (Figure D-14). This evaluation also suggests that pressures were approximately hydrostatic during trapping of most of the inclusions.

Inclusions within quartz cements are clearly diagenetic in origin, but inclusions in healed microfractures crossing detrital grains may or may not be. Microfractures can form and heal during burial of the reservoir unit, or be inherited from the provenance area. In this Garn Formation area the setting for microfractures in grains is ambiguous. Aqueous inclusion salinities are similar in both overgrowth and microfractures in grains, but in the microfractures, the homogenisation temperature range is much wider, both 2-phase and metastable and/or monophase types are present, and the inclusions are significantly undersaturated with methane. Methane saturation would be achieved at round 50 bars and 50°C, which provides a minimum constraint on their formation. If the inclusions are related to the present burial regime, the models indicate that they could have formed from the Cretaceous onward. In this case, however, the variable homogenisation temperatures would be interpreted as resulting from reequilibration. On the other hand, the data are consistent with a pre-Jurassic origin.

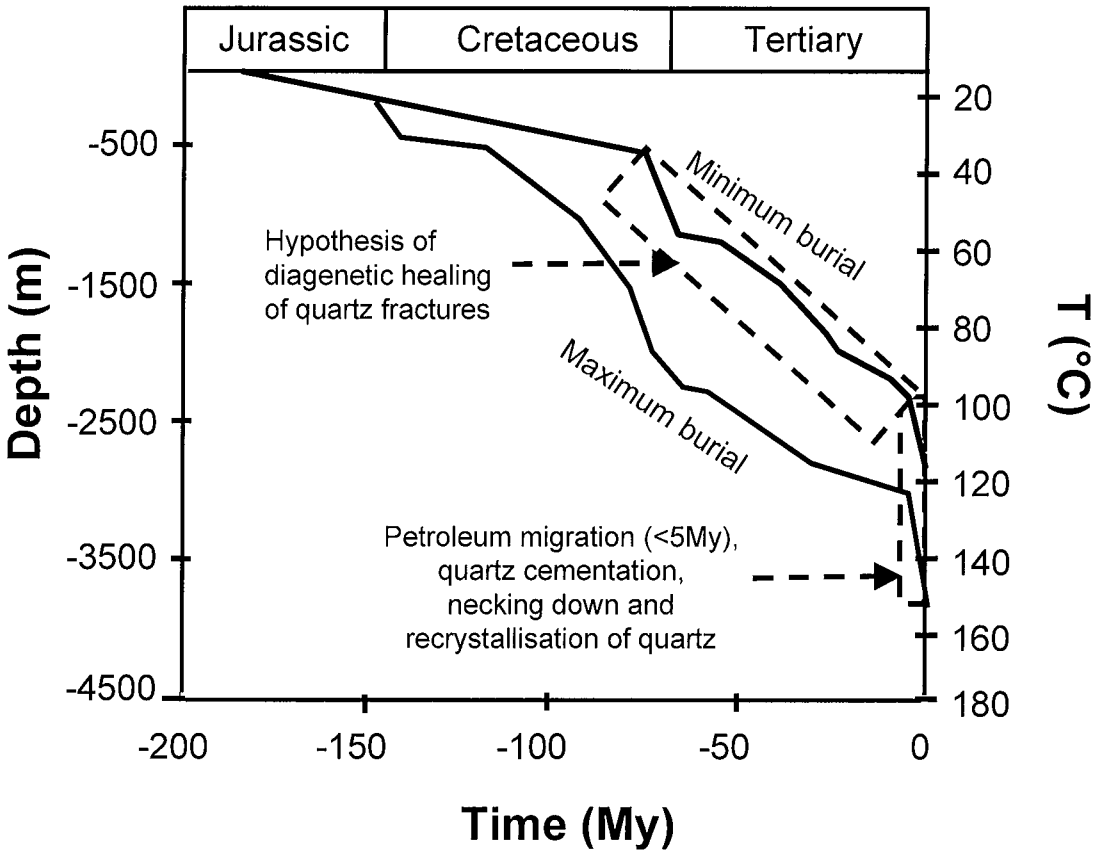

Figure D-14. Burial history curves of the Haltenbanken region (after Bjørlykke et al., 1986; Walderhaug, 1994b). Results of present work are superimposed using dotted boxes.

Implications for the effect on quartz cementation depend on the exact trapping mechanism for the inclusions. The data are ambiguous on this point. If the inner overgrowths have suffered wholesale recrystallisation, which is one interpretation of the CL evidence, then the quartz may have formed before petroleum emplacement, and there is no reason to postulate a bulk inhibitory effect. In this case there was clearly enough water to permit recrystallisation (and this can be observed in some inclusions), so some diagenesis can proceed with petroleum present. At the small scale of inclusions, irreducible water saturation in petroleum saturated reservoirs is probably sufficient for this process. A potential problem here is the means of access of fluids to the inner parts of overgrowths. If however, the edges of the inner zones are not sealed by the later outer overgrowths, i.e. quartz grains are not completely enclosed by the outer overgrowths, in regions of high inclusion density there will probably be channels for fluid infiltration. Experimental work is required to resolve this issue. On the other hand, if the irregular CL is an original feature of the quartz, and not due to recrystallisation then significant volumes of quartz have precipitated after petroleum emplacement. In this case the data can be interpreted to indicate that either petroleum does not halt bulk quartz cementation or that the reservoir equivalent of the inclusion charge has been subsequently lost, and the outer overgrowths precipitated in water-saturated pores. Although our data show that some quartz can precipitate with petroleum present, they cannot be used to

conclude that quartz cementation is not inhibited. Field scale integration of geochemical and quartz cement volume data are required to test that model.

5.6 Conclusion

The fluid inclusion data and PVTX modelling of inclusions in quartz overgrowths in this Garn Formation area reveal new insights into the evolution of petroleum compositions, inclusion trapping mechanisms and oil emplacement-quartz cementation relationships.

The inclusion petroleum consists of a wide range of liquid and vapour rich compositions in close proximity to each other, which exhibit a continuum of methane concentrations, and in which, unusually, the liquid portion separates into two liquids at low temperature. This low temperature behaviour is typical of a gas condensate/volatile mixture with high methane content and heavy alkanes. The variable liquid-vapour ratio, compositions and morphologies of all petroleum inclusions can be interpreted as a result of a combination of heterogeneous trapping and necking down. The petroleum fluid has evolved from a liquid/gas condensate petroleum fluid to a near-critical petroleum fluid, which is similar to the actual regional reservoir petroleum. Two main episodes of fluid entrapment can be distinguished. The first corresponds to the arrival of petroleum fluids at around 100-120°C and 190-230 bar. The second corresponds to the trapping of the majority of the petroleum inclusions, between 110-160ºC and 230-280 bar, including elements of necking down and possible recrystallisation of the inner overgrowths, made up of both liquid-rich and vapour-rich populations. This occurred during the last few million years of relatively rapid burial. Pre-petroleum fluids may be represented by aqueous fluid entrapment within microfractures in detrital quartz, at conditions above 50°C and 50 bar, but these may also have been inherited from the provenance area.

This study has shown that the data from fluid inclusions have to be carefully read to determine precise relationship and chronology between all diagenetic events (healing of quartz microfractures, growth of quartz, petroleum migration, quartz recrystallisation, necking-down, reequilibration of fluid inclusions...). However, another key-question still remains unsolved. This concerns the capability of petroleum or aqueous fluids to access through quartz overgrowth and quartz-overgrowth boundary during or after quartz cementation and/or recrystallisation processes. Solution of this problem will involve an experimental approach to analyse the control of all kinetic parameters such as temperature, pressure and fluid chemistry.

ACKNOWLEDGEMENTS

We would express our thanks to Norman Oxtoby and one anonymous journal reviewer for their constructive comments and suggestions. We are grateful to TotalFinaElf to have provided the rock samples.

REFERENCES

Aplin, A. C., MacLeod, G., Larter, S. R., Pedersen, K. S., Sorensen, H., & Booth, T. (1999). Combined use of Confocal Laser Scanning Microscopy and PVT simulation for estimating the composition and physical properties of petroleum in fluid inclusions. *Mar. Petrol. Geol., 16*, 97-110.

Bjorlykke, K., Aagaard, P., Dypvik, H., Hastings, D. S., & Harper, A. S. (1986). Diagenesis and reservoir properties of Jurassic sandstones from the Haltenbanken area, offshore mid Norway. *In A.M. Spencer, ed., Petroleum geology of the northern European margin: London, Graham and Trotman*, 285-292.

Duan, Z., Moller, N., Greenberg, J. H., & Weare, J.H., (1992). The prediction of methane solubility in natural waters to high ionic strength from 0 to 250°C and from 0 to 1600 bar. *Geochim. Cosmoschim. Acta, 56*, 1451-1460.

Dubessy, J., Buschaert, S., Lamb, W., Pironon, J., & Thiery, R. (2001). Methane-bearing aqueous fluid inclusions: Raman analysis, thermodynamic modelling and application to petroleum basins. *Chemical Geology, 1-3, 193-201.*

Ehrenberg, S. N. (1990). Relationship between diagenesis and reservoir quality in sandstones of the Garn formation, Haltenbanken, Mid-Norwegian continental shelf. *Am. Assoc. Petrol. Geol. Bull., 74*, 1538-1558.

Gluyas, J. G., Robinson, A. G., Emery, D., Grant, S. M., & Oxtoby, N. H. (1993). The link between petroleum emplacement and sandstone cementation. *Petroleum Geology of Northwest Europe: Proceedings of the 4th Conference. J.R. Parker Ed.*, 1395-1402.

Goldstein, R. H., & Reynolds, T. J. (1994). *Systematics of fluid inclusions in diagenetic minerals.* SEPM Short Course 31, Tulsa, 199 p.

Grant, S. M. & Oxtoby, N. H. (1992). The timing of quartz cementation in Mesozoic sandstones from Haltenbanken, offshore mi-Norway: fluid inclusion evidence. *J. Geol. Soc. Lond.*, 149, 479-482

Guillaume, D., Teinturier S., Dubessy, J., Pironon, J. (2002). Calibration of methane analysis by Raman spectroscopy in H_2O-NaCl-CH_4 fluid inclusions. Validation using natural hydrocarbon and aqueous fluid inclusions. *Chemical Geology Special issues for XVIth ECROFI meeting (in press).*

Karlsen, D. A., Nyland, B., Flood, B., Ohm, S. E., Brekke, T., Olsen, S., &Backer-Owe, K. (1995). Petroleum geochemistry of the Haltenbanken, Norwegian continental shelf. In J. M. Cubitt &

W. A. England, *The Geochemistry of Reservoirs*, Geol. Soc. London Spec. Publ. 86, pp. 203-256.

Luks, K. D., Merrill, R. C., & Kohn, J. P. (1983). Partial miscibility behavior in cryogenic natural gas systems. *Fluid Phase Equilibria, 14*, 193-201.

Odden, W., Patience, R. L., & Graas, G. W. (1998). Application of light hydrocarbons (C_4-C_{13}) to oil/source rock correlations: a study of the light hydrocarbon compositions of source rocks and test fluids from offshore Mid-Norway. *Org. Geochem., 28*, 823-847.

Pironon, J., Canals, M., Dubessy, J., Walgenwitz, F., & Laplace-Builhe, C. (1998). Volumetric reconstruction of individual oil inclusions by confocal scanning laser microscopy. *Eur. Journal Mineral., 10*, 1143-1150.

Pironon, J., Thiery, R., Ayt Ougougdal, M., Teinturier, S., Beaudoin, S., & Walgenwitz, F. (2001). FT-IR measurements of petroleum fluid inclusions: methane, n-alkanes and carbon dioxide quantitative analysis. *Geofluids, 1*, 2-10.

Poty, B., Leroy, J., & Jachimowicz, L. (1976). Un nouvel appareil pour la mesure des températures sous le microscope: l'installation de microthermométrie Chaixmeca. *Bull. Soc. fr. Minéral. Cristallogr., 99*, 182-186.

Ramm, M. (1992). Porosity-depth trends in reservoir sandstones: theoretical models related to Jurassic sandstones, offshore Norway. *Mar. Petrol. Geol., 9*, 324-327.

Saigal, G., Bjorlykke, K., & Larter, S. (1992). The effects of oil Emplacement on diagenetic processes - Examples from the Fulmar reservoir sandstones, Central North Sea. *Am. Assoc. Petrol. Geol. Bull., 76*, 1024-1033.

Swarbrick, R. E., & Edwards, S. C. (1993). Overpressure and Palaeopressure. In *Geofluid Seminar Serie* (ed. P. J.), pp. 333-337.

Thiéry, R., Pironon, J., Walgenwitz, F., & Montel, F. (2000). PIT (Petroleum Inclusion Thermodynamic): a new modeling tool for the characterization of hydrocarbon fluid inclusions from volumetric and microthermometric measurements. *J. Geoch. Expl., 69-70*, 701--704.

Walderhaug, O. (1990). A fluid inclusion study of quartz-cemented sandstones from offshore mid-norway - possible evidence for continued quartz cementation during oil emplacement. *Journal of Sedimentary Petrology, 60*, 203-210.

Walderhaug, O. (1994a). Precipitation rates for quartz cement in sandstones determined by fluid inclusion microthermometry and temperature history modelling. *Journal of sedimentary Petrology, 64*, 324-333.

Walderhaug, O. (1994b). Temperatures of quartz cementation in Jurassic sandstones from the Norwegian continental shelf - Evidence from fluid inclusions. *Journal of Sedimentary Petrology, 64*, 311-323.

Williams, L. B., Hervig, R. L., & Bjorlykke, K. (1997). New evidence for the origin of quartz cements in hydrocarbon reservoirs revealed by oxygen isotope microanalyses. *Geochim. Cosmoschim. Acta, 61*, 2529-2538.

Worden, R. H., & Morad, S. (2000). Quartz cementation in oil field sandstones: a review of the key controversies. In *Special Publication Number 29 of the International Association of Sedimentologists* (ed. R. H. Worden, Morad, S.). Blackwell Science, pp.1-20.

E. CONCLUSION GENERALE

CONCLUSION GENERALE

Les expériences réalisées en système silice±eau±sels±huile±gaz ont permis de simuler et d'approcher les conditions de la diagenèse siliceuse d'un réservoir pétrolier naturel et d'améliorer la compréhension des mécanismes de croissance de quartz et de formation des inclusions fluides en milieu aqueux et/ou hydrocarboné. Ce travail a également permis de développer de nouvelles approches analytiques.

Avancées analytiques

Des courbes de calibrage permettant de calculer la teneur en méthane des inclusions dans le système H_2O-CH_4-NaCl ont été obtenues à partir de l'analyse en spectroscopie Raman et grâce à la synthèse d'inclusions utilisées comme standards. Les fluides aqueux des inclusions de synthèse sont alors saturés vis à vis du méthane dans les conditions expérimentales. La concentration en méthane (mCH_4) des inclusions aqueuses peut être calculée grâce à l'équation suivante [1]:

$$mCH_4 = [I(CH_4)/I(H_2O)] \times [72 - 35 \times \exp(-1.1 \times mNaCl)] \qquad R^2 = 0.99 \qquad [1]$$

où mNaCl est la salinité (molalité) calculée à partir de la Tf des inclusions et $[I(CH_4)/I(H_2O)]$ représente le rapport d'aire des bandes du méthane et de l'eau obtenu en spectroscopie Raman.

L'utilisation d'inclusions synthétiques et naturelles de référence a permis un calibrage de l'analyse quantitative de CH_4, CO_2 et des alcanes des inclusions hydrocarbonées par spectroscopie FT-IR. Le couplage de ces données compositionnelles avec les modèles thermodynamiques permet d'affiner les conditions PVTX de piégeages des fluides hydrocarbonés et de suivre l'évolution de la composition de ces fluides au cours de leur(s) migration(s).

L'imagerie infrarouge est une nouvelle technique de cartographie moléculaire à l'échelle microscopique. Cette technique permet d'établir des images 2D et 3D en fonction des coordonnées x-y de la zone analysée et de l'intensité d'une bande d'absorption infrarouge. Les premiers tests ont permis de cartographier les composés hydrocarbonés situés dans les espaces poreux, dans les inclusions ainsi que dans les microfissures des quartz. Les zones plus ou moins riches en eau des grains de quartz détritiques, des auréoles de croissance, des microfractures et des inclusions peuvent être localisées. Cette technique peut donc servir à déterminer et visualiser en 2D et/ou en 3D les paléo-fissures drainant les fluides aqueux et/ou hydrocarbonés lors de

leur(s) migration(s) dans les bassins pétroliers. Cette technique apparaît désormais comme une technique complémentaire aux techniques d'imagerie appliquées à la diagenèse (cathodoluminescence, microscopie confocale...).

Outre la reconstitution des volumes d'huile et de gaz des inclusions hydrocarbonées, l'utilisation de la microscopie confocale en mode réflexion permet de visualiser des volumes relativement faibles d'eau, comme un film d'eau mouillant les parois d'une inclusion hydrocarbonée. Cependant, qu'ils soient importants ou non, ces volumes d'eau sont encore difficilement mesurables. Par conséquent, il est difficile de comparer précisément les rapports eau/huile/gaz des inclusions hydrocarbonées avec les rapports eau/huile/gaz utilisés lors du remplissage des autoclaves. En d'autres termes, il ne nous est pas encore possible de savoir précisément si la saturation en eau, en huile ou en gaz d'un bassin se reflète dans une inclusion.

Synthèse d'inclusions et cimentation de quartz en laboratoire

Des inclusions aqueuses ont été synthétisées dans des microfractures de grains de quartz, en présence de méthane dès 150°C-200 bar, en présence d'hydrocarbures à partir de 184°C-163 bar. Dans les surcroissances, des inclusions aqueuses en présence d'hydrocarbures ont été synthétisées à partir de 277°C-330 bar. Des inclusions hydrocarbonées ont été synthétisées avec différents rapports E/H, dans des microfractures de quartz (0<E/H<50%, 209-350°C; 175-400 bar), ainsi que dans des auréoles de croissance (10<E/H<50%, 289-350°C; 350-400 bar). La formation d'inclusions, la cicatrisation des fractures et la croissance de quartz sont des processus rapides (1 à 15 jours) dans les conditions expérimentales (150-400°C; 150-400 bar). En revanche, ces processus nécessitent une solution sursaturée en silice. Il a été notamment observé qu'une baisse de température entraînait la sursaturation de la silice et favorisait la cimentation de quartz et la synthèse d'inclusions. Au vu des résultats expérimentaux, il est donc possible que les fluctuations des conditions de températures des bassins puissent localement favoriser la croissance de quartz et le nombre d'inclusions fluides par des processus de sursaturation/précipitation. Dans les gammes de pression-température inférieures à 400°C-400 bar, l'effet de la pression sur la synthèse et la cimentation de quartz peut être considéré comme négligeable par rapport à l'effet de température, qui est le paramètre majeur. La croissance d'auréoles est plus importante pour un germe de quartz de synthèse que pour un germe de quartz naturel, en raison notamment du possible enrichissement en groupements silanol du quartz de synthèse. La combinaison de ces deux types de quartz est représentative de la plupart des quartz naturels des réservoirs. En effet, les réservoirs silicoclastiques contiennent des grains de quartz détritiques d'origines diverses (métamorphique, ignée, diagénétique, biogénique...) présentant des propriétés cristallochimiques variables.

Représentativité des inclusions fluides

La composition des inclusions hydrocarbonées est représentative de la composition du fluide parent jusqu'à des températures et pressions de 250°C et 212 bars respectivement. Les inclusions hydrocarbonées de synthèse ont permis de valider le modèle PIT (Petroleum Inclusion Thermodynamics) pour des températures inférieures à 250°C. En dessous de cette température, l'eau dissoute dans les inclusions est négligeable (<5%). En revanche, à 350°C-400 bar, des processus de cracking ont été mis en évidence aussi bien dans les inclusions fluides que dans l'huile parent. Par ailleurs, les propriétés PVTX des inclusions fluides hydrocarbonées sont modifiées par la présence d'eau à hautes températures (350°C). Dans ce cas, les isoplèthes et isochores caractéristiques des inclusions hydrocarbonées sont modifiées. La modélisation de la composition des huiles et la reconstitution des conditions de piégeage des inclusions piégées à haute température (>250°C) par les modèles thermodynamiques actuels restent imprécises car ces derniers ne prennent pas l'eau en compte.

Aucun processus de rééquilibrage et d'infiltration post-auréole n'ont été observés dans les auréoles des quartz lors d'une baisse continue de température. En revanche, quelques inclusions naturelles localisées dans des microfractures à l'intérieur ou en bordure des grains détritiques brésiliens dépourvus d'auréoles ont put être rééquilibrées et marquées au lithium ou au méthane. Ce rééquilibrage a été effectué à des températures expérimentales supérieures (150, 200 et 250°C) aux T_h des inclusions préexistantes (83 à 103°C).

Mécanisme de croissance du quartz en présence d'eau et d'hydrocarbures

Les expériences réalisées en autoclave à pression gaz (GPA) et à pression fluide (FPA) ont montré que la mouillabilité des quartz vis à vis de l'eau et/ou des hydrocarbures était un paramètre très important (Figure E-1 et E-2).

La figure E-1 (GPA; T<270°C; P<212bar) montre l'incidence de la mouillabilité des quartz par l'eau et/ou l'huile sur la taille des pyramides de croissance des quartz, le nombre d'inclusions fluides et la concentration en méthane des inclusions aqueuses contemporaines des inclusions hydrocarbonées à basse température. Lorsque le quartz est mouillé à l'eau (A), la cicatrisation de fracture, la croissance limitée de quartz (pyramides) et la formation d'inclusions fluides sont possibles. Les inclusions aqueuses de synthèse sont saturées vis à vis du méthane. Lorsque le quartz est mouillé à l'eau puis à l'huile, pour des rapports E/H variables (B et C), les pyramides de croissances sont relativement moins importantes que pour un système exclusivement aqueux. De plus, les inclusions aqueuses contemporaines des inclusions hydrocarbonées sont sous-saturées vis à vis du méthane par rapport à un système exclusivement aqueux. L'huile semble jouer un rôle de barrière entre l'eau et le gaz en inhibant les processus de diffusion du méthane dans l'eau. La ségrégation et les variations locales de la colonne eau-huile-gaz pourraient ainsi expliquer les

teneurs variables en méthane des inclusions aqueuses naturelles des bassins pétroliers. Lorsque le quartz est d'abord mouillé à l'huile, la cimentation de quartz et la formation d'inclusions fluides sont nulles. Les microfractures ne sont que très rarement cicatrisées. Lorsque les quartz sont mouillés à l'huile (E) pour un rapport E/H donné, la cimentation de quartz et la formation d'inclusions sont relativement limitées par rapport à B et C.

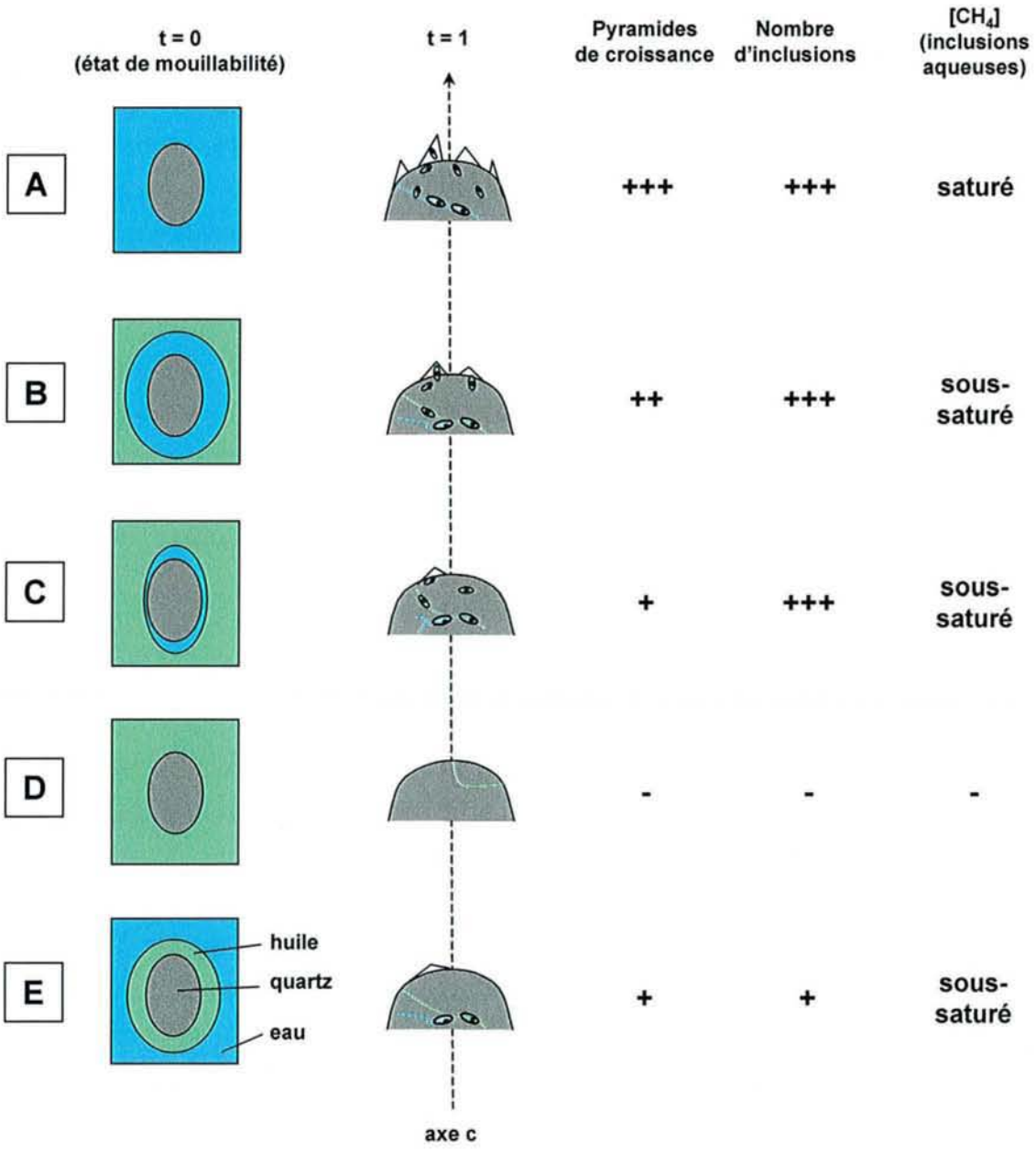

Figure E-1: Croissance de quartz en milieu aqueux et/ou hydrocarboné pour différents états de mouillabilité (A, B, C, D et E) pour les expériences réalisées en autoclave à pression gaz (T<270°C; P<212bar) : incidence sur la taille des pyramides de croissance des quartz, le nombre d'inclusions fluides et sur la concentration en méthane des inclusions aqueuses contemporaines des inclusions hydrocarbonées.

La figure E-2 (FPA; T=350-400°C; 400bar) montre l'incidence de la mouillabilité des quartz par l'eau et/ou l'huile sur la taille des auréoles, le nombre d'inclusions fluides et les valeurs isotopiques en $\delta^{18}O$ des auréoles de croissance à haute température. Lorsque le quartz est mouillé exclusivement à l'eau (A), la croissance d'auréoles de quartz et la formation d'inclusions fluides sont importantes. Lorsque le quartz est mouillé à l'eau, pour des rapports E/H variables (B et C), les surcroissances de quartz sont relativement moins importantes que pour un système exclusivement aqueux. Dans des conditions expérimentales (B), à 400 bar, 350°C et un rapport E/H = 10% (à 25°C), le fait que la quasi totalité de l'eau soit dissoute dans la phase hydrocarbonée implique que la présence d'un film d'eau résiduel suffit à faire pousser du quartz en milieu à forte saturation en huile, dans l'hypothèse ou l'eau reste le seul vecteur et transporteur de silice. Le recouvrement partiel d'un grain ou d'une auréole par l'huile ou par l'eau pourrait expliquer la présence et la répartition des différentes zones de croissance des quartz. Lorsque le quartz est mouillé exclusivement à l'huile (D), la cicatrisation des microfractures de quartz et la formation d'inclusions fluides sont très limitées, la croissance d'auréoles est nulle. Les données expérimentales obtenues en SIMS sur les auréoles de croissance des quartz en présence d'eau et d'hydrocarbures ont montré que les auréoles générées en présence d'huile (B et C) avaient des $\delta^{18}O$ supérieures, d'environ 10‰ par rapport à celles créées en milieu strictement aqueux (A) dans les mêmes conditions expérimentales à 350°C et 400 bar. Il est donc clair que la présence d'huile a une influence directe sur les valeurs de $\delta^{18}O$ des auréoles. Si l'hypothèse d'un fractionnement isotopique en oxygène entre l'huile et l'eau lors des processus de dissolution de l'eau dans l'huile est confirmée, il est envisageable que les valeurs de $\delta^{18}O$ puissent alors varier au sein même d'une auréole, selon le type d'huile et le rapport E/H. Outre un fractionnement eau-huile et/ou eau-quartz, un fractionnement additionnel direct entre l'huile et le quartz semble peu réaliste. En effet, cette hypothèse impliquerait que l'huile contienne de la silice dissoute en solution et soit le, ou un des vecteurs de la silicification des quartz. Si l'on fait le parallèle entre l'étude des auréoles naturelles des réservoirs pétroliers avec les auréoles expérimentales, il est fort probable que les valeurs maximales en $\delta^{18}O$ des auréoles naturelles puissent correspondre à une forte saturation en huile du réservoir ou du moins à un stade de migration d'hydrocarbures. Dans ce cas, les hypothèses d'un fluide météorique ou profond ne suffiraient plus à elles seules pour expliquer les fortes valeurs isotopiques en $\delta^{18}O$ des quartz diagénétiques.

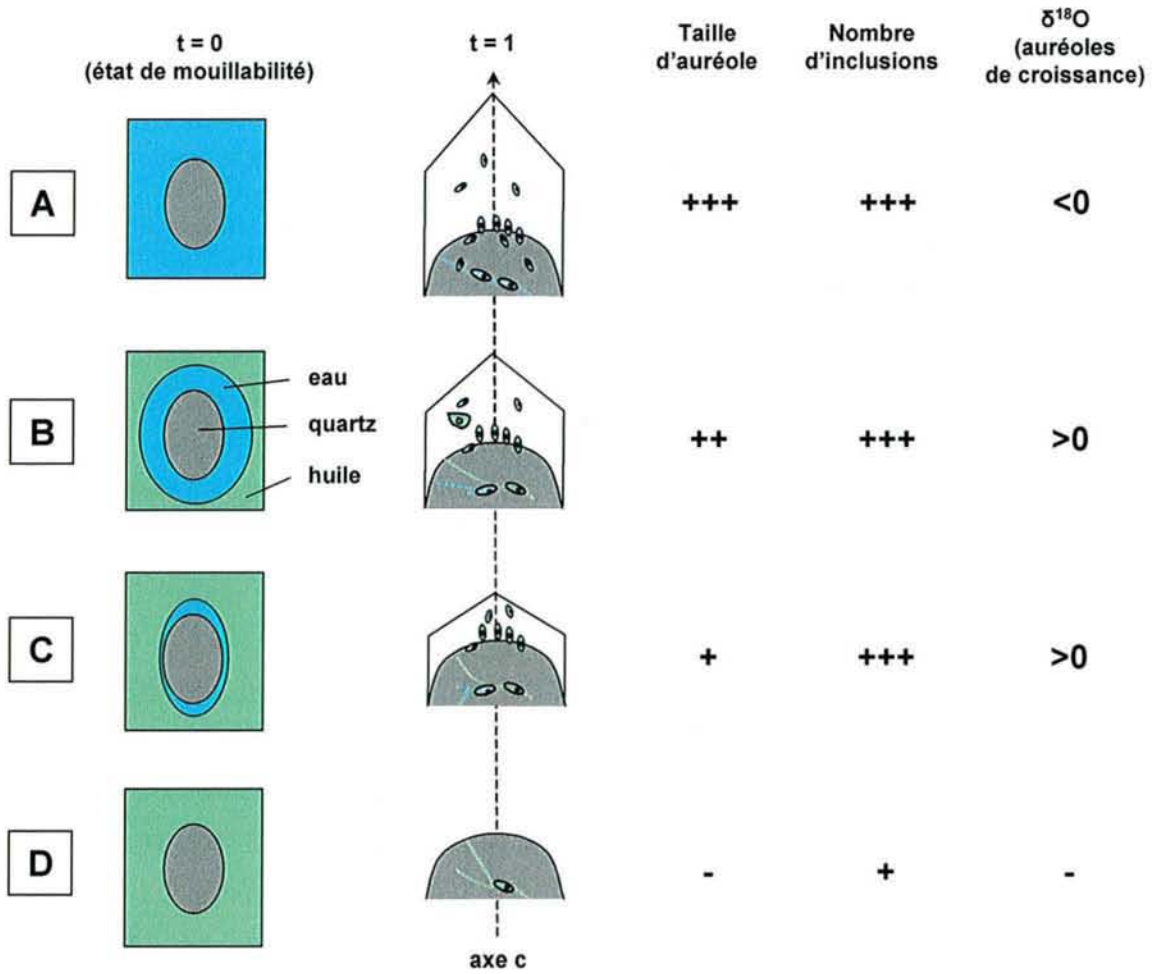

Figure E-2: Croissance de quartz en milieu aqueux et/ou hydrocarboné pour différents états de mouillabilité (A, B, C et D) pour les expériences réalisées en autoclave à pression fluide (T=350-400°C; 400bar) : incidence sur la taille des auréoles, le nombre d'inclusions fluides, les valeurs isotopiques en $\delta^{18}O$ des auréoles de croissance.

Perspectives

La croissance expérimentale de quartz et la formation d'inclusions fluides aqueuses et hydrocarbonées en présence d'eau et d'huile ouvrent de nombreuses voies de recherche dans le domaine de la diagenèse organique et minérale des bassins pétroliers.

L'utilisation d'une huile naturelle (gaz compris) dans les expériences permettrait d'approcher davantage les conditions naturelles des réservoirs pétroliers, d'améliorer et/ou valider les modèles thermodynamiques basées sur les inclusions fluides. Deux approches peuvent être envisagées. La première consisterait à utiliser un mélange d'alcanes légers en plus de l'huile morte et du méthane. Cependant, l'utilisation d'un mélange C_2-C_5 au sein du dispositif expérimental actuel induirait une baisse de pression (~100 bar à 200°C) qui risque de minimiser la formation d'inclusions et la cimentation de quartz. La deuxième approche consisterait à redonner "vie" à une huile morte par

des processus de cracking en modifiant la distribution et la composition de l'huile morte de départ. Par ailleurs, l'étude couplée des huiles avant et après expérience et des inclusions de synthèse permettrait d'étudier le cracking des huiles. En effet, les inclusions fluides piègent la signature de l'huile à un instant t, à un couple P-T donné. Les inclusions sont des microréacteurs qui permettent de s'affranchir des problèmes liés à la trempe et aux prélèvements des solutions expérimentales.

Le trend des huiles naturelles utilisé dans les modèles thermodynamiques pour la reconstitution PVTX des conditions de piégeage des pétroles pourrait être étendu à différents mélanges d'huiles ou de gaz par cette deuxième approche. D'autre part, la présence d'eau dans la phase hydrocarbonée a un impact relativement important sur les isoplèthes et les isochores caractéristiques des inclusions hydrocarbonées, essentiellement à des températures supérieures à 250°C. Il serait donc utile d'étudier l'influence du rapport E/H sur les changements des propriétés PVTX des inclusions et d'intégrer l'eau dans les modèles thermodynamiques. Cette démarche est à préconiser dans les synthèses d'inclusions hydrocarbonées de haute température, où la solubilité de l'eau dans l'huile est importante. Cependant, il est clair que la synthèse d'inclusions fluides à basses températures (<200°C) reste la solution la plus favorable mais la plus difficile.

En parallèle avec les outils utilisés lors de cette étude (sonde ionique, cathodoluminescence et imagerie infrarouge), la microscopie électronique à transmission (MET) en mode image, micro diffraction et perte d'énergie sur des coupes ultraminces de quartz permettraient de poursuivre l'étude de la caractérisation physique et chimique de la limite grain-auréole et de l'auréole. Ainsi, l'analyse élémentaire des nano-inclusions et l'observation de la nano-structure (cavités, fractures...) des quartz par MET pourraient être menées en utilisant des coupes microtomiques. Par ailleurs, l'utilisation de marqueurs fluorescents tels que des imprégnations de résines dans des quartz ou des carottes de quartz pourrait permettre l'observation tridimensionnelle des réseaux de fractures des quartz en microscopie confocale.

Enfin, les résultats isotopiques obtenus sur les auréoles de croissance des quartz générées en présence d'hydrocarbures ouvrent de nombreuses voies en géochimie isotopiques des huiles et sur l'étude des fractionnements minéral-eau-huile. Des expériences à différentes températures, pressions et rapports E/H permettraient notamment de quantifier les échanges isotopiques en oxygène entre l'huile et l'eau associée.

REFERENCES GENERALES

REFERENCES GENERALES

Abercrombrie H. J., Hutcheon I. E., Bloch J. D., and De Caritat P. (1994). Silica activity and the smectite-illite reaction. *Geology* 22, 539-542.

Aplin A. C., Warren E. A., Grant S. M., and Robinson A. G. (1993) Mechanisms of quartz cementation in North Sea reservoir sands: constraints from fluid compositions. In *Diagenesis and Basin Development. AAPG Studies in Geology*, Vol. 36 (ed. A. D. Horbury, Robinson, A.G.), pp. 7-22.

Aplin A. C. and Warren E. A. (1994). Oxygen isotopic indications of the mechanisms of silica transport and quartz cementation in deeply buried sandstones. *Geology* 22, 847-850.

Aplin A. C., MacLeod G., Larter S. R., Pedersen K. S., Sorensen H., and Booth T. (1999). Combined use of Confocal Laser Scanning Microscopy and PVT simulation for estimating the composition and physical properties of petroleum in fluid inclusions. *Marine And Petroleum Geology* 16(2), 97-110.

Anthony T. R. and Cline H. E. (1974). Thermomigration of liquid droplets in salt, 4th Symposium on Salt. *Northern Geological Society* 1, 313-321.

Auvray P. and Regreny A. (1973). Influence des germes sur la qualité radioéléctrique des monocristaux de quartz de synthèse. *Bull. Soc. fr. Minéral. Cristallogr.* 96, 267-273.

Ayalon A. and Longstaffe F. J. (1988) Oxygen isotope studies of diagenesis and porewater evolution in the western Canada Sedimentary basin: Evidence from the Upper Cretaceous basal Belly River sandstone. *Journal of Sedimentary Petrology* 58, 489-505.

Balitsky V. S., Balitskaya L. V., Bublikova T. M., Kalinichev A. G., Marina E. A., Iwasaki H., and Iwasaki F. (1998). Silica transfer and beta-quartz growth from supercritical aqueous fluids. *Journal of Supercritical Fluids* 13, 357-362.

Balitsky V. S., Kurashige M., Balitskaya L. V., and Iwasaki H. (2002). Kinetics of dissolution and state of silica in hydrothermal solutions of Na_2CO_3 and NaOH, and accelerated method for the quartz crystal characterization against growth rate. *Journal of Crystal Growth* 237-239, 828-832.

Barclay S. A. and Worden R. H. (2000). Effects of reservoir wettability on quartz cementation in oil fields. In *Quartz cementation in sandstones. Special publication of the International Assocation of Sedimentologists*, Vol. 29 (ed. W. R. H. a. M. S.), pp. 103-117.

Barrès, O., Burneau, A., Dubessy, J. & Pagel, M. (1987). Application of micro-FT-ir spectroscopy to individual hydrocarbon fluid inclusion analysis. *Appl. Spectrosc.*, 41, 1000-1008.

Behar, F., Kressmann, S., Rudkiewicz, J.L., Vandenbroucke, M. (1992). Experimental simulation in a confined system and kinetic modelling of kerogen and oil cracking. *Organic Geochemistry.* 19, 173-189.

Bertie, J. E. & Apelblat, Y. (1996). Infrared Intensities of liquids XIX: A simple and effective approximate method for the calculation of infrared optical constant spectra of liquids from transmission measurements. *Applied spectroscopy*, 50, 1039-1046.

Bird G., Boon J., and Stone T. (1986). Silica transport during steam injection into oil sands 1. Dissolution and Precipitation Kinetics of Quartz: New Results and Review of Existing Data. *Chemical Geology* 54, 69-80.

Bjoroy, M., Williams, J.A., Dolcater, D.L., Winters, J.C. (1988). Variations in hydrocarbon distribution in artificially matured oils. *Organic Geochemistry*. 13, 901-913.

Bjorlykke, K., Aagaard, P., Dypvik, H., Hastings, D. S., & Harper, A. S. (1986). Diagenesis and reservoir properties of Jurassic sandstones from the Haltenbanken area, offshore mid Norway. *In A.M. Spencer, ed., Petroleum Geology of the northern European margin: London, Graham and Trotman*, 285-292.

Blanchet A. (2002). Origine, conditions et processus de la silicification diagénétique de reservoirs gréseux en Mer du Nord. *Thèse* Université Paris XI.

Blatt H. (1987). Perspectives: Oxygen isotopes and the origin of quartz. *J. Sediment. Petrol.* 57, 373-377.

Bode, J.H.G., Smit, W.M.A., Visser, T. & Verkruijsse, H.D. (1980). The absolute infrared intensities of propyne-d/sub 0/ and propyne-d/sub 3/. *J. Chem. Phys.*, 72, 6560-70.

Bodnar R. J. and Sterner S. M. (1985). Synthetic fluid inclusions in natural quartz. III. Determination of phase equilibrium properties in the system $H_2$0-NaCl to 1000°C and 1500. *Geochimica et Cosmochimica Acta* 49, 1861-1873.

Bodnar, R.J., and Vityk, M.O. (1994). Interpretation of microthermometric data for H_2O-NaCl fluid inclusions. *In De Vivo, B. and Frezzotti, M.L. (eds.) Short Course of the Working Group (IMA) Fluid inclusions in minerals: Methods and Applications.* Virginia Tech, Blacksburg, 117-130.

Bohlmann E. G., Mesmer R. E., and Berlinski P. (1980). Kinetics of silica deposition from simulated geothermal brines. *Soc. Petrol. Eng. J.*, 239-248.

Bolt P. H. and van Santen R. A. (1997). A small angle X-ray scattering study on high pH silica precipitations. *Colloids and Surfaces A: Physicochemical and Engineering Aspects* 122, 183-187.

Bouhlel, S., Fortuné, J.P., Guilhaumou, N. & Touray, J.C. (1988). Les minéralisations stratiformes à F-Ba de Hammam Zriba, Jebel Guébli (Tunisie nord orientale) : l'apport des études d'inclusions fluides à la modélisation génétique. *Mineral. Deposita,* 23, 166-173.

Brantley, S.L. (1992). The effect of fluid chemistry on quartz microcrack lifetimes. *Earth and Planetary Science Letters*, 113, 145-156.

Bratus, M.D., Svoren, I.M., Danysh, V.V. (1975). Inclusions of hydrocarbons in "Marmorosh diamonds" from Carpathians as indicators of migration of oil fluids. Carbon and its compounds in endogenic processes of mineral formation. (abstract) *COFFI*, 8, 28.

Brint J. F., Hamilton P. J., Haszeldine R. S., Fallick A. E., and Brown S. (1991) Oxygen isotopic analysis of diagenetic quartz overgrowths from the Brent sands: a comparison of two preparation methods. *Journal of Sedimentary Petrology* 61(4), 527-533.

Caroll S., Mroczek E., Alai M., and Ebert M. (1998). Amorphous silica precipitation (60 to 120°C): Comparison of laboratory and field rates. *Geochimica et Cosmochimica Acta* 62(8), 1379-1396.

Carpenter S. J. and Lohmann K. C. (1997) Carbon isotope ratios of Phanerozoic marine cements: Re-evaluating the global carbon and sulfur systems. *Geochimica et Cosmochimica Acta* 61(22), 4831-4846.

Cassan J.-P., Garcia Palacios M. d. C., Fritz B., and Tardy Y. (1981). Diagenesis of sandstone reservoirs as shown by petrographical and geochemical analysis of oil bearing formations in the Gabon basin. *Société Nationale Elf Aquitaine (Production)*.

Charoy, B., de Donato, Ph., Barres, O. & Pinto-Coelho, C (1996): Channel occupancy in an alkali-poor beryl from serra branca (goias, brazil): spectroscopic characterization. *American Mineralogist*, 81, 395-403.

Cheilletz, A., de Donato, Ph., & Barres, O.(2001a) La traçabilité des émeraudes : une avancée décisive obtenue par microscopie infrarouge (μsirtf). *Revue de gemmologie*, a.f.g., n°141/142, 81-84.

Cheilletz, A., Barres, O., & de Donato, Ph. (2001b) L'emeraude : vers un génome minéral. *Le journal du cnrs*, n° 133, 12.

Cole D. R., Ohmoto H., and Lasaga A. C. (1983). Isotope exchange in mineral-fluid systems. I. Theoritical evaluation of oxygen isotope exchange accompanying surface reaction and diffusion. *Geochimica et Cosmochimica Acta* 47, 1681-1693.

Daridon, J.L. (1992). Mesure et représentation des équilibres de phases sous pression de mélanges d'eau, de paraffines et de dioxyde de carbone. Thèse, Université de Pau, France, 177 p.

Deneux-Mustin, S., Lartiges, B., Villemin, G., de Donato, Ph., Bersillon, J.L., Thomas, F. & Snidaro, D (1997) Morpho-chemistry in secondary sludge filtration cakes: a case study. *Wat. Sci.Tech.*, 6, n°11, 93-99.

Dennis P. F. (1984). Oxygen self-diffusion in quartz under hydrothermal conditions. *Journal of Geophysical Research* 89(B6), 4047-4057.

Dereppe, J.M., Pironon, J. & Moreau, C. (1994). Characterization of the composition of fluid inclusion in minerals by ^{1}H NMR. *American Mineralogist*, 79, 712-718.

Dennis P. F. (1984). Oxygen self-diffusion in quartz under hydrothermal conditions. *Journal of Geophysical Research* 89(B6), 4047-4057.

Dixon S. A., Summers D. M., and Surdam R. C. (1989). Diagenesis and prservation of porosity in Norphlet Formation (Upper Jurassic), southern Alabama. *AAPG Bulletin* 73, 707-728.

Donovan T. J., Friedman I., and Gleason D. (1974). Recognition of petroleum-bearing traps by unusual isotopic compositions of carbonate-cemented surface rocks. *Geology* 2, 351-354.

Doremus R. H. (1998). Diffusion of water and oxygen in quartz: reaction-diffusion model. *Earth and Planetary Science Letters* 163, 43-51.

Duan Z., Moller N., and J.H. W. (1992). An equation of state (EOS) for CH_4, CO_2 and H_2O. *Geochimica et Cosmoschimica Acta* 56, 2605-2618.

Duan, Z., Moller, N., Greenberg, J., Weare, J.H., (1992).. The prediction of methane solubility in natural waters to high ionic strength from 0 to 250°C and from 0 to 1600 bars. *Geochimica et Cosmochimica Acta* 56, 1451-1460.

Dubessy J., Buschaert S., Lamb W., Pironon J., and Thiery R. (2000). Methane-bearing aqueous fluid inclusions: Raman analysis, thermodynamic modelling and application to petroleum basins. *Chemical Geology* 173(1-3), 193-205.

Dubessy J., Guillaume D., Buschaert S., Fabre C., and Pironon J. (2000). Production of synthetic fluid inclusions in the H_2O-CH_4-NaCl system using laser-ablation in fluorite and quartz. *European Journal of Mineralogy* 12(6), 1083-1091.

Dubessy, J., L'Homme, T., Boiron, M.C., Rull, F. (2002). Determination of chlorinity in aqueous fluids using Raman spectroscopy of the stretching band od water at room temperature: application to fluid inclusions. *Applied Spectroscopy*, in press.

Dubina E. O. and Lakshtanov L. (1997). A kinetic model of isotopic exchange in dissolution-precipitation processes. *Geochimica et Cosmochimica Acta* 61(11), 2265-2273.

Dubois M., Weisbrod A., and Shtuka A. (1994). Experimental determination of the two-phase (liquid and vapour) region in water-alkali chloride binary systems at 500 et 600°C using synthetic fluid inclusions. *Chemical Geology* 115, 227-238.

Dutton S. P. and L.S. L. (1988) Cementation and burial history of a low-permeability quartzarenite, Lower Cretaceous Trabis Peak Formation, east Texas. *Geological Society of American Bulletin* 100, 1271-1282.

Egeberg P. K. and Aagaard P. (1989). Origin and evolution of formation water from oil fields on the Norvegian shelf. *Applied Geochemistry* 4, 131-142.

Ehrenberg, S. N. (1990). Relationship between diagenesis and reservoir quality in sandstones of the Garn formation, Haltenbanken, Mid-Norwegian continental shelf. *AAPG, 74*, 1538-1558.

Elphick S. C., Dennis P. F., and Graham C. M. (1986). An experimental study of the diffusion of oxygen in quartz and albite using an overgrowth technique. *Contributions to Mineralogy and Petrology* 92, 322-330.

Finkel, A.G. (1966). Experimental and theoretical study of absolute intensities in the infrared spectra of gaseous hydrocarbons. *Opt. And Spectrosc.*, 20, 432-435.

Fisher R. S. and Land L. S. (1986) Diagenetic hystory of Eocene Wilcox sandstones, south-central Texas. *Geochimica et Cosmochimica Acta* 50, 551-561.

Fleming B. A. (1986). Kinetics of reaction between silicic acid and amorphous silica surfaces in NaCl solutions. *J. Colloid Interface Sci.* 110, 40-64.

Furong C. (1995). The quality control of quartz growth: A chinese perspective. *Prog. Crystal Growth and Charact.* 30, 283-294.

Gautier J.-M. (1999). Etude expérimentale et modélisation de la cinétique de dissolution et de cristallisation des silicates en milieu hydrothermal : cas du quartz et du feldspath potassique, Paul Sabatier. Thèse Université Paul Sabatier, Toulouse, France, 180 p.

George, S.C., Krieger, F.W., Eadington, P.J., Quezada, R.A., Greenwood, P.F., Eisenberg, L.I., Hamilton, P.J. & Wilson, M.A. (1997). Geochemical comparison of oil-bearing fluid inclusions and produced oil from the Toro sandstone, Papua New Guinea. *Organic Geochemistry*, 26, 155-173.

Giles M. R., Indrelid S. L., Beynon G. V., and Amthor J. (2000). The origin of marge-scale quartz cementation: evidence from large data sets and coupled heat-fluid mass transport modelling. In *Special Publication Number 29 of the International Association of Sedimentologists*, Vol. 29 (ed. R. H. Worden, Morad, S.), pp. 21-38. Blackwell Science.

Giletti B. J. and Yund R. A. (1984). Oxygen diffusion in quartz. *Journal of Geophysical Research* 89(B6), 4039-4046.

Girard J.-P., Munz I. A., Johansen H., and Hill S. (2001). Conditions and timing of quartz cementation in Brent reservoirs, Hild Field, North Sea: constraints from fluid inclusions and SIMS oxygen isotope microanalysis. *Chemical Geology* 176, 73-92.

Gluyas J. G., Robinson A. G., Emery D., Grant S. M., and Oxtoby N. H. (1993). The link between petroleum emplacement and sandstone cementation. *Petroleum Geology of Northwest Europe: Proceedings of the 4th Conference. J.R. Parker Ed.*, 1395-1402.

Graham C. M., Valley J. W., and Winter B. L. (1996) Ion microprobe analysis of $^{18}O/^{16}O$ in authigenic and detrital quartz in the St. Peter Sandstone, Michigan Basin and Wisconsin Arch, USA: Constrasting diagenetic histories. *Geochimica et Cosmochimica Acta* 60(24), 5101-5116.

Grant, S. M. & Oxtoby, N. H. (1992). The timing of quartz cementation in Mesozoic sandstones from Haltenbanken, offshore mi-Norway: fluid inclusion evidence. *J. Geol. Soc. Lond.*, 149, 479-482

Greenwood, P.F., George, S.C. & Hall, K. (1998). Applications of laser micropyrolysis-gas chromatography-mass spectrometry. *Organic Geochemistry.*, 29, 1075-1089.

Gribov, L.A. (1964). *Intensity theory for infrared spectra of polyatomic molecules*, English translation by P.P. Sutton, Consultants Bureau, New-York, p. 106.

Goldstein R. H. and Reynolds T. J. (1994). *Systematics of fluid inclusions in diagenetic minerals*, 31, 199.

Guerrant, R.P., 1964. Hydrocarbon-water solubilities at high temperatures under vapor-liquid-liquid equilibrium conditions. Ph.D. Thesis, Pennsylvania State University, 124 p.

Guilhaumou, N., Touray, J.C. & Bouhlel, S. (1988). Stretching of hydrocarbon fluid inclusions in fluorite at 200 and 400 bars confining pressure. Application to low-pressure geobarometry. *Bull. Minéral.*, 111, 421-426.

Guilhaumou, N., Szydlowskii, N. & Pradier, B. (1990). Characterization of hydrocarbon fluid inclusions by infrared and fluorescence microspectrometry. *Mineralog. Mag.*, 54, 311-324.

Guilhaumou, N., Dumas, P., Ingrin, J., Carr, G.L. & Williams, G.P. (1999) Synchrotron infrared microspectrometry applied to petrography in micron scale range. *The Internet Journal of Vibrational Spectroscopy*, 3, 14 p.

Guillaume, D., Tkachenko, S., Dubessy, J., Pironon, J., (2001). High temperature and high pressure water solubility in ethylbenzene to 200°C and 1kbar and the acetic acid effect. *Geochimica et Cosmochimica Acta* 65, 3319-3324.

Guillaume D., Teinturier S., Dubessy J., and Pironon J. (2002, this volume) Calibration of methane analysis by Raman spectroscopy in H_2O-NaCl-CH_4 fluid inclusions. Validation using natural hydrocarbon and aqueous fluid inclusions. *Chemical Geology*(Special issues for XVIth ECROFI meeting), (in press).

Gunnarsson I. and Arnorsson S. (2000). Amorphous silica solubility and the thermodynamic properties of H_4SiO_4 in the range of 0° to 350°C at P_{sat}. *Geochimica et Cosmochimica Acta* 64(13), 2295-2307.

Gussoni, M. (1982). Infrared intensities by parametric methods ; a guided tour. Chap. 5. In: *Vibrational intensities in infrared and Raman spectroscopy*. W.B. Person & G. Zerbi, Eds. Elsevier, Amsterdam. 466 p.

Hassouta L. (1999). La comparaison de grès cimentés et de grès non cimentés par la calcite du groupe du Brent (Zone d'Alwyn, Mer du Nord). Une clé pour l'établissement de bilans de matière et la compréhension des processus de formation du quartz et des argiles (illite, kaolinite, dickite). Thèse de doctorat, Lille, France, 167 p.

Haszeldine R. S. and Osborne M. (1993). Fluid inclusion temperatures in diagenetic quartz reset by burial: implications for oil field cementation. *AAPG* 36, 35-46.

Heidman J. L., Tsonopoulos C., Brady C., and Wilson G. M. (1985). High-temperature mutual solubilities of hydrocarbons and water. Part II: ethylbenzene, ethylcyclohexane, and n-octane. *AIChE J.* 31, 376-384.

Hervig R. L., William L. B., Kirkland I. K., and Longstaffe F. (1995). Oxygen isotope microanalyses of diagenetic quartz: possible low temperature occlusion of pores. *Geochemica et Cosmochimica Acta* 59, 2537-2543.

Herzberg, G. (1968). *Molecular spectra and molecular structure. II. Infrared and Raman spectra*. Van Nostrand, London, 632 p.

Hinman N. W. (1998). Sequences of silica phase transitions: effects of Na, Mg, K, Al and Fe ions. *Marine Geology* 147, 13-24.

Hogg A. J. C., Pearson M. J., Fallick A. E., and Hamilton P. J. (1995) An integrated thermal and isotopic study of the diagenesis of the Brent Group, Alwyn South, U.K. North Sea. *Applied Geochemistry* 10, 531-546.

Holness M. B. and Watt G. R. (2001). Quartz recrystallization and fluid flow during contact metamorphism: a cathodoluminescence study. *Geofluids* 1(3), 215-228.

Horsfield, B. & Mc Limans, R.K. (1984). Geothermometry and geochemistry of aqueous and oil-bearing fluid inclusions from Fateh Field, Dubai. *Organic Geochemistry.*, 6, 733-740.

Horsfield, B., Schenk, H.J., Mills, N., Welte, D.H. (1992). An investigation of the in-reservoir conversion of oil to gas: compositional and kinetic findings from closed-system programmed-temperature pyrolysis. *Organic Geochemistry.* 19, 191-204.

Hosaka M., Miyata T., and Sunagawa I. (1995). Growth and morphology of quartz crystals synthesized above the transition temperature. *Journal of Crystal Growth* 152, 300-306.

Huang, D., (1999). Advances in hydrocarbon generation theory (I) Generation and evolution model for immature oils and hydrocarbon. *Journal Of Petroleum Science & Engineering*, 22: 121-130.

Huang, W.-L. and Otten, G.A., (2001). Cracking kinetics of crude oil and alkanes determined by diamond anvil cell-fluorescence spectroscopy pyrolysis: technique development and preliminary results. *Organic Geochemistry*, 32: 817-830.

Hurst A. R. (1981). A scale of dissolution for quartz and its implications for diagenetic processes in sandstones. *Sedimentology* 28, 451-459.

Ito Y. & Nakashima S. (2002) Water distribution in low-grade siliceous metamorphic rocks by micro-FTIR and its relation to grain size: a case from the Kanto Mountain region, Japan. *Chemical Geology*, 189, 1-18.

Iwasaki F., Iwasaki H., and Okabe Y. (1997). Growth rate anisotropy of synthetic quartz grown in Na_2CO_3 solution. *Journal of Crystal Growth* 178, 648-652.

Iwasaki H., Iwasaki F., Balitsky V. S., Balitskaya L. V., and Makhina I. B. (1998). Growth rates anisotropy of synthetic quartz crystals grown on Z-cut hexagonal seeds and computer simulations of growth process. *Journal of Crystal Growth* 187, 481-489.

Iwasaki F. and Iwasaki H. (2002). Historical review of quartz crystal growth. *Journal Of Crystal Growth* 237-239, 820-827.

Jones, R.N. & Sandorfy, C. (1956). Chemical Applications of Spectroscopy. IV Infrared and Raman spectrometry : applications. *Interscience*. 432 p.

Jourdan A., Thomas M., Brevart O., Robson P., Sommer F., and Sullivan M. (1987). Diagenesis as the control of the Brent sandstone reservoir properties in the Greater Alwyn area (East Shetland basin). In *Petroleum Geology of North West Europe.* (ed. J. Brooks and G. K.). Graham & Trotman.

Kalyuzhny V. A. (1982a). *Principles of knowledge about mineral-forming fluids.*

Karlsen, D. A., Nyland, B., Flood, B., Ohm, S. E., Brekke, T., Olsen, S., &Backer-Owe, K. (1995). Petroleum geochemistry of the Haltenbanken, Norwegian continental shelf. In J. M. Cubitt &

W. A. England, *The Geochemistry of Reservoirs*, Geol. Soc. London Spec. Publ. 86, pp. 203-256.

Kertes A. S. (1989). Hydrocarbons with water and seawater. Part II: C_8 to C_{36}. *Pergamon Press, New York* 38.

Kondo, S. & Saëki, S. (1973). Infrared absorption intensities of ethane and propane. *Spectrochimica Acta*, 29A, 735-751.

Kraishan G. M., Rezaee M. R., and Worden R. H. (2000). Significance of trace element composition of quartz cement as a key to reveal the origin of silica in sandstones: an example from the Cretaceous of the Barrow Sub-basin, Western Australia. In *Quartz Cementation in Sandstones. Special Publication of the International Association of Sedimentologists*, Vol. 29 (ed. R. H. Worden and S. Morad), pp. 317-331. Blackwell Science.

Lamb W. M., Popp R. K., and Boockoff L. A. (1996). The determination of phase relations in the CH_4-H_2O-NaCl system at 1 kbar, 400 to 600°C using synthetic fluid inclusions. *Geochimica et Cosmochimica Acta* 60(11), 1885-1897.

Landais, P., Michels, R., and Poty, B. (1989). Pyrolysis of organic matter in cold-seal pressure autoclaves. Experimental approach and applications. *Journal of Analytical and applied pyrolysis*, 16, 103-115.

Landais P. and Rochdi A. (1990) Reliability of semiquantitative data extracted from transmission microscopy-Fourier transform infrared spectra of coal. *Energy and Fuels*, 4, 290-295.

Larese R. E. and Hall D. L. (1996). Studying Petroleum migration with fluid inclusions: results from hydrothermal burial simulation experiments. *PACROFI VI*, 74-75.

Lasch P. and Naumann D. (1998) FT-IR microspectroscopic imaging of human carcinoma thin sections based on pattern recognition techniques. *Cell. Mol. Biol.*, 44, 189-202.

Lasch P., Chiriboga L., Yee H., Boese M. and Diem M. (2002) A new tool in medical diagnostics: infrared microspectroscopic imaging. *European Microscopy and Analysis*, 77, 13-15.

Laudise R. A. and Sullivan R. A. (1961). Solid State Physics, U.S.A., Vol. 12 (ed. S. e. Turnbull), pp. 149-222.

Lee M. and Savin S. M. (1985) Isolation of diagenetic quartz overgrowths on sand grains for oxygen isotopic analysis. *Geochemica et Cosmochimica Acta* 49, 497-501.

Lee Y. K., Bak R. H., and Chung S. J. (1997). The distribution of inclusions in synthetic quartz. *Journal of Crystal Growth* 182, 81-85.

Levine, J.R., Samson, I.M. & Hesse, R. (1991). Occurrence of fracture-hosted impsonite and petroleum fluid inclusions, Quebec City Region, Canada. *AAPG Bulletin*, 75, 139-155.

Lewis E.N., Treado P.J., Reeder R.C., Story G.M., Dowrey A.E., Marcott C., and Levin I.W. (1995) Fourier transform spectroscopic imaging using an infrared focal-plane array detector. Analytical Chemistry, 67, 3377-3381.

Linke, W.F. (1965). Solubilities of inorganic and metal-organic compounds. I and II, (4th edition). American Chemical Society, Washington, D. C.

Longstaffe F. J. (2000). An Introduction to stable oxygen and hydrogen isotopes an their use as fluid tracers in sedimentary system. In *Fluids and basin evolution*, Vol. 28 (ed. K. Kyser), pp. 115-160.

Longstaffe F. J. and Ayalon A. (1987). Oxygen-isotope studies of clastic diagenesis in the Lower Cretaceous Viking Formation, Alberta: Implication for the role of meteoric water. In *The diagenesis of sedimentary sequences. Geological Society of London Special Publication*, Vol. 36 (ed. J. D. Marshall), pp. 277-296.

Luks, K. D., Merrill, R.C. & Kohn, J.P. (1983). Partial miscibility behavior in cryogenic natural gas systems. *Fluid Phase Equilibria*, 14, 193-201.

Lyon I. C., Burley S. D., McKeever P. J., Saxton J. M., and Macaulay C. (2000) Oxygen isotope analysis of authigenic quartz in sandstones: a comparison of ion microprobe and conventional analytical techniques. *In Quartz Cementation in Sandstones. Special Publication of the International Association of Sedimentologists,* Vol. 29 (ed. R. H. Worden and S. Morad), pp. 299-316. Blackwell Science.

Mallet, J.L. (1992). Discrete smooth interpolation in geometric modelling. *Computer-Aided Design*, 24, 178-191.

Marchand A. M. E., Haszeldine R. S., Smalley P. C., Macaulay C. I., and Fallick A. E. (2001). Evidence for reduced quartz-cementation rates in oil-filled sandstones. *Geology* 29(10), 915-918.

Matsuhisa Y., Goldsmith J. R., and Clayton R. N. (1979). Isotopic fractionation in the system quartz-albite-anorthite-water. *Geochimica et Cosmochimica Acta* 43, 1131-1140.

McBride E. F. (1989) Quartz cementation in sandstones: A review. *Earth-Science Reviews* 26, 69-112.

McBride E. F., Land L. S., and Mack L. E. (1987) Diagenesis of eolian and fluviatil feldspathic sandtones, Norphlet Foramtion (Upper Jurassic), Rankin Country, Mississippi, and Mobile County, Alabama. *AAPG Bulletin* 71, 1019-1034.

McConnell J. D. C. (1995). The role of water in oxygen isotope exchange in quartz. *Earth and planetary Science Letters* 136, 97-107.

Meunier J. D. (1992). Precipitation of minerals between detrital quartz and quartz overgrowths in sandstones. *European Journal of Mineralogy* 4, 1401-1406.

Michels R., Langlois E., Ruau O., Mansuy L., Elie M., and Landais P. (1996). Evolution of asphaltenes during artificial maturation: A. Record of the chemical processes. *Energy & Fuels* 10(39-48).

Midtbo R. E. A., Rykkje J. M., and Ramm M. (2000). Deep burial diagenesis and reservoir quality along the eastern flank of the Viking Graben. Evidence for illitization and quartz cementation after hydrocarbon emplacement. *Clay Minerals* 35, 227-237.

Milliken K. L., Land L. S., and Loucks R. G. (1981) History of burial diagenesis determined from isotopic geochemistry, Frio Formation, Brazoria County, Texas. *AAPG Bulletin* 65, 1397-1413.

Muller E. (1985). The transportation of brine inclusions in rock salt in a temperature field of a heat source. *Cryst. Res. Technol.* 20(5), 677-682.

Odden W., Patience R. L., and Graas G. W. (1998). Application of light hydrocarbons (C_4-C_{13}) to oil/source rock correlations: a study of the light hydrocarbon compositions of source rocks and test fluids from offshore Mid-Norway. *Organic Geochemistry* 28(12), 823-847.

Oh S.J. and Koenig J.L. (1998) Phase and curing behavior of polybutadiene/diallyl phtalate blends monitored by FT-IR imaging using focal-plane array detection. Analytical Chemistry, 70, 1768-1772.

Onasch C. M. and Vennemann T. W. (1995). Disequilibrium partitioning of oxygen isotopes associated with sector zoning in quartz. *Geology* 23(12), 1103-1106.

Osborne M. and Haszeldine S. (1993). Evidence for resetting of fluid inclusion temperatures from quartz cements in oil fields. *Marine and Petroleum Geology* 10, 271-278.

Pagel M., Braun J.J., Disnar J.R., Martinez L., Renac C. and Vasseur G. (1997) thermal history constraints from studies of organic matter, clay minerals, fluid inclusions, and apatite fission tracks at the Ardèche paleo-margin (BA1 drill hole, GPF program), France. *Journal of Sedimentary Research*, 67, 235-245.

Pang L.S.K., George S.C. & Quezada R. A. (1998). A study of the gross compositions of oil-bearing fluid inclusions using high performance liquid chromatography. *Organic Geochemistry*, 29, 1149-1161.

Pironon J. (1990). Synthesis of hydrocarbon fluid inclusions at low temperature. *American Mineralogist* 75, 226-229.

Pironon, J., & Barrès, O. (1990). Semi-quantitative FT-IR microanalysis limits: Evidence from synthetic hydrocarbon fluid inclusions in sylvite:.*Geochimica et Cosmochimica Acta,* 54, 509-518.

Pironon, J., Sawatzki, J., & Dubessy, J. (1991). Nir FT-Raman microspectroscopy of fluid inclusions: comparisons with VIS Raman and FT-ir microspectroscopies. *Geochimica et Cosmochimica Acta*, 55, 3885-3891.

Pironon, J., & Barrès, O. (1992). Influence of brine-hydrocarbon interactions on FT-IR microspectroscopic analyses of intracrystalline liquid inclusions. *Geochimica et Cosmochimica Acta*, 56, 169-174.

Pironon, J. (1993). Estimation de la longueur de chaîne des hydrocarbures des inclusions fluides par spectrométrie Raman. *Compte-Rendus de l'Académie des Sciences, Paris*, t.316, Série II, 1075-1082.

Pironon J. and Canals M. (1997). Mise au point d'un protocole d'analyse des volumes des inclusions fluides d'hydrocarbures. Modélisation des propriétés PVT dans le but de reconstitutions thermobarométriques. *CONTRAT CREGU - EAP N°10839.*

Pironon J., Canals M., Dubessy J., Walgenwitz F., and Laplace-Builhe C. (1998). Volumetric reconstruction of individual oil inclusions by confocal scannig laser microscopy. *Eur. Journal Mineral.* 10, 1143-1150.

Pironon, J., Thiéry, R., Teinturier, S., Walgenwitz, F., (2000, this volume). Water in petroleum inclusions. Evidence from Raman and FT-IR measurements, PVT consequences. *Journal of Geochemical Exploration* 69-70, 663-668.

Pironon , J., Teinturier, S., Thiery, R. (2000). Etude et modélisation PVTX d'inclusions hydrocarbonées et aqueuses de la zone d'Alwyn (Mer du Nord). Rapport CREGU 00/09/01.

Pironon J., Thiery R., Ayt Ougougdal M., Teinturier S., Beaudoin S., and Walgenwitz F. (2001, this volume). FT-IR measurements of petroleum fluid inclusions: methane, n-alkanes and carbon dioxide quantitative analysis. *Geofluids* 1(1), 2-10.

Pironon J., Teinturier S., De Donato P. (2001) New developments in FT-IR measurements of petroleum fluid inclusions. *International Meeting on Organic Geochemistry, Nancy,* 10-14 septembre, Abstract, 2, 257-258.

Poty, B., Leroy, J. & Jachimowicz, L. (1976). Un nouvel appareil pour la mesure des températures sous le microscope: l'installation de microthermométrie Chaixmeca. *Bulletin de la Société française de Minéralogie et Cristallographie*, 99, 182-186.

Price, L.C., (1981). Aqueous solubility of crude oil to 400°C and 2,000 bar pressure in the presence of gas. *J. Pet. Geol.* 4, 195-223.

Ramboz, C., Pichavant, M., Weisbrod, A., (1982). Fluid immiscibility in natural processes: use and misuse of fluid inclusion data. II. Interpretation of fluid inclusion data in terms of immiscibility. *Chemical Geology* 37, 39-48.

Ramm M. (1992). Porosity-depth trends in reservoir sandstones: theoretical models related to Jurassic sandstones, offshore Norway. *Marine and Petroleum Geology* 9, 324-327.

Renders P. J. N., Gammons C. H., and Barnes H. L. (1995) Precipitation and dissolution rate constants for cristobalite from 150 to 300°C. *Geochimica et Cosmochimica Acta* 59(1), 77-85.

Richardson , C.K., Pinckney, D.M., (1984). The chemical and thermal evolution of the fluids in the Cave-in-Rock fluorspar district, Illinois; mineralogy, paragenesis, and fluid inclusions. *Economic Geology and the Bulletin of the Society of Economic Geologists* 79, 1833-1856.

Riley, G., Susuki, S. & Orville-Thomas, W.J. (1982) Dipole moment parameters and infrared band intensities. Chap. 8. In: *Vibrational intensities in infrared and Raman spectroscopy.* W.B. Person & G. Zerbi, Eds. Elsevier, Amsterdam. 466 p.

Rimstidt J. D. and Barnes H. L. (1980). The kinetics of silica-water reactions. *Geochimica et Cosmochimica Acta* 44, 1686-1699.

Robinson A., Grant S., and Oxtoby N. (1992). Evidence against natural deformation of fluid inclusions in diagenetic quartz. *Marine and Petroleum Geology* 9, 568-572.

Roedder E. and Kopp O. C. (1975). A check on the validity of the pressure correction in inclusion geothermometry, using hydrothermally grown quartz. *Fortschr. Mineral.* 52(Special), 431-446.

Roedder, E., (1984). Fluid inclusions. Reviews in Mineralogy 12. Mineralogical Society of America. 644 p.

Saigal G., Bjorlykke K., and Larter S. (1992). The effects of oil Emplacement on diagenetic processes - Examples from the Fulmar reservoir sandstones, Central North Sea. *American Association of Petroleum Geologists Bulletin* 76(7), 1024-1033.

Sawamura, S., Kitamura, K., Taniguchi, Y., (1989). Effect of pressure on the solubilities of benzene and alkylbenzenes in water. *J. Phys. Chem.* 93, 4931-4935.

Sawaki T., Sasada M., Sasaki M., Tsukimura K., Hyodo M., Okabe T., Uchida T., and Yagi M. (1997). Synthetic fluid inclusion logging to measure temperatures and sample fluids in the Kakkonda geothermal field, Japan. *Geothermics* 26(1), 281-303.

Sharp Z. D. and Kirschner D. L. (1994). Quartz-calcite oxygen isotope themometry:a calibration based on natural isotopic variations. *Geochimica et Cosmochimica Acta* 58, 4491-4501.

Shelton K. L. and Orville M. O. (1980). Formation of synthetic fluid inclusions in natural quartz. *American Mineralogist* 65, 1233-1236.

Smith, D.L., and Evans, B. (1984). Diffusional crack healing in quartz. *Journal of Geophysical research*, 89(b6), 4125-4135.

Spotl C., Houseknecht D. W., and Riciputi L. R. (2000). High-temperature quartz cement and the role of stylolites in a gas reservoir, Spiro Sandstone, Arkoma Basin, USA. In *Special Publication Number 29 of the International Association of Sedimentologists* (ed. R. H. Worden, Morad, S.), pp. 281-297

Stasiuk L. D. and Snowdon L. R. (1997). Fluorescence micro-spectrometry of synthetic and natural hydrocarbon fluid inclusions: crude oil chemistry, density and application to petroleum migration. *Applied Geochemistry* 12, 229-241.

Sterner S. M. and Bodnar R. J. (1984). Synthetic fluid inclusions in natural quartz I. Compositional types synthesized and applications to experimental geochemistry. *Geochimica et Cosmochimica Acta* 48, 2659-2668.

Swarbrick, R. E., & Edwards, S. C. (1993). Overpressure and Palaeopressure. In *Geofluid Seminar Serie* (ed. P. J.), pp. 333-337.

Swamy V., Saxena S. K., Sundman B., and Zhang J. (1994). A thermodynamic Assessment of silica phase diagrams. *Journal of Geophysical Research* 99(B6), 11787-11794.

Teinturier, S., Pironon, J., and Walgenwitz, F. (2002, this volume). Fluid inclusions and PVTX modelling: Examples from the Garn Formation, Haltenbanken, Mid-Norway. *Marine and Petroleum Geology*, 15(6) 755-765.

Teinturier S., Elie M., and Pironon J. (in review, this volume). Evidence of oil cracking using synthetic petroleum inclusion. *Journal Of Geochimical Exploration.*

Teinturier S. and Pironon J. (in review, this volume) .Time formation of individual fluid inclusion within fluorite crystal in H_2O-NH_4Cl and quartz in H_2O-NaCl system. *American Mineralogist.*

Teinturier S. and Pironon J. (in prep, this volume). Experimental diagenesis of quartz in petroleum environment. Part I: Fluid phases - Procedures and fluid trapping. *Geochimica et Cosmochimica Acta.*

Teinturier S. and Pironon J. (in prep, this volume). Experimental diagenesis of quartz in petroleum environment. Part II: Solid-liquid (dis)-equilibrium. *Geochimica et Cosmochimica Acta.*

Tester J. W., W.G. W., Robinson B. A., Grigsby C. O., and Feerer J. (1994). Correlating quartz dissolution kinetics in pure water from 25 to 625°C. *Geochimica et Cosmochimica Acta* 58(11), 2407-2420.

Thiéry R., Pironon J., Walgenwitz F., and Montel F. (2000). PIT (Petroleum Inclusion Thermodynamic): a new modeling tool for the characterization of hydrocarbon fluid inclusions from volumetric and microthermometric measurements. *Journal of Geochimical Exploration* 69-70, 701--704.

Tilley B. J. and Longstaffe F. J. (1989) Diagenesis and isotopic evolution of porewaters in the Alberta Deep Basin: The Falher Member and Cadomin Formation. *Geochimica et Cosmochimica Acta* 53, 2529-2546.

Tissot B. P. and Welte D. H. (1984). *Petroleum formation and occurrence, 2nd ed.*

Tsonopoulos, C., Wilson, G.M., (1983).. High-temperature mutual solubilities of hydrocarbons and water. Part I: benzene, cyclohexane and n-hexane. AIChE Journal 29, 990-999.

Vityk M. O., Pottorf R. J., Gray G. G., Larese D., and Hall D. (2001). Application of synthetic fluid inclusions to hydrocarbon system analysis. *ECROFI XVI*, 455-456.

Walderhaug O. (1990). A fluid inclusion study of quartz-cemented sandstones from offshore mid-norway - possible evidence for continued quartz cementation during oil emplacement. *Journal of Sedimentary Petrology* 60(2), 203-210.

Walderhaug, O. (1994a). Precipitation rates for quartz cement in sandstones determined by fluid inclusion microthermometry and temperature history modelling. *Journal of sedimentary Petrology, 64*, 324-333.

Walderhaug, O. (1994b). Temperatures of quartz cementation in Jurassic sandstones from the Norwegian continental shelf - Evidence from fluid inclusions. *Journal of Sedimentary Petrology, 64*, 311-323

Wilkinson M., Crowley S. F., and Marshall J. D. (1992). Model for the evolution of oxygen isotope ratios in the pore fluids of mudrocks during burial. *Marine and Petroleum Geology* 9, 98-105.

Williams L. B., Hervig R. L., and Bjorlykke K. (1997). New evidence for the origin of quartz cements in hydrocarbon reservoirs revealed by oxygen isotope microanalyses. *Geochimica et Cosmochimica Acta* 61(12), 2529-2538.

Wopenka, B., Pasteris, J. D. & Freeman, J. J. (1990). Analysis of individual fluid inclusions by Fourier transform infrared and Raman microspectroscopy. *Geochimica et Cosmochimica Acta* 54, 519-533.

Worden R. H., Oxtoby N. H., and Smalley P. C. (1998). Can oil emplacement prevent quartz cementation in sandstones? *Petroleum Geoscience* 4, 129-137.

Worden R. H. and Morad S. (2000). Quartz cementation in oil field sandstones: a review of the key controversies. In *Special Publication Number 29 of the International Association of Sedimentologists* (ed. R. H. Worden, Morad, S.). Blackwell Science.

Xie Z. and Walther J. V. (1993). Quartz solubilities in NaCl solutions with and without wollastonite at elevated temperatures and pressures. *Geochimica et Cosmochimica Acta* 57, 1947-1955.

Zecchini, P & Maitrallet, P.. (1998) : Les gisements d'émeraudes d'Inde. *in* "L'émeraude, connaissances actuelles et prospectives" *D. Giard, G. Giuliani, A. Cheilletz, E. Fritsch, E. Gonthier, eds. Association Française de Gemmologie (AFG), CNRS-ORSTOM, Paris,* 81-95.

Zhang Y. G. and Frantz J. D. (1987). Determination of the homogenisation temperatures and densities of supercritical fluids in the system NaCl-KCl-$CaCl_2$-H2O using synthetic fluid inclusions. *Chemical Geology* 64, 335-350.

Zhang Y., Stolper E. M., and Wasserburg G. J. (1991). Diffusion of a multi-species component and its role in oxygen and water transport in silicates. *Earth and Planetary Science Letters* 103, 228-240.

Zheng Y. F. (1993) Calculation of oxygen isotope fractionation in anhydrous silicate minerals. *Geochimica et Cosmochimica Acta* 57, 1079-1091.

Université HENRI POINCARÉ NANCY 1

Monsieur **TEINTURIER Stéphane**

DOCTORAT de l'UNIVERSITE HENRI POINCARE, NANCY 1

en SCIENCES DE L'UNIVERS

VU, APPROUVÉ ET PERMIS D'IMPRIMER n° 760

Nancy, le 25 novembre 2002

Le Président de l'Université
Pour le Président
et par délégation,
Le Vice-Président du
Conseil d'Administration,

Cl. BURLET

Marc GABRIEL

UNIVERSITÉ HENRI POINCARÉ, NANCY 1 * LE PRESIDENT

Université Henri Poincaré, Nancy I
24-30 rue Lionnois - B.P. 3069 - 54013 NANCY Cédex
Tél. : 03 83 68 20 00 - Fax : 03 83 68 21 00

Diagenèse expérimentale du quartz en présence d'hydrocarbures

Résumé: La cimentation du quartz est un processus diagénétique important puisqu'elle influence directement la qualité d'un réservoir pétrolier, notamment en régulant la porosité et donc son potentiel en huile ou en gaz. Les expériences réalisées en système silice±eau±sels±huile±gaz ont permis de simuler et d'approcher les conditions de la diagenèse siliceuse d'un réservoir pétrolier naturel et d'améliorer la compréhension des mécanismes de formation des inclusions fluides et de croissance de quartz en milieu aqueux et/ou hydrocarboné. Des courbes de calibrage permettant de calculer la teneur en méthane des inclusions dans le système H_2O-CH_4-NaCl ont été obtenues à partir de l'analyse en spectroscopie Raman et grâce à la synthèse d'inclusions utilisées comme standards. L'utilisation d'inclusions synthétiques et naturelles de référence a permis un calibrage de l'analyse quantitative de CH_4, CO_2 et des alcanes des inclusions hydrocarbonées par spectroscopie IR.

Des inclusions aqueuses ont été synthétisées dans des microfractures de grains de quartz, en présence de méthane dès 150°C-200 bar, en présence d'hydrocarbures à partir de 184°C-163 bar et dans des surcroissances en présence d'hydrocarbures à partir de 277°C-330 bar. Des inclusions hydrocarbonées ont été synthétisées avec différents rapports eau/huile (E/H), dans des microfractures de quartz (0<E/H<50%, 209-350°C; 175-400 bar), ainsi que dans des auréoles de croissance (10<E/H<50%, 289-350°C; 350-400 bar). La composition des inclusions hydrocarbonées est représentative de la composition du fluide parent jusqu'à des températures et pressions de 250°C et 212 bars respectivement. A 350°C-400 bar, des processus de cracking ont été mis en évidence aussi bien dans les inclusions fluides que dans l'huile parent et les propriétés PVTX des inclusions fluides hydrocarbonées sont modifiées par la présence d'eau dissoute dans l'huile en grande quantité. Aucun processus de rééquilibrage et d'infiltration post-auréole n'a été observé dans les auréoles des quartz lors d'une baisse de température. En revanche, quelques inclusions fluides ont pu être rééquilibrées et marquées au lithium ou au méthane en appliquant des températures expérimentales supérieures aux T_h des inclusions préexistantes.

La croissance de quartz et la formation d'inclusions fluides sont donc possibles même à forte saturation en hydrocarbures seulement si les quartz sont mouillés à l'eau. Dans des conditions expérimentales extrêmes (350°C-400 bar; E/H =10%), le fait que la quasi-totalité de l'eau soit dissoute dans la phase hydrocarbonée implique que la présence d'un film d'eau suffit à faire pousser du quartz en milieu à forte saturation en huile, dans l'hypothèse ou l'eau reste le seul vecteur et transporteur de silice. Les données expérimentales obtenues en SIMS ont montré que les auréoles générées en présence d'huile avaient des $\delta^{18}O$ supérieures, d'environ 10‰ par rapport à celles crées en milieu strictement aqueux dans les conditions expérimentales à 350°C et 400 bar. Si l'on fait le parallèle entre l'étude des auréoles naturelles des réservoirs pétroliers et les auréoles expérimentales, il est fort probable que les valeurs maximales en $\delta^{18}O$ des auréoles naturelles soient les témoins d'une saturation en huile du réservoir au moment de leur formation.

Mot-clés: quartz, hydrocarbures, expérimentation, diagenèse

Experimental diagenesis of quartz with petroleum

Abstract: Quartz cementation has a great impact on petroleum reservoir quality by controlling the porosity and thus the gas or oil storage. Experiments were carried out in a silica±water±salts±oil±gas system with the objective to simulate the siliceous diagenesis of natural petroleum reservoirs and to better understand the mechanisms of fluid inclusions formation and quartz cementation in a water and/or petroleum system. Calibration curves have been established using Raman microspectroscopy and synthetic reference inclusions to calculate the methane content of aqueous inclusions in the H_2O-CH_4-NaCl system. A quantitative procedure for FT-IR microspectrometry has been developed to obtain, from individual petroleum fluid inclusions, mole % concentrations of methane, alkanes and carbon dioxide as constraints to thermodynamic modelling.

Synthetic aqueous inclusions were created within quartz microfractures, with methane (from 150°C-200 bar), with petroleum (from 184°C-163 bar) and inside quartz overgrowths with the presence of hydrocarbons (from 277°C-300 bar). Synthetic petroleum inclusions were created with different water/oil ratios (W/O) within quartz microfractures (0<E/H<50%, 209-350°C; 175-400 bar), and in quartz overgrowths (10<E/H<50%, 289-350°C; 350-400 bar). The composition of the petroleum inclusions is representative to their parent oil composition up to 250°C and 212 bars. At 350°C-400 bar, cracking processes have been observed as well inside petroleum inclusions as for its residual parent oil in the autoclave. Moreover, the presence of water has modified the PVTX properties of fluid inclusions. On the other hand, no reequilibration processes have been observed with a continuous decrease of temperature. In contrast, few natural inclusions marked with lithium and methane have been reequilibrated by applying higher experimental temperatures than the trapping temperature of pre-existing fluid inclusions.

The quartz cementation as well as the fluid inclusion formation is thus possible even at high oil saturation. These processes require that the quartz is water-wet. In extreme experimental conditions (350°C-400 bar; E/H =10%), the almost entire dissolution of water into the petroleum phase involve that a simple water film is sufficient to generate quartz overgrowth into a high oil saturation. This hypothesis implies that water still remains the silica vector. SIMS profiles shows that $\delta^{18}O$ values of quartz overgrowths created with the presence of petroleum are higher (+10‰) than those created in a strict water system, at 350°C and 400 bar. If we project these observations in natural petroleum reservoirs, it could be possible that the maximum $\delta^{18}O$ values of diagenetic quartz overgrowths correspond to a possible episode of petroleum migration.

Keywords: quartz, petroleum, experiments, diagenesis

UMR G2R 7566 CNRS-CREGU-INPL-UHP Géologie et Gestion des Ressources Minérales et Energétiques
Université Henri Poincaré Nancy 1, Faculté des Sciences, BP 239, 54506 Vandoeuvre lès Nancy Cedex